Unveiling Hematopoietic Stem Cell Dynamics: Identification and Isolation of Hematopoietic Stem Cells at Single-Cell Level

INAUGURALDISSERTATION
zur Erlangung des Doktorgrades
der Naturwissenschaften

Dr. rer. nat.

Im Fachbereich Biologie und Chemie (FB 08)
der Justus-Liebig-Universität
in Giessen

von
Tessa Schmachtel
aus Frankfurt

JUSTUS-LIEBIG-
UNIVERSITÄT
GIESSEN

Giessen Juni 2025

2. Korrigierte Auflage, März 2026

Vom Fachbereich Biologie und Chemie (FB 08) der Justus-Liebig -Universität Gießen als Dissertation angenommen.

Dekan:	Prof. Dr. Holger Zorn
Gutachter:	PD Dr. habil. Oliver Rossbach Prof. Dr. Michael A. Rieger
Datum der Disputation:	27.11.2025

Erklärung

Ich erkläre hiermit, dass ich mich bisher keiner Doktorprüfung im Mathematisch-Naturwissenschaftlichen Bereich unterzogen habe.

Frankfurt am Main, den 20.03.2026 [redacted]

(Unterschrift Tessa Schmachtel)

Teile dieser Arbeit sind bereits in internationalen Fachzeitschriften veröffentlicht worden:

Komic, H.*, Schmachtel, T.*, Simoes, C.*, Kuelp, M.*, *et al.* Continuous map of early hematopoietic stem cell differentiation across human lifetime. *Nat Commun* 16, 2287 (2025). https://doi.org/10.1038/s41467-025-57096-y

***equal contribution as first author**

Schmachtel, T., Bonig, H., & Rieger, M. A. (2025). FACS-Based Assessment of Human Hematopoietic Stem and Progenitor Cells. International journal of molecular sciences, 26(17), 8381. https://doi.org/10.3390/ijms26178381

Versicherung

Ich erkläre: Ich habe die vorgelegte Dissertation selbstständig und ohne unerlaubte fremde Hilfe und nur mit den Hilfen angefertigt, die ich in der Dissertation angegeben habe. Alle Textstellen, die wörtlich oder sinngemäß aus veröffentlichten Schriften entnommen sind, und alle Angaben, die auf mündlichen Auskünften beruhen, sind als solche kenntlich gemacht. Ich stimme einer evtl. Überprüfung meiner Dissertation durch eine Antiplagiat-Software zu. Bei den von mir durchgeführten und in der Dissertation erwähnten Untersuchungen habe ich die Grundsätze guter wissenschaftlicher Praxis, wie sie in der „Satzung der Justus-Liebig-Universität Gießen zur Sicherung guter wissenschaftlicher Praxis“ niedergelegt sind, eingehalten.

Frankfurt am Main, den 20.03.2026 [redacted]

(Unterschrift Tessa Schmachtel)

Table of content

List of Figures

List of Tables

Abbreviations

% *Percent*

AbSeqs *Oligonucleotide-conjungated Antibodies*

AGM *Aorta-Gonad-Mesonephros*

BM *Bone Marrow*

c *Centi*

CB *Cord Blood*

CCA *Canonical Correlation Analysis*

CD *Cluster of Differentiation*

CFU-S *Spleen Colony forming Units*

CH *Clonal Hematopoiesis*

CHIP *Clonal Hematopoiesis of Indeterminate Potential*

CLOUD-HSPCs *Continuum of low-primed undifferentiated Hematopoietic Stem and Progenitor Cells*

CLPs *Common Lymphoid Progenitors*

CMPs *Common Myeloid Progenitors*

CS7 *Carnegie Stages*

dHSCs *Developmental Hematopoietic Stem Cells*

DMEM Dulbecco's Modified Eagle Medium

DMSO *Dimethyl Sulfoxide*

ECM *Extracellular Matrix*

EDTA *Ethylenediaminetetraacetic acid*

FACS *Fluorescence-activated Cell Sorting*, Fluorescence-Activated Cell Sorting

FCS *Fetal Calf Serum*

G-CSF *Granulocyte-Colony Stimulating Factor*, *Granulocyte-Colony Stimulating Factor*

GSEA *Gene Set Enrichment Analysis*

Gy *Grey*

HS *High Sensitivity*, *High Sensitivity*

HSCs *Hematopoeitic Stem Cells*

HSCT *Hematopoietic Stem Cell Transplantation*

HSPC *Hematopoietic Stem and Progenitor Cell*

kNN *K Nearest Neighbor*

L *Liter*

Lin *Lineage*, *Lineage*

LMPPs *Lympho-Myeloid primed Progenitors*

LT-HSCs *Long-Term Hematopoeitic Stem Cells*

LYP *Lymphoid Progenitors*

m mili, *Meter*

MDPs *Monocyte Dendritic Cell Progenitors*

MEPs Megakaryocyte-Erythroid Progenitors

MHC-II *Major Histocompatibility Complex II*

MLR *Mixed Lymphocyte Reaction*

MNC *Mononuclear Cells*

MPPs Multipotent Progenitors

NSG *NOD/SCID IL2ycnull mouse*, *NOD.Cg-Prkdc^{scid} Il2rg^{tm1Wjl}/SzJ*

PB *Peripherial Blood*

PBS *Phosphate Buffered Saline*

PCA *Principle Component Analysis*

PDCD1 *Programmed Cell Death Protein 1*

PD-L2 *Programmed Cell Death Ligand 2*

SEM *Standard Error of the Mean*

SFEM *Serum Free Exansion Medium*

TAE *TRIS-Acetat-EDTA*

TCM *Central Memory T-cells*

TEM *Effector Memory T-cells*

TLR *Toll-like Receptors*

TN *Naive T-cells*

Tregs *Regulatory T-cells*

UV *Ultraviolet*

w/o *Without*

wpt *Weeks post Transplantation*

WTA *Whole Transcriptome Analysis*

Summary

The human bone marrow constitutes the principal site of hematopoiesis, sustaining the continuous generation of platelets, erythrocytes and immune cells through the activity of hematopoietic stem and progenitor cells (HSPCs) residing within specialized microenvironmental niches. Within this compartment, a rare subset of hematopoietic stem cells (HSCs) maintains lifelong hematopoiesis by precisely regulating the balance between self-renewal and differentiation, predominantly persisting in a quiescent state under homeostatic conditions but capable of rapid activation in response to acute physiological stressors such as infection or hemorrhage. The equilibrium between steady-state and emergency hematopoiesis is fundamental to hematopoietic homeostasis; however, chronic inflammation and aging can disrupt this balance, leading to impaired blood cell production and increased risk of developing hematologic malignancies. Although substantial progress has been made in the characterization and prospective isolation of distinct human HSPC subsets using surface marker-based strategies, current strategies often yield in heterogeneous populations and several differentiation models have been proposed. To address this challenge and map differentiation trajectories, the presented research employed a single cell Transcriptomic/AbSeq approach, simultaneously quantifying the expression of 596 genes at mRNA level and 46 surface markers, on over 62,000 FACS-enriched HSPCs from 15 healthy donors across different age groups. Comprehensive computational analysis revealed four main lineage pathways, supporting a stepwise model of differentiation with an early branching point for megakaryocyte-erythroid progenitors. Notably, HSPCs from older donors exhibited a higher proportion of undifferentiated cells and diminished differentiation across all lineages. A key finding of this study is the identification of Programmed death ligand 2 (PD-L2/CD273) as a surface marker highly expressed on the most primitive HSPCs. CD273/PD-L2-positive HSPCs, isolated from mobilized PB samples, demonstrated a distinct molecular signature characterized by the enrichment of stemness genes such as *Thy1*, *DLK1* and *MPL*, as well as delayed entry into the cell cycle, reduced mitochondrial activity and delayed *in vitro* differentiation indicating a deeper quiescent state. Functional assays, including *in vitro* colony forming assays and *in vivo* xenograft experiments, confirmed that CD273/PD-L2^{high} HSPCs possess the capacity for multi-lineage reconstitution. Beyond their stem cell properties, CD273/PD-L2-expressing HSPCs exhibited notable immunomodulatory functions. In allogeneic lymphocyte reaction assays, these cells suppressed CD8+ T-cell proliferation and activation. Blocking PD-L2 promoted the secretion of pro-inflammatory cytokines (IFN-γ, TNF-α, IL-6), showed a reduced abundance of regulatory T-cells and a shift toward myeloid lineage bias in HSPCs, implying an increased inflammatory response reaction. These findings highlight a dual role for PD-L2: First **as a marker of more quiescent, primitive HSPCs** and second as **a mediator of immune regulation within the hematopoietic compartment**.

In summary, this integrated study provides valuable insights into the organization of human hematopoiesis and the identification of PD-L2/CD273 as a defining marker of a particularly quiescent, immunomodulatory HSPC subset. These discoveries may have important implications for stem cell transplantation and the treatment of blood malignancies, as understanding and manipulating these pathways may improve therapeutic outcomes and help maintaining healthy hematopoiesis throughout life.

Zusammenfassung

Das menschliche Knochenmark ist der zentrale Ort der Hämatopoese, in der hämatopoetische Stamm- und Vorläuferzellen (engl. *hematopoietic stem and progenitor cells*; HSPCs) die kontinuierliche Bildung aller Blutzelllinien gewährleisten. Eine seltene Subpopulation, die hämatopoetischen Stammzellen (engl. *hematopoietic stem cells*; HSCs), hält dieses System durch ein fein balanciertes Gleichgewicht zwischen Selbsterneuerung und Differenzierung lebenslang aufrecht. Unter normalen Bedingungen sind HSCs überwiegend inaktiv, können jedoch bei Stress wie Infektionen oder Blutverlust rasch aktiviert werden. Störungen durch chronische Entzündungen oder Alterungsprozesse beeinträchtigen dieses Gleichgewicht und erhöhen das Risiko für Bluterkrankungen. Trotz erheblicher Fortschritte bei der funktionalen Charakterisierung von HSPC-Subpopulationen führt die Oberflächenmarker-basierte Isolierung häufig zu heterogenen Zellgemischen. Dies hat unter anderem zur Folge, dass insbesondere die unterschiedlichen Modelle zur Organisation der Differenzierung weiterhin Gegenstand intensiver Diskussionen sind.

Um dieses Problem zu adressieren, wurde im Rahmen dieses Dissertationsprojekts mithilfe von Einzelzell-basierter Sequenzierung die Expression von 596 Genen und 46 Oberflächenmarkern in über 62.000 HSPCs aus dem Knochenmark von 15 gesunden Spendern unterschiedlichen Alters analysiert. Die bioinformatische Auswertung ergab vier Linienpfade und bestätigte ein stufenweises Differenzierungsmodell mit einem frühen Abzweigungspunkt für Megakaryozyten-Erythrozyten-Vorläufer. Auffällig war, dass HSPCs älterer Spender einen höheren Anteil undifferenzierter Zellen und eine verzögerte Differenzierung aufwiesen.

Ein weiteres zentrales Ergebnis dieser Studie ist die Identifikation von CD273/PD-L2 (engl. *Programmed death ligand 2*; PD-L2) als Marker, welcher auf den unreifen HSPCs stark exprimiert wird. Diese CD273/PD-L2-positiven Zellen zeichneten sich durch eine ausgeprägte Stammzell-Signatur, verlangsamten Zellzyklus, reduzierte mitochondriale Aktivität und verzögerte Differenzierung aus. Zusammen weisen diese Merkmale auf eine erhöhte Quieszenz der Zellen hin. Darüber hinaus bestätigten Xenotransplantations-Modelle die Fähigkeit von CD273/PD-L2^{high} HSPCs zur multilinearen Rekonstitution. Interessanterweise zeigte diese Zellpopulation nicht nur einen Stammzell-ähnlichen Phänotyp, sondern auch immunmodulatorische Eigenschaften. In einer Mischkultur aus unterschiedlichen Lymphozyten unterdrückte CD273/PD-L2 exprimierende HSPCs die Aktivierung und Proliferation von CD8+ T-Zellen. Im Gegensatz dazu führte die Blockade von CD273/PD-L2 zu einer verstärkten Immunreaktion, erkennbar an erhöhten Spiegeln proinflammatorischer Zytokine (IFN-γ, TNF-α, IL-6), einer verminderten Anzahl regulatorischer T-Zellen sowie einer vermehrten Differenzierung der HSPCs in myeloide Zelllinien. Diese Ergebnisse unterstreichen die doppelte Rolle von CD273/PD-L2: Einerseits als **Oberflächenmarker primitiver HSPCs**, andererseits als **Regulator immunologischer Prozesse im hämatopoetischen Kompartiment**.

Zusammenfassend liefert unsere Studie neue Einblicke in die Organisation der menschlichen Hämatopoese und identifiziert PD-L2/CD273 als Marker einer unreifen, immunmodulatorischen HSPC-Subpopulation. Diese Erkenntnisse könnten wichtige Impulse für die Optimierung von Stammzelltransplantationen und die Behandlung hämatologischer Erkrankungen geben.

1. Introduction

The human bone marrow (BM), once described as a "waste product (*excrementum ossium*)" by the esteemed philosopher Aristotle, is now recognized as the primary source of the vital blood cells that are essential for the maintenance of our human body functions (Dechambre A, 1877). Over the centuries, theories about the role of the BM varied, with some suggesting it was simply a source of nutrients for the bones, others challenging these hypotheses by stating the formation of the marrow takes place after the bone is built (Cooper, 2011; Robin C., 1875). It was not until the late 18th century that Neumann's hypothesis that the bone marrow was "the seat of blood formation" emerged, a statement that remains the cornerstone of the contemporary hematopoietic research paradigm (Neumann, 1868).

Besides its remarkable properties, the BM cannot function in isolation. Rather more, it needs to be considered as part of the hematopoietic system, a large mobile tissue that not only is the seat of the blood cell formation but connects all different organs in the human body. By that, blood cells encompass for supplying oxygen, mediating tissue repair and orchestrating our immune response in exposure to pathogens. To take care of all these functions, the hematopoietic system gives rise to producing around 350 billion platelets, 180 billion erythrocytes and 12 billion lymphocytes per day (Rieger and Schroeder, 2012). These cells varied in morphology and function but most of them arise from multipotent hematopoietic stem and progenitor cells (HSPCs) in an adult system (Weissman and Shizuru, 2008; Seita and Weissman, 2010). HSPCs reside in the BM niche, a microenvironment that functions as important gatekeeper in maintaining the blood cell system and exerts its regulatory activity on HSPCs and their progeny. Advancements in molecular, genetic and cellular technologies have unveiled the intricacies of the hematopoietic system with unprecedented clarity, revealing a complex landscape characterized by dynamic interactions between HSPCs and their microenvironment within the BM niche (Fröbel et al., 2021). The intricate crosstalk between these cellular elements orchestrates the finely tuned balance of hematopoiesis, ensuring the adaptive responsiveness of the system to environmental cues and physiological demands (Fröbel et al., 2021; Kode et al., 2014; Walkley et al., 2007).

It is essential to recognize that the hematopoietic system encompasses various components, including HSPCs, a broad variety of functional effector cells and even non-hematopoietic cells. Alongside these cellular components, hematopoiesis is influenced by extracellular factors like the extracellular matrix (ECM) and chemical and physical factors (Zanetti & Krause, 2020). Understanding these complex interactions among these elements requires ongoing research efforts to elucidate the intricacies of HSPC biology and their interactions within the BM niche.

1.1. The hematopoietic system – A brief journey through different developmental stages

Hematopoiesis is the generation of blood cells throughout the lifespan and therefore plays a major role in health and disease. It is a highly regenerative process that produces over one trillion (10^{12}) cells daily to maintain steady-state blood cell replacement and to adequately compensate for acute blood loss associated with emergency hematopoiesis (Rieger and Schroeder, 2012). While in the adult hematopoietic system all cells arise from hematopoietic stem cells (HSCs), embryonic hematopoiesis initiates through a distinct process where the first red blood cells emerge from an alternative source. To gain insight into adult hematopoiesis and gain a comprehensive understanding of the mechanisms guiding HSC identity and location, it is crucial to embark a brief exploration of its diverse developmental stages.

1.1.1. Developmental hematopoiesis

The mammalian developmental hematopoiesis takes place in multiple anatomical locations and occurs in various successive stages, also determined as "hematopoietic waves". It can be separated into 3 distinct waves: primitive, transient-definitive and definitive as illustrated in **Figure 1**. Primitive and transient-definitive waves are described as HSC-independent stage (Bertrand & Traver, 2009; Calvanese & Mikkola, 2023; McGrath et al., 2015; Palis, 2014; Tober et al., 2007). During these embryonic waves, the hematopoietic system must expand the blood cell compartment and produce progenitor cells while differentiating into different tissues (Canu & Ruhrberg, 2021; Dzierzak & Bigas, 2018; Vink et al., 2022). The primitive progenitor wave starts in humans by carnegie stage 7-8 (CS7-8) (2.5 weeks). These early stages are needed for the generation of primitive erythroid progenitors (oxygenation), embryonic macrophages (tissue remodeling and defense) and megakaryocytes precursors (vascular maintenance) (Bertrand & Traver, 2009; Gao et al., 2018; Kingsley et al., 2004; Palis, 2014). As these initial stages of hematopoiesis progress, a cohort of circulating red blood cells is formed, characterized by their large size and embryonic globin expression with higher oxygen carrying capacity (ζ/ε globins) (Steiner and Vogel, 1973; Peschle et al., 1984; Wilkinson et al., 1987; Manning et al., 2020). These erythroblasts are the first blood-forming cells and derive from the yolk sac. During murine primitive hematopoiesis, they are formed within embryonic day 7-8 (E7-8) (Calvanese & Mikkola, 2023; Haar & Ackerman, 1971; Luckett, 1978).

The transient-defined wave of hematopoiesis takes place within CS8-9 (3.25 weeks) in humans and E8-9 in mice (Calvanese & Mikkola, 2023). Following the development, the initialization of the heartbeat marks the phenotypical switch between primitive erythroblasts and the fetal erythroid lineage. After erythroblasts enter the circulation during E8-9 in mice and CS10-12 in humans, they are replaced by enucleated and globin α/γ-synthesizing erythrocytes which are synthesized in the fetal liver (Fraser et al., 2007; Hikspoors et al., 2022; Tavian et al., 1999). Hematopoiesis in the fetal liver is capable of differentiating into myeloid, megakaryocytic and lymphoid cells (Houssaint, 1981; Moore & Metcalf, 1970).

Following the HSC-independent hematopoiesis, the third and definitive developmental wave starts at stage E11.5/CS14-16 and initiates the synthesis of developmental HSCs (dHSCs). These dHSCs are capable of fully repopulating the hematopoietic system and have true multilineage potential. However, their number is very limited, with an estimated one dHSC per hematopoietic organ. They originate from the aorta-gonad-mesonephros (AGM) region and are reported to be a potent source of dHSC activity (Kumaravelu et al., 2002; Medvinsky & Dzierzak, 1996; Müller et al., 1994). At stage E12.5, these dHSC colonize the fetal liver, mediated by β1 integrin. Their subsequent proliferative expansion is transmitted by angiopoietin-like factors and the SOX17 transcription factor (Hirsch et al., 1996; I. Kim et al., 2007; Potocnik et al., 2000; C. C. Zhang et al., 2006). Despite previous publications, recent studies using lineage tracing strategies revealed only a two-fold increase in adult-blood-fated HSC precursors during this period. While fetal liver HSCs proliferate extensively, many exhibit differentiation bias over self-renewal, suggesting earlier developmental constraints limit adult-repopulating HSC expansion (Ganuza et al., 2022; Calvanese and Mikkola, 2023). In humans, dHSC colonization of the fetal liver is conveyed by the 6-gene signature (*RUNX1*, *HOXA9*, *MLLT3*, *MECOM*, *HLF*, *SPINK2*) in stage CS17 (Bian et al., 2020; Calvanese & Mikkola, 2023). The involvement of the fetal liver and the in-depth analysis of HLF^+ HSCs shown evidence for a decreased expression of proliferative genes during the end of the embryonic period, implying a shift towards homoeostatic HSC in the first trimester and marking the start for the feta period (Calvanese et al., 2022). During the transition from embryonic to fetal period, human BM hematopoiesis begins with the myeloid cell colonization of the cavity of long bone cavities following vascularization around week 8 (Charbord et al., 1996). By week 12, long-term engraftable HSCs (LT-HSCs) are detectable and a fully active BM hematopoiesis is established by week 14 (Charbord et al., 1996; Z. Zheng et al., 2022). While transforming to fetal BM is associated with a shift towards a more quiescent state between week 17-22, further research is necessary to elucidate the changes in the niche supporting HSC maturation and lifelong maintenance between fetal liver and BM (Ranzoni et al., 2021).

As illustrated in **Figure 1** murine and human developmental hematopoiesis show tremendous differences when it comes to anatomy and pregnancy duration. Nevertheless, these initial sites of hematopoiesis are largely conserved among vertebrates and can be used to gain further understanding of early developments and their impacts on adult hematopoiesis (Medvinsky et al., 2011).

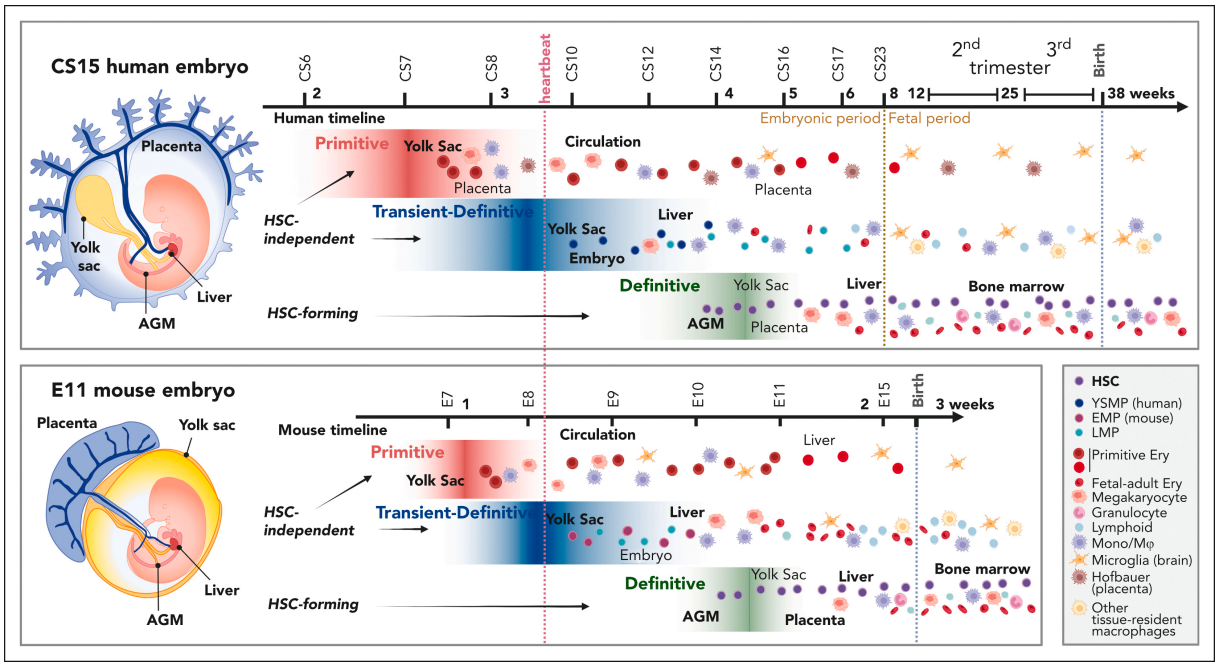

Figure 1. Developmental hematopoiesis in human and mouse embryos.

Hematopoiesis is conserved in mammals but differs in anatomical sites, timing, and progenitor output between humans and mice. In humans, hematopoiesis begins at 2.5 weeks in the yolk sac with primitive progenitors, producing nucleated erythroblasts and macrophages. By 3.25 weeks, a second wave of definitive progenitors emerges, contributing to tissue-resident macrophages and lymphoid cells. The third wave at 4–6 weeks originates hematopoietic stem cells (HSCs) in the AGM, which seed the liver, mature, and later migrate to the bone marrow by the second trimester. In mice, similar developmental waves occur but within a shorter timeframe, leading to overlaps. Mouse yolk sac progenitors favor erythromyeloid differentiation, while human progenitors exhibit myeloid skewing. Key developmental milestones, such as heartbeat onset and the embryonic-to-fetal transition, occur at different stages between species (taken from Calvanese and Mikkola, 2023).

1.1.2. Adult hematopoiesis

After outlining the various developmental stages that illustrate HSC migration from the AGM to the fetal liver and ultimately into the BM, where they remain throughout adulthood, this thesis will focus on investigating adult hematopoiesis.

As described above, adult hematopoiesis has an enormous quantity of blood cells produced every day. This highly regenerative organ is fully based on the proliferation and differentiation of HSCs. In contrast to the embryonic hematopoiesis, blood cell formation in adulthood cannot be HSC-independent. Studies indicate that the small population of HSCs, estimated to be less than 1.3 million, is responsible for generating mature peripheral blood cells throughout an individual's lifespan. However, this number can vary, ranging from a few hundred active HSCs to 50,000 - 600,000 HSCs in steady-state adult hematopoiesis (Abkowitz et al., 2002; Watson et al., 2020). Recent studies comparing different age cohorts have shown, that under the age of 65 approximately 20,000 – 200,000 HSC/MPPs are stably contributing to our blood production (Mitchell et al., 2022). Under homeostatic conditions most HSCs remain in quiescence (G0 phase), with infrequently proliferation occurring to ensure their long-term maintenance (Bigas & Waskow, 2016; Dzierzak & Bigas, 2018; Rossi et al., 2007). Nevertheless, the plasticity of the hematopoietic system is most evident during emergency situations such as induced stress, physical trauma, anemia or infections, when cell counts can

rapidly increase (Rieger and Schroeder, 2012). These emergency situations require an adaptive regulation of the hematopoietic system to generate specific cell types in appropriate numbers and locations depending on various circumstances. Consequently, precise mechanisms must be orchestrated to ensure correct fate decisions. Over recent decades, numerous models have been proposed to elucidate the organization of our hematopoietic system and the initiation of differentiation. Advancements in technology have provided deeper insights into the factors influencing these cell fate decisions and response mechanisms. In the following chapter, we will examine these various models and their associated hypotheses.

1.2. Modules of hematopoiesis

1.2.1. Classical module of hematopoiesis

1.2.1.1. Hierarchical tree model

The classical model of hematopoiesis places HSCs at the apex of the hematopoietic hierarchy. Alexander A. Maximow was the first to propose this theory, which elucidated the diverse cellular morphologies observed in cells across different blood lineages and developmental stages (Doulatov et al., 2012a; Maximow, 1909). According to that model HSCs restrict their self-renewal capacity to generate MPPs through stepwise differentiation into oligo-, bi- and unipotent progenitors (Kondo et al., 1997; Velten et al., 2017). This paradigm was proofed over the last century by endless studies exploring our understanding of HSC self-renewal and differentiation properties through transplantation assays (Olson et al., 2020b). The downstream located MPPs exhibit self-renewal capacity while maintaining multipotency (Busch et al., 2015). That construct of stepwise restriction of lineage potential at binary branching points results in a tree-like model (Haas et al., 2018) (**Figure 2A**). Subsequently, MPPs differentiate into oligopotent progenitors that have limited lineage differentiation capacity, forming common myloied progenitors (CMPs) or common lymphoid progenitors (CLPs) (Akashi et al., 2000; Cabezas-Wallscheid, 2014; Kondo et al., 1997; E. Pietras, 2015). Afterwards, these progenitors produce lineage-restricted precursors and mature cell types of the blood and immune systems (Haas et al., 2018; Seita & Weissman, 2010b). While the hierarchical organization of the hematopoietic system has been emphasized for the past century, recent publications exploring the clonal composition of the HSC compartment suggest that multiple HSCs contribute concurrently to peripheral blood cell production, resulting in stable hematopoiesis (Carrelha et al., 2018; Drize et al., 1996; Goyal & Zandstra, 2015). Technological advancements over the last two decades have led to the emergence of an alternative, more flexible model of hematopoiesis, challenging its strict hierarchical structure with a more heterogeneous HSC population summiting at the top. Consequently, hematopoiesis is inherently polyclonal with new clones of mature cells successively arising, due to the finite life span of the previously expanded primary pool.

1.2.1.2. The clonal succession model

The initial incorporation of genetic barcoding and next-generation sequencing techniques peaked in the so-called “clonal succession models”, offering insights into the dynamic nature of hematopoiesis. As stated before, these models suggest that numerous HSC clones participate in the process over time (Biasco et al., 2016; Gerrits et al., 2010; Glimm et al., 2011; S. Kim et al., 2014; Six et al., 2020). Following this hypothesis, the combination of the barcoding-based labeling with cell sorting revealed that a predominant fraction of transplanted clones consistently contributes to hematopoiesis over extended periods. However, the clonal composition of specific effector populations—such as granulocytes, T cells, and B cells—varies substantially over time. Individual clones show dynamic behavior, with many expanding, declining or changing their contribution to hematopoiesis throughout the observation period (Verovskaya et al., 2013). Importantly, clone sets may differ between varied compartments, such as PB and BM (Biasco et al., 2015, 2016).

This perspective was further confirmed by another model based on transposon system established in transgenic mice, called “Sleeping Beauty”, which enabled *in situ* labelling and clonal tracking of hematopoietic cells. The successive measurement of progenitors through their common location of transposons could be used to detect their cellular origins, lineage relationships and dynamics of native blood production progenitors (R. Lu, 2014; Sun et al., 2014). Furthermore, this model enables their analysis *in vivo* over different time points without prior transplantation. The results shown strikingly different clones at different time points supported steady state hematopoiesis. Recent publications investigating the clonal composition in steady-state hematopoiesis using single-cell techniques were able to quantify the lineage output of distinct HSC clones. The tracing approach of mature hematopoietic cells demonstrated that 50 % of HSC clones gave rise to 60 % of progenitor and mature cells over different time points (Weng et al., 2024). These results of the observed clonal dynamic are consistent with the clonal succession model, stating that the putative clonal diversity is much higher than previously demonstrated and can differ to different time points and inquiries.

In addition to providing detailed insights into clonal expansion, single-cell technologies have facilitated thorough examinations of phenotypically homogeneous populations. These analyses incorporate factors such as epigenetic, transcriptomic and metabolic states, challenging the concept that progenitor populations represent distinct cell types. Instead, they suggest that progenitors should be viewed as transitional states and displayed temporal dominance of different HSC clones in a demand-driven application. These revelations, among others, have revolutionized our comprehension of HSCs and their role in lineage commitment and build a new perspective on how HSCs contribute to blood production over time.

1.2.3. The continuous differentiation model

Building on these insights, single-cell transplantations showed significant functional heterogeneity within the HSC compartment further contradicting the classical hierarchical model. Multiple studies indicate that

true oligopotency is confined to a minority of HSCs, while the majority exhibit a stable predisposition—or lineage bias—toward the generation of specific blood cell lineages (Alejo E. Rodriguez-Fraticelli, 2018; Karamitros et al., 2018; Notta, 2016; Paul, 2015; Perié et al., 2015; Velten et al., 2017). These results underscore the influence of cell-intrinsic regulators on cell fate decisions, occurring at early stages of hematopoietic differentiation (CE Müller-Sieburg, 2002; Yu, 2016). Subsequent advances in large-scale single-cell gene expression profiling have enabled the reconstruction of developmental trajectories independently of traditional surface marker-based classification, displaying a gradual acquisition of lineage-committed transcriptomic states by HSCs, rather than an abrupt transitions between stable intermediate states (Karamitros et al., 2018; Nestorowa et al., 2016; Pina et al., 2012; Tusi et al., 2018; Velten et al., 2017). In addition to that, lineage tracing experiments have demonstrated the direct emergence of the megakaryocyte lineage from HSCs, a phenomenon challenging the traditional tree model (Alejo E. Rodriguez-Fraticelli, 2018). The identification of lineage-biased HSCs suggests that lineage separation begins early during hematopoietic development. At this stage, emerging barriers between lineages remain plastic but become increasingly restrictive over time, reflecting a gradual loss of multipotency and culminating in lineage commitment. Early transcriptional priming likely corresponds to multipotent cells with a bias toward specific lineages, whereas uni-lineage transcriptional signatures mark cells that are functionally committed (Velten et al., 2017). In such a model, progenitor cells are not defined as discrete entities but rather as transitional states along a continuous differentiation spectrum. This model accommodates the substantial heterogeneity observed within the HSC compartment, is consistent with the variable lineage output of single HSC clones following transplantation, and is supported by evidence of transcriptional priming, functional biases and early lineage divergence (Grover et al., 2016; Karamitros et al., 2018; Nestorowa et al., 2016; Pina et al., 2012; Tusi et al., 2018; Velten et al., 2017). Accordingly, hematopoietic differentiation is characterized by a gradual acquisition of lineage-biased gene expression without clear-cut boundaries between progenitor populations (**Figure 2B**). The continuous model of hematopoiesis proposes that differentiation trajectories are initiated early and, while still responsive to extrinsic signals, these early biases help explain the lineage output preferences observed throughout hematopoietic development (Laurenti & Göttgens, 2018).

These findings underscore the complexity of hematopoietic regulation and suggest a hierarchical organization within the hematopoietic system, where various progenitor cells contribute to specific lineages of mature blood cells. Overall, a comprehensive understanding of the different models explaining adult hematopoiesis is essential for unraveling the intricacies of blood cell development and homeostasis.

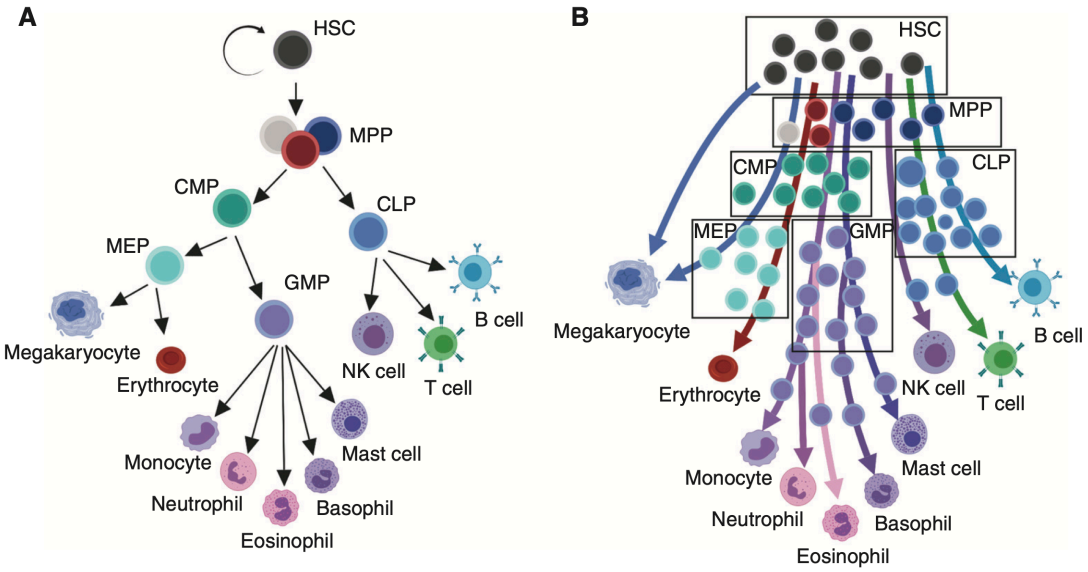

Figure 2. Models of HSC lineage commitment.

(**A**) The classical tree-like model depicts hematopoietic stem cells (HSCs) differentiating into multipotent progenitors, which generate lineage-restricted progenitors and eventually all mature hematopoietic cells. This model assumes uniform developmental stages and uniform lineage decisions, driven either stochastically or by instructive cytokines. (**B**) The continuous differentiation model highlights gradual lineage specification and transcriptional bias emerging earlier than full lineage commitment. Progenitor states, defined by phenotypic markers, demonstrate the heterogeneity within these populations (taken from Olson, Kang and Passegué, 2020).

1.3. A hierarchy roadmap through the hematopoietic compartment

To introduce the various cells within the hematopoietic compartment, we will refer to the traditional hematopoietic hierarchy to simplify the understanding (**Figure 3**).

Independent of the model explaining the hematopoietic system, it is widely established that HSCs are the parental population of all other hematopoietic cells (Laurenti & Göttgens, 2018). The ability to isolate and characterize different stem cells or their subsequent progenitor cells opens avenues to understand how hematopoiesis is regulated. Selecting these populations for studies is based on a series of cell surface markers. These protein markers are mostly declared as cluster of differentiation (CD) and used for their prospective isolation using fluorescence-activated cell sorting (FACS). Despite the fact, that many hematopoietic studies have been performed in mice, there is a lack of congruence than it comes to the expression of their cell surface markers. In the following abstract we will predominantly focus on human CD markers and not discuss murine markers.

In the clinical setting CD34+ cells isolated through direct aspiration or granulocyte-colony stimulating factor (G-CSF) directed mobilization are commonly used as stem cell source material. CD34 was first described around 1990 and since then is one of the cornerstones in immunophenotypic analysis for HSPCs (Civin et al., 1984; Krause et al., 1996). These cells compromise approximately 1 - 1.5 % of BM mononucleated cells and are capable of reconstituting hematopoiesis in patients undergoing autologous bone marrow refusion

following myeloablation therapy, resulting in sustained durable donor-derived hematopoietic reconstitution. Therefore, CD34+ cells have been widely confirmed in clinical applications to define human stem and progenitor cells (Anjos-Afonso & Bonnet, 2023; Link et al., 1996). Although CD34 is considered the *bona fide* human HSC marker, it encounters diverse mixture of different progenitor populations. Because of that, researchers have to use a more refined isolation method to specifically identify and study the most primitive stem cells.

CD90 (Thy1) was one of the first markers which in combination with CD34 described a small population containing multilineage capacity (Baum et al., 1992; Murray et al., 1995). Over the following decade further studies postulated the absence of CD45RA and CD38 expression leads to a more enriched HSC population. As a result, HSCs have been described as CD34+CD38-CD45RA-CD90+ cells until recent years (Bhatia et al., 1997; Conneally et al., 1997; Lansdorp et al., 1990). This isolation strategy could only be refined by work from Notta *et al*., who proposed the addition of the integrin α6 (CD49f). As a result, the predominantly applied marker combination to prospectively isolate human HSCs is defined as Lin-CD34+CD38-CD45RA-CD90+CD49f+ cells (Notta et al., 2011).

According to the hierarchical structure of hematopoiesis, HSCs give rise to MPPs, which exhibit reduced self-renewal capacity and increased cell-cycle activity (Adolfsson, 2005; Forsberg et al., 2006). As outlined in the previous chapter, distinct transcriptional stages within a progenitor population drive lineage priming, resulting in the subdivision of MPPs based on their differentiation potential and lineage bias. This process has been extensively characterized in murine models. In human fetal samples, the research group of John Dick identified bipotent megakaryocytic-erythroid progenitors using $CD34^{+}CD38^{-}$ HSPCs. By incorporating the surface markers BAH1 and CD71, they distinguished two MPP subpopulations: $BAH1^{-}CD71^{+}$ (F2; ~1.23 %) and $BAH1^{+}CD71^{+}$ (F3; ~0.01 %). These findings suggest that, during developmental hematopoiesis, lineage-restricted progenitors can emerge directly from multipotent progenitors without transitioning through an oligopotent stage. In adult bone marrow samples, the frequencies of F2 and F3 MPPs are significantly lower (~0.01 %). Consequently, MPPs in adult samples are commonly isolated using the marker combination $Lin^{-}CD34^{+}CD38^{-}CD45RA^{-}CD90^{-}CD49f^{-}$ (Notta et al., 2011, 2016; R Majeti, 2007).

Downstream of MPPs the megakaryocyte-erythrocyte differentiation branch is one of the earliest differentiation steps (Alejo E. Rodriguez-Fraticelli, 2018; Carrelha et al., 2018). Megakaryocyte-erythrocyte progenitors (MEPs) can be isolated using the marker combination $Lin^{-}CD34^{+}CD38^{+}CD123^{-}CD45RA^{-}CD135^{-}CD10^{-}$ (Doulatov, 2010; Manz et al., 2002; R Majeti, 2007).

In parallel, MPPs give rise to lympho-myeloid primed progenitors (LMPPs), characterized by the marker profile $CD34^{+}CD38^{-}Thy1^{-/lo}CD45RA^{+}$, which represents approximately 1 % of $CD34^{+}$ cells. Although these cells exhibit multilineage lymphoid potential (B, T, and NK cells), previous studies indicated an absence of *in vivo* repopulating activity, suggesting a more lineage-restricted progenitor state (R Majeti, 2007). The differentiation of LMPPs progresses towards the formation of CMPs, granulocyte-monocyte progenitors (GMPs), and CLPs. CMPs are defined by the marker profile

Lin⁻CD34⁺CD38⁺CD123lowCD45RA⁻CD135⁺CD10⁻, while GMPs express Lin⁻CD34⁺CD38⁺CD123⁺CD45RA⁺CD135⁺CD10⁻. CLPs, committed to lymphoid differentiation, are characterized as Lin⁻CD34⁺CD38⁻CD45RA⁺CD7⁺CD10⁺CD135⁺. Notably, myeloid progenitors express CD123 and CD135, whereas erythroid progenitors lack these markers. The transition from CMPs to GMPs is marked by the acquisition of CD45RA. Furthermore, single CD135⁺CD45RA⁻ CMPs have been demonstrated to produce all myeloid, but not lymphoid, lineages both in vitro and following transplantation (Doulatov, 2010; Edvardsson et al., 2006; Manz et al., 2002). Regarding lymphoid commitment, CD7 and CD10 are recognized as early markers for T and B cell precursors, respectively. Hoa *et al*. reported that CD7⁺ cells within the CD34⁺CD38⁻ HSPC population possess the potential to differentiate into B and NK cells but lack myeloid and erythroid potential. Consequently, CLPs are restricted to the lymphoid lineage, giving rise to T, B, and NK cells, while CMPs are committed to the myeloid-erythroid pathway.

This stepwise differentiation trajectory highlights how multipotent, lineage-biased progenitors progressively give rise to lineage-specific, committed progenitors, underscoring the complexity and regulation of hematopoietic differentiation (Olson et al., 2020b).

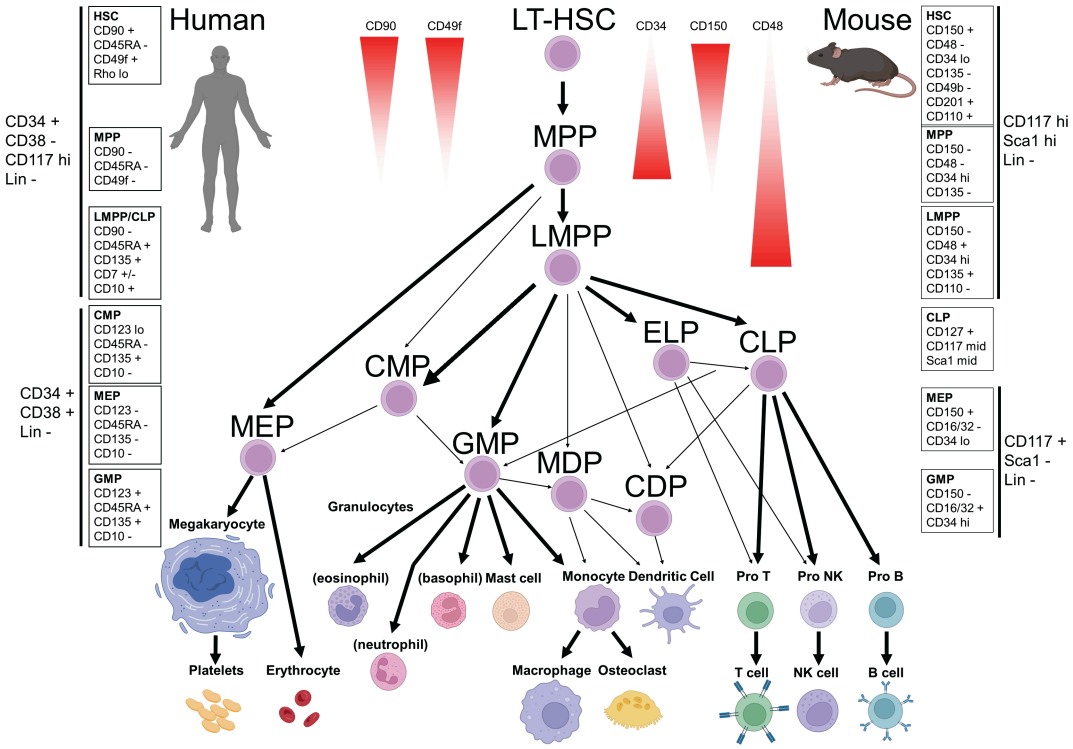

Figure 3. Differentiation hierarchy displaying the lineage determination in adult mouse and humans.

The major stem and progenitor cell populations are defined by their cell surface phenotypes, as listed next to each population and in the red bars below the schematics. Terminally differentiated cells are shown on the bottom, with arrows indicating inferred lineage relationships. In mice (right), hematopoietic stem cells (HSCs) give rise to transiently engrafting multipotent progenitors (MPPs) and immature lymphoid-biased progenitors, such as lympho-myeloid primed progenitors (LMPPs), which undergo gradual lymphoid specification. Myeloid and erythroid differentiation proceeds through well-defined progenitor populations, including common myeloid progenitors (CMPs), granulocyte-macrophage progenitors (GMPs), and megakaryocyte-erythroid progenitors (MEPs). In humans (left), HSCs are identified by the expression of CD49f and other markers, with multipotent progenitors (MPPs) characterized by the loss of CD49f expression. Similar to mice, human hematopoiesis includes well-defined myelo-erythroid progenitor populations (CMPs, GMPs, and MEPs).

After introducing the different lineages that emerge from HSCs, we will shift our focus primarily to HSCs and their heterogeneity. As previously mentioned, numerous experiments have demonstrated that the HSC population is much more heterogeneous than initially thought. Thus, in the following chapter, we will explore the definitional framework to characterize HSCs and the various factors influencing HSC heterogeneity in greater depth.

1.4. The definition of hematopoietic stem cells

1.4.1. The terminological framework

HSCs are defined by their ability to self-renew and replenish all the cell types presented in the hematopoietic system. Their multipotency was first defined in the middle of the 20th century by the first successful mouse transplantation of lethally irradiated mice (LO Jacobson, 1951). Following *in vivo* experiments using syngeneic BM cells transplanted into mice resulting in myeloid and erythroid colonies cells found in the spleen. These experiments gave more insight into the estimated stem cell numbers of these spleen colony forming units (CFU-S). It could be estimated that within 10,000 BM cells, 1 cell is capable of colonizing the spleen (AJ Becker, 1963; JE Till, 1961). In the 1990s, single-cell transplantation experiments were performed to truly show the capacity of a single blood-forming HSC to generate all hematopoietic lineages (Osawa et al., 1996). With these advances in technology, HSCs could be separated in LT-HSCs with a long-term reconstitution capacity over 3 - 4 months and ST-HSCs, multipotent cells which are only able to sustain hematopoiesis over a short period of time (approximately < 1 month), without durable and serial reconstitution ability. With these stepwise differentiation steps, progenitor populations limit their self-renewal potential (Yang et al., 2005). Until today, serial transplantation (secondary or tertiary recipient) displays the gold standard to interpret the self-renewal capacity of a hematopoietic subpopulation (Dykstra et al., 2007). To test human hematopoietic cell engraftment and multilineage reconstitution, the population of interest is injected into sublethal irradiated immune-deficient mice (NOD/SCID IL2γc^{null} mouse, referred to as NSG) as xenograft model (M. Ito et al., 2002). While HSC transplantation models offer significant advantages and valuable insights, it is important to acknowledge their limitations: these models create artificially induced conditions that compel the cells to expand, thereby failing to provide an uncompromised view of their natural fate in an unperturbed environment. As a result, they reveal the cells' "potential" fate rather than their actual behavior under physiological conditions (Haas et al., 2018).

1.4.2. Heterogeneity of HSCs

As discussed in the previous chapter, HSCs are typically defined based on their immunophenotypic profiles, characterized by the expression of specific surface markers (Lin-CD34+CD38-CD45RA-CD90+CD49f+). While prospective isolation using monoclonal antibodies and FACS is a widely used and straightforward method, it often results in a relatively heterogeneous cell population, as it overlooks crucial factors contributing to HSC diversity, such as genetic and epigenetic variations, metabolic states, and cell cycle dynamics (Haas et

al., 2018). To gain a deeper understanding of HSC heterogeneity, it is essential to explore and dissect these underlying factors in greater detail. As displayed in **Figure 4A** the BM microenvironment plays a pivotal role in shaping HSC heterogeneity. HSCs localize to distinct niches composed of various cell types (e.g., stromal, endothelial, and immune cells), each delivering unique biochemical and biophysical signals and influencing (Acar et al., 2015; Bruns et al., 2014; Ding & Morrison, 2013; Greenbaum et al., 2013; Sugimura et al., 2012; M. Zhao et al., 2014). Cytokines, extracellular matrix stiffness and niche-specific signals influence HSC function and lineage decisions (Anthony & Link, 2014; Asada et al., 2017; Çelebi et al., 2011; Choi et al., 2015; Ehninger & Trumpp, 2011; Lee-Thedieck et al., 2012; Mossadegh-Keller et al., 2013; Pinho & Frenette, 2019; Rieger et al., 2009; Uckelmann et al., 2016). HSC heterogeneity is also driven by chromatin accessibility, epigenetic alterations (e.g., DNA methylation and chromatin remodeling) and genetic mutation acquired over time (Beerman et al., 2013; Bock et al., 2012; Cabezas-Wallscheid, 2014; Cui et al., 2009; Farlik et al., 2016; Lara-Astiaso et al., 2014; Lipka et al., 2014; Pastore & Levine, 2016). These changes affect HSC maintenance, lineage commitment and response to stress or aging, contributing to variability in their function (**Figure 4B+C**). Variations in HSC cellular states (e.g., cell cycle phase, metabolic activity, and quiescence) further contribute to heterogeneity. Quiescent HSCs often rely on glycolysis to minimize reactive oxygen species (ROS) production, protecting DNA integrity, while active HSCs show increased biosynthesis and oxidative phosphorylation (**Figure 4D**) (K. Ito et al., 2012; K. Ito & Suda, 2014; Qian et al., 2016). Asymmetric segregation of cellular components, such as proteins and organelles, during cell division may lead to distinct fates in daughter cells (Beckmann et al., 2007). While mechanisms like Cdc42-mediated polarity have been observed, their precise role in HSC fate determination requires further exploration (**Figure 4E**) (Florian et al., 2012). The biochemical reactions and their stochastic nature taking place during cellular processes such as transcription or translation generate variability among HSCs, even in identical conditions (**Figure 4F**) (Elowitz et al., 2002; Raj & van Oudenaarden, 2008).

To understand how lineage bias arises from HSC heterogeneity and how extrinsic signals affect the lineage output it is essential to understand the hematopoietic regulation during physiological stress, which will be further discussed in the following chapter.

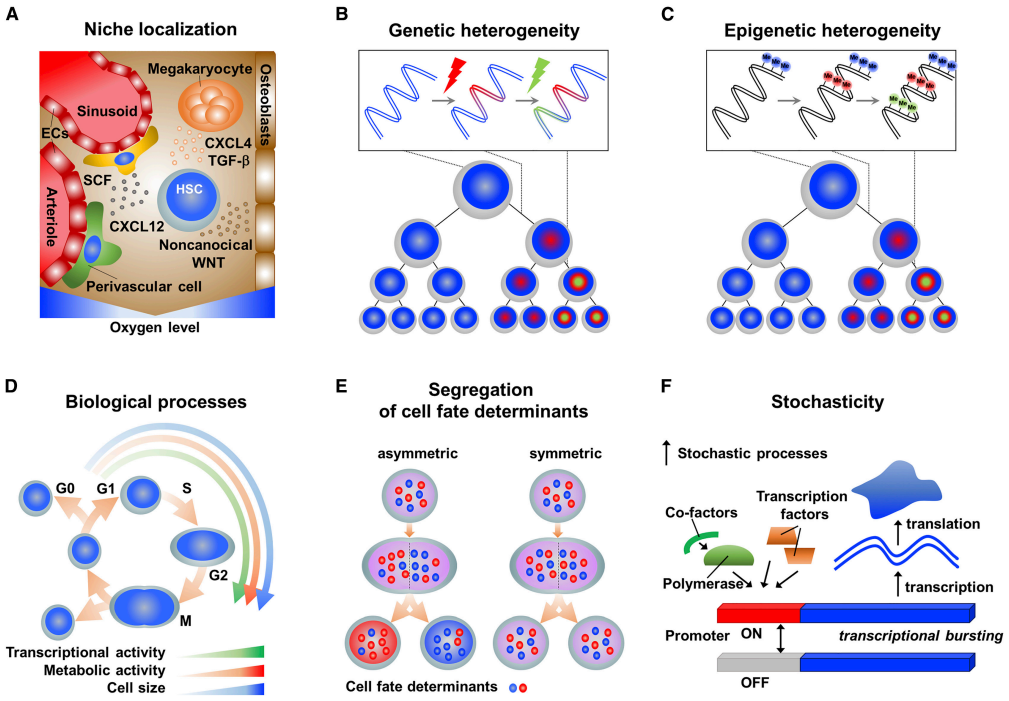

Figure 4. Distinct sources contribute to heterogeneity within the HSC compartment.

(**A**) HSCs localize to distinct bone marrow niches, each characterized by unique biochemical and biophysical microenvironments that influence HSC fate and function. (**B**) Somatic mutations in HSCs and their progeny can give rise to genetic mosaics, leading to altered functional properties and contributing to clonal diversity. (**C**) Differential epigenetic modifications, including DNA methylation and histone modifications, across individual HSCs generate epigenetic heterogeneity that impacts lineage commitment and differentiation potential. (**D**) Variability in cellular states, such as differences in cell cycle phase, metabolic activity, or quiescence, contributes to biomolecular heterogeneity within the HSC population. (**E**) Asymmetric segregation of cellular components during HSC division can result in daughter cells with distinct functional capacities, further contributing to intra-compartmental diversity. (**F**) Intrinsic stochastic processes, including random fluctuations in gene expression and molecular interactions, drive cellular variability and influence HSC behavior and differentiation outcomes (taken from Haas, Trumpp and Milsom, 2018).

1.5. Emergency hematopoiesis

Hematopoiesis must be very adaptable and responsive system to external stimuli like infection, chemotherapy or blood loss and tailor their lineage output and cell production to a specific demand. Pathogen driven infections and associated inflammations mobilize present innate immune effector cells as first line of defense (Cronkite & Strutt, 2018). These cells are rapidly used and need to be continuously replenished. This need shifts the steady state hematopoiesis into emergency hematopoiesis through activation of HSCs, increased proliferation and temporary expansion of the HSC pool to boost immune cell production (King & Goodell, 2011; E. M. Pietras, 2017; Takizawa et al., 2012). As stated in the previous chapter, HSCs are responsive to cytokines and chemokines through their extracellular and intracellular receptors. Especially inflammatory cytokines like Interferon I and II (IFN), Interleukin 6 (IL-6) or granulocyte colony stimulating factor (G-CSF) lead to HSC activation and emergency myelopoiesis and granulopoiesis to initiate the innate immune response (Baldridge et al., 2010a; Boettcher & Manz, 2017; Essers et al., 2009; Hirche et al., 2017; Schuettpelz & Link, 2013; Wilson, 2008). During this process, the lineage-biased HSCs play an important role to drive emergency production into certain cell lines and serve as an emergency backup for stress, capable of efficiently and specifically counter-balance the sudden loss of certain cell

types. Haas *et al.* demonstrated this mechanism with megakaryocytic-restricted progenitors expressing von Willebrand factor (VWF) in a phenotypic HSC compartment which drive an emergency megakaryopoiesis in demand-driven response to infections or tissue damage (Haas, 2015; Haas et al., 2018). Despite target-driven manners, broader homeostatic perturbations can elicit similar effects on differentiation trajectories. The same HSC-like megakaryocyte progenitors activated by thrombopoietin-depended mechanism result in rapid expansion of the megakaryocyte lineage after platelet depletion (Olson et al., 2020b; Sanjuan-Pla et al., 2013). In addition to cytokine driven inflammatory reactions which can influence HSC biology indirectly, circulating HSPCs can directly sense infectious agents through pathogen-associated molecular patterns (PAMPs) by their expressed toll-like receptors (TLR) (J. M. Kim et al., 2005; Nagai et al., 2006; Sioud et al., 2006). The recognition by TLR can induce HSPC activation and differentiation into the myeloid lineages, stimulate cytokine release and boost the immune cell production (**Figure 5**) (Sezaki et al., 2020). These mechanisms collectively demonstrate the remarkable adaptability of the hematopoietic system, allowing for rapid and targeted responses to diverse physiological challenges, whether they be infectious threats or acute cellular depletions, ensuring the maintenance of hematopoietic homeostasis.

Multiple protection mechanisms allow activated HSCs to restore their quiescence after induced inflammatory stress to ensure lifelong fitness of the hematopoietic system. For instance, in the lab of Emmanuelle Passegué It was shown that after acute stimulation, HSCs become desensitized to IFN-1 signaling and desensitize to further stimulation, terminating the response as a negative feedback loop (E. M. Pietras et al., 2014). On the contrary to acute inflammatory reactions, which can be balanced back to steady-state homeostasis, chronic inflammation or recurring infections can lead to decreased self-renewal and repopulating capacity of HSCs (Essers et al., 2009; Florez et al., 2020; E. M. Pietras, 2017). These effects are adding during the increased lifespan of a being. Therefore, aging is often associated with chronic low-grade inflammation and distinct lineage bias and molecular signatures which are further discussed in the following chapter (Vasto et al., 2007).

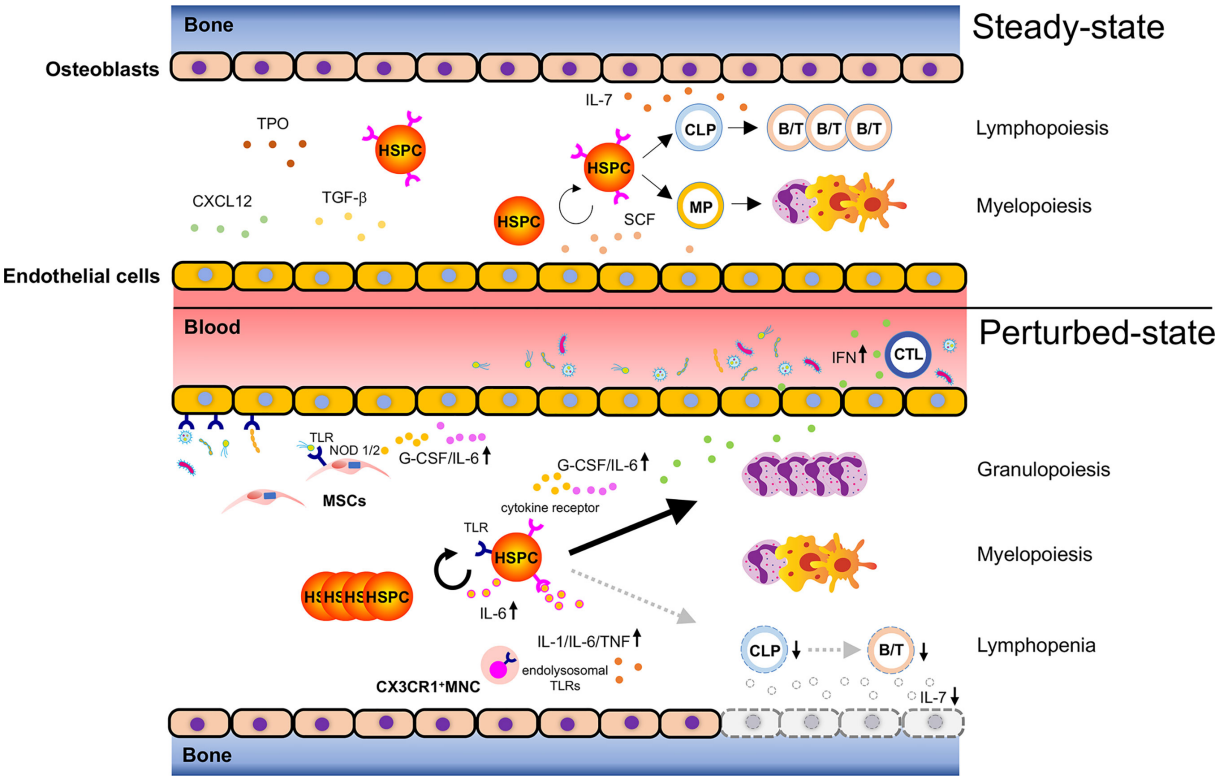

Figure 5. Mechanism of emergency hematopoiesis induced by pathogen exposure.

Steady-state hematopoiesis is characterized by the maintenance of lifelong blood cell production through the tightly regulated processes of self-renewal and differentiation of hematopoietic stem and progenitor cells (HSPCs). This homeostatic mechanism ensures the continuous replenishment of lymphoid and myeloid progenitors, sustaining the hematopoietic trajectory. This tightly regulated and balanced process can be perturbed by infections, entering the bone marrow via systemic blood circulation. Through various pattern recognition receptors (like toll-like receptors-TLR) HSPCs are activated, which induces proliferation and differentiation biases towards myeloid lineages. Pro-inflammatory cytokines (G-CSF/IL-6/IL-1/TNF) further stimulate granulopoiesis and myelopoiesis, prioritizing the generation of innate immune cells crucial for pathogen clearance (taken from Sezaki et al., 2020).

1.6. Aging

Since the beginning of the 19th century, human life expectancy has doubled, rising from less than 30 years to over 72 years (Finch, 2009). This increase presents the unique challenges for HSCs to maintain their fitness during their significantly extended lifespan while exposure of various stressors accumulates over time (Mansell et al., 2023). In general, aging is associate with profound molecular and functional changes in both mature and immature hematopoietic cells, leading to a decline in the adaptive and immature immune response and HSC function (Kovtonyuk et al., 2016). These age-related alterations increase the susceptibility to infections and development of autoimmunity and hematologic malignancies (Dorshkind et al., 2009). Aged HSCs exhibit expanded pool sizes but diminished self-renewal capacity, accompanied by a bias toward myeloid differentiation (Chambers et al., 2007; Dykstra et al., 2011; Harrison & Astle, 1982; Morrison et al., 1996; Rossi et al., 2005; Sudo et al., 2000). In murine models, phenotypic HSCs upregulate the myeloid marker CD150, resulting in an increased prevalence of myeloid-biased HSCs (**Figure 6**). Transplantation studies further confirm that aged HSCs preferentially reconstitute myeloid lineages over serial transplantations (Beerman et al., 2010; Challen et al., 2010; Rossi et al., 2005). Similar tendencies

were reported for the human hematopoietic system with aged immunophenotypic HSCs (Lin-CD34+CD38-CD90+CD45RA-) showing increased cell frequency, decreased quiescent and detectable myeloid differentiation bias (Pang et al., 2011). The increased myelopoiesis aligns with the hematopoietic alterations during inflammations discussed previously.

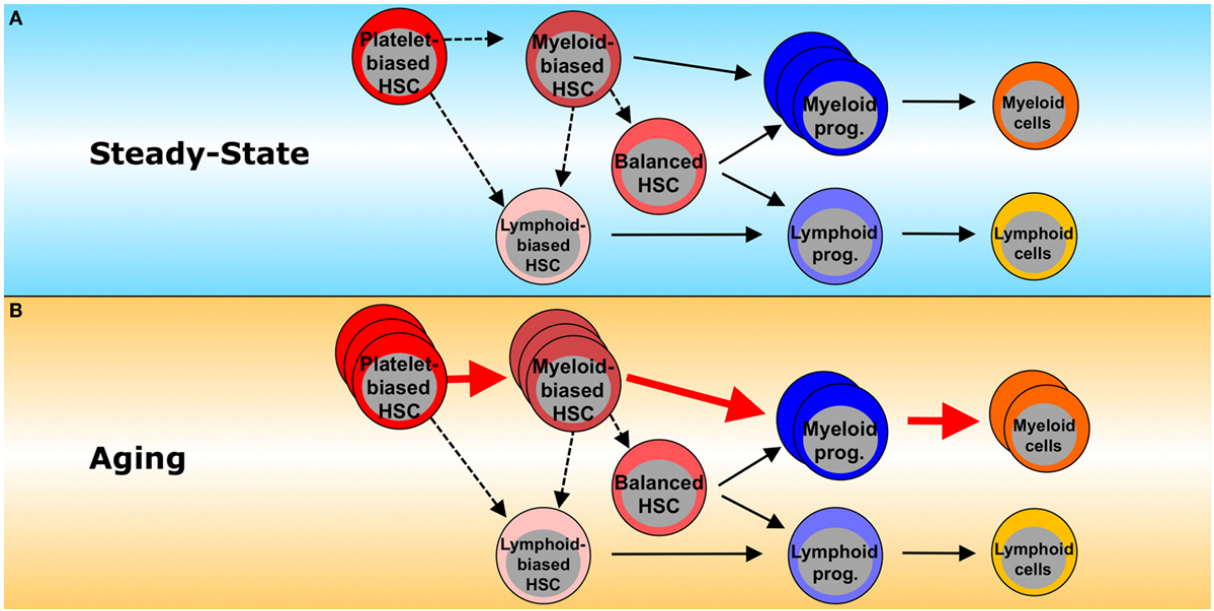

Figure 6. Age-related changes in lineage output.

A) Steady-state hematopoiesis: Diverse HSC subsets, including platelet-biased, lymphoid-biased, myeloid-biased and balanced HSCs, contribute equally to maintain equilibrium between myeloid and lymphoid lineages. **B**) Aged hematopoiesis: Aging induces an increased frequency of myeloid-biased HSCs, including platelet-biased HSCs. This shift results in enhanced production of myeloid progenitors and mature myeloid cells, leading to the characteristic myeloid bias observed in elderly individuals (taken from Kovtonyuk et al., 2016; Oakley C. Olson, Kang and Passegué, 2020).

Besides lineage bias and increased HSC frequency, intrinsic aging mechanism impact HSC functionality. The accumulation of DNA damages, oxidative stress, telomer shortening as well as epigenetic and transcriptomic alterations highlight the complex interplay between cellular damage and transcriptional reprogramming driving hematopoietic dysfunction over time (Collado et al., 2007; K. Ito & Suda, 2014; Rossi et al., 2007). Especially somatic mutation in genes involved in epigenetic regulations such as *DNMT3A, ASXL1* or *TET2* show driving effects in the age-related clonal hematopoiesis (CH) (Busque et al., 2012; Dorsheimer et al., 2019; Jaiswal & Ebert, 2019; Pardali et al., 2020). These mutations are rare (<1 %) in younger individuals but become increasingly common with age. By the age of 70, >10 % of individuals harbor clones of appreciable size. Clinically, the presence of specific hematopoietic clones is described as clonal hematopoiesis of indeterminate potential (CHIP), characterized by an expanded somatic blood cell clone (>4 %) without other hematological abnormalities (Genovese et al., 2014; Jaiswal et al., 2014; Jaiswal & Ebert, 2019; Steensma et al., 2015). While CHIP has been reported to be associated with increased risk of developing blood malignancies, only 0.5 -1 % of individuals harboring CHIP develop these with various factors as clone size, mutation numbers and the specify of the mutated gene influencing the outcome (Genovese et al., 2014; Jaiswal & Ebert, 2019). Interestingly, recent publication showed a significant

correlation of CHIP in *TET2* and *DNMT3A* with poor prognosis in chronic heart failure patients underlying the complex interplay between the hematopoietic system with other organs (Dorsheimer et al., 2019).
These observations highlight the molecular alterations that affect hematopoietic fitness during aging and emphasize the importance of understanding HSC biology in the context of extended human lifespans.

1.7. Objectives of the Present Study

Over the past six decades, HSCs have been extensively studied and characterized for their pivotal role in hematopoiesis. Significant advancements have been made in the murine model, where the isolation of a relatively homogeneous immature subpopulation using phenotypic markers has enabled detailed functional characterization. However, the human HSC compartment remains less well-defined, with current isolation strategies yielding heterogeneous populations due to a lack of specific prospective markers.

This study aims to identify and isolate highly purified human HSCs from healthy donors across different age cohorts, through an integrated multi-omics approach. By integrating FACS-based enrichment of human HSPC subpopulations (CD34+ and CD34+CD38-) with high-resolution single-cell sequencing technologies, the presented project aims to comprehensively profile both the transcriptome and surface proteome of these cells. This multi-omics approach seeks to **uncover novel surface markers specific to undifferentiated HSC** populations and **elucidate their differentiation trajectories** with unprecedented detail. Leveraging single-cell methodologies, we intend to dissect the heterogeneity within phenotypically similar HSCs and distinguish them from multipotent progenitors and potentially revealing distinct HSC subsets and their molecular signature. Newly identified markers will undergo functional validation through *in vitro* molecular characterization and *in vivo* transplantation assays to assess long-term repopulating potential.
The findings of this study have the potential to refine HSC enrichment strategies, enhance our understanding of human hematopoiesis and contribute to improved therapeutic and clinical applications in the field of stem cell biology and regenerative medicine.

2. Materials and Methods

The methods and materials outlined below are primarily standardized protocols from Prof. Michael Rieger's group (Department of Medicine, Hematology/Oncology, Goethe University Hospital Frankfurt/Main, Germany) and have been adapted from general work instructions. Some methods are described in already published articles and cited accordingly. Graphical illustrations were created using BioRender.com.

2.1. Materials

2.1.1. Chemicals and Reagents

Table 1. Chemicals and reagents used in the presented thesis.

Chemical	Company
Agencourt AMPure XP	Beckman Coulter, Brea, California, USA
Dimethylsulfoxide (DMSO)	AppliChem, Darmstadt, Germany
EDTA solution 0.5 M, pH 8.0	Invitrogen by Thermo Fisher Scientific, Waltham, Messachusetts USA
Ethanol, absolute (≥99.8 %)	Roth, Karlsruhe, Germany
Hank's Balanced Salt Solution (HBSS)	Sigma, St.Louis, Missouri, USA
Isopropanol	Sigma Aldrich, St.Louis, Missouri, USA
PhiX Sequencing Control V3	Illumina, San Diego, California, USA
Picric acid, saturated aqueous solution	Sigma, St.Louis, Missouri, USA
Sodium azide (NaN_3)	Sigma, St.Louis, Missouri, USA
Trypan blue	Sigma, St.Louis, Missouri, USA

2.1.2. Enzymes

Table 2. Enzymes used in the presented thesis.

Enzymes	Company
Deoxyribonuclease (DNase) I solution (1 mg/mL)	Stem cell technologies, Vancouver, Canada
NEBNext® High-Fidelity 2× PCR Master Mix	New England Biolabs GmbH, Frankfurt/Main, Germany
Q5® Hot Start High-Fidelity DNA Polymerase	New England Biolabs GmbH, Frankfurt/Main, Germany

2.1.3. Antibodies

2.1.3.1. Fluorochrome conjugated antibodies used for flow cytometry analysis

Table 3. Fluorochrome conjugated antibodies used in the presented thesis.

Antigen	Clone	Conjugate	Company
CD2	RPA-2.10	Biotin	eBioscience by Thermo Fisher Scientific, Waltham, Massachusetts, USA
CD3	OKT3	Biotin BV510, PerCP-Cy5.5	eBioscience by Thermo Fisher Scientific, Waltham, Massachusetts, USA BD Bioscience, Frankling Lakes, New Jersey, USA
CD4	SK3	FITC	BD Bioscience, Frankling Lakes, New Jersey, USA
CD10	HI10a	PE-Cy7	BD Bioscience, Frankling Lakes, New Jersey, USA
CD14	61D3	Biotin	eBioscience by Thermo Fisher Scientific, Waltham, Massachusetts, USA
CD16	CB16	Biotin	eBioscience by Thermo Fisher Scientific, Waltham, Massachusetts, USA
CD19	HIB19	Biotin, PE, PE-Cy7	eBioscience by Thermo Fisher Scientific, Waltham, Massachusetts, USA; BD Bioscience, Frankling Lakes, New Jersey, USA
CD25		PE	BD Bioscience, Frankling Lakes, New Jersey, USA
CD33	P67.6	APC	BD Bioscience, Frankling Lakes, New Jersey, USA
CD34	8G12	APC, FITC	BD Bioscience, Frankling Lakes, New Jersey, USA
CD38	HB7	APC-H7, PE	BD Bioscience, Frankling Lakes, New Jersey, USA; eBioscience by Thermo Fisher Scientific, Waltham, Massachusetts, USA
CD49f	GoH3	PE-Cy5	eBioscience by Thermo Fisher Scientific, Waltham, Massachusetts, USA
CD45	2D1, HI30	FITC, V450-c, BV711	BD Bioscience, Frankling Lakes, New Jersey, USA
CD45RA	HI100	BV570	BioLegend, San Diego, California, USA
CD45.1	A20	PerCP-Cy5.5, PE	eBioscience by Thermo Fisher Scientific, Waltham, Massachusetts, USA /BioLegend
CD56	CMSSB (NCAM)	Biotin	eBioscience by Thermo Fisher Scientific, Waltham, Massachusetts, USA
CD69	FN50	R718	BD Bioscience, Frankling Lakes, New Jersey, USA
CD71	OKT9	FITC	eBioscience by Thermo Fisher Scientific, Waltham, Massachusetts, USA
CD90/Thy1	5E10	PerCP-Cy5.5	BD Bioscience, Frankling Lakes, New Jersey, USA
CD110/BAH1	BAH-1	PE	BD Bioscience, Frankling Lakes, New Jersey, USA
CD123	9F5	BV421	BD Bioscience, Frankling Lakes, New Jersey, USA

CD133	AC133	APC	Miltenyi Biotec B.V. & Co. KG, Bergisch Gladbach, Germany
CD197 (CCR7)	2-L1-A	RB780	BD Bioscience, Frankling Lakes, New Jersey, USA
CD235a	HIR2	Biotin	eBioscience by Thermo Fisher Scientific, Waltham, Massachusetts, USA
CD273 (PD-L2)	MIH18	BV711, BV650	BD Bioscience, Frankling Lakes, New Jersey, USA
CD274 (PDL1)	MIH1	PE-Cy7	BD Bioscience, Frankling Lakes, New Jersey, USA
CD278 (ICOS)	DX29	BV650	BD Bioscience, Frankling Lakes, New Jersey, USA
CD279 (PD1)	EH12.1	BV786	BD Bioscience, Frankling Lakes, New Jersey, USA
FoxP3	236A/E7	R718	BD Bioscience, Frankling Lakes, New Jersey, USA
KI67		FITC	BD Bioscience, Frankling Lakes, New Jersey, USA
TER119	TER-119	APC-eFlour®780	eBioscience by Thermo Fisher Scientific, Waltham, Massachusetts, USA
Streptavidin		PE-Dazzle 594	BioLegend, San Diego, California, USA
Fixable viability dye		eFluor®780, eFluor®506	eBioscience by Thermo Fisher Scientific, Waltham, Massachusetts, USA

2.1.3.2. Unconjugated Primary antibodies used for protein analysis and neutralization

Table 4. Unconjugated primary antibodies used in the presented thesis.

Antibody	Company
Monoclonal PD-L2	Cell Signaling Technology, Danvers, Massachusetts, USA
Polyclonal HLF	Thermo Fischer Scientific, Waltham, MA, USA
Monoclonal ATP1B1	Cell Signaling Technology, Danvers, Massachusetts, USA
Monoclonal α Tubulin	Cell Signaling Technology, Danvers, Massachusetts, USA
Human PD-L2/B7-DC Antibody	R&D Systems, Minneapolis, USA
Normal Goat IgG Control	R&D Systems, Minneapolis, USA

2.1.4. Cytokines and small molecules used for human cell culture

Table 5. Cytokines and small molecules used in the presented thesis.

Cytokines	Company
Recombinant human SCF	Peprotech by Thermo Fisher Scientific, Waltham, Massachusetts, USA
Recombinant human TPO	Peprotech by Thermo Fisher Scientific, Waltham, Massachusetts, USA

Recombinant human FLT-3	Peprotech by Thermo Fisher Scientific, Waltham, Massachusetts, USA
Recombinant human IL-3	Peprotech by Thermo Fisher Scientific, Waltham, Massachusetts, USA
Recombinant human IL-2	Peprotech by Thermo Fisher Scientific, Waltham, Massachusetts, USA
TNF-α	Peprotech by Thermo Fisher Scientific, Waltham, Massachusetts, USA
UM171	STEMCELL Technologies, Vancouver, Canada
Human LDL	STEMCELL Technologies, Vancouver, Canada

2.1.5. Cell culture medium

Table 6. Medias used in the presented thesis.

Medium	Components
MLR assay media	SFEM II, 100 ng/ml human SCF, 100 ng/ml human TPO, 100 ng/ml human FLT-3, 100 ng/ml human IL-3, 50 UE human IL-2, 38 nM UM171, 50ng/ml human LDL and 1 % Pen Strep
HSPCs media	SFEM II, 100 ng/ml human SCF, 100 ng/ml human TPO, 100 ng/ml human FLT-3, 100 ng/ml human IL-3, 38 nM UM171, 50ng/ml human LDL and 1 % Pen Strep
TNF α media	SFEM II, 100 ng/ml human SCF, 100 ng/ml human TPO, 100 ng/ml human FLT-3, 100 ng/ml human IL-3, 38 nM UM171, 50ng/ml human LDL, 1 µg/ml human TNF α and 1 % Pen Strep
BSA control media	SFEM II, 100 ng/ml human SCF, 100 ng/ml human TPO, 100 ng/ml human FLT-3, 100 ng/ml human IL-3, 38 nM UM171, 50ng/ml human LDL, 0.001 % BSA and 1 % Pen Strep
Freezing medium I	50 % StemSpan SFEM II, 50 % FCS
Freezing medium II	50 % StemSpan SFEM II, 30 % FCS, 20 % DMSO
Thawing medium	DMEM, 2 % FCS

2.1.6. Kits

Table 7. Kits used in the presented thesis.

Kit	Company
Anti-Rabbit Detection Module for Jess, Wes, Peggy Sue or Sally Sue	Protein Simple, San Jose, USA
BD Pharmingen™ FITC Mouse Anti-Ki-67 Set	BD Bioscience, Franklin Lakes, New Jersey, USA
BD Pharmingen™ Transcription Factor Buffer Set	BD Bioscience, Franklin Lakes, New Jersey, USA
BD Rhapsody™ Cartridge Kit	BD Bioscience, Franklin Lakes, New Jersey, USA
BD Rhapsody™ Cartridge Reagent Kit	BD Bioscience, Franklin Lakes, New Jersey, USA

BD Rhapsody™ cDNA kit	BD Bioscience, Franklin Lakes, New Jersey, USA
BD Rhapsody™ WTA Amplification Kit	BD Bioscience, Franklin Lakes, New Jersey, USA
BD™ single-Cell Multiplexing Kit Human Immune Sample Tag	BD Bioscience, Franklin Lakes, New Jersey, USA
CD34 MicroBead Kit UltraPure, human	Miltenyi Biotec, Bergisch Gladbach, Germany
High Sensitivity DNA ScreenTape Analysis	Agilent Technologies, Santa Clara, California, USA
High Sensitivity RNA ScreenTape Analysis	Agilent Technologies, Santa Clara, California, USA
LEGENDplex™ Human CD8/NK Panel (13-plex) w/ VbP V02	BioLegend, San Diego, California, USA
LEGENDplex™ Human HSC Myeloid Panel (7-plex) with V-bottom Plate	BioLegend, San Diego, California, USA
NextSeq 2000 P3 Reagents (200 Cycles)	Illumina, San Diego, California, USA
NextSeq 500/550 Mid Output	Illumina, San Diego, California, USA
miRNeasy Micro Kit	Qiagen, Venlo, Netherlands
Qubit dsDNA HS Assay Kit	Thermo Fisher Scientific, Waltham, Massachusetts, USA
Qubit RNA HS Assay Kit	Thermo Fisher Scientific, Waltham, Massachusetts, USA
SMART®-Seq HT Kit	Talara, San Jose, USA
T-cell Activation/Expansion Kit, human	Miltenyi Biotec, Bergisch Gladbach, Germany

2.1.7. Consumables

Table 8. Instruments used in the presented thesis.

Instrument	Company
2100 Bioanalyzer	Agilent Technologies, Santa Clara, California, USA
BD FACSAriaIII cell sorter	BD Bioscience, Franklin Lakes, New Jersey, USA
BD FACSCelesta	BD Bioscience, Franklin Lakes, New Jersey, USA
BD LSRFortessaII	BD Bioscience, Franklin Lakes, New Jersey, USA
CellObserver 430 optical microscope	Carl Zeiss AG, Oberkochen, Germany
Centrifuge Rotanta 460R	Hettich, Tuttlingen, Germany
Centrifuge, Heraeus Megafuge 1.0R	Thermo Fisher Scientific, Waltham, Massachusetts, USA
Centrifuge, tabletop (Rotanta 200, 220R)	Hettich, Tuttlingen, Germany
Clean bench, HERAsafe KSP	Thermo Fisher Scientific, Waltham, Massachusetts, USA
CO_2 Incubator, HERAcell 150i	Thermo Fisher Scientific, Waltham, Massachusetts, USA

DNA electrophoresis chamber	BioRad, Hercules, California, USA
Freezer - 20° C and refrigerators	Liebherr, Bulle, Switzerland
Freezer - 80° C, Heraeus	Thermo Fisher Scientific, Waltham, Massachusetts, USA
Incubator, Heraeus	Thermo Fisher Scientific, Waltham, Massachusetts, USA
Leica CM3050 S Kryostat	Leica Mikrosysteme Vertrieb GmbH, Wetzlar, Germany
MiSeq	Illumina, San Diego, Carlifornia, USA
Nano-Drop 1000 spectrometer	Thermo Fischer Scientific, Waltham, MA, USA
NextSeq 500	Illumina, San Diego, Carlifornia, USA
Qubit 3 Fluorometer	Invitrogen by Thermo Fischer Scientific, Waltham, MA, USA
Qubit 4 Fluorometer	Invitrogen by Thermo Fischer Scientific, Waltham, MA, USA
T100 Thermal cycler	BioRad, Hercules, Berkeley, CA, USA
Thermomixer	Biometra, Analytik Jena, Jena, Germany
Ultracentrifuge Optima L-90K	Beckman Coulter, Pasadena, CA, USA
UV-Transilluminator GelDoc 2000	BioRad, Hercules, Berkeley, CA USA
Vacuum pump	Integra Biosciences, Fernwald, Germany
Vortex Minishaker	Roth, Karlsruhe, Germany

2.1.8. Laboratory equipment

Table 9. Laboratory equipment used in the presented thesis.

Laboratory equipment	Company
Aspiration pipettes (2 mL)	BD Bioscience, Franklin Lakes, New Jersey, USA
Cell culture flasks (25, 75 and 175 cm2)	BD Bioscience, Franklin Lakes, New Jersey, USA
Combitips plus (1, 5 and 10 mL)	Hettich, Tuttlingen, Germany
Conical polystyrene tubes	Hettich, Tuttlingen, Germany
Counting chamber C-Chip, Neubauer improved	Thermo Fisher Scientific, Waltham, Massachusetts, USA
Cryotubes (1 and 2 mL)	Thermo Fisher Scientific, Waltham, Massachusetts, USA
DNA LoBind Tubes	Eppendorf, Hamburg, Germany
Disposable base mold, 15×15 mm	Thermo Fisher Scientific, Waltham, Massachusetts, USA
Falcon sterile centrifuge tubes (5, 15 and 50 mL)	Greiner Bio-One, Frickenhausen, Germany
Freezing box	neoLab, Heidelberg, Germany

Insulin syringe	BD Bioscience, Franklin Lakes, New Jersey, USA
Microvette	Sarstedt, Nümbrecht, Germany
Non-tissue culture plates (6 well)	BD Bioscience, Franklin Lakes, New Jersey, USA
Pasteur pipettes (glas)	Roth, Karlsruhe, Germany
Petri dishes, Greiner	Greiner Bio-One, Frickenhausen, Germany
Pipette tips (10, 100, 200 and 1000 µL)	Gilson, Limburg-Offheim, Germany
Polypropylene tube, sterile, round bottom, with cap, 5 mL	Greiner Bio-One, Frickenhausen, Germany
Protection gloves (Latex, Nitril)	Meditrade, Kiefersfelden, Germany
Reaction tubes (0.1, 0.2, 1.5 and 2 mL)	Eppendorf, Hamburg, Germany
Scalpels	mediware Servoprax, Wesel, Germany
Silicon stem cell inserts	IBIDI, München, Germany
Sterile cell strainer	BD, Franklin Lakes, New Jersey, USA
Sterile filters (0.22 and 0.50 µm)	Merck Millipore, Billerica, Massachusetts, USA
Sterile pipettes (2, 5, 10 and 25 mL)	Costar, Corning, New York, USA
Syringes (5,10 and 20 mL)	Braun, Melsungen, Germany
Thermo Scientific™ SuperFrost Plus™ Adhesion slides	Thermo Fisher Scientific, Waltham, Massachusetts, USA
Tissue culture dishes (3.5 and 10 cm)	Greiner Bio-One, Frickenhausen, Germany
Tissue culture plates (6, 12, 24, 96 well)	Costar by Corning, Corning, New York, USA

2.1.9. Buffers and Solutions

Table 10. Buffer and Solutions used in the presented thesis.

Buffer/Solution	Ingrediens/Source
BD Pharm Lyse, Lysis Buffer	BD Bioscience, Franklin Lakes, New Jersey, USA
Buffer AL Lysis Buffer	QIAGEN, Hilden, Germany
DNA loading buffer (6×)	New England Biolabs, Ipswich, MA, USA
Dimethyl sulfoxide (DMSO)	Invitrogen by Thermo Fischer Scientific, Waltham, MA, USA
Dulbecco's Modified Eagle Medium (DMEM)	Gibco, Life Technologies, Darmstadt, Germany
FACS buffer	PBS, 2 % FCS, 0.05 % NaN3, EDTA 0.5 µM
FACS buffer w/o acide	PBS, 2 % FCS, EDTA 0.5 µM

Fetal calf serum (FCS)	PAA Laboratories, Pasching, Austria
Ficoll-Histopaque 1083	Sigma Aldrich, St.Louis, Missouri, USA
Human Pancoll (density: 1.077 g/mL)	PAN-Biotech, Aidenbach, Germany
MethoCult™ H4034 Optimum	STEMCELL Technologies, Vancouver, Canada
Phosphate Buffered Saline (PBS)	PAA Laboratories, Pasching, Austria
Sodium Acetate 3M, pH 5.2	Merck, Darmstadt, Germany
StemSpan; serum free expansion medium (SFEM II)	STEMCELL Technologies, Vancouver, Canada
TAE buffer (10×)	Roth, Karlsruhe, Germany

2.1.10. BD™ AbSeq Antibody-oligonucleotide conjugates

In order to get surface marker expression pattern during scCITEseq analysis we used oligonucleotide-conjugated antibodies (AbSeqs) from BD Bioscience. These AbSeq panels are customized. Panel 1 was used for the primary scCITEseq analysis using BM samples from different age groups (**Table 11**). Panel 2 was used to analyze specific HSC and T-cell expression pattern after mixed lymphocyte reaction (MLR) assay (**Table 12**).

Table 11. BD™ AbSeqs panel for adult BM analysis.

AbSeq	Clone	Catalogue no.
B7-H4	MIH43	940100
CD1a	HI149	940063
CD1c	F10/21A3	940024
CD3	SK7	940000
CD7	MT701	940029
CD9	M-L13	940078
CD10	HI10a	940045
CD11b	M1/70	940008
CD11c	B-ly6	940024
CD13	WM15	940044
CD14	MFp9	940005
CD15	W6D3	940274
CD19	SJ25C1	940004

CD22	HIB22	940273
CD25 (IL2RA)	2A3	940009
CD26 (DPP4)	M-A261	940101
CD32	FLI8.26	940069
CD33	WM53	940031
CD34	581	940021
CD38	HIT2	940013
CD45	HI30	940002
CD45RA	HI100	940011
CD45RO	UCHL1	940022
CD47	B6H12	940082
CD56	NCAM16.2	940007
CD62L	DREG-56	940041
CD81	JS-81	940052
CD90	5E10	940032
CD93	R139	940215
CD96	6F9	940272
CD117 (cKIT)	YB5.B8	940051
CD123 (IL3RA)	763	940020
CD124 (IL4R)	hIL4R-M57	940092
CD126 (IL6R)	M5	940090
CD133	W6B3C1	940095
CD137	4B4-1	940055
CD155 (PVR)	TX24	940055
CD184 (CXCR4)	12G5	940056
CD235ab	GA-R2 (HIR2)	940040
CD273 (PD-L2)	MIH18	940071
CD274 (PD-L1)	MIH1	940035
CD366 (TIM3)	7D3	940066
CD371 (CLEC12A)	50C1	940212

HLA-ABC	G46-2.6	940062
HLA-DR	G46-6	940010
GPR56	CG4.rMAb	460005

Table 12. Abseq panel for mixed lymphocyte reaction assay.

AbSeq	Clone	Catalogue no.
CD1a	HI149	940063
CD1c	F10/21A3	940083
CD1d	CD1d42	940296
CD2	RPA-2.10	940046
CD3	SK7	940000
CD4	SK3	940001
CD5	UCHT2	940038
CD7	M-T701	940029
CD8	SK1	940305
CD10	HI10a	940045
CD11b	ICRF44	940266
CD11c	B-ly6	940024
CD13	WM15	940044
CD14	MϕP9	940005
CD15	W6D3	940008
CD16	B73.1	940314
CD18	6.7	940086
CD19	SJ25C1	940004
CD21	B-ly4	940048
CD22	HIB22	940273
CD26	M-A261	940101
CD27	L128	940319
CD28	CD28.2	940017
CD32	FLI8.26	940069

CD33	WM53	940031
CD34	581	940021
CD38	HIT2	940013
CD39	TU66	940073
CD40	5c3	940049
CD45	HI30	940002
CD45RA	HI100	940011
CD45RO	UCHL1	940022
CD47	B6H12	940082
CD56	NCAM16.2	940007
CD62L	DREG-56	940041
CD64	MD22	940262
CD69	FN50	940019
CD81(TAPA-1)	JS-81	940052
CD90	5E10	940032
CD94	HP-3D9	940081
CD95(Fas)	DX2	940037
CD102	CBR-IC2/2	940241
CD103	Ber-ACT8	940067
CD117 (c-kit)	YB5.B8	940051
CD122	Mik-β3/IL2RB	940232
CD123 (IL3Ra)	7G3	940020
CD124	HIL4R-M57	940092
CD126 (IL6R)	M5	940090
CD127	HIL-7R-M21	940012
CD133	W6B3C1	940095
CD137	4B4-1	940055
CD155 (PVR)	TX24	940102
CD161	DX12	940070
CD215 (IL-15Rα)	JM7A4	940290

CD226	DX11	940075
CD235a/b	GA-R2 (HIR2)	940040
CD273 (PD-L2)	MIH18	940071
CD274 (B7-H1)	MIH1	940035
CD279	EH12.1	940015
CD366 (Tim3)	7D3	940066
CX3CR1	2A9-1	940216
GPR56	CG4.rMAb	460005
HLA-DR	G46-6	940010
HLA-A,B,C	G46-2.6	940062
IgD	IA6-2	940026
IgG	G18-145	940027
IgM	G20-127	940276
TCRαβ(TCRab)	IP26	940074
TCRγδ(TCRgd)	11F2	940365

2.1.11. Customized BD™ Rhapspody gene panel

The custom gene panel employed in the presented study comprised 596 genes carefully selected for hematopoietic and progenitor cells, leukemia stem cells, clonal hematopoiesis-related genes and for cell surface and cell cycle listed in **Table 13**. All primers were purchased from BD Bioscience.

Table 13. BD Rhapsody gene panel.

Gene	Order no.	ADGRG1	NM_005682.6	ALAS2	NM_000032.4
ABCB1	NM_000927.4	ADGRG6	NM_198569.2	ALCAM	NM_001627.3
ABCG1	NM_004915.3	ADM	NM_001124.2	ANGPT1	NM_001146.4
ABL1	NM_007313.2	AGER	NM_001136.4	ANK1	NM_020476.2
ACO1	NM_001278352.1	AHCYL1	NM_006621.5	ANK3	NM_020987.4
ACTB	NM_001101.3	AHSP	NM_016633.3	ANKRD27	NM_032139.2
ADA2	NM_001282225.1	AIF1L	NM_031426.3	APEX1	NM_001641.3
ADAM19	NM_033274.4	AIM2	NM_004833.1	AQP9	NM_020980.4
ADGRA3	NM_145290.3	AKR1C3	NM_003739.5	ARFGEF1	NM_006421.4
		AKT1	NM_001014431.1	ARFIP2	NM_012402.3

ARHGAP22	NM_021226.3	C2CD2	NM_015500.1	CD4	NM_000616.4
ARL3	NM_004311.3	C2orf69	NM_153689.5	CD47	NM_198793.2
ARMC8	XM_006713564.3	C5orf30	NM_001316968.1	CD48	NM_001778.3
ARPP19	NM_001306195.1	CACNB2	NM_201596.2	CD58	NM_001779.2
ASRGL1	NM_001083926.1	CALN1	NM_001017440.2	CD74	NM_001025159.2
ATP1B1	NM_001677.3	CALR	NM_004343.3	CD8A	NM_001145873.1
ATP8B4	NM_024837.3	CALU	NM_001219.4	CD93	NM_012072.3
ATRX	NM_000489.4	CAT	NM_001752.3	CD96	NM_198196.2
ATXN7L3B	NM_001136262.1	CBL	NM_005188.3	CD99	NM_002414.4
B2M	NM_004048.2	CBLB	NM_170662.4	CDIP1	NM_001199054.1
BAALC	NM_024812.2	CBLC	NM_012116.3	CDK12	NM_016507.3
BAG6	NM_001098534.1	CCNA2	NM_001237.3	CDK2	NM_001798.4
BAMBI	NM_012342.2	CCNB1	NM_031966.3	CDK4	NM_000075.3
BCL11A	XM_017004334.1	CCNB2	NM_004701.3	CDK6	NM_001145306.1
BCL2	NM_000633.2	CCND1	NM_053056.2	CDK7	NM_001799.3
BCL2L1	NM_001322242.1	CCNE1	NM_001238.3	CDKN2A	NM_058195.3
BCL2L2	NM_004050.4	CCNJ	NM_001134375.1	CDKN2C	NM_001262.2
BCL6	NM_001130845.1	CD109	NM_133493.4	CEBPA	NM_004364.4
BCOR	NM_001123383.1	CD14	NM_000591.3	CEBPE	NM_001805.3
BCORL1	NM_021946.4	CD19	NM_001770.5	CENPU	NM_024629.3
BEX1	NM_018476.3	CD2	NM_001767.3	CEP95	NM_138363.2
BEX3	NM_206915.2	CD244	NM_016382.3	CFL1	NM_005507.2
BIRC5	NM_001168.2	CD247	NM_198053.2	CHEK1	NM_001114121.2
BIVM	NM_017693.3	CD274	NM_014143.3	CHEK2	NM_007194.3
BMI1	NM_005180.8	CD276	NM_001024736.1	CHST15	NM_001270764.1
BMS1	NM_014753.3	CD34	NM_001025109.1	CIDECP	NR_002786.1
BRAF	NM_004333.4	CD36	NM_000072.3	CKAP4	NM_006825.3
BTBD11	NM_001018072.1	CD38	NM_001775.3	CKAP5	NM_001008938.3
BTK	NM_000061.2	CD3D	NM_000732.4	CLEC12A	NM_138337.5
C1QTNF6	NM_031910.3	CD3E	NM_000733.3	CLEC2B	NM_005127.2
C20orf96	NM_153269.2	CD3G	NM_000073.2	CLEC2B	NM_005127.2

CLN5	ENST00000636183.1	DLAT	NM_001931.4	FAM169A	NM_015566.2
CNRIP1	NM_015463.2	DLC1	NM_182643.2	FAM171A1	NM_001010924.1
COG3	NM_031431.3	DLK1	NM_003836.6	FAM212A	NM_203370.1
COL24A1	NM_152890.5	DNAJB9	NM_012328.2	FAM30A	NR_026800.2
COL5A1	NM_000093.4	DNAJC6	NM_001256864.1	FAM3C	NM_014888.2
CPXM1	NM_019609.4	DNMT3A	ENST00000402667.1	FAM69B	NM_152421.3
CRHBP	NM_001882.3	DNMT3B	NM_006892.3	FANCI	NM_001113378.1
CRIM1	NM_016441.2	DPP4	NM_001935.3	FBXO7	NM_012179.3
CSDE1	NM_001007553.2	DPYSL3	NM_001387.2	FBXW7	NM_033632.3
CSF3R	NM_000760.3	DRAM1	NM_018370.2	FCGR2A	NM_021642.3
CSNK2A1	NM_001895.3	DST	NM_015548.4	FCGR3B	NM_000570.4
CTNNB1	NM_001098209.1	DTL	NM_016448.3	FCN1	NM_002003.3
CTNNBL1	NM_030877.4	DUSP6	NM_001946.3	FCRL3	NM_052939.3
CTPS1	NM_001905.3	DUT	NM_001948.3	FCRLA	NM_032738.3
CTSH	NM_004390.4	E2F5	NM_001951.3	FECH	NM_000140.3
CTSL	NM_001912.4	EEF1AKMT3	NM_015433.2	FGD5	NM_152536.3
CUL4A	NM_001008895.2	EFEMP2	NM_016938.4	FGFR1	NM_023110.2
CUX1	NM_181552.3	EIF2AK1	NM_014413.3	FGR	NM_001042729.1
CXCL16	NM_001100812.1	EIF2S1	NM_004094.4	FKBP14	NM_017946.3
CXCR4	NM_001008540.1	EIF2S3	NM_001415.3	FLT3	NM_004119.2
CYBA	NM_000101.3	EIF5	NM_001969.4	FMR1	NM_002024.5
CYBB	NM_000397.3	EIF5B	NM_015904.3	FNBP1	NM_015033.2
CYLD	NM_001042355.1	ELK3	NM_005230.3	FOSL1	NM_005438.4
DACH1	NM_080759.5	ELOA	ENST00000609199.1	FOXO1	NM_002015.3
DAPK1	NM_001288729.1	EMP1	NM_001423.2	FRMD4B	NM_015123.2
DCAF7	NM_005828.4	EPC1	NM_001272004.1	FSCN1	NM_003088.3
DDAH1	NM_012137.3	EPDR1	NM_017549.4	GADD45A	NM_001924.3
DDIT3	NM_001195057.1	EREG	NM_001432.2	GADD45B	NM_015675.3
DDX5	NM_004396.4	ERG	NM_182918.3	GADD45G	NM_006705.3
DDX6	NM_001257191.2	ETV6	NM_001987.4	GAPDH	NM_001289745.1
DGUOKAS1	NR_104029.1	EZH2	NM_004456.4	GATA1	NM_002049.3

GATA2	NM_001145661.1	HIST1H2BI	NM_003525.2	IL10RA	NM_001558.3
GCNT2	NM_145655.3	HLA-A	NM_002116.7	IL18RAP	NM_003853.3
GCSAML	NM_001281853.1	HLA-B	NM_005514.7	IL1RAP	NM_001167928.1
GIMAP4	NM_018326.2	HLA-C	NM_002117.5	IL2RA	NM_000417.2
GINS2	NM_016095.2	HLA-DRB4	NM_021983.4	IL2RB	NM_000878.3
GNAS	NM_001077489.3	HLA-E	NM_005516.5	IL3RA	NM_002183.3
GNB1	NM_001282539.1	HLA-F	NM_001098479.1	INPP4B	NM_001101669.1
GNL1	NM_005275.3	HLF	NM_002126.4	INSIG1	NM_005542.4
GNLY	NM_006433.4	HMGA2	NM_003483.4	IPO5	XM_005254052.3
GPSM1	NM_001145638.2	HMGB1	NM_001313892.1	IQGAP2	NM_006633.3
GPX1	NM_000581.2	HMGN2	NM_005517.3	IQGAP2	NM_006633.3
GUCY1A3	NM_000856.5	HMGXB4	NM_001003681.2	IRGQ	NM_001007561.2
GYPA	NM_002099.7	HMOX1	NM_002133.2	ISG20	NM_002201.5
GZMA	NM_006144.3	HNRNPR	NM_005826.4	ITGA6	NM_000210.3
GZMB	NM_004131.4	HOPX	NM_001145459.1	ITPR3	NM_002224.3
GZMH	NM_033423.4	HOXA5	NM_019102.3	ITSN2	NM_006277.2
H2AFY2	NM_018649.2	HOXA6	NM_024014.3	JAK2	NM_004972.3
HAUS6	NM_017645.4	HOXA9	NM_152739.3	JAK3	NM_000215.3
HBA1	NM_000558.4	HOXB2	NM_002145.3	JAZF1	NM_175061.3
HBA2	NM_000517.4	HOXB3	NM_002146.4	JUN	NM_002228.3
HBB	NM_000518.4	HRAS	NM_001130442.2	KAT6A	NM_006766.4
HBM	NM_001003938.3	HRH1	NM_000861.3	KAT6A	NM_006766.4
HBS1L	NM_006620.3	HRH2	NM_022304.2	KBTBD8	NM_032505.2
HDC	NM_002112.3	HS2ST1	NM_012262.3	KCNK17	NM_031460.3
HES1	NM_005524.3	HSP90AA1	NM_005348.3	KCNQ5	NM_019842.3
HIRA	NM_003325.3	HTR1F	NM_000866.4	KDM2A	NM_012308.2
HIST1H2AC	NM_003512.3	IDE	NM_004969.3	KDM6A	NM_021140.3
HIST1H2BC	NM_003526.2	IDH1	NM_001282386.1	KDR	NM_002253.2
HIST1H2BD	NM_021063.3	IDH2	NM_002168.3	KEAP1	NM_012289.3
HIST1H2BE	NM_003523.2	IDH3A	NM_005530.2	KIFAP3	NM_014970.3
HIST1H2BG	NM_003518.3	IKZF1	NM_006060.5	KIT	NM_000222.2

KLF3-AS1	NR_026804.1	MEIS1	NM_002398.2	NAB1	NM_001321312.1
KLF4	NM_004235.5	METAP2	NM_006838.3	NCAM1	ENST00000615112.4
KLK10	NM_001077500.1	METTL14	NM_020961.3	NCBP1	NM_002486.4
KLRB1	NM_002258.2	MEX3B	NM_032246.4	NCF1	NM_000265.5
KMT2A	NM_005933.3	MICA	NM_001177519.2	NCF2	NM_000433.3
KNTC1	NM_014708.4	MICAL2	NM_014632.3	NCR3LG1	NM_001202439.2
KRAS	NM_033360.3	MICB	NM_005931.4	NDC1	NM_018087.4
KSR1	XM_017025271.1	MINPP1	NM_004897.4	NDC80	NM_006101.2
LANCL2	NM_018697.3	MIPEP	NM_005932.3	NECTIN2	NM_002856.2
LAPTM4B	ENST00000521545.6	MKI67	NM_002417.4	NET1	NM_005863.4
LDHB	NM_001174097.2	MLLT3	NM_004529.3	NF1	NM_000267.3
LHFPL2	NM_005779.2	MME	NM_000902.3	NFE2L2	NM_001145413.3
LILRA5	NM_021250.3	MMRN1	NM_007351.2	NFKBIB	NM_002503.4
LINC01278	NR_015353.1	MPL	NM_005373.2	NHP2	NM_017838.3
LONP2	NM_031490.3	MRE11	NM_005591.3	NIPAL2	NM_001321635.1
LPP	NM_001167671.2	MREG	NM_018000.2	NOTCH1	NM_017617.4
LRPPRC	NM_133259.3	MRPL35	NM_016622.3	NOX1	NM_007052.4
LRRC61	NM_001142928.1	MSH3	NM_002439.4	NOX3	NM_015718.2
LRRC8B	NM_015350.2	MSI2	NM_138962.3	NOX4	NM_016931.4
LRRFIP2	NM_017724.2	MSMO1	NM_006745.4	NOX5	NR_033672.1
LYSMD3	NM_198273.2	MTHFD2	NM_006636.3	NPL	NM_030769.2
M6PR	NM_002355.3	MTMR2	NM_016156.5	NPM1	NM_002520.6
MAFK	NM_002360.3	MTPAP	NM_018109.3	NPR3	NM_000908.3
MALAT1	XR_001748267.1	MTSS1	NM_014751.5	NRAS	NM_002524.4
MAMDC2	NM_153267.4	MXD1	NM_002357.3	NYNRIN	NM_025081.2
MAP3K7	NM_145331.2	MYC	ENST00000613283.2	ODC1	NM_001287189.1
MAPK1IP1L	NM_144578.3	MYCN	NM_005378.5	OGG1	NM_016821.2
MARCH5	NM_017824.4	MYCNOS	ENST00000419083.5	OGT	NM_181672.2
MCTP1	NM_024717.5	MYD88	NM_002468.4	OSER1	NM_016470.7
MCUB	NM_017918.4	MYO5C	NM_018728.3	P2RY1	NM_002563.4
MECOM	NM_001105078.3	NAA38	NM_001320925.1	PAICS	NM_001079524.1

PAM	NM_000919.3	POLE2	NM_002692.3	RBM38	NM_017495.5
PAN3-AS1	NR_029383.1	POLR2G	NM_002696.2	RBM48	NM_032120.3
PAQR6	NM_198406.2	POLR3F	NM_006466.3	RBM7	NM_016090.3
PARP12	NM_022750.3	PPIG	NM_004792.2	RBPMS	NM_001008712.2
PARP6	NM_001323532.1	PPM1D	NM_003620.3	RELA	NM_021975.3
PCAT6	NR_046325.1	PPP1R10	NM_002714.3	RFC3	NM_002915.3
PCLAF	NM_014736.5	PPP1R16B	NM_015568.3	RFX7	XM_011521925.2
PCNX1	NM_014982.2	PRDX1	NM_002574.3	RGCC	NM_014059.2
PCTP	NM_021213.3	PRDX2	NM_005809.5	RHAG	NM_000324.2
PDCD1LG2	NM_025239.3	PRDX3	NM_006793.4	RIMKLB	NM_001297776.1
PDE10A	NM_006661.3	PRDX4	NM_006406.1	RLIM	NM_016120.3
PDGFRA	NM_006206.4	PRKAR2B	NM_002736.2	RMDN1	NM_016033.2
PDLIM1	NM_020992.3	PRKCH	NM_006255.4	RNF10	XM_006719717.2
PDZD8	NM_173791.4	PRKDC	NM_006904.6	RNF125	NM_017831.3
PEX5	NM_001131025.1	PROM1	NM_006017.2	RPL31	NM_000993.4
PHB	NM_001281496.1	PSMD1	NM_002807.3	RRM1	NM_001033.4
PHF1	NM_024165.2	PTCD2	NM_024754.4	RSL1D1	NM_015659.2
PHF6	NM_001015877.1	PTEN	NM_000314.6	RUNX1	NM_001754.4
PIAS2	NM_004671.4	PTK2	NM_153831.3	RUNX2	NM_001024630.3
PIK3CD	NM_005026.3	PTPN11	NM_002834.3	RYR3	NM_001036.4
PIM1	NM_002648.3	PTPRC	NM_002838.4	SAMHD1	NM_015474.3
PLBD1	NM_024829.5	PVR	NM_006505.4	SART3	NM_014706.3
PLCH1	NM_014996.2	RAB5C	NM_004583.3	SCD	NM_005063.4
PLIN2	NM_001122.3	RABGAP1	NM_012197.3	SEL1L3	NM_015187.4
PLK4	NM_014264.4	RAC1	NM_006908.4	SERTAD2	NM_014755.2
PLSCR4	NM_001128304.1	RAC2	NM_002872.4	SETBP1	NM_015559.2
PMP22	NM_000304.3	RACGAP1	NM_001126103.2	SETDB1	NM_012432.3
PNISR	NM_015491.2	RAD21	NM_006265.2	SF3B1	NM_012433.3
PNP	NM_000270.3	RAF1	NM_002880.3	SFXN3	ENST00000393459.5
PNPLA4	NM_001142389.1	RARA	NM_000964.3	SGK1	NM_005627.3
POLA1	NM_016937.3	RB1	NM_000321.2	SHANK3	NM_033517.1

SKIDA1	NM_207371.3	STEAP3	NM_001008410.1	TRIP13	NM_004237.3
SKIV2L2	NM_015360.4	STMN1	NM_005563.3	TRIT1	NM_017646.5
SLC15A3	NM_016582.2	SUPT16H	NM_007192.3	TRMT5	NM_020810.3
SLC17A9	NM_022082.3	SYF2	NM_015484.4	TSPYL2	NM_022117.3
SLC25A36	NM_018155.2	TAL1	NM_001287347.2	TUBB	NM_178014.3
SLC25A37	NM_016612.3	TAPT1	NM_153365.2	TXN	NM_003329.3
SLC25A5	NM_001152.4	TCEAL9	NM_001006613.1	TXN2	NM_012473.3
SLC27A2	NM_003645.3	TCF12	NM_207036.1	TXNRD1	NM_182729.2
SLC4A1	NM_000342.3	TET2	NM_001127208.2	U2AF1	NM_006758.2
SLC9A7	NM_032591.2	TFAM	NM_003201.2	UBR2	NM_015255.2
SLF1	NM_032290.3	TFE3	NM_006521.5	UBR5	NM_015902.5
SMARCA1	NM_003069.4	TFPI	NM_006287.4	UBXN1	NM_001286077.1
SMARCD3	NM_001003801.1	TFRC	NM_001128148.2	ULBP1	NM_025218.3
SMC1A	NM_006306.3	TGIF2	NM_001199514.1	ULBP2	NM_025217.3
SMC3	NM_005445.3	TGM2	NM_004613.3	ULBP3	NM_024518.2
SMIM24	NM_001136503.1	THY1	NM_001311160.1	UMPS	NM_000373.3
SNHG20	NR_027058.1	TIPIN	NM_017858.2	USP32P2	NR_003554.1
SOCS2	NM_001270467.1	TLR4	NM_138554.4	VGLL4	NM_001128219.2
SOD1	NM_000454.4	TM9SF3	NM_020123.3	VWF	NM_000552.4
SOD2	NM_000636.3	TMEM107	NM_032354.3	WASF1	NM_001024934.1
SORD	NM_003104.5	TMEM200A	NM_001258276.1	WDR91	NM_014149.3
SPINK2	NM_021114.3	TMEM38B	NM_018112.2	WRN	NM_000553.4
SPNS2	NM_001124758.1	TMEM97	NM_014573.2	WT1	ENST00000640146.1
SPTA1	NM_003126.2	TMOD3	NM_014547.4	XBP1	NM_005080.3
SPTBN1	NM_003128.2	TNFRSF4	NM_003327.3	XK	NM_021083.2
SRSF2	NM_001195427.1	TNIK	NM_015028.3	YES1	NM_005433.3
SSPO	NM_198455.2	TP53	NM_000546.5	ZBTB39	NM_014830.2
SSX2IP	NM_001166293.1	TPM1	NM_001018006.1	ZBTB4	NM_001128833.1
ST3GAL6	NM_001271146.1	TPR	NM_003292.2	ZBTB46	XM_005260196.3
STAG2	NM_001042751.1	TPT1	NM_003295.3	ZDHHC21	NM_178566.4
STAM	NM_003473.3	TRAF3IP2	NM_147686.3	ZEB1	NM_030751.5

ZFP30	NM_001320666.1
ZNF165	NM_003447.3
ZNF219	NM_001101672.1
ZNF225	NM_013362.3
ZNF304	NM_020657.3
ZNF500	NM_021646.3
ZRSR2	NM_005089.3
ZSWIM8	NM_001242487.1
ZWINT	NM_007057.3

2.1.12. Software and Algorisms

Table 14. Software and algorism used in the presented thesis.

Software	Developer
BD FACSDiva™ (v 8.0)	BD Bioscience, Frankling Lakes, New Jersey, USA
Compass for SW™ (v. 5.0 and earlier)	Protein Simple, San Jose, USA
ChatGPT (v. 4 and earlier)	OpenAI, San Francisco, California, USA
FlowJo™ (v. 10.10 and earlier)	BD Bioscience, Frankling Lakes, New Jersey, USA
GitHub	Microsoft, San Francisco, California, USA
GraphPad Prism (v. 10 and earlier)	GraphPad Software, Inc. , San Diego, California, USA
Microsoft Office 365	Microsoft Corporation, Redmon, Washington, USA
Mendeley Cite	Elsevier, Amsterdam, Netherlands
Perplexity AI	Perplexity AI , San Francisco, California, USA
R programming language (v. 4.5.0. and earlier)	R Core Team
R Studio (v. 2024.12.1 and earlier)	Posit, Cambridge, Massachusetts, USA
Seven Bridges Genomics platform (v. 2 and earlier)	BD Bioscience, Frankling Lakes, New Jersey, USA
Agilent Tapestation System (v. 5.1 and earlier)	Agilent Technologies, Santa Clara, California, USA

2.2. Methods

2.2.1. Cell culture methods

2.2.1.1. Human sample collection

Biological specimens were collected in accordance with the Declaration of Helsinki and approved by the Ethical Review Board of the Medical Faculty of the University Hospital Frankfurt (Frankfurt, Germany, ethical permit #329/10), the Ethical Review Board of the Sahlgrenska University Hospital (Gothenburg, Sweden, ethical permit #011-17) and the Ethical Review Board of the Clínica Universidad de Navarra (Pamplona, Spain, ethical permit #2019.143). BM samples from middle age and old donors were collected from the femur of osteoarthritic patients undergoing hip replacement surgery at the Sahlgrenska University Hospital (Mölndal, Sweden). Young age BM aspirates were obtained from Clínica Universidad de Navarra (Pamplona, Spain). The primary scCITEseq analysis included 15 BM samples in this study, five of young age (20-23 years old), six of middle age (52-65 years old) and four of old age (70-84 years old). In total, there were eight male and seven female participants, with equal distribution in age groups. The prospective isolation of $CD273^{high}$ and $CD273^{low}$ HSPCs was performed using G-CSF mobilized peripheral blood samples (mPB) after leukapheresis from several healthy stem cell donors at the DRK-Blutspendedienst Baden-

Württemberg in Frankfurt (Germany). The secondary scCITEseq analysis included three G-CSF leukapheresis products of healthy donors. All subjects gave written informed consent prior to sampling (Komic et al., 2025).

2.2.1.2. Isolation and purification of human hematopoietic subpopulations

All freshly collected primary samples were processed within 24h as presented in **Figure 7**. Mononuclear cells were isolated using Pancoll density gradient centrifugation (Pancoll human, density: 1.077 g/mL, PAN Biotech). The samples were diluted in a 1:1 ratio with PBS, carefully layered onto pre-warmed and pre-aliquoted Pancoll, and centrifuged at 300 x g for 30 minutes without interruption. The interphase containing the mononuclear cells (MNCs) was collected and washed twice with 1x PBS. $CD34^+$ cells were enriched using the CD34 MicroBead Kit (Miltenyi Biotec) following the manufacturer's instructions. For flow cytometric analysis and sorting of marker-defined hematopoietic stem and progenitor cell (HSPC) subpopulations, lineage-positive cells were labeled with a cocktail of biotinylated antibodies targeting lineage-specific markers (CD2, CD3, CD14, CD16, CD19, CD56, CD235a), followed by Streptavidin-PE-Dazzle staining. To identify viable HSPC subsets, mononuclear cells (MNCs) were stained with fluorochrome-conjugated antibodies, including those specific for CD10 (clone HI10a), CD34 (clone 8G12), CD38 (clone HB7), CD45RA (clone HI100), CD90 (clone 5E10), CD123 (clone 9F5) and CD273 (clone MIH18) and Fixable Viability Dye. Antibodies were purchased according to the listed companies in **Table 3**. HSPC populations were analyzed using an LSRFortessa™ Cell Analyzer (BD Bioscience), FACSCelesta™ Cell Analyzer (BD Bioscience).

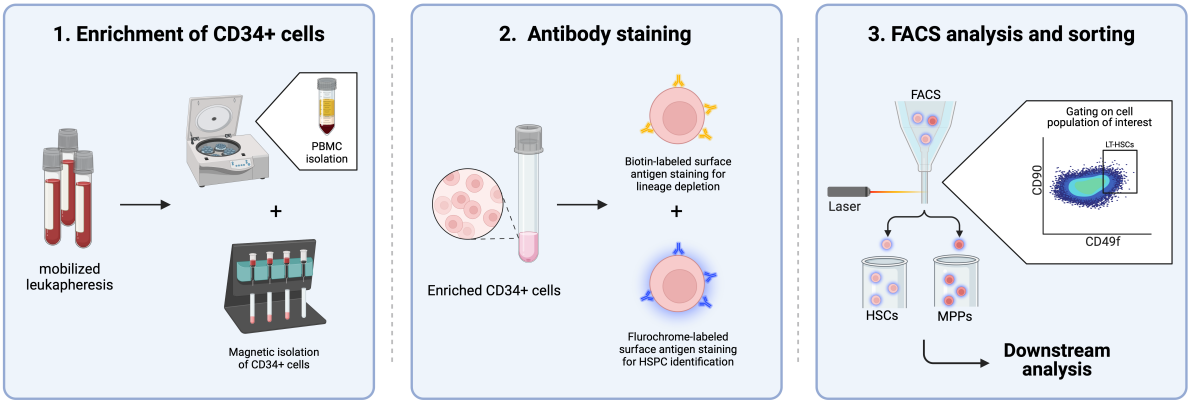

Figure 7. Graphical representation of FACS-based assessment of human HSPCs (Schmachtel et al., 2025).

Different HSPC subpopulations were defined by the marker combination published by Notta *et al*. 2016, as well as our own marker candidate which was used for subsequent analysis and is defined as PD-$L2^{high}$ and PD-$L2^{low}$ (**Table 15**). PD-$L2^{high}$ and PD-$L2^{low}$ cells were sorted using a 70 µm nozzle and the FACSAria™ III Cell Sorter (BD Bioscience). For *in vitro* analysis cells were sorted directly into HSPC medium supplemented as described in **Table 6**. Cells isolated for protein analysis; RNA bulk sequencing or xenograft transplantation

were sorted into PBS and further processed according to required protocol. Sorting purity was verified by a test sort and reanalysis prior to sorting. Purity of the desired populations was >90 %.

Table 15. Characterization of HSPC subpopulations.

Population	Antibody combination
HSC	$Lin^-CD34^+CD38^{-/lo}CD45RA^-CD90^+CD49f^+$
MPP	$Lin^-CD34^+CD38^{-/lo}CD45RA^-CD90^-CD49f^-$
CMP	$Lin^-CD34^+CD38^+CD10^-CD45RA^-CD123^+$
LMP	$Lin^-CD34^+CD38^+CD10^+$
MEP	$Lin^-CD34^+CD38^+CD10^-CD45RA^-CD123^-$
PD-L2^{high}	$Lin^-CD34^+CD38^-CD45RA^-CD273^+$/PD-L2^{hi}
PD-L2^{low}	$Lin^-CD34^+CD38^-CD45RA^-CD273^-$/PD-L2^{lo}

2.2.1.3. Isolation, activation and CellTrace™ staining of human T-cells

MNCs from healthy donors using leukapheresis products were isolated by density gradient as described before. After counting the cell number, CD3+ T-cells were magnetically isolated using the PAN T-cell isolation kit (Miltenyi Biotec) according to manufacturer's protocol. Isolated T-cells were stimulated with CD2, CD3, CD28 antibody coated beads in ratio 1:4 (T-cells/Beads) using the T-cell Activation/Expansion kit (Miltenyi Biotec) according to manufacturer's protocol. T-cells were incubated at 37°C, 5 % CO_2 for 2h. To trace T-cell proliferation, cells were stained with CellTrace™ Violet (Thermo Fisher Scientific) according to manufacturer's protocol. After 20 min of incubation at 37 °C, 5 % CO_2 in the dark, staining solution was diluted with five times the initial staining volume containing at least 1 % of protein to remove any free dye. T-cells were pelleted by centrifugation at 300 x g and rt. Activation and CellTrace™ staining were performed 2,5h prior to co-culture with HSPCs. Different T-cell/bead ratio were tested to get an adequate activation of T-cells without causing T-cell exhaustion (**Figure 8**). For MLR reaction assay, ratio from 1:4 T-cells/beads was used.

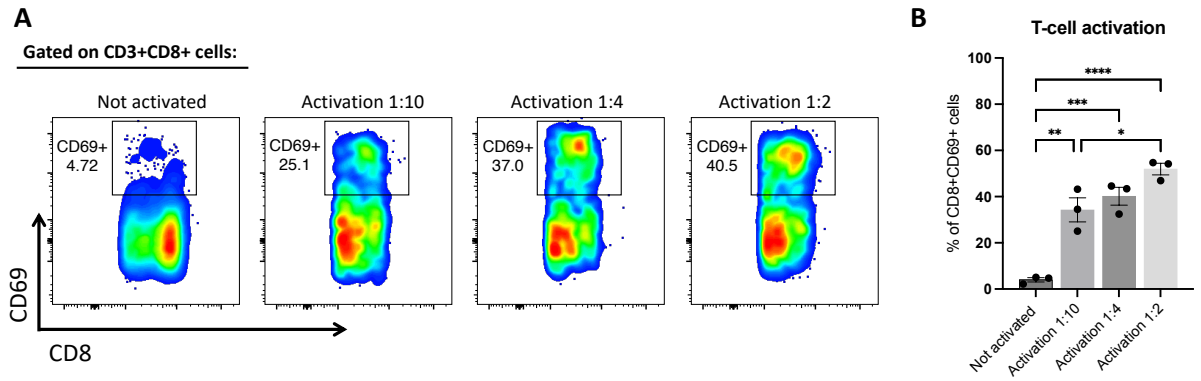

Figure 8. Experimental setting for T-cell activation.

A) Representative flow cytometry plots (pseudocolour density) of CD69 expression on CD8+ T-cells with different bead ratios. **B**) Percentage of T-cell activation measured as displayed in A. *P* values were calculated by one-way ANOVA with Turkeys multiple comparison. No significance = ns, P<0.05 *, P<0.01 **, P<0.001 ***, P<0.0001 ****. Bars represent mean with SEM.

2.2.1.4. Mixed lymphocyte reaction assay

Mixed lymphocyte reaction assays were performed by co-culturing $1x10^4$ CD34+ HSPCs with $1x10^4$ activated T-cells from unrelated donors. While T-cells were activated and stained, CD34 enriched HSPCs were incubated with 20 µg α-PD-L2 neutralization or IgG goat control antibody (both R&D Systems). Co-cultured cells were incubated in 100 µl MLR assay media which is described in **Table 6**. Besides co-cultured cells with α-PD-L2 or IgG antibody, T-cells and CD34+ HSPCs were cultured alone as reference. To compare expression profiles and proliferation of T-cells before and after incubation flow cytometry analysis of CellTrace™ staining, T-cell activation marker profile and intracellular T-cell staining were performed on day 0. Antibody panels were combined as following:

- Surface protein staining panel to assess HSPC differentiation and T-cell activation/proliferation: CellTrace™ Violet, CD3, CD4, CD8, CD25, CD34, CD45RA, CD69, CD133.
- Intracellular staining panel to assess T-cell differentiation: CellTrace™ Violet, CD3, CD4, CD8, CD25, CD34, CD45RA, CD197(CCR7), FoxP3.

Antibodies were purchased according to the listed companies in **Table 3**. Additional expression profiling, cytokine profiling and scCITEseq analysis were performed after 3 days of incubation to assess the immune modulations happening during coculturing. The complete workflow of our newly established mixed lymphocyte reaction assay is illustrated in **Figure 9**.

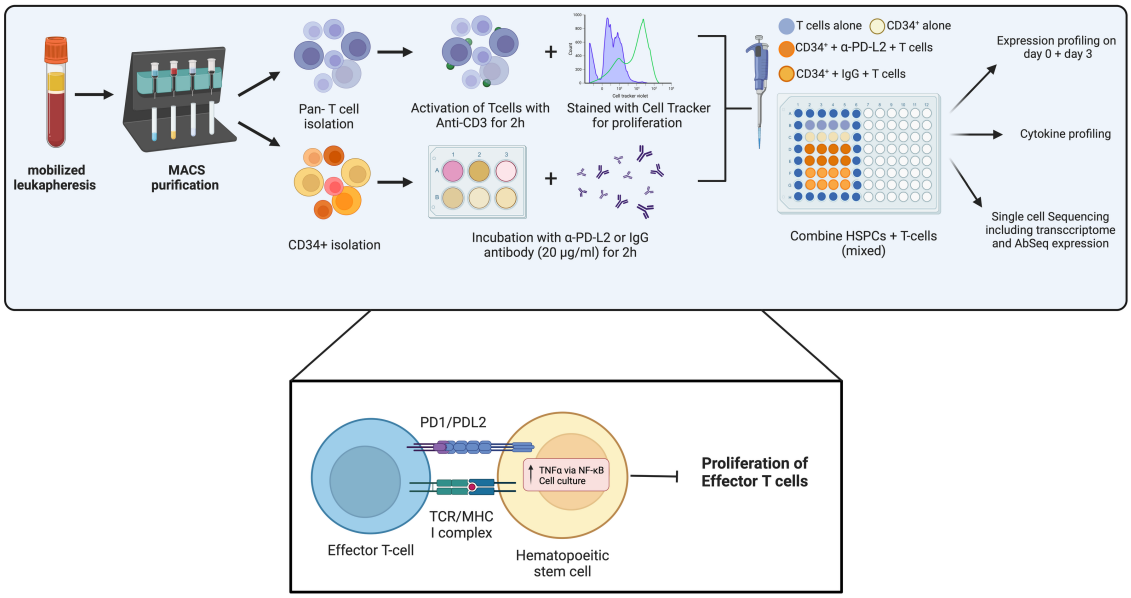

Figure 9. Graphical representation displaying the workflow for MLR assays.

2.2.1.5. T-cell proliferation index

The following method was performed as previously described in Komic et al., 2025.

T-cell proliferation was monitored before and after MLR assay using CellTrace™ Violet (Thermo Fisher Scientific) staining and fluorescence assessment according to the manufacturer's protocol and proliferation index was calculated as previously described (Hernández-Malmierca et al., 2022).

2.2.1.6. *Ex vivo* expansion and differentiation assay

The following method was performed as previously described in Komic et al., 2025.

Ex vivo expansion and differentiation assay was accomplished using FACS-sorted PD-L2^{high} and PD-L2^{low} HSPCs. Cells were counted and 3000 cells were seeded in 200 µl HSPC media as described in **Table 6**. Cells were cultured at 37 °C with 5 % CO_2 for 7 days. Each condition was plated in duplicate. On the day of analysis, cells were harvested, and 10 µl of the cell suspension was used for cell counting. The remaining cells were pelleted by centrifugation (290 × g, 7 minutes, 4 °C) and resuspended in 50 µl of Brilliant Stain Buffer (BD Biosciences). Cells were then stained with fluorochrome-conjugated antibodies against CD201 (EPCR), CD90, CD34, CD45RA, and CD133, along with a Fixable Viability Dye, to assess differentiation status by flow cytometry using a BD FACS FORTESSA (BD Biosciences).

2.2.1.7. Colony forming assay

The following method was performed as previously described in Komic et al., 2025.

Colony forming assays were conducted by seeding 300 freshly sorted PD-L2^{high} and PD-L2^{low} HSPCs in MethoCult™ (H4034, STEMCELL Technologies) and incubated for 14 days at 37 °C with 5 % CO_2 in a cell incubator. Colonies were scored microscopically (CellObserver, Zeiss) for colony formation and lineage distribution.

2.2.1.8. Time-lapse imaging and subsequent single cell tracking

Time-lapse imaging using video-microscopy and subsequent single cell tracking was performed as previously described (Komic et al., 2025; Rieger et al., 2009). Fifty FACS-sorted $CD273^{high}$ and $CD273^{low}$ HSPCs were seeded into 4-well micro-inserts (IBIDI) placed within 24-well NUNC tissue culture plates (Thermo Fisher Scientific). Following a 12-hour initial incubation, the plates were saturated with 5 % CO_2 and gas-tight sealed using adhesive tape. Cultures were then transferred to a Zeiss CellObserver Z1 microscope equipped with a 37 °C environmental chamber. Phase-contrast images were acquired every 2 minutes using a 10× objective and an AxioCam HRm camera (1388 × 1040 pixel resolution), operated via a custom VBA module controlling Zeiss AxioVision 4.8 software. Cells were imaged continuously for 7 days and tracked manually using a custom software tool ("The Tracking Tool TTT") developed by Timm Schroeder, until the fate of all third-generation progeny was established (Rieger et al., 2009). The time of first division was defined as the interval between the start of time-lapse imaging and the first observed cytokinesis. Cell death was identified morphologically by cell shrinkage, loss of refractivity, and immobility. No automated or unsupervised tracking algorithms were used in this analysis .

2.2.1.9. TNF-α culture of *in vitro* culture HSPCs

CD34 enriched HSPCs were counted and 30,000 cells were cultured in 200 µl TNF-α media or BSA control media supplemented as described in **Table 6**. Surface protein expression was profiled every 24h for 7 days using BD FACSCelesta™ Cell Analyzer (BD Bioscience) and the following antibodies: CD34 (clone 8G12), CD38 (clone HB7), CD90 (clone 5E10), CD133 (clone AC133), CD273 (clone MIH18), CD274 (clone MIH1). Live/Dead cell exclusion as determined using a fixable viability dye. Antibodies were purchased according to the listed companies in **Table 3**.

2.2.1.10. JC1 staining

The measurement of mitochondrial membrane potential was performed using JC-1 dye (5,5',6,6'-tetrachloro1,1',3,3'-tetraethylbenzimidazolocarbocyanine iodide; Thermo Fisher Scientific) staining which allows the separation of mito-low (green fluorescence emission ~529 nm) or mito-high (green fluorescence emission ~529 nm and red fluorescence emission shift ~590nm) fractions. CD34 enriched HSPCs were incubated with 2 µM JC-1 at 37 °C, 5 % CO_2 for 30 min. Additional surface markers were stained afterwards as described before.

2.2.2. *In vivo* models

All described *in vivo* experiments were performed according to the German animal welfare legislation and were approved by the relevant authorities based in Regional Council Darmstadt (approval number #FK2024). The following experiment were conducted using NOD.Cg-*Prkdc*^{scid} *Il2rg*^{tm1Wjl}/SzJ (referred to as NSG) (Ishikawa et al., 2002; JM et al., 1988; Shultz et al., 2005; van der Loo et al., 1998). All mice were

bred and maintained under specific pathogen-free conditions at the mouse facility, located at the Georg-Speyer-House in Frankfurt, Germany.

2.2.2.1. Xenotransplantation assay

Transplantation was performed by Tjeerd Petrus Sijmonsma, German Cancer Consortium (DKTK) and German Cancer Research Center (DKFZ), Heidelberg, Germany. FACS sorted lin$^-$CD34$^+$CD273^{high} and lin$^-$CD34$^+$CD273^{low} HSPCs, as well as FACS-sorted lin$^-$CD34$^+$ HSPCs treated with α-PD-L2 neutralization antibody or IgG control (R&D Systems) were counted and 30,000 human HSPCs were tail-vein injected into sub-lethally irradiated (2.4 Gy) 5 – 8 week-old NSG mice. PB analysis was performed every 4 weeks post transplantation as illustrated in **Figure 10**. RBCs were lysed (PharmLysisBuffer, BD Bioscience) and residuals erythrocytes were excluded by anti-murine Ter119 staining (APC-H7). Fixable Viability Dye was used for live/dead staining. Chimerism of xenotransplants was determined by staining leukocytes with mCD45.1 and human CD45, using clone 2D1 (BV421) in combination with clone HI30 (BV711). Multi-lineage reconstitution was distinguished by staining with anti-human antibodies: CD3 (BV510), CD19 (PE-Cy7), CD33 (APC), CD34 (FITC) and CD38 (PE).

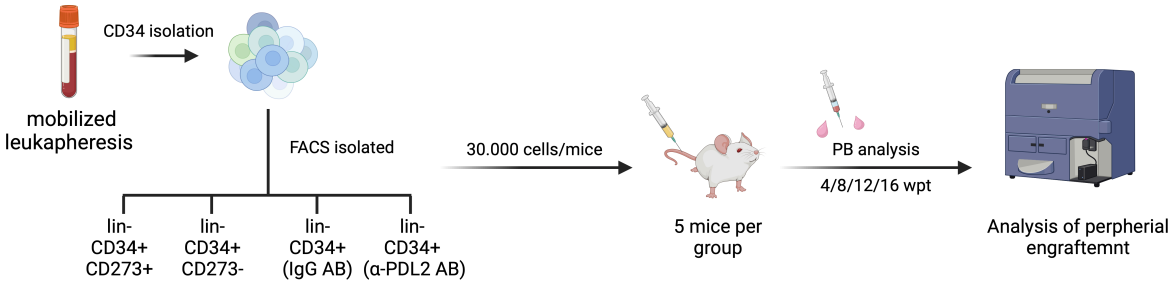

Figure 10. Graphical representation of xenotransplantation assay in primary recipients.

2.2.2.2. Isolation, Purification and Analysis of Human Hematopoietic Cells after Xenotransplantation from bone marrow and spleen

Endpoint analysis of xenotransplantation was performed by isolating the femurs, tibias and spleens from recipient mice. Isolated bones were flushed and MNCs were enriched by density gradient. Spleen were weighted and cells were purified by meshing them through a 100 µm nylon cell strainer (Corning). For analyzing engraftment chimerism and multilineage reconstitution the following three staining panels were used:

- Lineage depletion: CD2, CD3, CD10, CD14, CD16, CD19, CD235a
- Progenitor staining: CD10, CD34, CD38, mCD45.1, hCD45, CD45RA, CD49f, CD90, CD123, Strep
- Lineage staining: CD3, CD19, CD33, CD34, CD38, mCD45.1, hCD45, mTer119

Chimerism was determined as described in the previous paragraph. Different human populations were characterized based on the displayed marker combination from **Table 16** and **Table 17**.

Table 16. Marker combination for multilineage analysis of xenograft endanalysis.

Population	Marker combination
HSC	$Lin^-CD34^+CD38^{-/lo}CD45RA^-CD90^+CD49f^+$
MPP	$Lin^-CD34^+CD38^{-/lo}CD45RA^-CD90^-CD49f^-$
CMP	$Lin^-CD34^+CD38^+CD10^-CD45RA^-CD123^+$
LMP	$Lin^-CD34^+CD38^+CD10^+$
MEP	$Lin^-CD34^+CD38^+CD10^-CD45RA^-CD123^-$
PD-L2^{high}	$Lin^-CD34^+CD38^-CD45RA^-CD273^+$/PD-L2^{hi}
PD-L2^{low}	$Lin^-CD34^+CD38^-CD45RA^-CD273^-$/PD-L2^{lo}

Table 17. Marker combination for progenitor analysis of xenograft endanalysis.

Population	Marker combination
T-cells	hCD45+CD33-CD3+
B-cells	hCD45+CD33-CD19+
Myeloid cells	hCD45+CD33+

2.2.3. Molecular and Biochemical Methods

2.2.3.1. Protein analysis

The following method was performed as previously described in Komic et al., 2025.

A total of 5,000 CD273^{high} and CD273^{low} HSPCs were FACS-sorted directly into 15 µl of ice-cold lysis buffer (M-PER™ Mammalian Protein Extraction Reagent, Thermo Fisher Scientific) supplemented with Pierce™ Protease and Phosphatase Inhibitor Mini Tablets (Thermo Fisher Scientific). For each sample and lane, 3 µl of the resulting lysate was used for protein detection. Cartridge preparation, sample loading, and capillary electrophoresis were carried out according to the manufacturer's instructions using the Jess or Wes Separation Module with 8 × 25 capillary cartridges (ProteinSimple). Primary antibodies were used at a dilution of 1:30. Protein detection was validated using High Dynamic Range (HDR) multi-image acquisition, and data analysis was performed with Compass Software v5.0.0 (ProteinSimple).

2.2.3.2. RNA bulk sequencing

The following method was performed as previously described in Komic et al., 2025.

RNA quality was assessed using High Sensitivity RNA ScreenTape analysis on the 4200 TapeStation System (Agilent). Between 1–5 ng of total RNA served as input for cDNA synthesis and amplification using the SMART®-Seq HT Kit (Takara). Sequencing was carried out on the Illumina NextSeq 500 platform using v2 chemistry in a 1 × 75 bp single-end configuration, in collaboration with Dr. Stefan Günther (Max Planck Institute for Heart and Lung Research, CPI – DNA & RNA Technologies, DZHK – Advanced Molecular Analytics Platform RheinMain, Bad Nauheim, Germany). Raw sequencing reads were evaluated for quality metrics, adapter contamination, and duplication rates using FastQC. Read trimming was performed with Trimmomatic v0.39, removing bases with an average Phred score below Q15 within a 5-nucleotide sliding window. Reads ranging from 15 to 75 nucleotides were retained for downstream analysis. Trimmed reads were aligned to the human reference genome (Ensembl GRCh38/hg38, release 104) using STAR v2.7.10a (Dobin et al., 2013). Gene-level quantification was performed using featureCounts v2.0.4, counting only reads uniquely mapping to exonic regions and excluding reads overlapping multiple genes. Differential gene expression analysis was conducted using DESeq2 v1.36.0, with contrasts generated from a batch-corrected raw count matrix (Love et al., 2014).

2.2.3.3. Cytokine profiling

The following method was performed as previously described in Komic et al., 2025.

Cytokine levels were quantified using the LEGENDplex™ Human CD8/NK Panel (13-plex) with VbP V02 (BioLegend) according to the manufacturer's protocol. Prior to flow cytometry analysis, 80 µL of supernatant were frozen at -80°C and processed in the following days. The samples were undiluted, and 25 µL of supernatant were used for subsequent analysis. All samples were pipetted in technical duplicates, and flow cytometry analysis was conducted using the BD FACSCelesta™ Analyzer system equipped with a high-throughput sampler for 96-well plates.

2.2.3.4. Single cell sequencing

Single cell sequencing was performed using the BD Rhapsody™ platform. For the presented studies in this thesis enriched HSPCs from BM and leukapheresis products were processed as described in paragraph **2.2.1.1**. **Human sample collection**. Afterwards HSPCs were resuspended in BD Stain Buffer (BD Bioscience). To pool different donors per sequencing run samples were stained with the BD® Single-Cell Multiplexing Kits according to manufacturer's protocol. BM samples were stained with CD14, CD34 and CD38 fluorochrome-conjugated antibodies and isolated via FACS. Leukapheresis samples were cultured in MLR assays as described in paragraph **2.2.1.4**. After 3 days of incubation cells were collected from wells and

washed with 1x PBS. A detailed overview for all samples used for scCITEseq analysis is provided in **Table 18** and **Table 19**.

Table 18. Sample overview for scCITESeq analysis of adult BM samples.

Age cohort	Donor name	Gender	Sample age	Sorted Subpopulation	Cell count
Old	#004	M	71	CD34+	4534
				CD34+CD38-	2396
	#018	M	71	CD34+	3276
				CD34+CD38-	2432
	#012	F	76	CD34+	4674
				CD34+CD38-	1509
	#019	F	80	CD34+	1176
				CD34+CD38-	961
Midage	#002	M	52	CD34+	2459
				CD34+CD38-	620
	#014	F	64	CD34+	3406
				CD34+CD38-	1148
	#008	M	62	CD34+	5453
				CD34+CD38-	1197
	#011	F	65	CD34+	2012
				CD34+CD38-	471
	#010	M	58	CD34+	5019
				CD34+CD38-	1282
	#015	F	63	CD34+	3782
				CD34+CD38-	1230
Young	HD2	M	20	CD34+	534
	HD3	M	21	CD34+	1623
	HD4	F	23	CD34+	3681
	HD5	M	20	CD34+	3368
	HD6	F	23	CD34+	4034

Table 19. Sample overview from mPB samples used for scCITE Seq in MLR reaction assay.

Donor name	Gender	Sample age	Donor combination	Cell population/ MLR condition	Cell number
Donor 1	M	21	HSPCs Donor 1 & T-cells Donor 5	CD34+ HSPCs	881
				CD3+ T-cells	1514
				IgG Coculture	3641
				PD-L2 Coculture	3700
Donor 2	F	31	HSPCs Donor 2 & T-cells Donor 4	CD34+	170
				IgG Coculture	1582
				PD-L2 Coculture	1826
Donor 3	M	36	HSPCs Donor 3 & T-cells Donor 1	CD34+	1502
				IgG Coculture	2611
				PD-L2 Coculture	2834
Donor 4	M	33		CD3+	1582
Donor 5	M	23		CD3+	1438

2.2.3.4.1. Single cell capture and cDNA synthesis

The following method was performed as previously described in Bexte et al., 2024 and Komic et al., 2025. For single cell capturing, cells were washed with 3 ml of Stain Buffer (BD Biosciences) and resuspended in 100 µl of Stain Buffer. A master mix containing 2 µl of each BD AbSeq oligonucleotide-conjugated antibody (BD Biosciences) was prepared and added to the cell suspension, followed by incubation for 40 minutes on ice. The AbSeq panels used in this thesis are listed in **Table 11** and **Table 12**. The cells were then washed twice with 3 ml of BD Stain Buffer and resuspended in 620 µl of BD Sample Buffer (BD Biosciences).

To assess cellular concentration and viability, cells were stained with Calcein AM (2 mM, BD Biosciences) and Draq7 (BD Biosciences) and analyzed using a disposable hemocytometer (Incyto) with the BD Rhapsody scanner. 40,000 – 50,000 cells were captured and loaded onto the BD Rhapsody™ microwell cartridge (BD Biosciences) according to the manufacturer's instructions. Oligonucleotide-labeled beads were added to the cartridge, followed by a washing step. Cells were then lysed by adding lysis buffer (5 mM DTT) and incubating for 2 minutes at room temperature. Beads with captured mRNA were retrieved from the BD Rhapsody™ cartridge (BD Biosciences). Reverse transcription and exonuclease I treatment were performed according to the manufacturer's protocol.

2.2.3.4.2. Library preparation and sequencing

The transcriptomic analysis of bone marrow (BM) cells was conducted using a custom gene panel consisting of 596 genes listed in **Table 13**. Single-cell cDNA libraries for this targeted panel were prepared using the BD Rhapsody™ Targeted mRNA kit, following the manufacturer's protocol. Leukapheresis samples cultured for the mixed lymphocyte reaction (MLR) assay were analyzed with the mRNA Whole Transcriptome Analysis (WTA) kit.

For both Rhapsody™ runs, AbSeq and Sample Tag libraries were prepared using the AbSeq Amplification and BD Single-Cell Multiplexing kits, adhering to the protocols provided by BD Biosciences. Quality control and concentration of final libraries were assessed using the Qubit™ dsDNA HS assay kit (Thermo Fisher Scientific) and the Agilent TapeStation 4150 (Agilent).

Sequencing was performed in collaboration with Dr. Stefan Günther at the Max-Planck-Institute for Heart- and Lung Research, CPI - DNA & RNA Technologies, DZHK - Advanced Molecular Analytics Platform RheinMain, Bad Nauheim, Germany. The final libraries, each at a concentration of 1 nM, were sequenced with either 20 % (BM samples) or 3 % (MLR assay) PhiX control DNA to enhance sequence complexity. Sequencing was conducted on an Illumina NextSeq 2000 sequencer with a P3 flow cell, generating 2x75 bp reads.

The described workflow for Single cell capture and cDNA synthesis and Library preparation and sequencing was executed in collaboration with Weijia Yu (Goethe University Hospital Frankfurt, Germany) and Alec Gessner (Goethe University Hospital Frankfurt, Germany), Hana Komic (University of Gothenburg, Sweden) and Catia Simoes (Cancer Center Clínica Universidad de Navarra, Pamplonam, Spain).

2.2.4. Computational analysis

The computational analysis of the BM samples was conducted in collaboration with BD Biosciences and bioinformatics scientists Edyta Kowalczyk and Yujuan Gui. Their work encompassed quality control, cell filtering, normalization, cartridge combination, batch effect correction using the CCA method, and the generation of Seurat objects. While detailed descriptions of these procedures are beyond the scope of this thesis, they are available in the following GitHub repository: https://github.com/TessaSchm/Early-HSC-differentiation and published in Komic et al., 2025.

2.2.4.1. Alignment and transcript quantification

Single-cell FASTQ files were aligned using the BD Rhapsody™ Primary Pipeline (versions 1.10.1 and 2.2) on the Seven Bridges Genomics platform (sevenbridges.com). Post-Illumina sequencing, FASTQ files and reference sequences for mRNAs and AbSeqs were uploaded to the platform and processed with default pipeline settings.

The workflow included read quality filtering, read alignment, and merging of read pairs into raw molecules. Unique Molecular Identifiers (UMIs) were corrected using Recursive Substitution Error Correction (RSEC)

and distribution-based error correction (DBEC). Additional steps involved cell label filtering and the determination of sample origins and multiplets via sample tag reads. Low-quality read pairs were discarded, while high-quality R1 reads were mapped to identify cell labels and UMIs. R2 reads were aligned to the GRCh38 reference, collapsing reads with identical cell labels, UMIs, and reference genes into single molecules. The RSEC algorithm corrected molecule counts for sequencing errors, and sample tags were mapped to cells.

High-quality singlets were defined as cells with >75 % of sample tag reads originating from a single tag, with other tags considered noise. To enhance cell recovery, noise counts were subtracted from each sample tag. Cells with two or more sample tags exceeding the threshold were labeled as multiplets, indicating multiple cells per microwell, while ambiguous cases were marked as undetermined.

The final output consisted of single-cell gene and protein expression matrices, based on reference files containing final library fragment sequences for the whole transcriptome/targeted gene panels and AbSeq panels.

Subsequently, scCITEseq data analysis was carried out in R (version 5.2.0 and earlier) employing the Seurat package (version 5.1.0 and earlier) (Hao et al., 2023).

2.2.4.2. Quality control, batch effect correction, filtering and normalization

Expression matrices from BM samples and targeted transcriptomic profiling were imported into R for analysis. Data were converted into Seurat objects using Seurat's "*CreateSeuratObject*" function (v4.1.1) with default settings. Batch correction for samples processed in different cartridges was conducted using the Canonical Correlation Analysis (CCA) method (**Figure 11**).

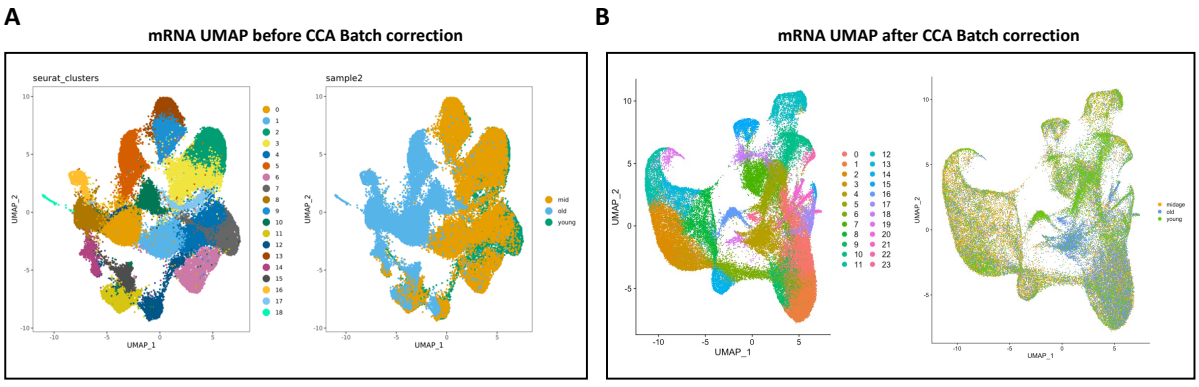

Figure 11. CCA batch effect correction.

A) mRNA UMAP projection before CCA batch correction. **B**) mRNA UMAP projection after CCA Batch correction. Analysis was performed by Edyta Kowalczyk.

The merged dataset was then split into individual samples for downstream analysis. Normalization and scaling were performed using default settings: log normalization for mRNA counts and centered log-ratio (CLR) transformation for AbSeq data. These analyses were performed by Edyta Kowalczyk and Yujuan Gui from BD Bioscience in collaboration of the BD Multiomic Alliance.

The WTA dataset from the MLR reaction assay was exported as a Seurat object from the BD Seven Bridges Genomics platform (v2.2). Quality control involved filtering out cells based on the following criteria:

- nCount_RNA (UMI counts per cell): Excluded if >450 or <3,000, as multiplets tend to have higher UMI counts.
- nFeature_RNA (Gene counts per cell): Included only if >300 to ensure sufficient gene representation.
- percent.mt (Mitochondrial gene percentage): Excluded if >25 % to remove apoptotic or necrotic cells.
- percent.ribo (Ribosomal gene percentage) and percent.globin (Hemoglobin gene percentage).

These metrics were also considered to detect and exclude low-quality cells as displayed in **Figure 12**.

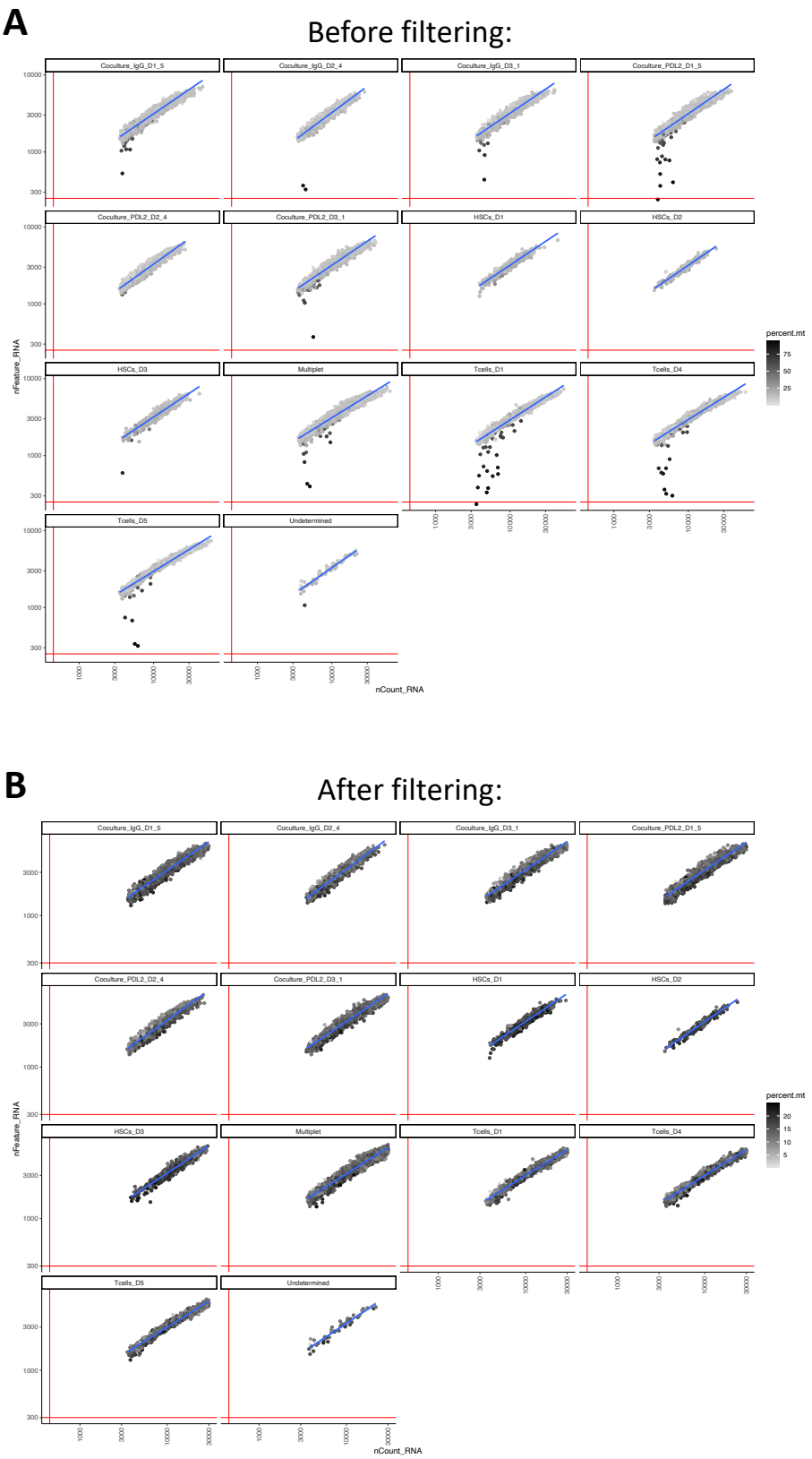

Figure 12. Exclusion of low quality cells.

A-B) Plot display nFeatures_RNA (UMI count) versus nCount_RNA (Gene count) per cell. Low quality cells are characterized by low nFeature_RNA and high nCount_RNA (**A**). Cut-off for filtering are nFeature_RNA <300 and nCount_RNA <400 and >3000.

Subsequent scaling and normalization followed the same approach as the BM samples, using log normalization for mRNA counts and CLR transformation for AbSeq data.

2.2.4.3. Dimensional reduction and clustering

All the mRNA across the analyzed datasets were used as input variables for the identification of integration anchors. Anchor detection was performed using the "*FindIntegrationAnchors"* function implemented in Seurat, leveraging canonical correlation analysis (CCA) for dimensionality reduction. The first 30 CCA dimensions were employed to define the neighborhood search space, with 20 nearest neighbors selected via a k-nearest neighbor (kNN) algorithm. Data integration across samples was executed using the "*IntegrateData"* function, utilizing the same 30 CCA dimensions, which resulted in the identification of 24 transcriptionally distinct cell clusters. The integrated, batch-corrected expression matrix was stored as an independent assay within the merged Seurat object.

For the WTA dataset, no batch effect correction was performed, due to the experimental set-up performed in one run. 15 dimensions from the principal component analysis were used to run UMAP function. Different resolutions were tested using the "*ClusterTree"* function and dataset was analyzed using res0.2 to ensure distinct separation between different cell types without over-clustering.

2.2.4.4. Cell label transfer

Initial cluster annotations were manually assigned based on established marker genes and cell surface proteins from previously published studies and datasets. To validate these annotations, we integrated a publicly available WTA dataset of complete bone marrow cells from Triana *et al*. We processed the reference dataset by performing log-normalization of mRNA counts, scaling features using the "*ScaleData"* function, and applying dimensionality reduction through principal component analysis (RunPCA). To transfer labels, we identified anchors between Seurat objects using the "*FindTransferAnchors"* function with k = 30. We then mapped the "Prediction_HCA" labels from the reference dataset (Version 3, 2023) onto our query dataset using the "*TransferData"* function. The resulting predictions were stored in the metadata under the label "Predicted_Label" without applying a cutoff. This approach combines manual curation with computational validation, ensuring robust cluster identification while preserving subtle biological variations in our dataset. In addition, Seurat function "*Azimuth"* was used to performed cell label prediction for WTA dataset with previous published references for PBMC and BM cell type annotations.

2.2.4.5. Immature cell analysis

To reconstruct cell lineages from the single-cell targeted gene expression data, we focused on a subset of cell populations including HSC/MPP, MPP/MK-Ery, MPP/LMPP, MEP, MDP-1, GMP-1, GMP-Neut, and LyP. We recalculated principal components (PCs) and performed clustering using 17 PCs at a resolution of 0.4, resulting in 9 distinct clusters. This refined embedding served as the foundation for trajectory analysis using

Slingshot (version 2.4.0). We designated cluster 0, representing the most immature HSC-1 population, as the starting point for the trajectory. To identify genes differentially expressed along these trajectories, we employed tradeSeq (version 1.10.0). The "*patternTest*" function was used to visualize and compare expression patterns between lineages. We conducted all pairwise comparisons (6 pairs in total) and assessed the significance of expression pattern differences using an adjusted p-value (FDA) threshold of 0.05.

2.2.4.6. Differentiation expression analysis

For the differential expression analysis and visualization, we employed log-normalized RNA counts and centered log-ratio (CLR) normalized AbSeq counts. We identified cluster-specific gene markers using the "*FindAllMarkers*" function, which applies a Wilcoxon Rank Sum test. For CD34+ HSPCs, we set criteria of a minimum 20 % of cells expressing the marker and a log2 fold change greater than 1. For re-clustered immature HSPCs, we maintained the 20 % expression threshold but lowered the log2 fold change to greater than 0.25. When identifying differentially expressed proteins between HSC1 and HSC2, we required a minimum of 25 % of cells to express the protein, without applying a fold change filter. To visualize these differentially expressed genes and proteins, we used "*FeaturePlot*" to display expression patterns across UMAPs, complemented by dotplots and violin plots generated with ggplot2 (v3.4.0) and RColorBrewer (v1.1.3). For a more robust analysis of immature subsets, we conducted pseudobulk analysis. Using the unnormalized count matrix, we generated pseudobulks per sample for each relevant cluster using the "P*seudobulk"* function from the glmGamPoi package (v1.12.2). We then performed differential gene expression analysis on these pseudobulks using the DESeq2 package (v1.40.2) with the "*DESeq*" function. In comparing HSC1 and HSC2 clusters, we included the sample of origin as a covariate in the design formula (sample + condition) and applied an adjusted p-value threshold of <0.05 to identify differentially expressed genes.

2.2.5. Statistics

Statistical analyses were performed using GraphPad Prism software (version 10.0, STATCON). Data were tested for normality, and appropriate statistical tests were applied based on the distribution (as specified in the figure legends). Continuous variables are shown as mean ± standard error of the mean (SEM), unless stated otherwise.

The significance level for all tests was set to $\alpha = 5$ %. *, p-value <0.05; **, p-value <0.01; ***, p-value <0.001; ****.

3. Results

Most of the results shown in this section are part of a published manuscript (Komic et al., 2025). Some segments of the text, figures and figure legends have been taken or adapted from the previously mentioned manuscript, originally co-written by me (see author contributions for more details).

3.1. Proteo-transcriptomic profiling of adult BM HSPCs

To create a comprehensive single-cell transcriptomic and surface protein expression map of human bone marrow HSPCs across the aging trajectory, 596 genes covering early human hematopoietic differentiation stages and LSC markers were selected, as well as 46 oligonucleotide-labeled antibodies (AbSeqs) commonly used in hematopoietic flow cytometry analysis using the BD Rhapsody™ technology platform (**Table 11** and **Table 13**). This targeted panel was designed to capture key aspects of human HSPC biology, including leukemia stem cells, clonal hematopoiesis and myeloid neoplasms, while also incorporating immune modulatory receptors and cell cycle reporters. Using this approach, deep single-cell CITE-seq analysis on 62,277 FACS-enriched high quality CD34+ HSPCs was conducted, including 13,000 high quality CD34+CD38- sorted cells, which were collected from 15 healthy donors, categorized into three age groups: young (n=5, average age 22.4 years), mid-age (n=6, average age 59.7 years), and old (n=4, average age 75.3 years) (**Figure 13**).

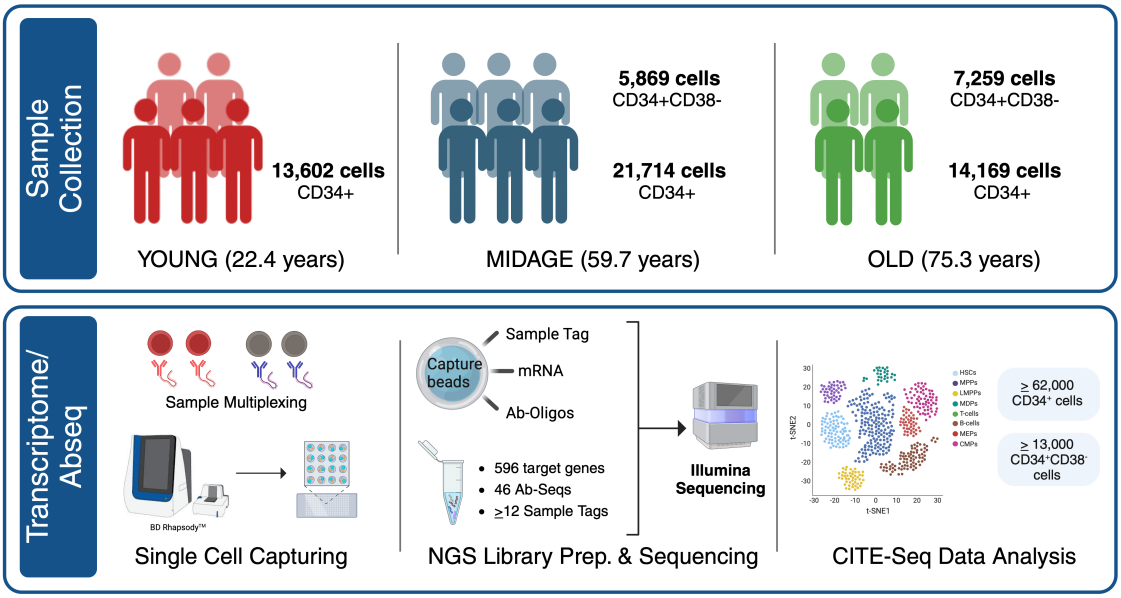

Figure 13. Overview experimental workflow for BM analysis.

HSPCs were isolated from 15 healthy donors of three different age groups (Sample collection). After sample multiplexing and antibody-based sequencing (AbSeq) staining for surface proteins, transcriptome analysis was performed using the BD Rhapsody platform. Transcriptome/AbSeq data analysis was performed on >62,000 CD34+ and >13,000 CD34+CD38- cells passing quality control. Created in BioRender. (Rieger, A. (2025) https://BioRender.com/n82a359)

Following the initial processing, integration and batch effect correction, 24 distinct clusters were identified through UMAP-based dimensional reduction based on their transcriptome (**Figure 14A**). Automated cell

label transfer, using the reference dataset from Triana *et al*., revealed a high proportion of immature cells labeled as CD34+ HSPCs at the bottom tip of the UMAP and two extending differentiation branches (**Figure 14B**). Further characterization was done by using well-established progenitor and lineage-specific marker genes. The human HSPC markers *HLF, CRHBP* and *HOPX* displaying a distinct upregulation at the tip of the UMAP confirmed the identity of the most immature. The erythrocyte branch was validated using *GATA1*, *GATA2* and *HBB* expression profiles (Ferreira et al., 2007; Moriguchi & Yamamoto, 2014), while monocyte-dendritic cell progenitors (MDPs) were characterized by the genes *CYBB*, *FGR* and *IL3RA* (Villani et al., 2017). GMPs showed distinct expression patterns of *CEBPA*, *CSF3R* and *CD48* (Boles et al., 2011; Ma et al., 2014) and lymphoid progenitors (LYP) were confirmed by the marker genes *MME*, *CD19* and *ISG20* (Rumfelt et al., 2006; Scheuermann & Racila, 1995) (**Figure 14C**). These expression pattern together with the automated annotations guided the manual labeling of the 24 cell clusters, which showed a high overlapping with the labels retrieved from the Triana dataset and displayed in a correlation matrix comparing both (**Figure 14D, Figure 15A**).

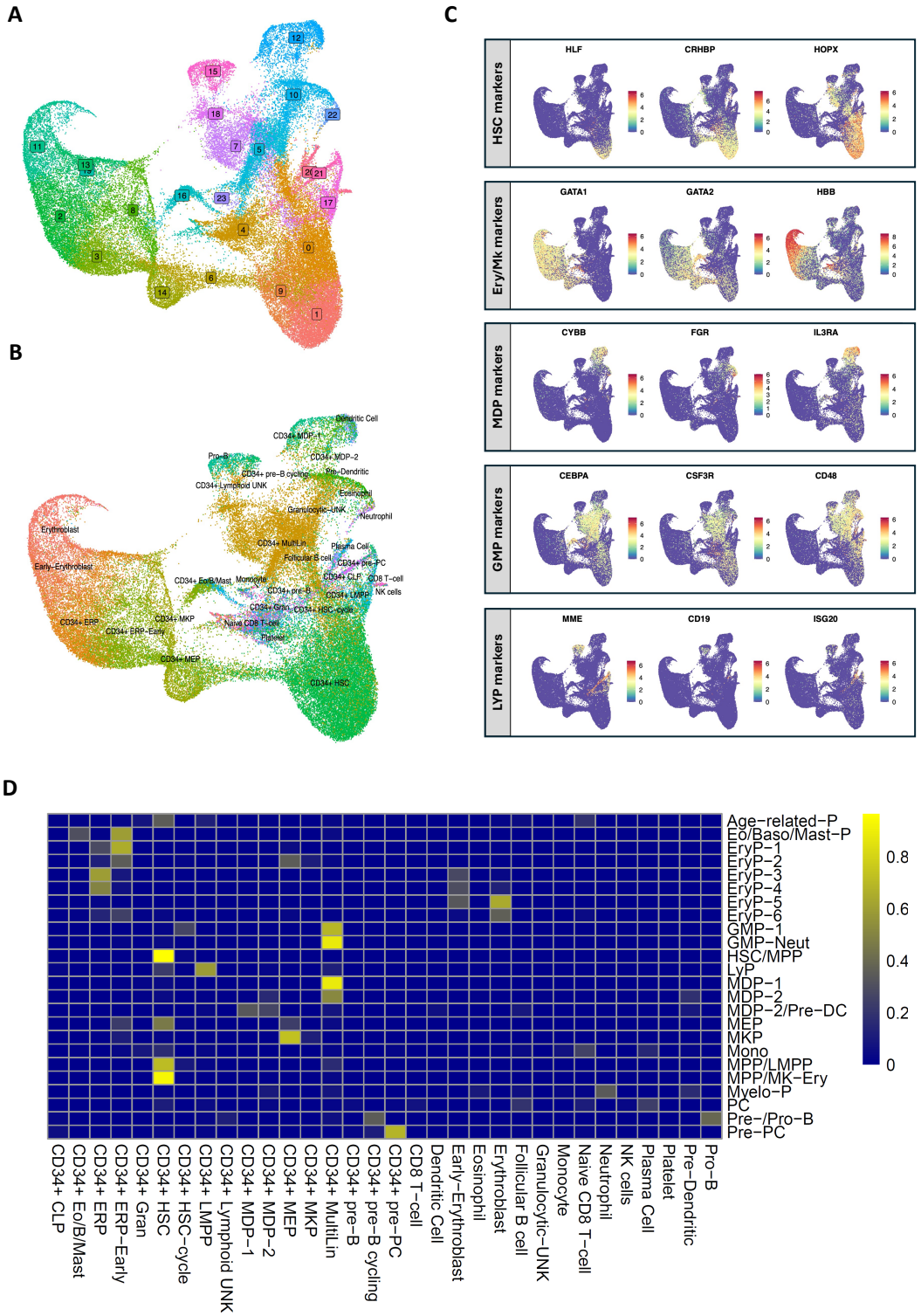

Figure 14. Proteo-transcriptomic profiling of CD34+cells from human BM.

A) UMAP visualization of gene expression-based clustering analysis of 62,277 CD34+ cells from 15 donors. Seurat clusters are color-coded. **B**) Cell label transfer was performed using the published dataset from Triana *et al.* 2021. **C**) Feature plots of selected lineage-specific marker genes to identify different cell populations. **D**) Correlation matrix of automated label transfer from reference dataset Triana *et al.* 2021 and manual annotations: X axis=predicted labels from cell label transfer, Y-axis= our manual annotation.

Combining the transcriptomic classification of cell types with their surface marker expression showed differential protein expression of the known HSPC surface markers CD90, CD34 and the absence of CD45RA

and CD38 for cluster HSC/MPP (**Figure 15B**). Each separate cluster shed a distinct clustering and surface marker expression for their respective population (**Figure 15C+D**).

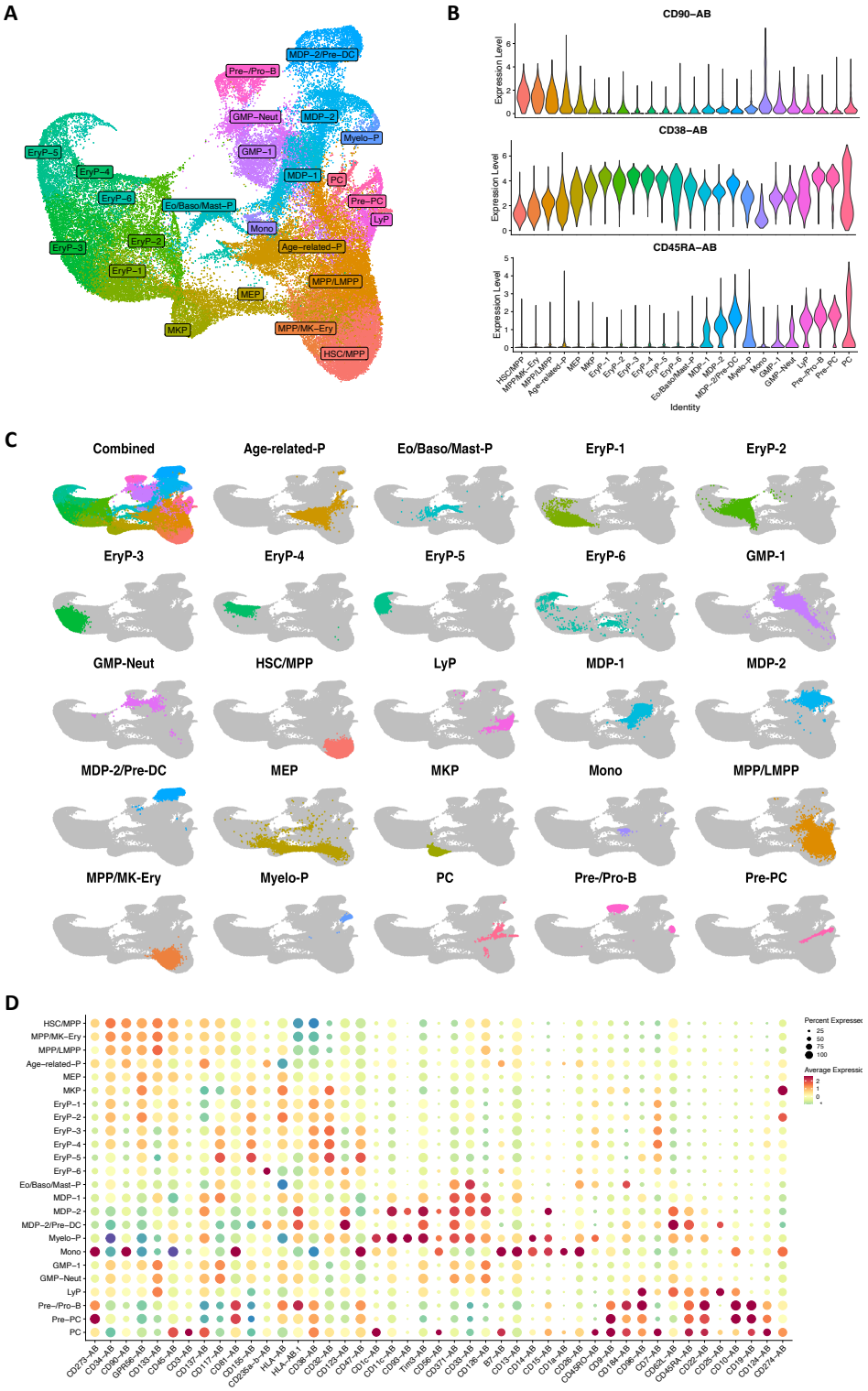

Figure 15. Association of surface marker expression with manual annotated cell clusters.

A) UMAP visualization of gene expression-based clustering analysis of 62,277 CD34+ cells from 15 donors with cluster annotation. **B**) Violin plots showing the surface protein expression of CD90, CD38 and CD45RA, detected by Transcriptomic/AbSeq. **C**) Visualization of individual separated clusters in UMAP projection. **D**) Dot-plot visualization of protein expression of previously defined cell type-specific markers.

The cluster composition between different age groups revealed some age-related differences. Besides the Age-related-Progenitor cluster nearly exclusively composed by the old age group, more mono-dendritic progenitors in the young age group could be detected and no myeloid bias for BM samples were retrieved from individuals with an average age of 75.3 years (**Figure 16A+B**).

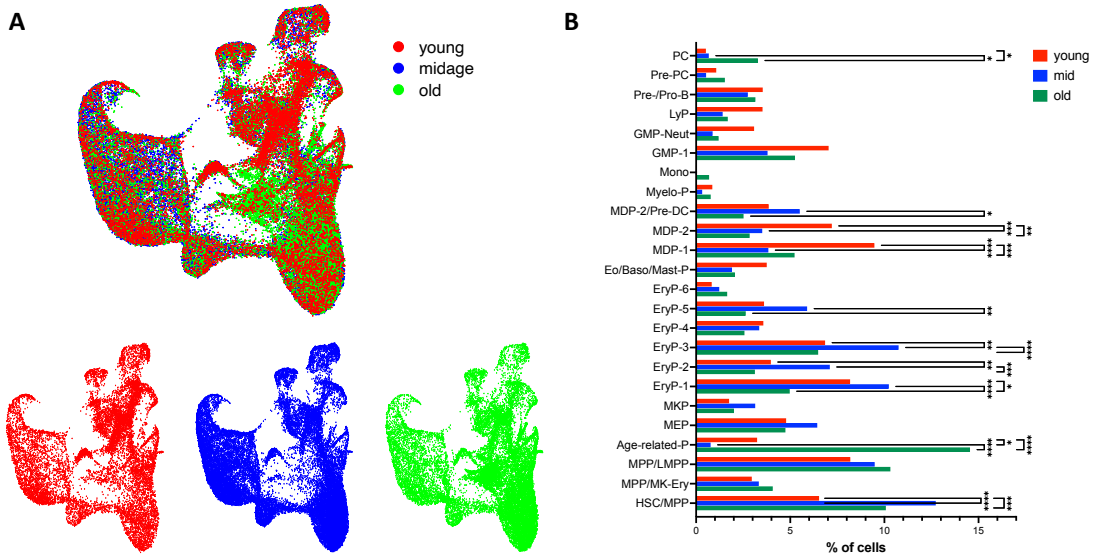

Figure 16. Distribution of CD34+ HSPCs from three age groups after batch effect correction.

A) UMAP display of 62,277 single cells from 15 donors of three age groups after CCA batch effect correction. Superimposed and isolated UMAP plots are shown. **B**) Distribution of cells per cluster from each age group. P values are from Wilcoxon Ran Sum test with Holm-Bonferroni correction. Bars represent the mean with SEM. Comparison of cell numbers of different cluster among age groups. No significance = ns, P<0.05 *, P<0.01 **, P<0.001 ***, P<0.0001 ****.

3.2. Proteo-transcriptomic analysis of early HSPCs

To focus on the earliest transitions of immature HSPCs into multi- and oligopotent progenitors, the clusters HSC/MPP, MPP/MK-Ery, MPP/LMPP, MEP, MDP-1, GMP-1, GMP-Neut and LyP, composing of 21,395 cells, were selected for a refined clustering analysis. These clusters showed a high abundance of CD34+CD38- sorted cells, which could be deciphered by sample tag labeling (**Figure 17A**). The most immature cluster HSC/MPP was used as trajectory anchor for re-clustering (**Figure 17B**). The number of clusters separating different subpopulations is depended on the used resolution to display the dimensional reduction, with higher resolutions resulting in higher cluster numbers (Zappia & Oshlack, 2018) (**Figure 17C**). The clustering tree analysis visualizes how clusters split over different resolution and display the probability of cells changing their identity (**Figure 17D**). To get a distinct separation and identifying rare cell types within an already HSPC enriched cell subset, resolution 0.4 was chosen for downstream analysis. The resolution resulted in nine cell clusters coded by different coloring (**Figure 17E**). As done for the previous analysis, automated label transfer with the reference dataset from Triana *et al.* was used to characterize the different cell identities with CD34+ HSPCs showing the highest representation and localized at the right tip of the UMAP (**Figure 17F**).

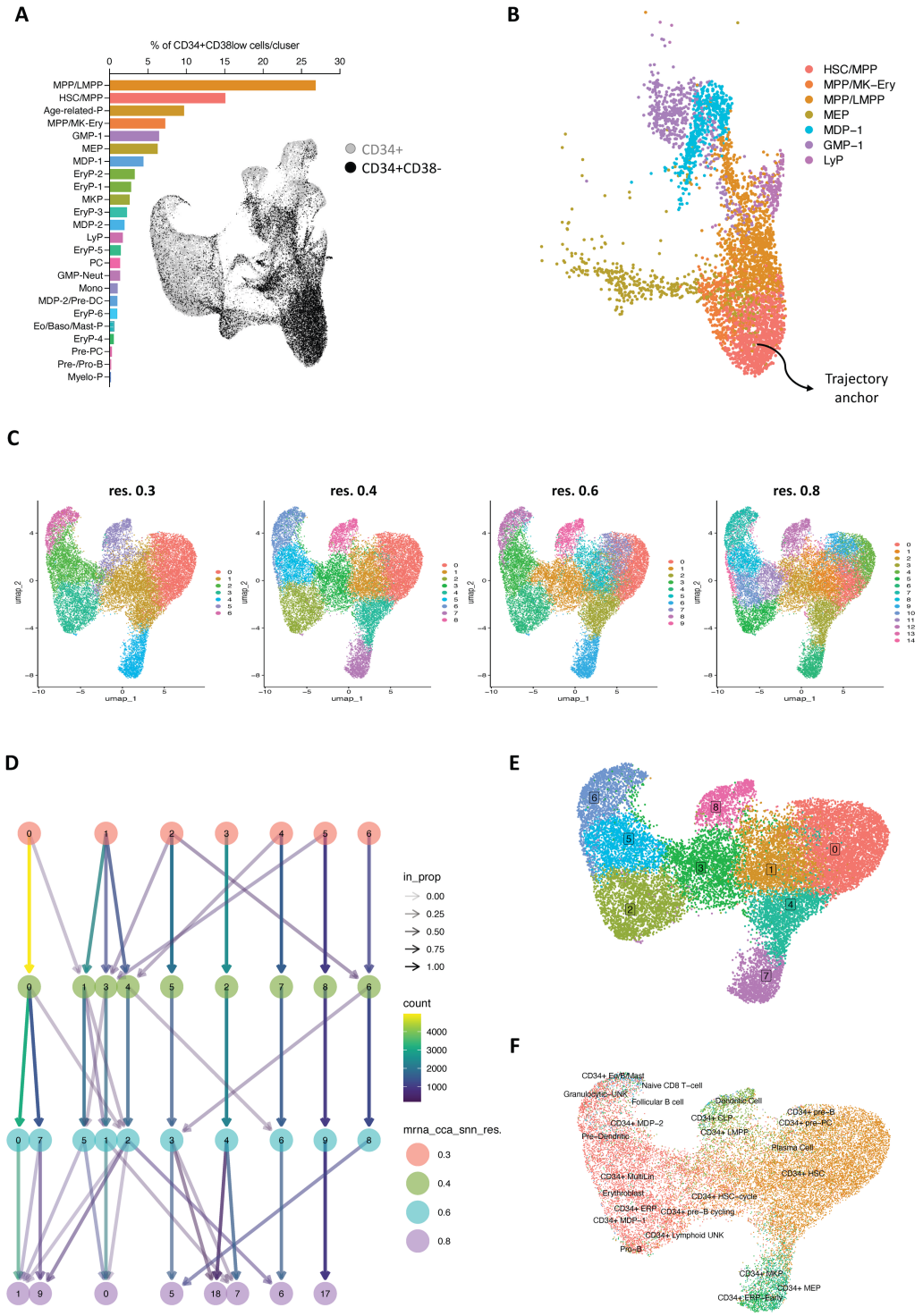

Figure 17. Re-clustering of early immature HSPCs.

A) Distribution of FACS-sorted CD34+CD38- cells in respective clusters and visualized on the UMAP demonstrating, enrichment in most immature cell clusters. **B**) UMAP visualization of clusters HSC/MPP, MPP/MK-Ery, MPP/LMPP, MEP, MDP-1, GMP-1, GMP-Neut, LyP used for re-clustering analysis, with HSC/MPP cluster functioning as trajectory anchor. **C**) Cell clustering among different resolution for re-clustered immature subpopulation. **D**) Cluster tree analysis displaying how clusters split and change their identity over different resolutions. **E**) UMAP projection of 21,395 cells with resolution 0.4 resulting in 9 distinct subpopulations. **F**) Automated label transfer projected onto immature UMAP with reference dataset from Triana *et al*. 2021.

Based on their transcriptomic and surface marker expression the nine cell clusters were annotated in two HSC clusters (HSC-1, HSC-2), one MPP cluster (MPP) and six early committed progenitors (MEP-1, MEP-2,

LYP, MDP-1, MDP-2, GMP) (**Figure 18A**). HSC-1 accounted for 4,982 cells and displayed the highest expression of well-described stem cell genes (*HLF, HOPX, PROM1, CRHBP, MLLT3*), as well the stem cell surface markers CD34, CD90 and CD133 (**Figure 18B**). Hierarchical gating using the Transcriptomic/Abseq expression of HSPC protein markers led to a relatively heterogenous cluster composition within the CD34+ cells. The CD34+CD38- displayed substantial increase of the HSC-1 cluster (~52 %). Using the HSC marker combination of CD34+CD38-CD45RA-CD90+, which is used for HSC sorting in flow cytometry, led to near depletion of the committed progenitor population with over 80 % of cells composing of HSC-1 or HSC-2 cells (**Figure 18C**).

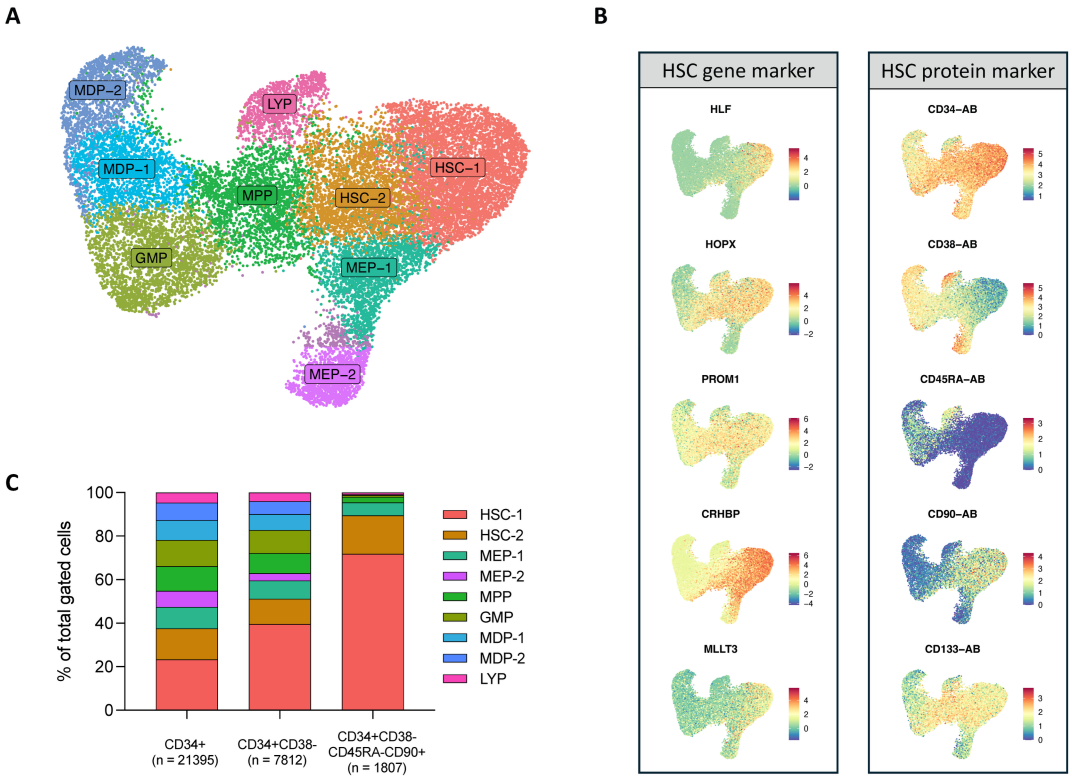

Figure 18. Annotation and proteo-transcriptomic analysis of immature HSPCs.

A) UMAP visualization of 21,395 immature HSPCs with manual annotated clusters using known stem cell markers. **B**) Feature plots of known HSC gene and surface protein markers. **C**) Hierarchical gating of HSPC population based on the Transcriptomic/Abseq surface protein expression and distribution in clusters.

Lineage signature scores derived from published gene set for HSCs, MEPs, GMPs and MLPs were used to further confirm the annotation of early progenitors and showed high correlation scores (**Figure 19A + B**).

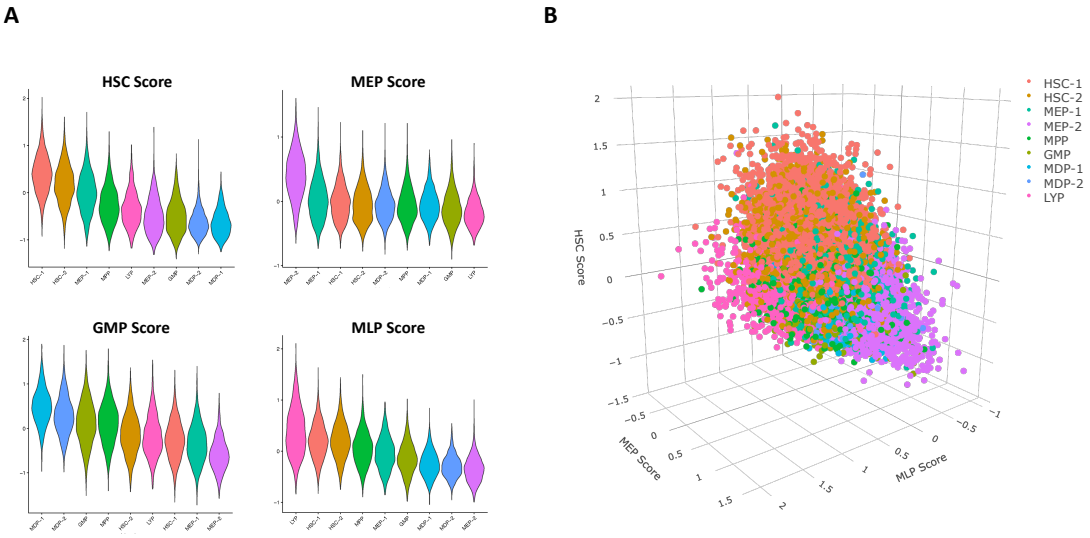

Figure 19. Stem cell and lineage scores of early immature HSPCs.

A-**B**) Violin plots (**A**) and three-dimensional plots (**B**) of lineage- and HSC-scores calculated for each cell by using published gene sets by Mende *et al*. enriched in prospectively isolated HSPC subsets.

3.3. Continuous pseudotime expression of immature HSPCs

To further investigate cellular changes among the human lifespan the distribution of each subpopulation in all three age groups was compared (**Figure 20A**). While the HSC-1 and HSC-2 cluster of young samples were smaller than later progenitor subpopulations, the fraction of cells residing in these clusters was markedly increased in BM obtained from mid-aged and old donors which is in agreement with published reports of HSC expansion upon aging (**Figure 20B**) (Pang et al., 2011). Lineage trajectories between different age groups showed no major differences in slingshot pseudotime analysis (**Figure 20C**). Several studies declared a decreased lymphopoiesis with age with could not be observed in our LYP cluster upon aging (Linton & Dorshkind, 2004; Miller & Allman, 2003; Su et al., 2024; Sudo et al., 2000). In contrast to that, the presented analysis revealed a reduced percentage of GMP and MDP-1 and -2 in BM from aged individuals, in comparison to young donors (**Figure 20B**)**.** Next, the density of cells along pseudotime was compared across the four trajectories (**Figure 20D**). The findings suggest that hematopoietic cells from young donors exhibit increased lineage commitment and higher overall differentiation activity. In contrast, samples from middle-aged and elderly donors display an accumulation of cells in the most immature compartments, accompanied by a marked reduction in differentiated progenitor populations, particularly within the lymphoid lineage.

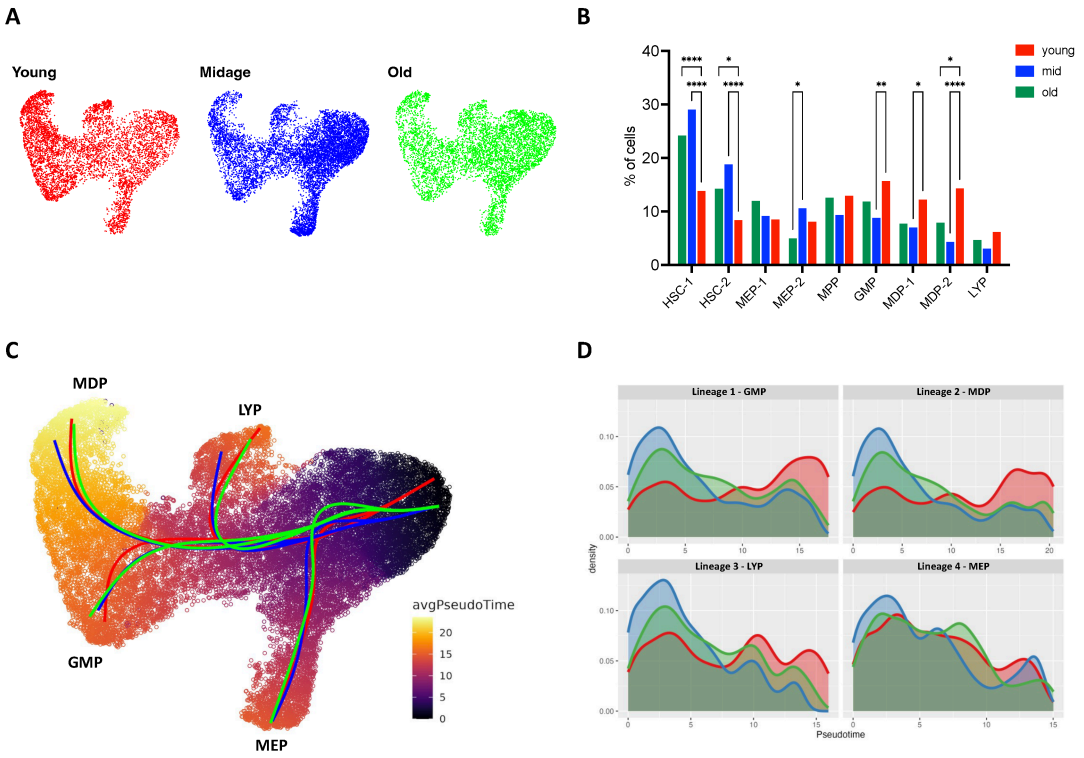

Figure 20. Age and pseudotime comparison of early immature cells.

A) UMAP visualization of cells from each age group. **B**) Distribution of cells per cluster from each age group. *P* values were calculated by Wilcoxon Rank Sum test with Holm-Bonferroni correction. **C**) Slingshot pseudotime analysis identified four trajectories. D) Density plots along pseudotime for each trajectory show age-group specific difference. P<0.05 *, P<0.01 **, P<0.001 ***, P<0.0001 ****.

After separating the cells from each age group, the comparison of the differential gene expression in HSC-1 and HSC-2 among age groups using DESeq2 pseudobulk analysis revealed highly overlapping genes, especially for the *bona fide* stem cell genes *HLF*, *MLLT3* and *MECOM* (**Figure 21A-C**). Among these genes was also the myeloproliferative leukemia protein (*MPL,* thrombopietin receptor) which showed a higher expression for the most immature cluster HSC-1 which is in line with previous reports indicating a role of thrombopoietin signaling for stemness and quiescence (Nakajima-Takagi et al., 2014).

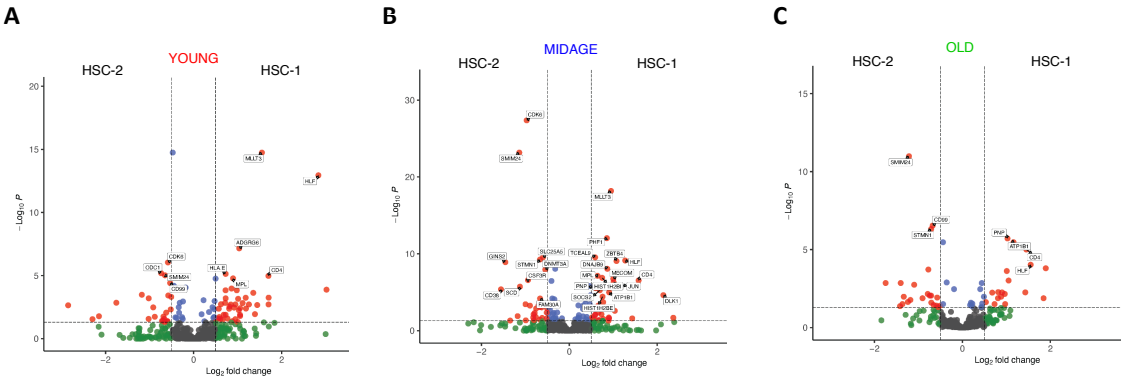

Figure 21. Differential gene expression of HSC-1 and HSC-2 pseudobulk according to age.

A-C) Volcano plots depict the results of DESeq2 analysis on pseudobulk data, comparing HSC-1 and HSC-2 cluster cells, within each age group. **A**) young, **B**) midage, **C**) old.

The analysis identified 16 genes that are upregulated in HSC-1 in all three age groups (**Figure 22A**). However, some stem cell genes showed age-dependent specific expression pattern (**Figure 22B**). For instance, mRNA levels of established stemness-associated genes like HLF, MECOM, CRHBP, and KLF4 were reduced in HSC-1 cells from young donors. The age-related upregulation of these genes was further evidenced by the intermediate expression levels observed in donors of middle age. A notable example is DLK1, which was specifically expressed in immature HSPCs and exhibited a marked increase in expression with age. Clonal hematopoiesis (CH) can arise from individual somatic mutations in genes associated with myeloid neoplasms within HSPCs (Dorsheimer et al., 2019). The mechanism by which these mutations lead to clonal dominance in HSPCs is not uniform. It depends on the affected gene and its expression pattern during hematopoietic differentiation (Pardali et al., 2020; Walsh et al., 2022). To explore this phenomenon, the targeted gene panel incorporated genes known to be associated with CH and examined their expression dynamics across cells from the HSC-1, HSC-2, and MPP clusters (**Figure 22C**). The following analysis revealed an intriguing pattern: the majority of genes recognized as CH drivers showed low expression levels in the HSC-1 population but were notably upregulated at the MPP stage. Particularly striking was the expression profile of the most common CH driver genes *DNMT3A* and *TET2.* Both genes are frequently mutated in CH and were almost undetectable in HSC-1 cells (Jaiswal et al., 2014; Kovtonyuk et al., 2016; Xie et al., 2014). Given that most reported mutations of these epigenetic regulators result in loss of function, this observation suggests that the upregulation observed in MPPs plays a crucial role in initiating differentiation. Interestingly, only four genes could be identified that exhibited high expression in HSC-1 cells and were subsequently downregulated during myeloid differentiation. Among these were well-known stemness genes, including *GATA2, KMT2A* and *MPL*. This pattern implies that CH pathogenesis likely involves a delicate balance between the delayed activation of genes associated with differentiation and the gradual silencing of factors that maintain stemness.

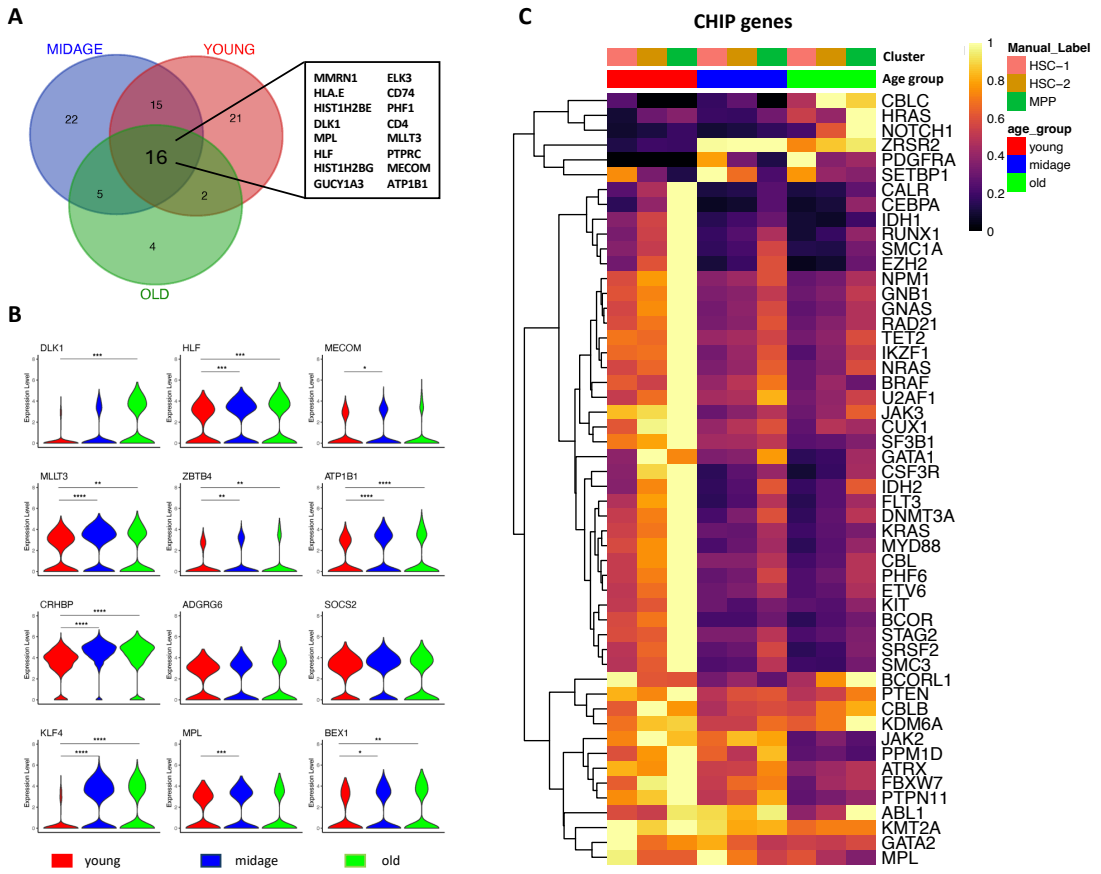

Figure 22. Upregulated genes in HSC-1 cells among all age groups and comparison of CHIP driver genes in immature cells.

A) Venn-diagram showing comparison of upregulated genes in cluster HSC-1 between individual age group. **B**) Violin plots pf expression of stem cell-related genes from cells in cluster HSC-1 of each age group. **C**) Heatmap of clonal hematopoiesis driver genes in clusters HSC-1, HSC-2 and MPP. *P* values were calculated by two-sided Wal test with Benjamini-Hochberg correction. P<0.05 *, P<0.01 **, P<0.001 ***, P<0.0001 ****.

3.4. Differential gene and surface protein expression of HSCs

To focus on the earliest HSPC clusters, 4,982 cells from cluster HSC-1 and 3,064 cells from cluster HSC-2 were analyzed as pseudobulk. Differential gene expression analysis revealed 49 upregulated and 30 downregulated genes in HSC-1 with a fold change >0.5 (log2) (**Figure 23A**). The HSC-1 cluster exhibited upregulation of well-established genes associated with stemness and HSC identity, including *CRHBP*, *MLLT3, HLF* and *MECOM*. Notably, *FGD5*, previously utilized as a marker for murine long-term HSCs in transgenic models, was also upregulated in this cluster (Gazit et al., 2014). Several other genes showed heightened expression in HSC-1 compared to HSC-2, such as DLK1, *ADGRG6*, *GUCY1A3*, *KLF4* and *BEX1*. Of particular interest was *DLK1*, a non-canonical Notch ligand crucial for maintaining adult long-term repopulating HSCs and stem cell quiescence in murine hematopoiesis (Huang et al., 2023). The potential of DLK1 to regulate cell proliferation, differentiation and tissue regeneration through both Notch-dependent and independent mechanisms underscores its significance (Falix et al., 2012). *ADGRG6*, encoding the mechanosensitive adhesion G-protein coupled receptor GPR126, was also highly expressed in HSC-1 (Q. Li et al., 2024; Musa

et al., 2019). Intriguingly, ADGRG6 expression is elevated in MLL-rearranged AML, a high-risk subtype, though its specific role in HSPC biology remains to be elucidated (Maiga et al., 2016). In contrast, the HSC-2 cluster displayed increased expression of genes involved in cell cycle entry and regulation, such as *CDK6*, *CCNE1* and *MYC*. This suggests that HSC-2 cells may be transitioning from quiescence (G0) to the G1 phase of the cell cycle. Correspondingly, quiescence-associated genes like *SOCS2* and *HLF* showed higher expression in HSC-1 cells. Furthermore, HSC-2 cells exhibited elevated expression of early HSPC differentiation markers, including *FLT3*, *IL3RA*, and *CSF3R* (G-CSF receptor), as well as the epigenetic regulator *DNMT3B*. These findings collectively indicate a more primed state for cell cycle re-entry and early differentiation in the HSC-2 population compared to the more quiescent HSC-1 cells. The differentiation trajectory from HSC-1 to HSC-2 show a nice gradient expression profile with stemness markers *HLF, DLK1, SOCS, MLLT3* and *JUN* being highly expressed during early pseudotime (0 – 7.5) and cell markers for cell cycle (*CDK6*) and lineage committed progenitors (*STMN1*, *SMIM24*) highly expressed during pseudo 7.5 – 15, which marks the transition from HSCs to MPPs (**Figure 23B**). TradeSeq analysis along pseudotime displayed a distinct upregulation of *DLK1* and *ADGRG6*, with was in alignment with the expression profile observed for the stemness marker *HLF* (**Figure 23C**).

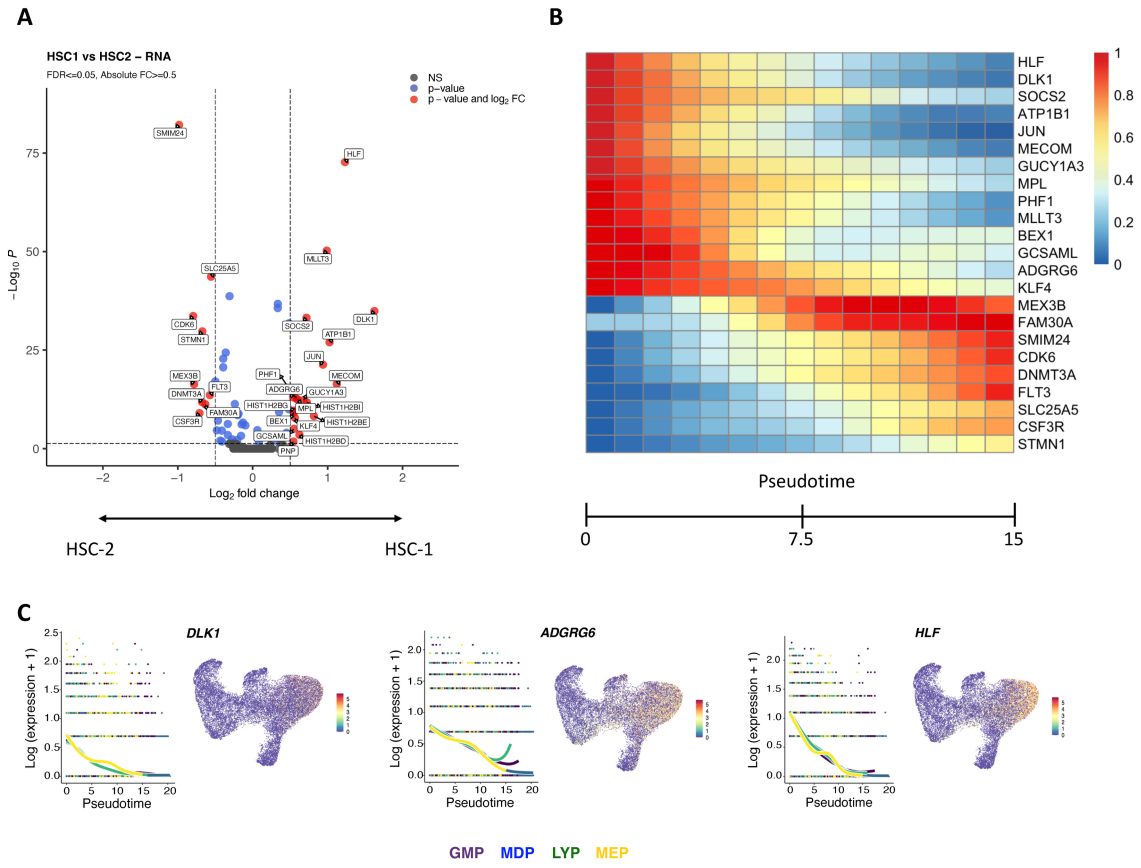

Figure 23. Transcriptomic profiling and differential gene expression of HSC-1 and HSC-2 specific cells.

A) Volcano plots decipher the differential gene expression in HSC-1 and HSC-2 pseudobulk. Two-sided Wald test with Benjamini-Hochberg correction **B**) Pheatmap displaying the differential expression HSC-1 specific genes among pseudotime. **C**) Gene expression along pseudotime of selected HSC-1 markers.

3.5. Surface marker analysis of HSC-1 revealed expression of CD273/PD-L2 on immature HSPCs

A key advantage of the Transcriptomic/AbSeq approach lies in its ability to simultaneously profile transcriptomes and surface protein expression at single-cell resolution. This enables the direct identification of novel surface markers and the evaluation of corresponding antibodies for cellular phenotyping. In this study, the expression of 46 surface proteins was selected to encompass established markers of HSPC subsets. Overall, the transcriptome-based annotation of cell clusters was consistent with their corresponding surface protein expression profiles. Notably, the most primitive subsets, HSC-1 and HSC-2, were defined by high levels of CD34 and CD90, along with the absence of early differentiation markers CD38 and CD45RA (**Figure 24A**). A progressive decline in CD34 and CD90 expression was observed from the HSC-1 to the MPP cluster, indicating the early onset of differentiation. Cells within the MEP-2 cluster exhibited a marked upregulation of CD38 and a concomitant loss of CD90, consistent with their commitment toward the megakaryocyte-erythroid lineage. Intriguingly, these MEP-2 cells also expressed high levels of CD123, a marker typically associated with multipotent and lymphoid progenitors, suggesting that CD123 expression may persist despite MEP lineage commitment. The MDP-1 and MDP-2 clusters were distinguished by robust upregulation of CD371 and CD33, indicative of myeloid lineage specification. Among all surface proteins analyzed, CD273 and CD62L were the only markers significantly upregulated in HSC-1 compared to HSC-2, highlighting their potential utility in further refining the phenotypic characterization of the most primitive HSPC subsets (**Figure 24B**). CD62L has previously been published as marker for lymphoid primed BM cells upregulated before the expression of CD10 (L. A. Kohn et al., 2012). In the presented analysis, CD273 expression was significantly elevated in the HSC-1 cluster compared to HSC-2, suggesting that CD273 may serve as a marker for the most primitive hematopoietic stem cell subset (**Figure 24C**).

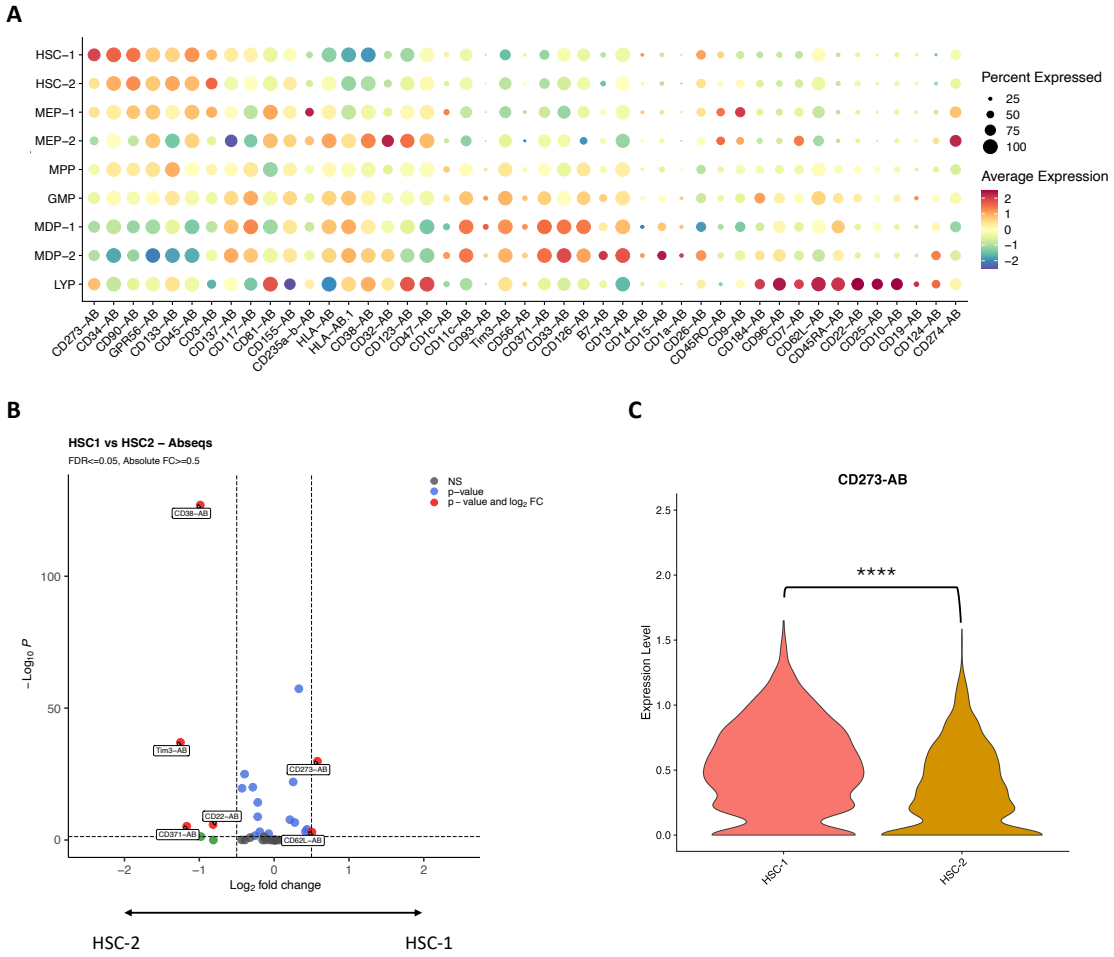

Figure 24. Surface protein expression on immature HSPCs.

A) Dot-plot visualization of surface marker expression for cell clusters of immature HSPCs. **B**) Volcano plot deciphering differential AbSeq expression in HSC-1 and HSC-2 cells. Wilcoxon Rank Sum test with Bonferroni correction. **C**) Violin plot of CD273 in cells from cluster HSC-1 and HSC-2. Wilcoxon Rank Sum test with Bonferroni correction. P<0.0001 ****.

CD273 is also known as programmed cell death ligand 2 (PD-L2). To explore whether CD273+ HSPCs are enriched in stem cell molecular signatures (HSC-1) within the HSPC populations, hierarchical gating was performed using AbSeq expression. Within different HSPC subpopulation the inclusion CD273 expressing cells elevated the level of the molecular signature of HSC-1 with CD34+CD273+ composing of ~ 54 % HSC-1 compared to ~ 28 % in CD34+ and ~ 19 % in CD34+CD273- cells (**Figure 25A**). Comparing the expression level of CD273 in different cell clusters showed modest expression for HSC-1 (**Figure 25B**). The bloodspot database further confirmed high expression of CD273 in HSCs and exhibited lower expression in MPPs and distinct progenitor populations (**Figure 25C**). Reference datasets from Triana *et al*. showed few CD273 expressing cells within their HSC/MPP cluster (**Figure 25D**).

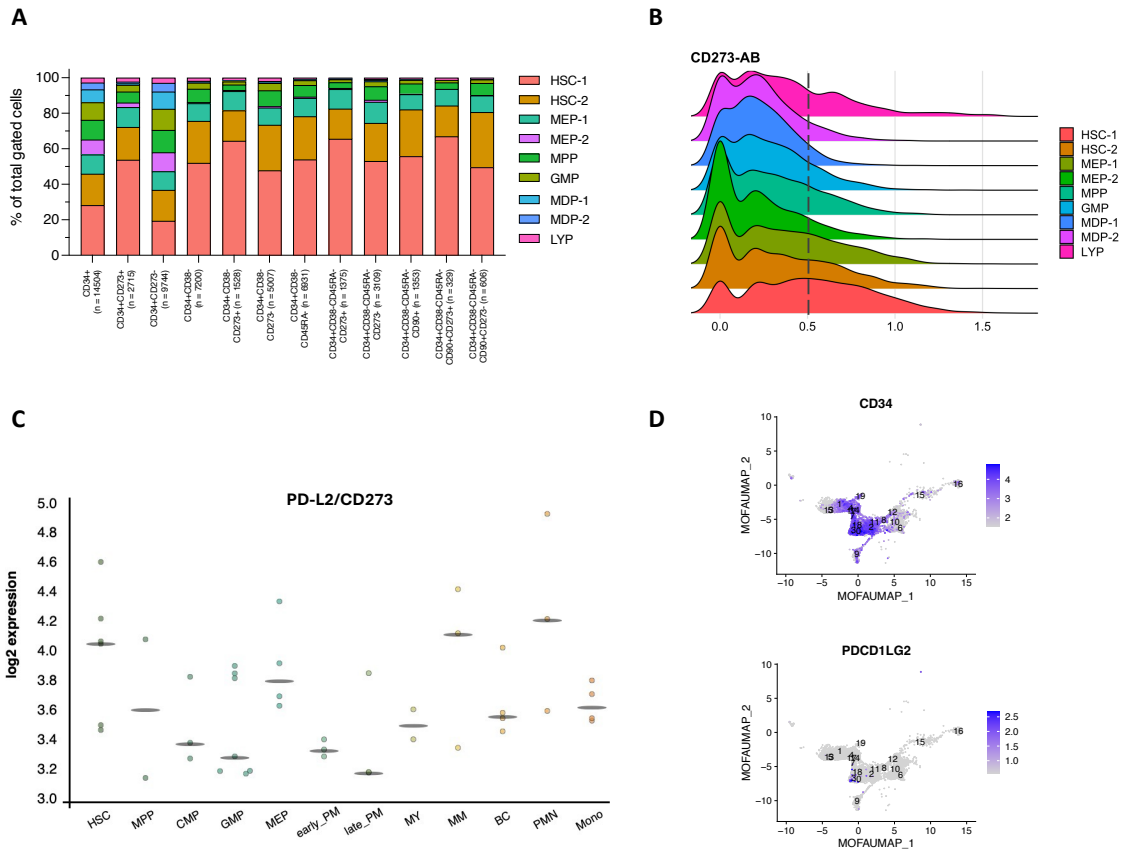

Figure 25. Expression of PD-L2/CD273 in different progenitor populations.

A) Hierarchical gating of HSPC population based on the AbSeq surface protein expression and distribution in clusters. **B**) Ridgeplot displaying the expression of CD273 among all cluster of immature HSPCs. **C**) CD273 (PD-L2) expression in cells of the hematopoietic system. Taken from bloodsplot.eu (Bagger et al., 2016). **D**) Feature plot of CD34 and PDCD1LG2 (CD273/PD-L2) expression in dataset from Triana et al., 2021.

Although single-cell proteo-transcriptomic analysis provides valuable insights into the molecular signatures of distinct cell types and facilitates the identification of novel potential stem cell markers, results derived from multi-omic datasets require rigorous functional validation to establish their biological relevance. Therefore, primary samples were utilized from adult HSPC sources to corroborate the findings and functionally characterize CD273-expressing HSPCs.

3.6. CD273 is significantly upregulated in most immature HSPC compartments

First, the differential expression of CD273 on the surface of human HSPCs derived from mPB samples was tested by performing flow cytometry analysis using a well-established HSPC gating strategy, which included CD90 and CD49f to enrich for immature HSCs (Notta et al., 2011) (**Figure 26A**). The analysis demonstrated that CD90+ and CD90+CD49f+ HSCs showed an increased expression level of CD273 (**Figure 26B**).

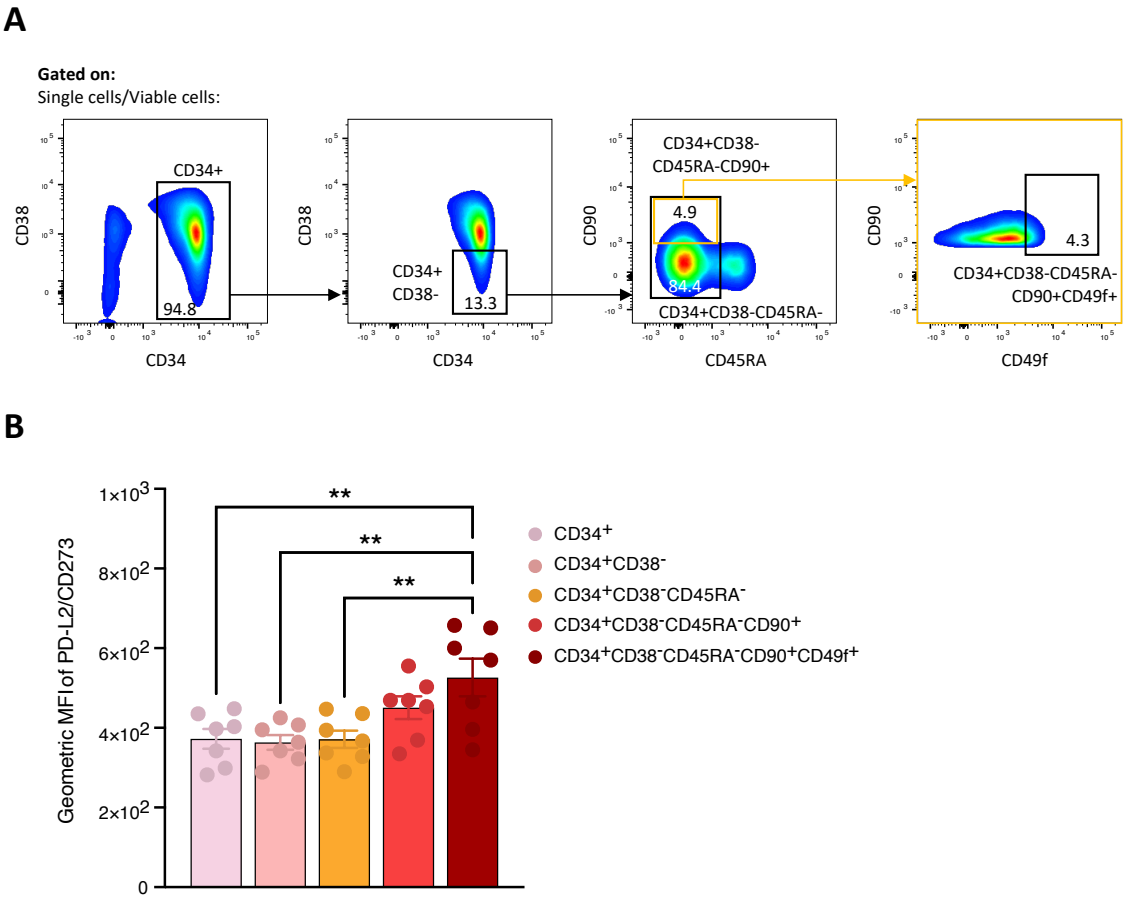

Figure 26. CD273 surface expression on different HSPC population.

A) Representative flow cytometry plots (pseudocolour density plot) for analyzing CD273 expression levels on defined HSPC subpopulations with their percentages. **B**) CD273 surface expression level on different HSPC population (*n*= 7 donors) by flow cytometry. *P* values were calculated by one way ANOVA with Tukey's multiple comparison test. P<0.01 **.

3.7. *In vitro* characterization of CD273^{high} and CD273^{low} HSPCs

To functionally test CD273 expressing HSPCs a hierarchical gating strategy on human HSPCs (CD34+CD38-CD45RA-Lin-) was applied for the prospective isolation of CD273^{high} and CD273^{low} expressing HSPCs (**Figure 27A**). The expression level of CD273 showed comparable percentages from 3.7 % for BM aspirations and 4.5 % for mPB samples. CD34+ showed slightly decreased CD273 expression (**Figure 27B-C**). For the following analysis, CD34+CD38-CD45RA-CD273+ and CD34+CD38-CD45RA-CD273- HSPCs were isolated from mPB samples are referred to as CD273^{high} and CD273^{low} (**Figure 27D, Table 16**).

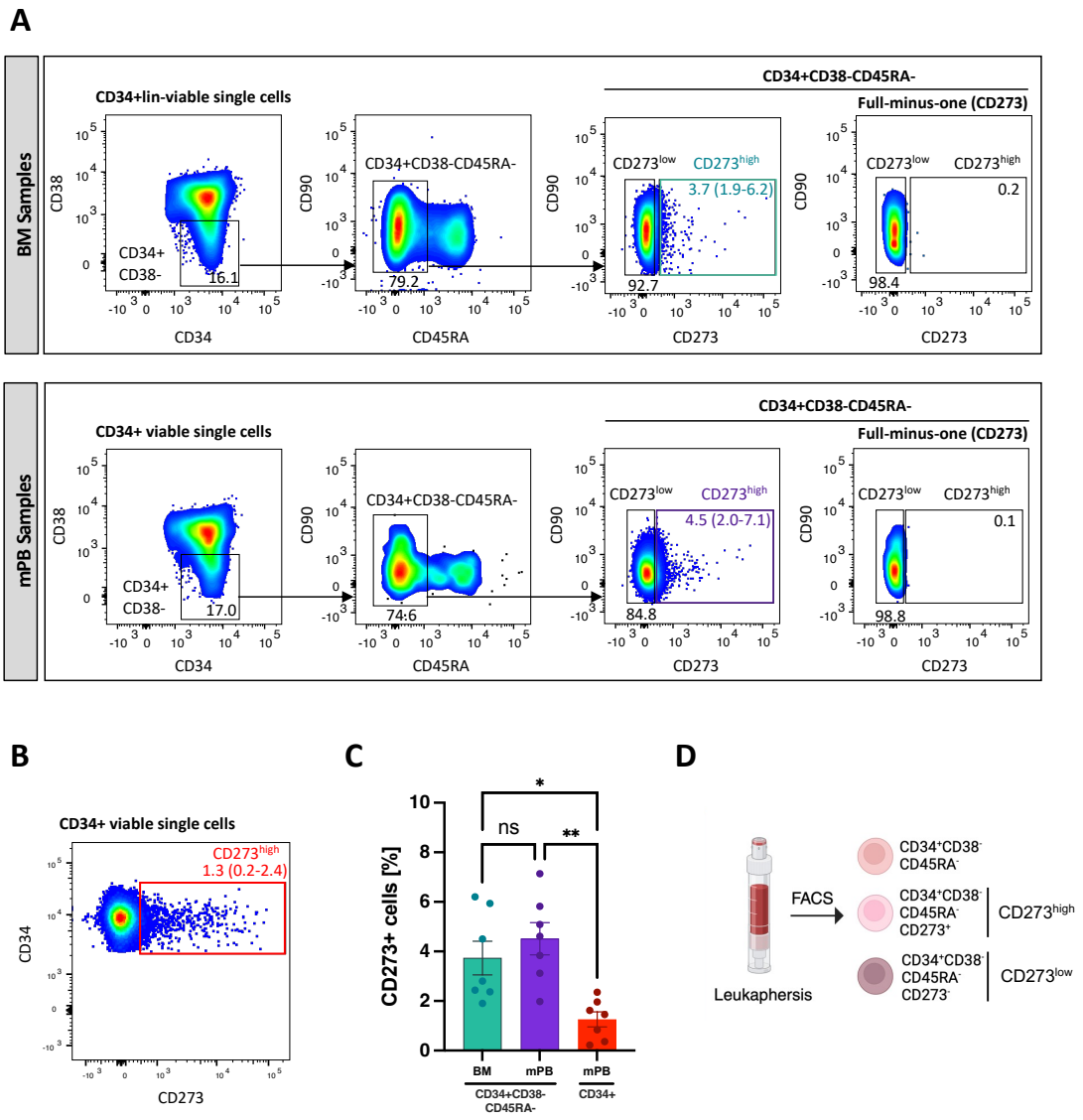

Figure 27. FACS sorting strategy for isolation of CD273^{high} and CD273^{low} HSPCs.

A) Representative flow cytometry plots (pseudocolour density plots) illustrating the hierarchical gating strategy used for isolation of Lin-CD34+CD38-CD45RA- HSPCs for bone marrow (BM) samples and CD34+CD38-CD45RA- HSPCs for mobilized peripheral blood (mPB) samples. **B**) CD273 expression of CD34+ MACS-enriched mPB. **C**) Percentage of CD273^{high} cells within the indicated populations. Bars represent the mean with SEM (n = 7 donors). *P* values were calculated with one way ANOVA with Tukey's multiple comparison test. No significance = ns, P<0.05 *, P<0.01 **. **D**) Graphical illustration for isolating CD273^{high} and CD273^{low} cells for functional validation.

3.7.1. CD273^{high} cells show delayed differentiation profile

To investigate the *in vitro* differentiation kinetics of CD273^{high} and CD273^{low} HSPCs, sorted populations were cultured for 7 days and flow cytometry analysis of stem cell markers EPCR, CD90 and CD133 on CD34+ cells was conducted (**Figure 28A**). CD273^{high} showed a delayed differentiation phenotype with an elevated CD90 and CD133 expression upon culture (**Figure 28B**).

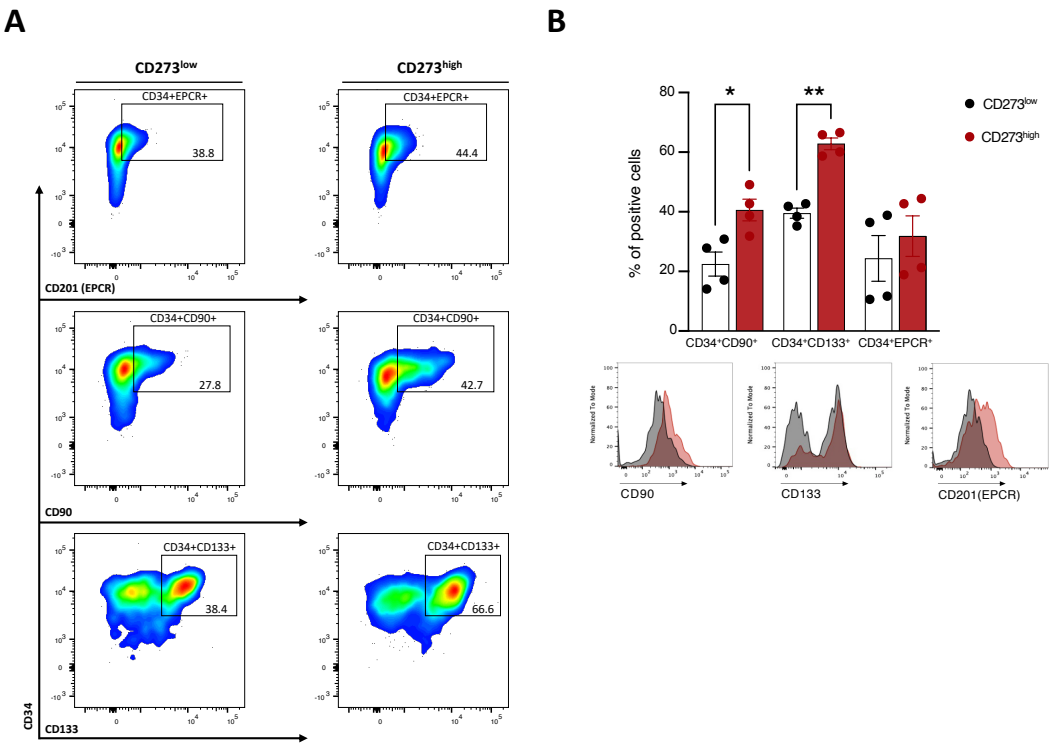

Figure 28. *In vitro* differentiation assay of CD273^{high} and CD273^{low} HSPCs.

A) Representative flow cytometry plots (pseudocolour density plot) illustrating the gating strategy for in vitro cultured CD273high and CD273low sorted HSPCs. Gates show CD34+ cells with expression of CD201(EPCR), CD90 and CD133 and their percentages. **B**) CD273high HSPCs show delayed in vitro differentiation. Cells were analyzed after 7 days of culture by flow cytometry (n = 4 donors). *P* values were calculated using two-way ANOVA with Šídák's multiple comparisons test. P<0.05 *, P<0.01 **.

3.7.2. CD273^{high} and CD273^{low} display similar colony forming potential

Colony forming assays are frequently used to test the potency of HSPCs (Bradley & Metcalf, 1966). They enable the identification of multipotent (CFU-GEMM), bipotent (BFU-E, CFU-GM) or unipotent (CFU-M, CFU-G, CFU-E) cells (**Figure 29A**). To analyze their potential 100 FACS-sorted HSPCs (CD34+CD38-CD45RA-Lin-), CD273^{high}, CD273^{low} and HSCs (CD90+CD49f+CD34+CD38-CD45RA-Lin-) were seeded in methylcellulose including cytokines for multi-lineage differentiation (permissive). Primary plating revealed multipotent potential and similar colony numbers of all tested subpopulation with CD273^{high} and CD273^{low} HSPCs both giving rise to ~16 % CFU-GEMMs and around 40 colonies per plate (**Figure 29B + C**). Serial replating between these populations demonstrated equal but not superior *in vitro* capacity of CD273^{high} HSPCs as CD90+CD49f+ HSCs (**Figure 29D + E**).

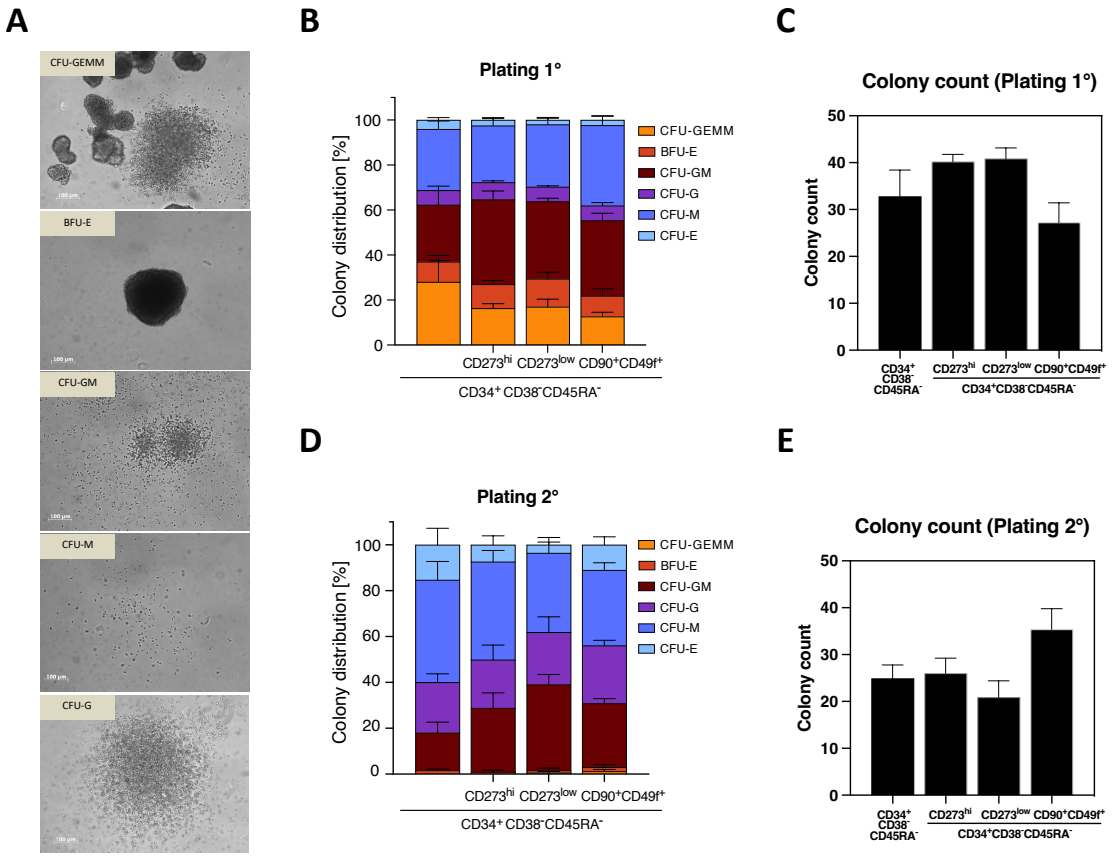

Figure 29. Colony forming analysis of CD273^{high} and CD273^{low} HSPCs.

A) Microscopic pictures of colony forming unit (CFU) assays. Multipotent cells form colonies composed of granulocytes, erythrocytes, macrophage and megakaryocytes (CFU-GEMM). Bipotent colonies can be differentiated between erythroid burst-form unit (BFU-E) or CFU-granulocyte-macrophage (CFU-GM). Unipotent cells give rise to either CFU-macrophage, CFU-erythroid or CFU-granulocyte (CFU-G). **B**) Colonies of FACS-sorted CD34+CD38-CD45RA- (parental population), CD273^{high}, CD273^{low} HSPCs and CD90+CD49f+ HSCs determined after 14 days *in vitro* culture (*n* = 5 donors). *P* values were calculated by two-way ANOVA with Tukey's multiple comparisons test. **C**) Colony count of primary plating. **D**) Scoring of replated colonies after 14 days (*n* = 4 donors). **E**) Colony count of replated CFUs. Bars represent the mean with SEM.

3.7.3. CD273^{high} showed lower mitochondrial potential

With most quiescent HSCs within the BM showing low mitochondrial membrane potential, JC-1 dye can be used as cationic carbocyanine dye that accumulates in the mitochondria and indicate the shift from low to high mitochondrial potential by shifting its fluorescence from green (~525 nm) to red (~590 nm) (Umemoto et al., 2018). CD34+ cell from mPB were analyzed for their mitochondrial potential in different HSPC subpopulation using flow cytometry (**Figure 30A**). The analysis showed ~80 % of human HSPCs (CD34+CD38-CD45RA-Lin-) were JC-1 low, compared to ~90 % of CD273^{high} and ~47 % of CD273^{low} cells, indicating an increased activation of CD273^{low} HSPCs (**Figure 30B**).

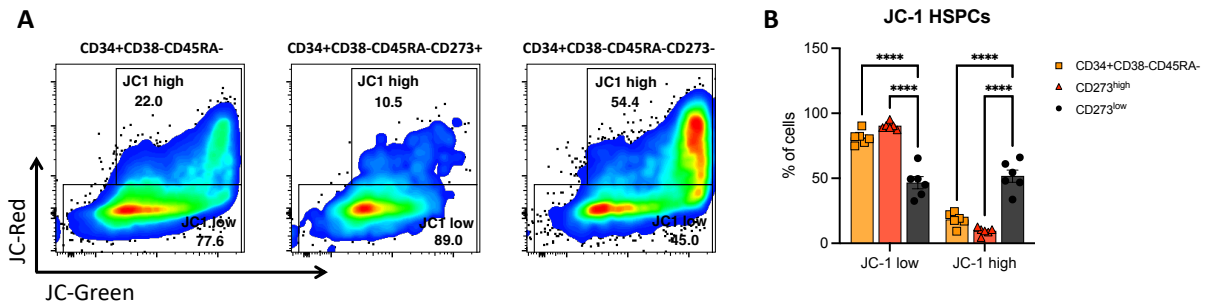

Figure 30. Mitochondrial potential of CD273^{high} and CD273^{low} HSPCs.

A) Representative flow cytometry plot (pseudocolour density plot) showing the mitochondrial potential using JC-1 staining of CD34+CD38-CD45RA-, CD273^{high} and CD273^{low} HSPCs. **B**) Comparison of mitochondrial potential in different HSPC subpopulations. *P* values were calculated using two-way ANOVA with Šídák's multiple comparisons test. P<0.0001 ****. Bars represent the mean with SEM.

3.7.4. CD273^{high} presented delayed entry into cell cycle

Higher mitochondrial potential can induce entry into cell cycle and cause proliferation and expansion of cells. To test the *in vitro* proliferation, 300 CD273^{high} and CD273^{low} HSPCs were seeded and cell counts were conducted on day 1, day 3, day 5 and day 7 (**Figure 31A**). Both populations showed similar expansion curves, with CD273^{low} HSPCs having a high expansion rate from day 1 to day 3 (**Figure 31B**). More accurate determination of cell-cycle behavior can be obtained via time-lapse microscopy-based single cell tracking. After culturing around 50 CD273^{high} and CD273^{low} cells per microwell for 7 days, the images can be used to track the timepoint of first division (entry into cell cycle with the transition from G0 to G1) (**Figure 31C**) (Eilken et al., 2009). Single-cell tracking revealed that CD273^{high} HSPCs displayed a delayed entry into cell cycle and first division (~58 h) as compared with their CD273^{low} counterparts (~70 h) (**Figure 31D**).

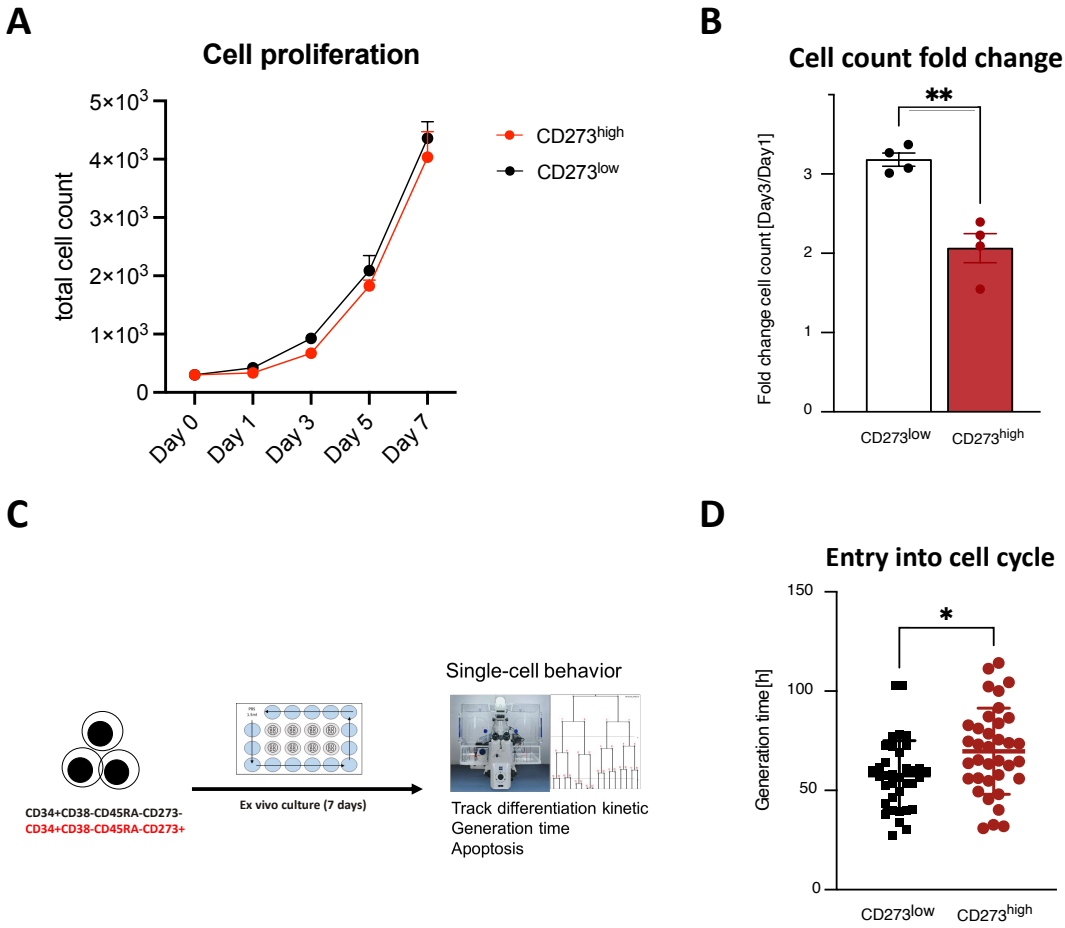

Figure 31. *In vitro* cell expansion and proliferation analysis of CD273^{high} and CD273^{low} HSPCs.

A) Cell proliferation of FACS-sorted CD273^{high} and CD273^{low} HSPCs (*n* = 4 donors) over 7 days *in vitro* culture. **B**) Fold expansion from day 1 to day 3 of cells from A. *P* values were calculated by two-tailed unpaired t-test. **C**) Workflow of videomicroscopy-based single-cell tracking. **D**) Single-cell tracking of FACS-sorted CD273^{high} and CD273^{low} HSPCs after 7 days *in vitro* culture (*n* > 35 cells). P values were calculated by two-tailed unpaired t-test. P<0.05 *, P<0.01 **. Bars represent means with SEM.

3.7.5. Transcriptomic analysis CD273^{high} versus CD273^{low} HSPCs

To gain further insight into the molecular signature of CD273^{high} and CD273^{low} HSPCs, bulk RNA-Seq was performed to assess potential alterations in gene expression profiles and expand the understanding of differentially regulated genes. Principal component analysis (PCA) was conducted to visualize variance within the dataset, with principal component 1 (PC1) explaining the highest proportion of variance and principal component 2 (PC2) the second highest (Ringnér, 2008). The analysis revealed distinct clustering of CD273^{high} and CD273^{low} HSPCs, with PC1 accounting for 66 % and PC2 for 19 % of the variance, indicating that these subpopulations possess distinct transcriptomic signatures (**Figure 32A**). The stem cell-associated genes *Thy1, DLK1, HOPX, BEX1, MLLT3, KLF4* and *MPL* exhibited increased expression levels in CD273^{high} HSPCs. In correlation with the previously observed delayed entry into cell cycle of CD273^{high} HSPCs, the early cell cycle regulator *CDK6* was significantly downregulated in this population (**Figure 32B**). Previous studies in the laboratory of John Dick demonstrated that the level *CDK6* regulates the exit of HSC quiescence, with

LT-HSCs lacing its expression and ST-HSCs already containing high *CDK6* protein levels enabling rapid cell cycle entry (Laurenti et al., 2015). These results were highly concordant with the gene expression measured in the previously presented Transcriptomic/AbSeq data set of early immature HSPCs, using similar hierarchical gating strategy for CD273^{high} and CD273^{low} HSPCs (**Figure 32C**). These transcriptomic changes between both HSPC subpopulation could be further confirmed by protein detection using the Simple Western system which is feasible for low input (Nguyen et al., 2011). CDK6 showed distinct protein upregulation in CD273^{low} HSPCs, whereas the stem cell markers HLF and ATP1B1 were slightly increased for CD273^{high} HSPCs, which is in accordance with the previously presented mRNA DEG analysis of HSC-1 vs HSC-2 cells (**Figure 32D**).

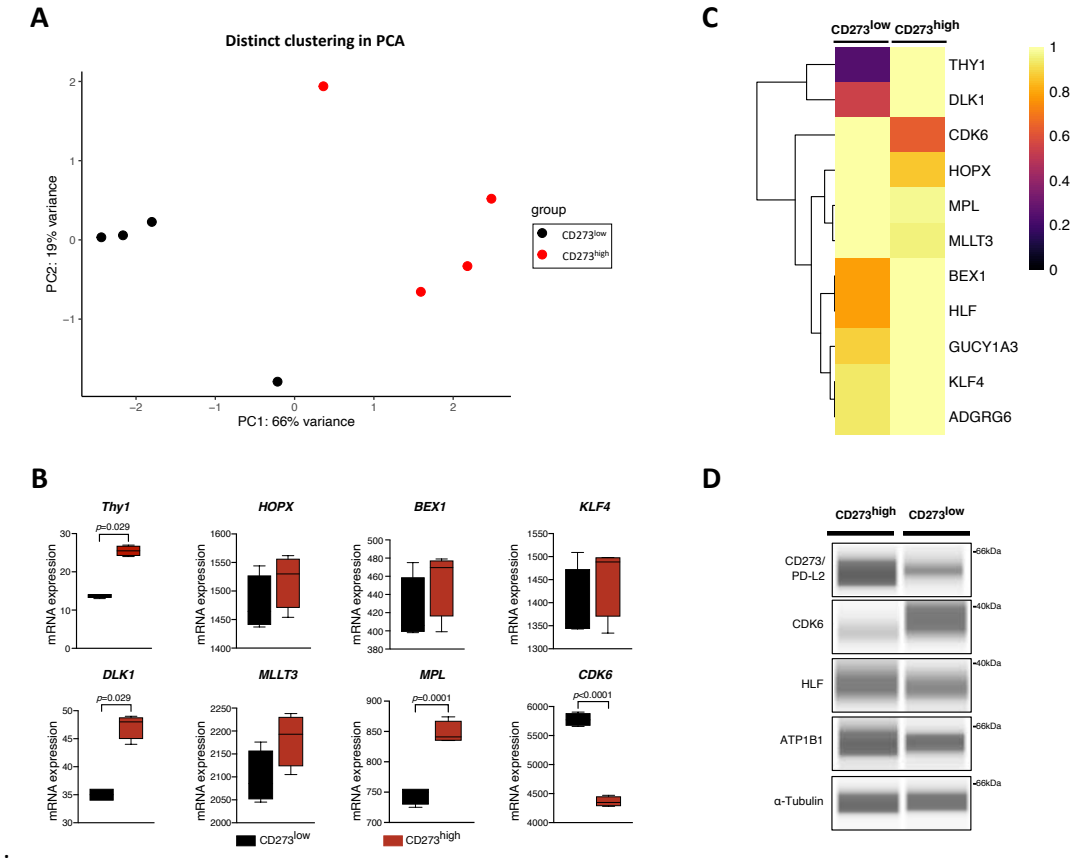

Figure 32.Transcriptomic and protein analysis of CD273^{high} and CD273^{low} HSPCs.

A) Principal component analysis (PCA) of transcriptome measured by bulk RNA-Seq of FACS-sorted CD273^{high} and CD273^{low} HSPCs (*n* = 4 donors). **B**) Expression of stem cell signature genes. Box extends from 25th–75th percentiles, marking the mean with a distinct line. The whiskers reach out to the maximum and minimum data point. Two-tailed Mann-Whitney test (*THY1, BEX1, KLF4, DLK1*) and two-tailed unpaired t-test (*HOPX, MLLT3, MPL, CDK6*). **C**) Expression of stem cell signature genes measured on hierarchically gated CD273^{high} and CD273l^{ow} HSPCs from AbSeq analysis showed the same pattern as bulk RNA-Seq in **B**. **D**) Protein expression of CD273 and stem cell-related marker proteins in FACS-sorted CD273^{high} and CD273^{low} HSPCs determined by Simple Western technology.

Taken together, the comprehensive functional validation of CD273^{high} HSPCs *in vitro* revealed several characteristics indicative for enhanced stemness. CD273^{high} HSPCs exhibited delayed differentiation kinetics, multipotent repopulating capacity, lower mitochondrial membrane potential and increased quiescence, as evidenced by delayed entry into the cell cycle. Moreover, CD273^{high} HSPCs displayed a

distinct molecular signature characterized by upregulation of stemness-associated genes, aligning with the presented single-cell transcriptomic dataset, corroborating the stem cell-like properties of CD273-expressing HSPCs. Although these assays confirm a more stemness characteristics of $CD273^{high}$ HSPCs, additional *in vivo* investigations will provide crucial evidence to validate the functional significance of CD273 expression in maintaining HSPC stemness and its potential role in hematopoietic hierarchy.

3.8. Xenotransplantation model showed no advantage of $CD273^{high}$ HSPCs in multilineage engraftment

Bona fide HSCs are characterized by their self-renewal ability and long-term multilineage reconstitution potential utilizing repopulation assays (GJ Spangrude, 1988). For the human compartment xenograft models using immunodeficient NSG mice (NOD-scid $IL2Rg^{null}$) are employed to determine immunophenotypes of human HSCs (Dick, 1996, 2008).

3.8.1. Engraftment chimerism in peripheral blood

To assess the multilineage reconstitution potential of CD273 expressing HSPCs, $CD34+CD273^{high}$ and $CD34+CD273^{low}$ subsets were isolated via FACS and transplanted into NSG mice. In parallel, CD34+ cells, representing the parental population, were sorted and treated with either a CD273/PD-L2 neutralizing antibody (referred to as: α-PD-L2) or an IgG control to determine the impact of CD273 signaling on engraftment efficiency. Since adult CD34+ HSPCs demonstrate significantly reduced engraftment potential in immunodeficient mice compared to fetal liver- or cord blood-derived CD34+ cells, a more heterogeneous parental population was selected to ensure sufficient cell numbers for experimental reproducibility (Rongvaux et al., 2014; Song et al., 2019). Each tested subpopulation was intravenously injected into sub-lethally irradiated NSG recipients, with five mice per group receiving 30,000 cells each. Engraftment and lineage reconstitution was analyzed every 4 weeks through PB analysis of transplanted recipients (**Figure 10**). To investigate the chimerism in the PB the proportion of human $CD45^+$ ($hCD45^+$) cells relative to murine $CD45^+$ ($mCD45^+$) cells within the viable cell population were quantified by flow cytometry (**Figure 33A**). Across all transplanted subpopulations, PB chimerism remained low over time, with $CD34+CD273^{low}$ exhibiting the highest engraftment efficiency, reaching 1.45 % at 8 weeks post-transplantation (wpt) (**Figure 33B**).

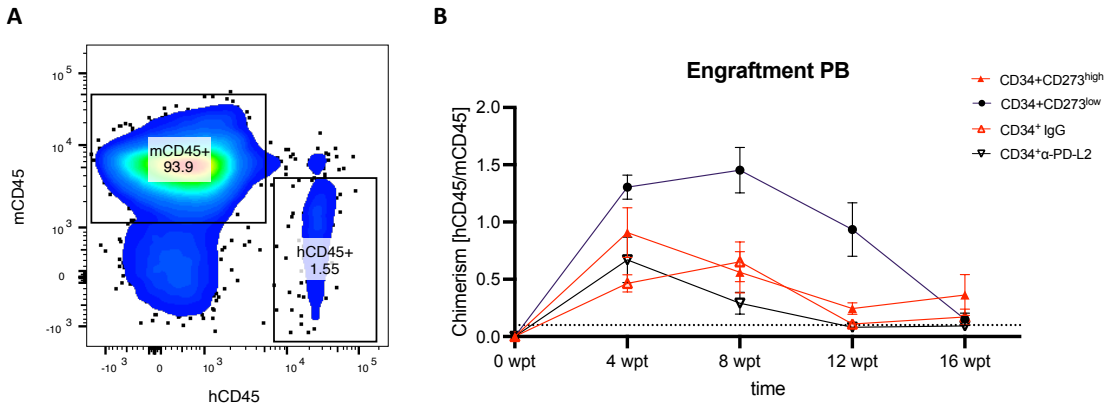

Figure 33. PB engraftment of CD273^{high}, CD273^{low} HSPCs and CD34+ cells treated with IgG or α-PD-L2 antibody.

A) Flow cytometry representation of mCD45+ and hCD45+ visualizing the chimerism in recipients. **B**) Engraftment kinetics of hCD45/mCD45 of NOD-SCID mice in peripheral blood (PB) over 16 weeks post transplantation (wpt) (*n* = 5 recipients). Four different group were transplanted as illustrated in **Figure 10**.

Lineage reconstitution was measured by monitoring the PB for myeloid cells (CD33+, **Figure 34A**), T-cells (CD3+, **Figure 34B**) and B-cells (CD19+, **Figure 34C**). The frequencies of these subsets were quantified as the proportion of lineage-positive cells relative to the total human CD45+ (hCD45+) population. In all groups, PB grafts demonstrated a predominance of myeloid cells within 4 wpt. Over time, a rapid decrease in myeloid cells relative to T- and B-cells was observed. B-cells reached their peak percentages at 12 wpt before declining. T-cells showed a gradual increase starting at week 12, with the highest percentage observed at 16 wpt. These observations align with previously published studies on long-term leukocyte reconstitution in NSG mice (Audigé et al., 2017; Wunderlich et al., 2018). Interestingly, CD34+CD273^{high} cells gave rise to more B-cells 16 wpt than CD34+CD273^{low} cells. Thus, no lineage bias in any of the reconstituted populations were detected.

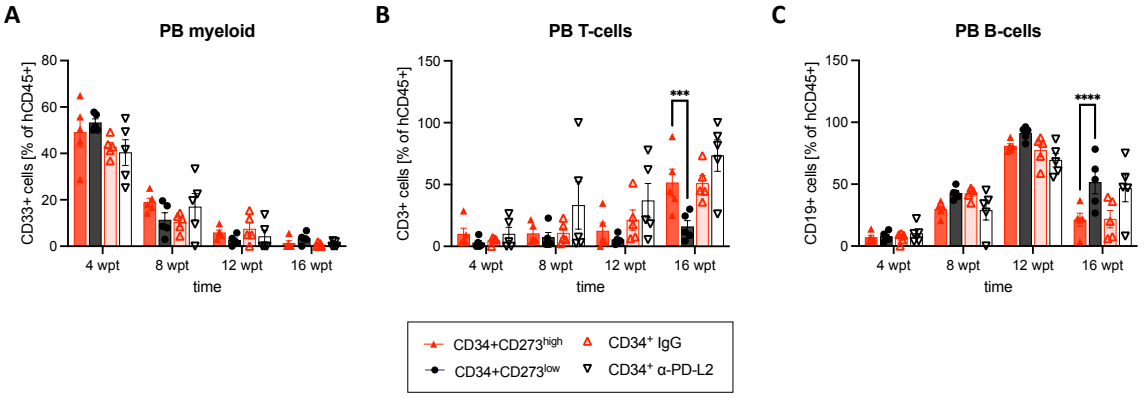

Figure 34. Lineage reconstitution in PB of CD273^{high}, CD273^{low} HSPCs and CD34+ cells treated with IgG or α-PD-L2 antibody.

Donor cell chimerism of leukocytes including myeloid cells (**A**), T-cells (**B**) and B-cells (**C**) in peripheral blood (PB) from recipients. Percentages of represented subpopulations were calculated from hCD45+ donor cells (*n* = 5 recipients). *P* values were calculated by two-way ANOVA with Šídák's multiple comparisons test. P<0.001 ***, P<0.0001 ****. Bars represent mean with SEM.

3.8.2. Endpoint analysis of BM and spleen

Endpoint analysis of xenotransplantation was performed 18 wpt. BM and spleens of all recipients were isolated and analyzed for engraftment chimerism and reconstitution of different lineages. In all transplanted groups, BM chimerism was relatively low, with CD34+CD273^{low} subpopulation showing the highest engraftment rate ~ 1 % (**Figure 35A**). Notably, lineage reconstitution in BM grafts showed a myeloid bias for CD34+CD273^{high} transplanted cells (**Figure 35B**). T-cells were negligible in the BM, which is in correlation with previous published studies in NSGs (Wunderlich et al., 2018). Analysis of distinct HSPC populations in the BM further validated the lineage bias of CD34^{+}CD273^{high} transplanted cells, which exhibited a significant increase in lymphoid-myeloid progenitors compared to other transplanted populations (**Figure 35C**). No significant differences were observed in other lineage compartments.

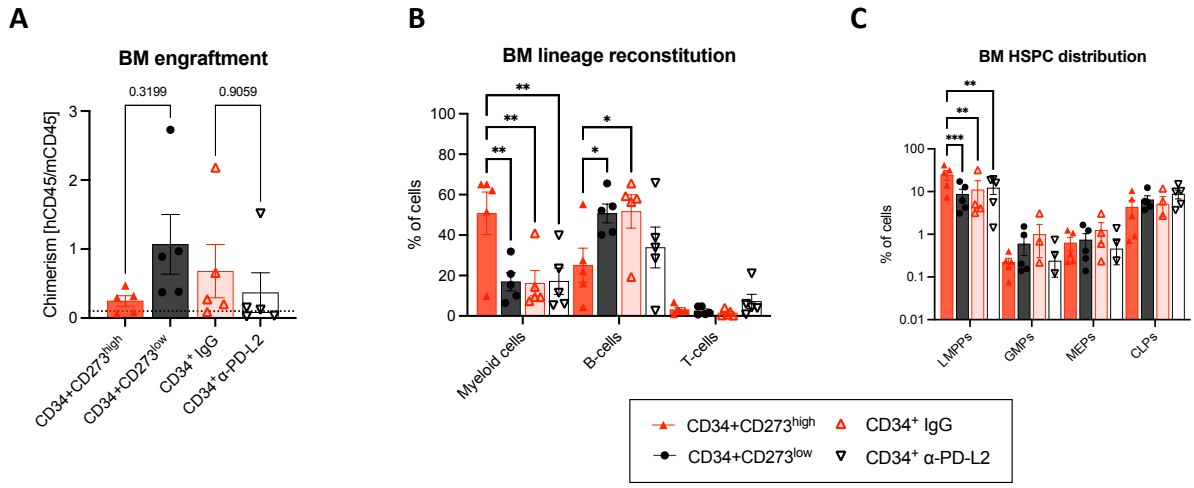

Figure 35. Engraftment and reconstitution in the BM of CD273^{high}, CD273^{low} HSPCs and CD34+ cells treated with IgG or α-PD-L2 antibody.

A) Bone marrow (BM) engraftment of hCD45/mCD45 cells 18 weeks post transplantation. **B**) Percentage of lineage reconstitution in the BM of recipients. **C**) Distribution of hematopoietic stem and progenitor populations in the BM. P values were calculated by two-way ANOVA with Šídák's multiple comparisons test. P<0.05 *, P<0.01 **, P<0.001 ***. Bars represent mean with SEM (*n* = 5 recipients).

NSG mice exhibit a small spleen, due to their immunodeficiency and lack of mature lymphoid lineages but still function as primary organs for hematopoietic engraftment (Blümich et al., 2021; Santagostino et al., 2017). Therefore, spleens of transplanted recipients were analyzed for cell number (**Figure 36A**), weight (**Figure 36B**), engraftment (**Figure 36C**) and lineage reconstitution (**Figure 36D**). Although CD34+CD273^{low} recipients showed a significant higher cell number in the spleen, these findings could not be supported by the spleen weight, which showed no differences between groups. Spleen chimerism showed no engraftment advantage of any transplanted subpopulation. Interestingly, B-cell reconstitution was higher for CD34+CD273^{low} and CD34+IgG HSPCs with 15 – 16 % for both groups, compared to >5 % in the other two groups. Overall, spleens showed low myeloid reconstitution in the spleen, whereas lymphoid cells

displayed high reconstitution potential which was reported in previous studies (Audigé et al., 2017; Wunderlich et al., 2018).

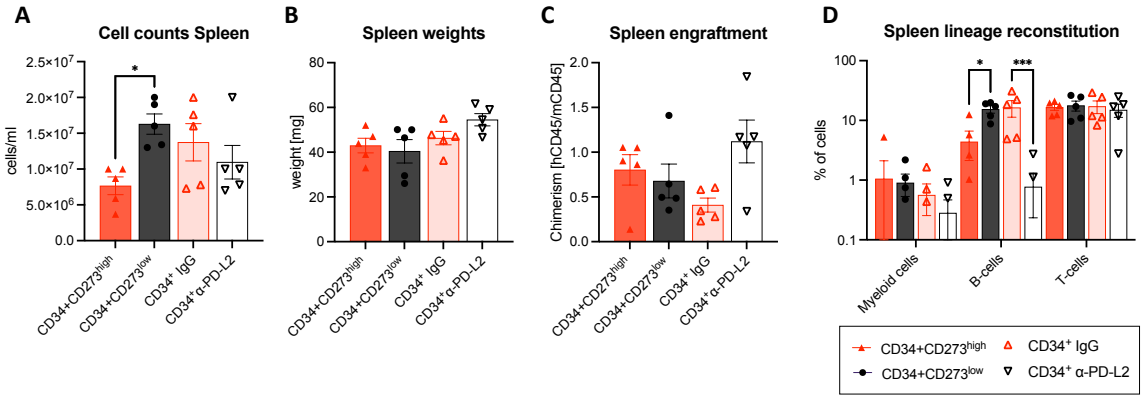

Figure 36. Engraftment and lineage reconstitution in the spleen of CD273^{high}, CD273^{low} HSPCs and CD34+ cells treated with IgG or α-PD-L2 antibody.

A) Cell counts of spleens. **B**) Weight of spleens. **C**) Spleen engraftment of hCD45/mCD45 cells 18 weeks post transplantation. **D**) Percentage of lineage reconstitution in the spleen recipients. *P* values were calculated by two-way ANOVA with Šídák's multiple comparisons test. P<0.05 *, P<0.001 ***. Bars represent mean with SEM (*n* = 5 recipients).

Despite the enhanced stemness characteristics observed *in vitro*, the following *in vivo* analysis in NSG mice did not demonstrate increased engraftment potential of CD273^{high} HSPCs, highlighting the complexity of stem cell behavior in different environments. To reconcile these findings and further elucidate the role of CD273, we next investigated its expression under pro-inflammatory cell culture conditions, which may more closely mimic stress-induced hematopoiesis and reveal context-dependent functions of this marker.

3.9. Upregulation of CD273 in pro-inflammatory culture

Studies by Passegué and collogues revealed that TNF-α promotes HSC survival by activating a NF- kB-dependent gene program which leads to an upregulation of CD273/PD-L2 on murine HSCs mediating a pro-survival mechanism (Yamashita & Passegué, 2019). To investigate the impact of TNF-α on HSPCs, CD34+ cells isolated from mPB samples were cultured *in vitro* for seven days with or without 1 µg/mL TNF-α. In the absence of TNF-α, CD273 expression exhibited only a modest increase over time (**Figure 37A + B**). Similarly, exposure to TNF-α resulted in a 1.5-fold upregulation of CD273 expression in relative proportion to the expression level of untreated HSPCs on day of culture (**Figure 37C + D**).

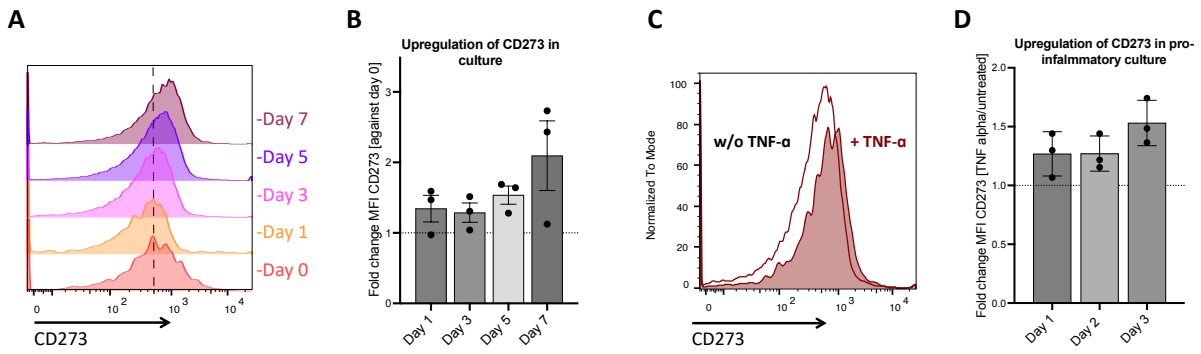

Figure 37. CD273 expression upon steady-state and pro-inflammatory *in vitro* culture.

A) Histogram of CD273 expression on CD34+ MACS-enriched samples from mobilized peripheral blood (mPB) over 7 days *in vitro* culture. **B**) MFI fold change of CD273 in culture calculated against expression on day 0 (n = 3 donors). **C**) Histogram of CD273 expression on CD34+ MACS-enriched samples cultured ± TNFα for 3 days. **D**) MFI fold change of CD273 on TNFα treated samples vs. untreated samples (n = 3 donors). Bars represent the mean with SEM.

The observed upregulation of CD273 on human HSPCs under pro-inflammatory culture conditions suggests a potential immunomodulatory survival mechanism in stress-induced environments as reported for the murine compartment. This finding is particularly intriguing given CD273's role as an inhibitory ligand for the programmed cell death receptor 1 (PD-1), a well-established immune checkpoint (Latchman et al., 2001). This connection opens a novel avenue for investigating CD273-expressing HSPCs in the context of their immunomodulatory capabilities.

3.10. The immunomodulatory role of CD273/PD-L2 on HSPCs

Immune checkpoint blockade has emerged as a pivotal focus in cancer research, with numerous therapeutic approaches targeting PD-1 and its ligands. These molecules play a crucial role in mediating cancer cell immune escape and impacting the overall prognosis, varying across different cancer types and microenvironments (He & Xu, 2020; Jia et al., 2018; Topalian et al., 2015). As a second ligand to PD-1, CD273/PD-L2 expressing HSPCs should be investigated in their immunomodulating function. STRING network analysis of CD273 revealed significant pathway enrichments associated with the regulation of T-cell proliferation and activation (**Figure 38A+B**). To evaluate these functionalities, a mixed lymphocyte reaction (MLR) assay was performed by co-culturing CD34+ HSPCs and allogeneic T-cells isolated from healthy donors. Donor-individual HSPCs were pre-treated with a neutralizing CD273/PD-L2 antibody or an IgG isotype control and co-cultured with unmatched T-cells isolated from another donor, leading to individual allogeneic pairs. The co-cultured cells were compared to control conditions, where T-cells were cultured without HSPCs. All conditions were cultured for three days as outlined in **chapter 2.2.1.4**.

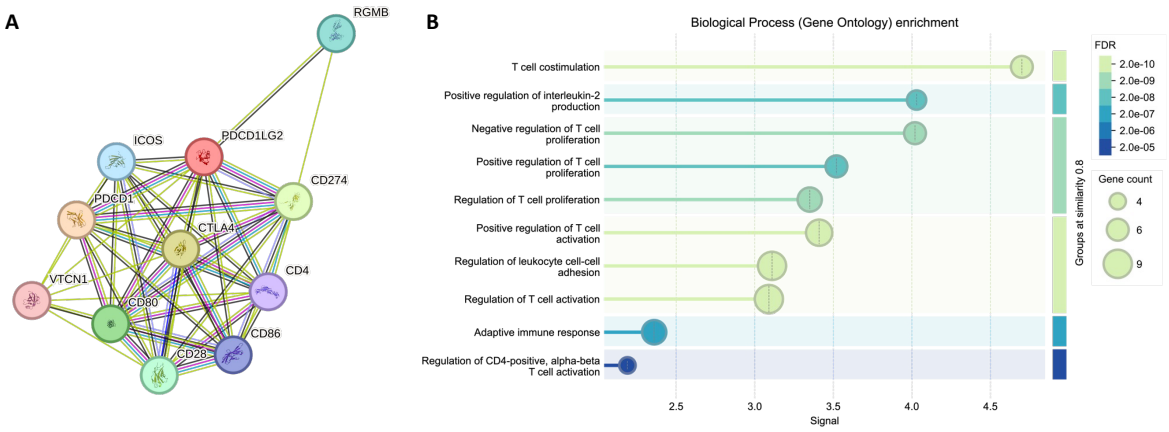

Figure 38. STRING analysis of PDCD1LG2 (CD273/PD-L2).

A-B) The protein network of the programmed cell death 1 ligand 2 (PDCD1LG2/CD273/PD-L2) interacts as direct ligand with programmed cell death protein 1 (PDCD1) and the repulsive guidance molecule B (RGMB) (**A**) and shows high immunomodulating functions for the T-cell compartment, regulating their activation and proliferation (**B**)(von Mering et al., 2005).

3.10.1. Neutralization of CD273/PD-L2 increases activation and proliferation of T-cells

To monitor the effects of CD273/PD-L2 neutralization on co-cultured T-cells, activation of CD8+ T-cells was measured via flow cytometry after 3 days of culture (**Figure 39A**). The expression level of the activation marker CD69 on CD8+ T-cells was significantly increased compared to the IgG control and the mono-cultured T-cells (**Figure 39B**).

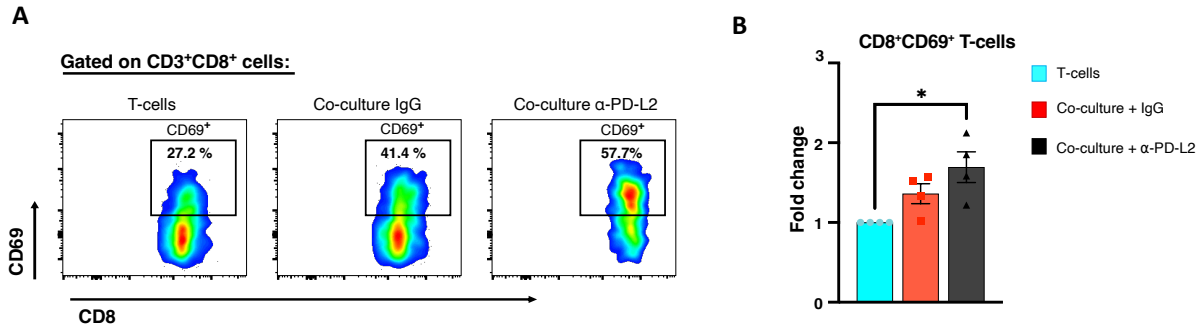

Figure 39. Increased activation of CD8+ T-cells upon CD273/PD-L2 neutralization.

A) Representative flow cytometry plots (pseudocolour density) of CD69 expression on CD8+ T-cells in different culture conditions. **B**) Percentage of T-cell activation measured as displayed in A (n = 4 donors). P values were calculated by one-way ANOVA with Holm-Šídák's multiple comparisons test. P<0.05 *. Bars represent mean with SEM.

Besides T-cell activation, gene ontology analysis suggested an influence of PD-L2 on T-cell proliferation. To monitor T-cell expansion dynamics in distinct T-cell subtypes over time during co-culture, T-cells were stained with CSFE (CellTrace™) and cell surface markers (**Figure 40A**). The number of generations was tracked on day 3 of co-culture in CD4+ and CD8+ T-cells. The co-culture with HSPCs suppressed the proliferation of CD8+ T-cells in comparison to T-cells alone. Importantly, increased CD8+ T-cell proliferation

was effectively rescued by blocking CD273/PD-L2 (**Figure 40B**). This observation suggests that HSPCs suppress CD8+ T-cell proliferation through PD-L2 interactions. In contrast, the proliferation of CD4+ T-cells was not altered by the MLR itself, indicating that CD4+ T-cells might not be as sensitive to HSPC-mediated suppression as CD8+ T-cells under these conditions. However, when CD273/PD-L2 was blocked, there was a marked increase in CD4+ T-cell proliferation. This suggests a delicate balance between T-cell stimulation and suppression within the co-culture environment, and that blocking CD273/PD-L2 may tip this balance towards stronger CD4+ T-cell activation.

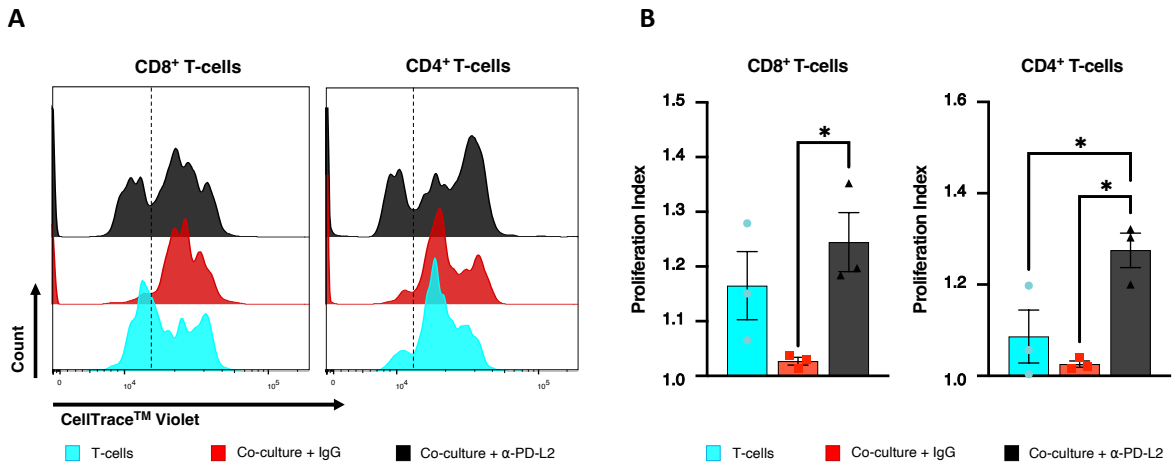

Figure 40. Increased proliferation of T-cells upon CD273/PD-L2 neutralization.

A) Proliferation of CD4+ and CD8+ T-cells by CFSE labeling. **B**) Proliferation index of CD4+ and CD8+ T-cells (*n* = 3 donors). *P* values were calculated by one-way ANOVA with with Holm-Šídák's multiple comparisons test. P<0.05 *. Bars represent mean with SEM.

Increased T-cell activation and expansion mediated by an inflammatory reaction needs to return to steady state cell numbers to inhibit chronic inflammation. Therefore, T-cell apoptosis is critical to terminate inflammation (Orteu et al., 1998). In has been reported that activated T-cells in MLR assays upregulate the expression of the pro-apoptotic enzyme caspase 8 (*FLICE*) within 3 days of co-culturing (O'Flaherty et al., 2000). To test the apoptosis regulation in the presented MLR assay, T-cells were stained with 7-AAD and Annexin V staining and distribution of living, apoptotic and dead cells was exploited via flow cytometry (**Figure 41A**). The analysis displayed a decreased percentage of viable cells for co-cultured CD4+ and CD8+ T-cells compared to mono-cultured T-cells. Notably, CD273/PD-L2 neutralization did not influence the survival rate and showed similar proportions as IgG control (**Figure 41B**). Similar effects could be detected by total cell counts, presenting a decreased overall cell number for co-culture setting (**Figure 41C**).

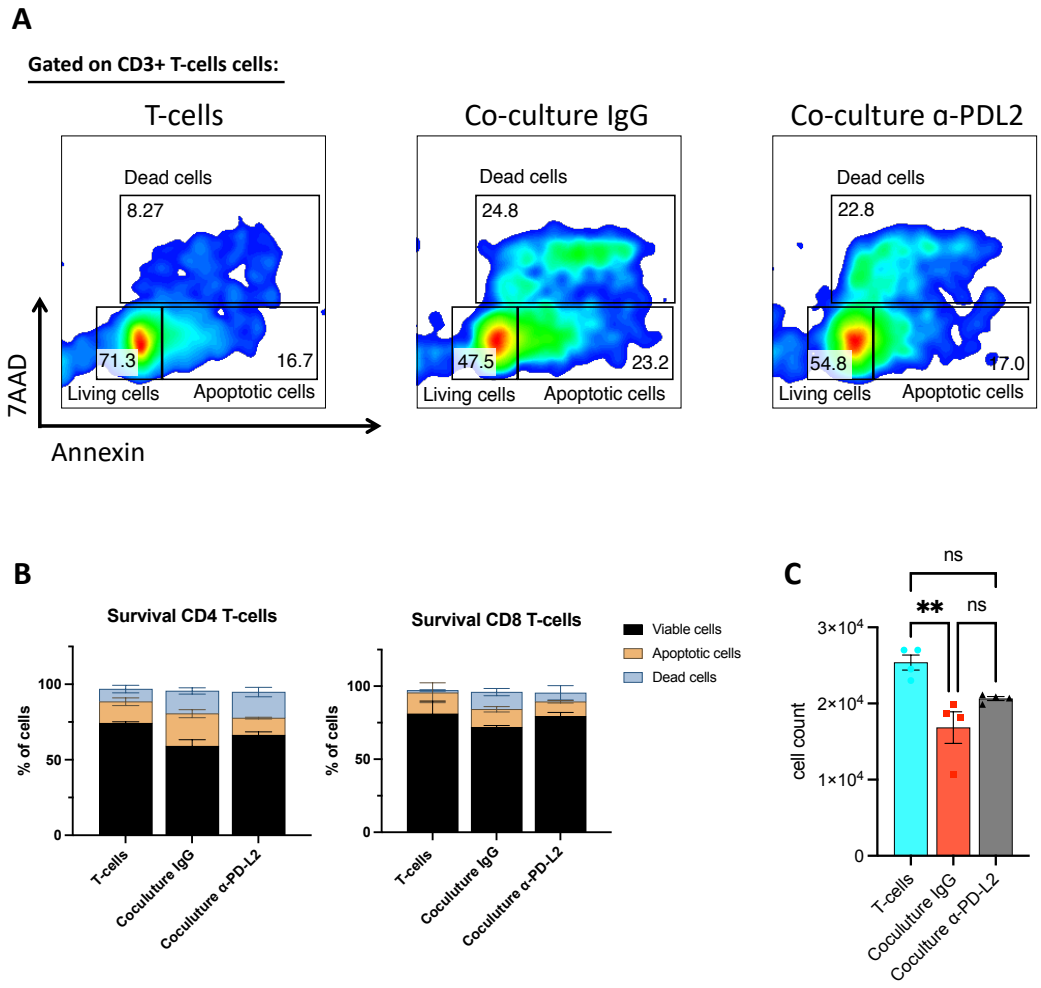

Figure 41. Survival of T-cell in MLR assay.

A) Representative flow cytometry plot (pseudocolour density) of 7AAD/Annexin staining for CD3+ T-cells in different MLR assay conditions. **B**) Percentage of CD4+ and CD8+ T-cells survival detected by 7AAD/Annexin staining in MLR assay conditions. **C**) Cell counts of MLR assay *P* values were calculated by one-way ANOVA with Turkey's multiple comparisons test. No significance = ns, *P*<0.01 **. Bars represent mean with SEM.

3.10.2. Neutralization of CD273/PD-L2 increases Tregs abundance and proinflammatory cytokine release

MLR assays with monocyte-derived dendritic cells (MoDcs) and T-cells from another donor alter the cell composition and abundance of central memory T-cells (TEM), as well as regulatory T-cells (Tregs) (Mangelinck et al., 2023). To check whether the previously described experimental settings could correspond to these findings, different T-cell subtypes were analyzed by flow cytometry. CD273/PD-L2 blockade resulted in a notable reduction of the fraction of CD4+CD25hiFOXP3+ Tregs (**Figure 42A + B**). These findings suggest that CD273/PD-L2 may contribute to immune suppression through two complementary mechanisms: (**1**) direct inhibition of T-cell activation via receptor-ligand interaction, and (**2**) indirect modulation through the induction and expansion of Tregs. To further investigate the impact of HSPC co-culture on memory T-cell subsets, flow cytometric analysis was performed. The results revealed a reduction naïve T-cell (TN) and central memory T-cell (TCM) populations, while effector memory T-cells (TEM)

increased upon MLR, indicating that HSPC contact drives T-cell differentiation toward more activated phenotypes (**Figure 42C**).

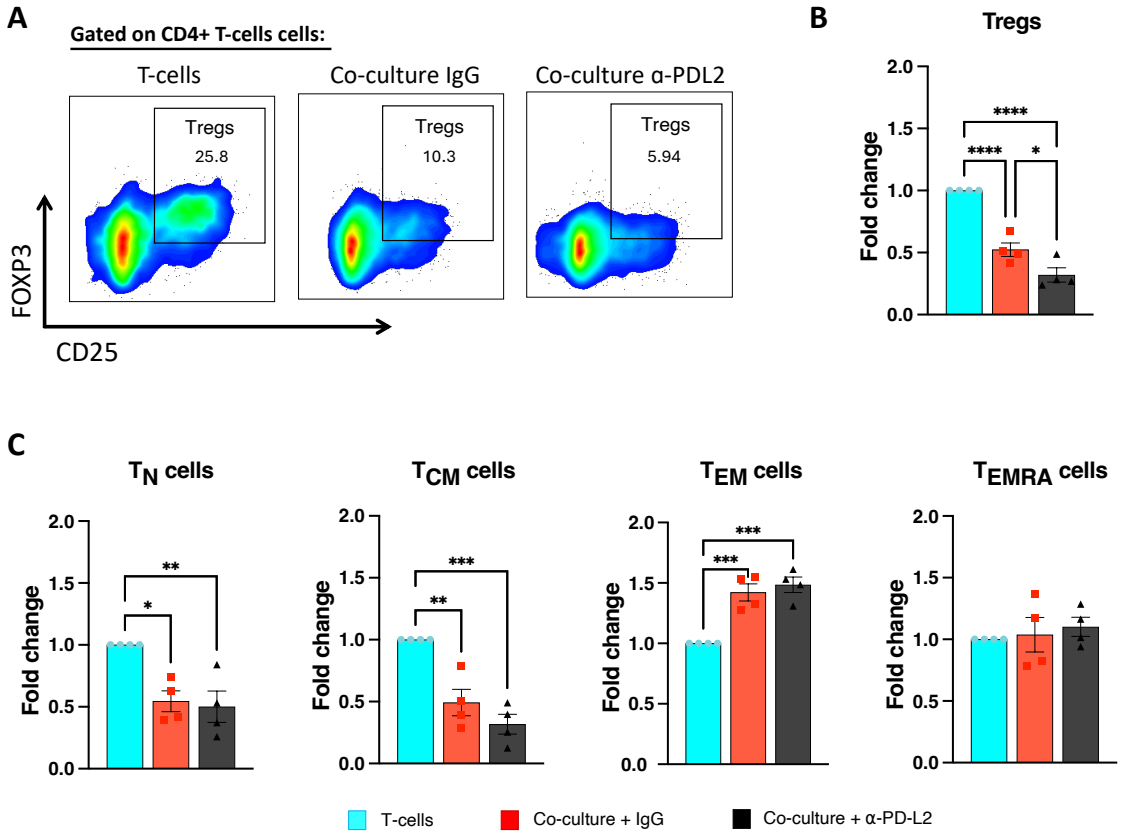

Figure 42. Proportion of different T-cell subsets in MLR assay.

A) Representative flow cytometry plot (pseudocolour density) of regulatory T-cell (Tregs) proportion in MLR assay. **B**) Percentage of Tregs relative to T-cell mono-culture. **C**) T-cell subtype abundance relative to T-cell mono-culture (n = 4 donors). T_N naïve T-cells, T_{CM} central memory T-cells; T_{EM} effector memory T-cells; T_{EMRA} terminally differentiated effector memory T-cells. One-way ANOVA with Holm-Šídák's multiple comparisons test. No significance = ns, P<0.05 *, P<0.01 **, P<0.001 ***, P<0.0001 ****. Bars represent mean with SEM.

To substantiate phenotypic changes in T-cell subsets, T-cell function was evaluated by analyzing cytokine levels in the supernatants of the co-cultures using multi-cytokine assays (**Figure 43**). Levels of the T-cell activation-associated cytokines IFN-γ, TNF-α, and IL-6 were elevated in CD273/PD-L2-blocked co-cultures compared to T-cell mono-cultures. In contrast, co-culture of T cells with HSPCs led to reduced secretion of the pro-inflammatory cytokine IL-17A, whereas neutralization of CD273/PD-L2 significantly increased IL-17A production. These results support the notion that CD273/PD-L2 interactions contribute to the establishment of an immunosuppressive microenvironment, characterized by dampened T-cell activation and inflammatory cytokine release.

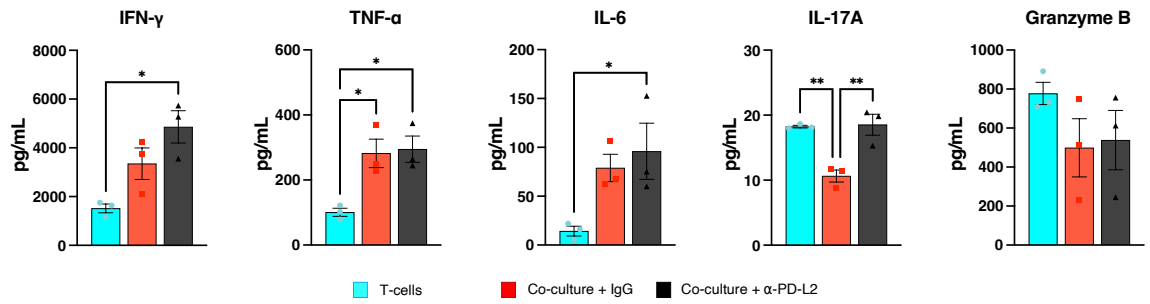

Figure 43. Cytokine secretion in MLR assay.

Cytokine-bead array assay of co-cultured and mono-cultured T-cell supernatant (*n* = 3 donors). One-way ANOA with Turkey's multiple comparison test. No significance = ns, *P*<0.05 *, *P*<0.01 **. All bars represent the mean with SEM.

3.10.3. Co-cultured HSPCs showed increased myeloid lineage differentiation and decreased stem-cell phenotype

Multiple studies have shown that pro-inflammatory cytokines influence HSC activation and differentiation to enable a dynamic response toward inflammation and emergency hematopoiesis (Baldridge et al., 2010b; De Bruin et al., 2013; Yamashita & Passegué, 2019; J. L. Zhao et al., 2014). By staining the HSPCs for CD34, CD133, and CD45RA, different progenitor subpopulations (HSCs/MPPs, LMPPs, EMPs and GMPs) could be distinguished from each other (Radtke et al., 2016) (**Figure 44B**). Flow cytometry analysis revealed enhanced myelopoiesis, characterized by increased frequencies of GMPs and LMPPs, upon co-culture of HSPCs with allogeneic T-cells (**Figure 44A**). This observation was further corroborated by cytokine quantification, which showed a significant upregulation of granulocyte-monocyte colony-stimulating factor (GM-CSF) in the supernatant of co-cultured HSPCs—a cytokine absent in mono-cultured HSPCs—explaining the elevated abundance of myeloid cell types (**Figure 44C**) (R. A. Lang et al., 1987; Metcalf et al., 1986; Regan-Komito et al., 2020). Interestingly, CD34+CD133+CD45RA− cells, which are phenotypically used to define HSCs and MPPs, showed reduced proportions in mono-cultured HSPCs. This finding contrasts with the expected reduction in differentiation in monoculture conditions and may point to technical limitations of the current approach, as well as highlight the need to incorporate additional markers in future analyses to achieve a more accurate and comprehensive characterization of HSPC subpopulations.

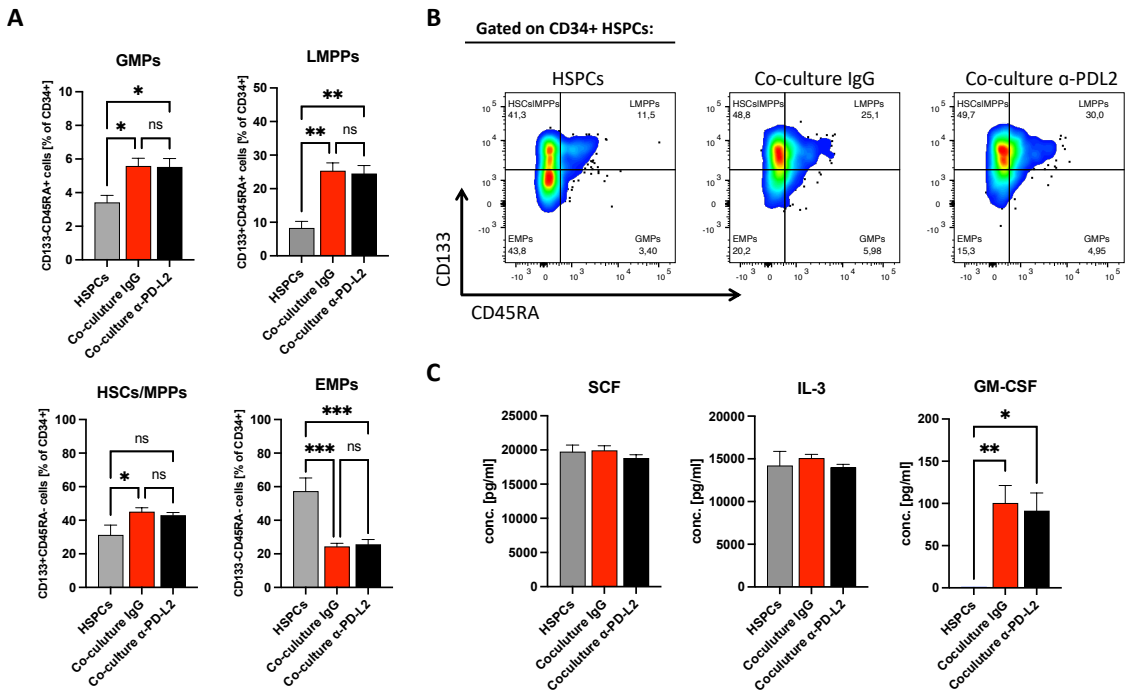

Figure 44. HSPC differentiation in MLR assay.

A) Distribution of HSPC subpopulations in MLR assay (*n* = 4 donors). GMPs = granulocyte-macrophage progenitor; LMPPs= lympho-myeloid primed progenitor; HSCs/MPPs= hematopoietic stem cells/ multipotent progenitors; EMPs = erythro-myeloid progenitor. *P* values were calculated by one-way ANOVA with Turkey's multiple comparison. **B**) Representative flow cytometry plot (pseudocolour density) of HSPC subpopulation in different MLR assay conditions presented in A. **C**) Cytokine- bead array assay of co-cultured and mono-cultured HSPCs (*n* = 4 donors). *P* values were calculated by one-way ANOVA with Turkey's multiple comparison. No significance = ns, P<0.05 *, P<0.01 **, P<0.001 ***, P<0.0001 ****. Bars represent mean with SEM.

The presented study demonstrated the immune-modulatory role of CD273/PD-L2 on HSPCs in suppressing T-cell activation, proliferation and decrease the abundance of Tregs through MLR assays. Building on these findings, single-cell proteo-transcriptomic analysis were utilized to uncover the molecular mechanisms underlying CD273/PD-L2 expression and its impact on HSPC differentiation and function.

3.11. Proteo-transcriptomic analysis of MLR assay

3.11.1. HSPCs and T-cells showed distinct clustering in dimensional reduction

To elucidate molecular mechanisms underlying HSPC-T cell interactions in MLR, a multi-modal single-cell analysis of three allogeneic donor pairs was conducted (**Table 19**). Monocultured and co-cultured HSPC-T-cell systems were profiled using whole-transcriptome sequencing paired with AbSeq proteomics, encompassing 86 surface markers (**Table 12**). Integrated analysis of 23,214 cells revealed distinct transcriptional states between HSPCs and T cells through unsupervised clustering (**Figure 45A**). Notably, co-cultured HSPCs exhibited significant transcriptomic remodeling compared to monocultures (**Figure 45B**). Unexpectedly, PD-L2-blocked co-cultures preserved cluster architecture compared to IgG controls, despite functional suppression of T cell activation observed in parallel assays (**Figure 39 + Figure 40**).

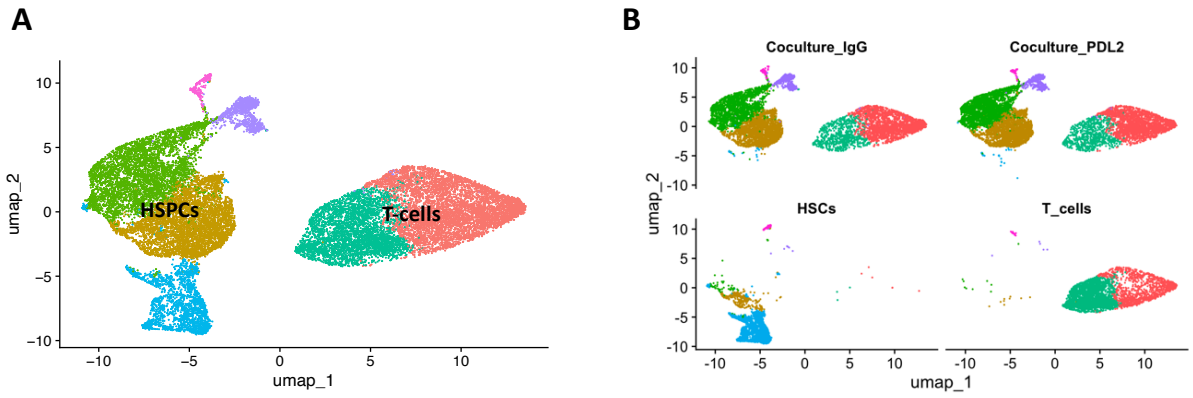

Figure 45. UMAP projection of MLR assay.

A) UMAP projection of 23,281 cells from MLR assay visualizing seurat clusters distribution. **B**) Separated UMAPs of different culture conditions in MLR assay.

3.11.2. Transcriptomic analysis confirmed delayed proliferation and activation of co-cultured T-cells

To further investigate the functional dynamics of co-cultured T-cells, a multi-tiered analytical approach was applied and T-cells were subsetted for subsequent re-analysis and re-clustering (data not shown). For robust cell type classification, we utilized the *Azimuth()* function within the Seurat computational framework. This algorithm implements a reference-based annotation strategy, leveraging curated datasets from both PBMCs (Hao et al., 2021) and BM (Granja et al., 2019; Oetjen et al., 2018) to assign probabilistic cell type identities (Stuart et al., 2019). The computational label transfer analysis corroborated with the *in vitro* MLR assay findings, demonstrating a reduced abundance of proliferating CD8+ T-cells in T-cell populations cultured with IgG control, which was reversed by PD-L2 neutralization (**Figure 46A**). Notably, an increase in T_{EM}-cells was observed following PD-L2 blockade, implicating an enhanced inflammatory reaction (**Figure 46B**). Gene set enrichment analysis (GSEA) comparing mono-cultured and co-cultured T-cells revealed upregulated pathways associated with T-cell differentiation and activation, aligning with the previously presented data (**Figure 46C**). Differential gene expression analysis corroborated the enhanced proliferative capacity of mono-cultured T-cells versus T-cells co-cultured with HSPCs (IgG) in the experimental system (**Figure 46D**). A significant upregulation of key cell cycle regulators could be observed, including the proliferation marker *MKI67*, DNA synthesis initiators thymidine kinase 1 (*TK1*), cyclins A2 (*CCNA2*), B2 (*CCNB2*) and D1 (*CDK1*), as well as the mitotic regulator polo-like kinase 1 (*PLK1*) (Gerdes et al., 1983; Gobran et al., 2025; J. M. Li et al., 2021; Pines & Hunter, 1991). Notably, co-cultured T-cells exhibited significant upregulation of HLA-B and HLA-C, key components of the MHC class I complex. Recent studies have demonstrated that enhanced expression of MHC class I molecules confers a survival advantage to neoplastic T-cells in malignant settings. This upregulation may represent an adaptive mechanism in co-cultured T-cells, potentially increasing their resistance to cell death and enhancing their persistence in the inflammatory microenvironment (Chang et al., 2024). Additionally, an upregulation of growth arrest was

noted and DNA damage-inducible proteins GADD45A and GADD45B, which are signatures for pro-inflammatory signals in T-cells and mediate cell cycle arrest, were elevated (B. Lu et al., 2004; Salvador et al., 2005). Interestingly, the long non-coding RNA *MALAT1* showed differential expression between conditions, with its upregulation in co-cultured cells aligning with recent findings associating *MALAT1* suppression with T-cell activation and proliferation (Dey et al., 2023). These molecular profiles provide compelling evidence for the divergent functional states of T-cells under mono-culture and co-culture conditions. These findings not only validate the proliferative response in the co-culture setting but also offer insights into the maintenance of a more naïve T-cell population in mono-culture. This comprehensive gene expression analysis enhances our understanding of T-cell activation dynamics and may inform future strategies for modulating T-cell responses in various immunological contexts. Surface proteome analysis further supported the displayed findings, showing increased expression of key activation markers in co-cultured T-cells. These included components of the TCR complex (CD3ε/ζ), the early activation marker CD69 (as shown in **Figure 39**), the adhesion molecule CD2, and the co-stimulatory receptor CD275 (ICOS) (**Figure 46E**). This expression pattern is consistent with *in vitro* data, indicating robust T-cell activation in the co-culture condition. Interestingly, mono-cultured T-cells exhibited the highest expression of several markers, including the pan-T-cell marker CD3, lineage markers CD4 and CD8, the IL-2 receptor alpha chain CD25, the B7 family member CD80, the IL-7 receptor alpha chain CD127, and the co-stimulatory molecule CD278 (ICOS-L). Notably, the exhaustion marker CD279 (PD-1) was also elevated in mono-cultured T-cells (Y. Liu et al., 2020). This distinct expression profile in mono-cultured T-cells suggests a complex interplay of activation, regulation, and potential exhaustion mechanisms in the absence of allogenic stimulation typical of MLR assays. These findings collectively provide a comprehensive view of T-cell dynamics in the depicted experimental system, highlighting the impact of PD-L2 blockade on T-cell proliferation and differentiation, while also revealing nuanced differences in activation states between mono-cultured and co-cultured T-cells.

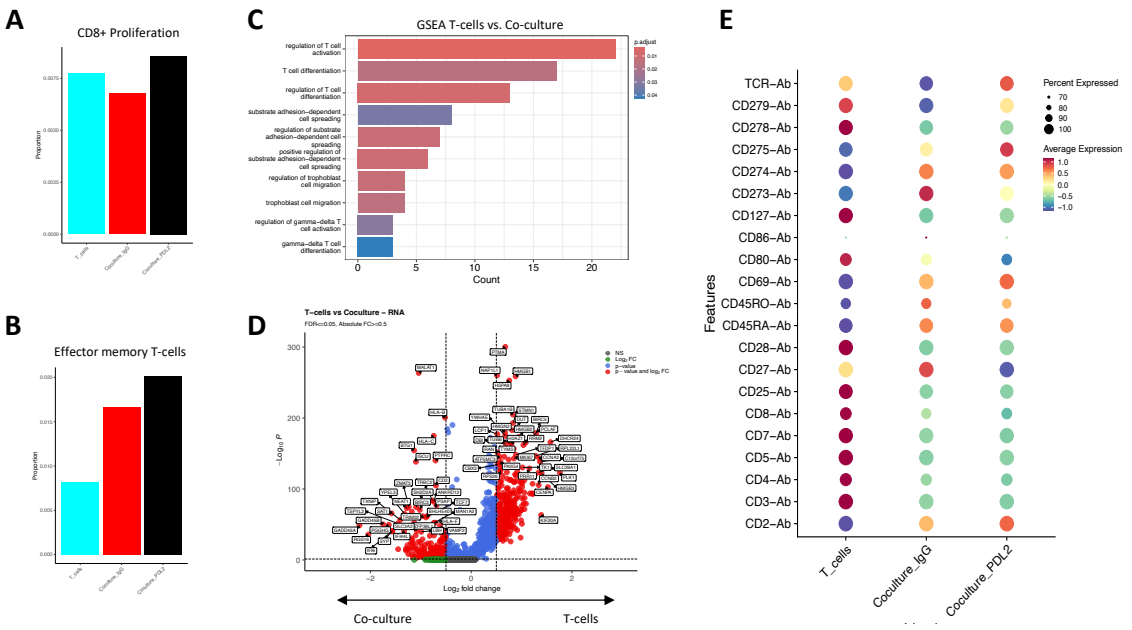

Figure 46. Analysis of T-cells in MLR assay.

A-B) Label transfer performed with reference dataset displayed increased abundance of proliferating CD8+ T-cells (**A**) and effector memory T-cells (**B**) in presence of PD-L2 neutralization antibody. **C**) GSEA analysis of co-cultured T-cells vs. mono-cultured T-cells. **D**) Differential gene analysis of T-cells vs. Coculture. **E**) Dotplot of T-cell specific AbSeqs.

3.11.3. HSPCs co-cultured with unmatched T-cells showed distinct clustering, myeloid differentiation and upregulation of pro-inflammatory regulators

HSPCs exhibited a distinct differentiation profile *in vitro*, prompting a detailed multi-omic analysis similar to that previously performed on T-cells. Re-clustering of 3,890 HSPCs revealed clear segregation between mono-cultured and co-cultured populations (**Figure 47A**). Surface proteome analysis demonstrated high expression of CD34 and the stem cell marker CD117 (c-Kit) for mono-cultured HSPCs (**Figure 47B**). Notably, HSPCs treated with PD-L2 neutralizing antibodies showed elevated expression of the differentiation marker CD45RA and the myeloid progenitor marker CD33. These findings suggest that PD-L2 blockade may influence HSPC differentiation trajectories, potentially favoring myeloid lineage commitment.

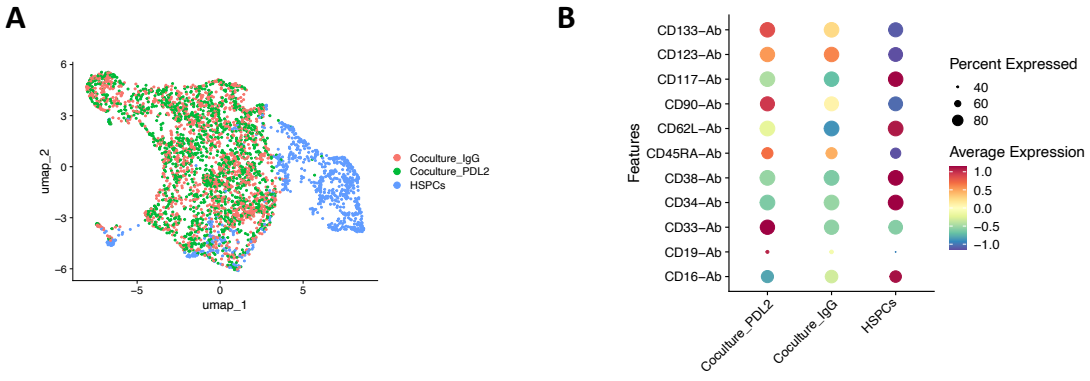

Figure 47. Analysis of HSPCs in MLR assay.

A) UMAP projection of 3,890 sub-clustered HSPCs. **B**) Dotplot of HSPC specific AbSeqs.

Differential gene expression analysis revealed a highly upregulated transcriptomic signature in co-cultured HSPCs (**Figure 48A**). Among the most prominently upregulated genes were MHC class II molecules, including *HLA-DR86, HLA-E, HLA-DOA*, and *HLA-DMA*. This suggests an immunological role for co-cultured HSPCs, consistent with recent findings that murine HSCs express MHC class II molecules and can function as APCs, actively interacting with CD4+ T cells to modulate adaptive immune responses (Hernández-Malmierca et al., 2022). These observations further underline the potential of HSPCs to act as active participants in immune regulation, rather than passive contributors to hematopoiesis. Additionally, genes driving hematopoietic differentiation, such as Runt-related transcription factor 3 (*RUNX3*), Colony Stimulating Factor 2 Receptor Beta (*CSF2RB*), Kruppel-like transcription factor-6 (*KLF6*), Galectin-3-binding protein (*LGALS3BP*) and the non-coding RNA miR-155 were significantly upregulated in co-cultured HSPCs. These genes are known to regulate lineage commitment and differentiation pathways, particularly favoring myeloid-specific development (Balogh et al., 2020; Carrelha et al., 2024; El Bannoudi et al., 2023; Goodman et al., 2016; Hung et al., 2020; O'Connell et al., 2008; Van Overmeire et al., 2016; Zafar et al., 2021). This aligns with the GSEA results that demonstrated coordinated regulation of myeloid differentiation pathways, consistent with pro-inflammatory responses and a myeloid bias for immune defense mechanisms (Yamashita & Passegué, 2019) (**Figure 48B**). In contrast, mono-cultured HSPCs showed elevated expression of canonical stem cell markers such as CD34, LIM domain only 2 (*LMO2*), and brain and acute leukemia cytoplasmic protein (*BAALC*) (Baldus et al., 2003; Chin et al., 2018; Zhu et al., 2005). These markers were accompanied by upregulation of genes influencing stemness, including *SPINK2*, *SOCS2*, *CDK6*, *BEX1* and *CEBPA* which are genes upregulated in the HSC-1/HSC-2 clusters (**Figure 23 + Table Appendix 1**). Together, these findings suggest that mono-cultured HSPCs maintain a more primitive, quiescent phenotype associated with self-renewal and long-term hematopoietic potential. These results provide compelling evidence for the functional plasticity of HSPCs under different culture conditions. Co-culture promotes differentiation and immune activation through MHC class II-mediated antigen presentation and myeloid-specific pathways, while mono-culture preserves stemness and quiescence. This duality underscores the dynamic interplay between hematopoietic differentiation and immune modulation within the HSPC niche, offering insights into their roles in tissue homeostasis and inflammatory responses.

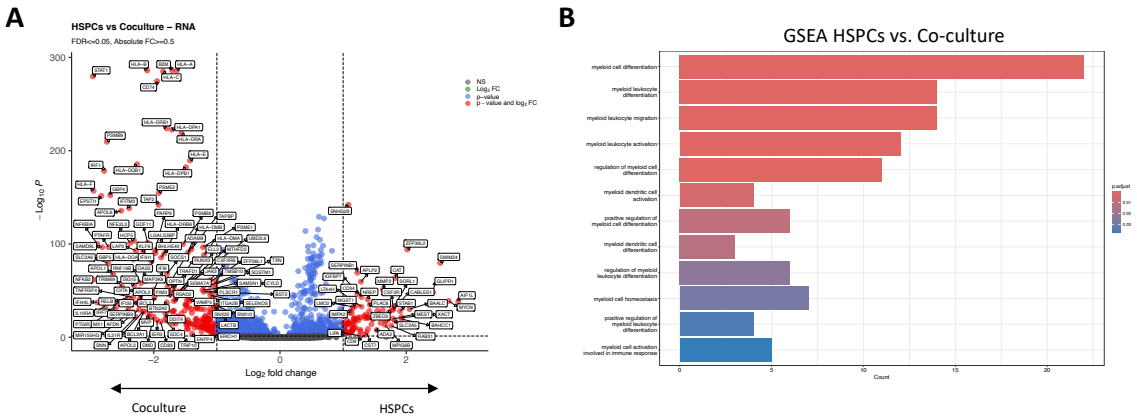

Figure 48. Differential gene expression and GSEA of HSPCs in MLR assay.

A) Differential gene expression analysis of HSPCs mono- vs, cocultured. **B**) GSEA analysis of myeloid differentiation pathways upregulated in co-cultured HSPCs vs. mono-cultured HSPCs.

Recent work by John Dick's lab identified a regulatory signature in HSPCs that retains memory of prior inflammatory stress, dividing HSCs into two subsets: normal HSCs (HSC-I) and inflammatory memory HSCs (HSC-II), which accumulate with age and clonal hematopoiesis (Zeng et al., 2023). The analysis presented here identified differential expression of these regulatory signatures in HSPCs. Mono-cultured HSPCs exhibited upregulation of canonical regulators associated with healthy, quiescent HSCs, while co-cultured HSPCs showed increased expression of inflammatory memory-associated regulators (**Figure 49**). Notably, pro-inflammatory genes such as Nuclear Factor Kappa B Subunit 1 and 2 (*NFKB1*, *NFKB2*), FosB Proto-Oncogene - AP-1 Transcription Factor Subunit (*FOSB*), C-X-C Motif Chemokine Ligand 10 (*CXCL10*) and the Interferon Regulatory Factor 1 and 7 (*IRF1*, *IRF7*) were highly expressed in co-cultured HSPCs treated with PD-L2 neutralizing antibodies but were minimally expressed in mono-cultured HSPCs.

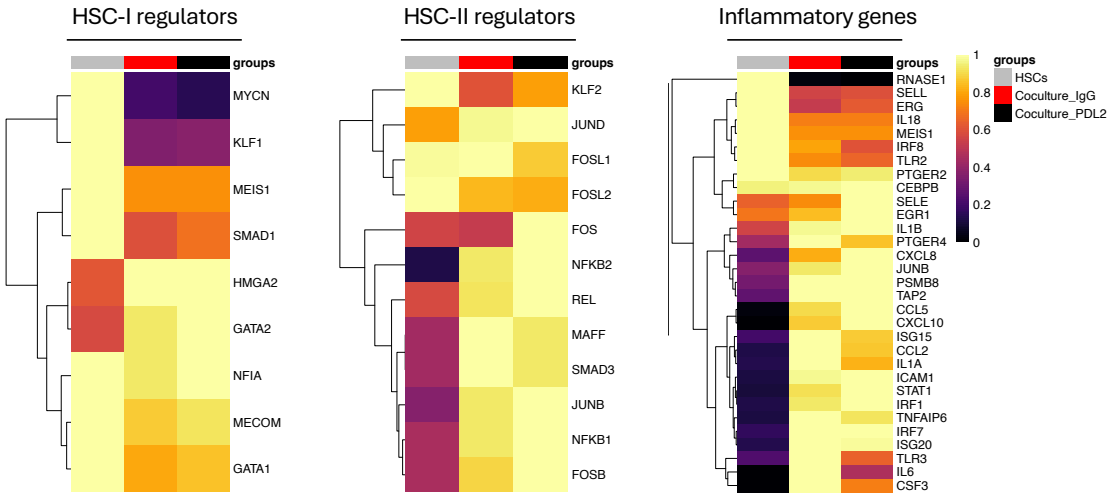

Figure 49. Differential gene analysis of inflammatory HSPC regulators.

Differential expression of marker genes for proinflammatory signatures in HSPCs (Zeng et al., 2023).

These findings suggest that PD-L2 blockade amplifies inflammatory signaling in HSPCs, promoting an inflammatory memory phenotype towards HSC-II signature. This highlights the potential role of PD-L2 in

modulating inflammatory responses and maintaining immune homeostasis within the hematopoietic niche. The presented study provides a high-resolution map of HSPC-T cell interactions, offering insights into the molecular basis of immunomodulation in hematopoietic niches.

4. Discussion

While advances in single-cell multi-omics have enhanced resolution of HSPC biology, the molecular identity of HSCs and their differentiation trajectories remain incompletely defined, owing to persistent heterogeneity and unknown dynamic lineage priming within these populations. To address this gap, a comprehensive proteo-transcriptomic analysis of >62,000 CD34+ HSPCs isolated from healthy donors across age groups was conducted, in combination with integrating single-cell RNA sequencing incoperating 46 AbSeqs to resolve immunophenotypic signatures of primitive HSCs. By coupling pseudotime mapping and differential expression of 596 genes with proteomic validation, this study aimed to decode transcriptional programs governing HSC identity, lineage commitment and age-associated functional decline, while identifying novel surface markers that demarcate immature subsets with distinct differentiation potentials.

4.1. Lineage trajectory analysis over pseudotime confirmed a stepwise differentiation process

“HSCs are placed on top of the hematopoietic hierarchy and defined by their self-renewal potential and their ability to differentiate into all mature blood lineages throughout the lifespan”. This definition builds the cornerstone in hematology and usually introduces most scientific studies on hematopoiesis. However, our understating of HSC differentiation trajectories still sparks debates in the field with different models being postulated over recent years.

As previously reviewed, two main models of hematopoietic differentiation have emerged (Olson et al., 2020a) (**Figure 2**):

Model 1: The classical hierarchical model, proposing a stepwise differentiation process resembling a tree structure with multipotent HSCs placed at the apex of the hierarchy (Akashi et al., 2000; Kondo et al., 1997; Manz et al., 2002; Morrison et al., 1997).

Model 2: The continuous differentiation model, suggesting a gradual acquisition of lineage-restricted features with a “continuum” of multiple low-primed, lineage biased HSCs (Velten et al., 2017).

This study's findings align with the hierarchical organization (**Model 1**), which has been postulated for the murine compartments over decades and was recently confirmed by studies performed using human BM and cord blood (CB) samples (Anjos-Afonso et al., 2022; Kaufmann et al., 2021; Weng et al., 2024). Through pseudotime and tradeSeq analysis, the presented study confirms a stepwise commitment process of HSCs and suggests that most HSCs are multipotent. These analyses contribute to the ongoing refinement of our understanding of HSC differentiation and stay in direct contrast with the concept of the continuum of low-primed undifferentiated hematopoietic stem and progenitor cells, referred to as “CLOUD-HSPCs”, postulated by Velten *et al*. 2017.

Although, the results revealed an early branching point of the MEP lineage, the delay in pseudotime suggests that multipotency is maintained after the earliest steps of differentiation differing from clone-tracing studies performed in the murine compartment which suggest a direct differentiation pathway from multipotent HSCs to megakaryocytic-erythrocytic progenitors (Alejo E. Rodriguez-Fraticelli, 2018; Perié et al., 2015). To further confirm this, additional experiments using barcoding strategies to assess the clonal lineage output of singular transplanted HSCs must be performed. This strategy would gain further insights in terms of their multipotency.

4.2. Re-analysis of early HSPCs identified two HSC compartments with distinct transcriptional state

Besides various differentiation models, the heterogeneity observed within the phenotypically defined stem cell compartment displays another major challenge in the field of hematopoietic research (Haas et al., 2018). Previous studies using CD34+HSPCs from CB samples showed distinct myeloid-lineage bias in long-term repopulating HSCs (Matsuoka et al., 2015). To further decipher the different molecular signatures of the most immature cells, the dataset was segmented and extracted 7 distinct stem and early progenitor clusters for re-analysis, which resulted in a UMAP consistent of >21,000 cells and 9 distinct cell clusters. In accordance with recent literature the most immature clusters (HSC-1/HSC-2) displayed a high expression of the stem cell genes *HLF, HOPX* and *MLLT3* and successively downregulated upon differentiation (**Figure 18**). *HLF* is one of the most specific human HSC genes, which was reported to maintain quiescence of HSCs and protect the stem cell pool during regeneration (Komorowska et al., 2017). Furthermore, MAC-1^{+} HSCs, which primarily represent non-cycling HSCs, were shown to express high levels of *HLF* (Tang et al., 2021). High *HLF* activity thus marks human HSCs and appears as central master regulator of self-renewal and differentiation in acute leukemia and HSC identity in blood reprogramming (Lehnertz et al., 2021). Additionally, new potential stem cell markers could be identified on the transcriptomic level: *DLK1* and *ADGRG6* (**Figure 23**). As previously described *DLK1* is a non-canonical Notch ligand, regulating cell proliferation and differentiation as well as tissue regeneration and has already been reported to influence self-renewal and repopulation of murine HSCs (Falix et al., 2012; Huang et al., 2023; Qian et al., 2016). Since *DLK1* encodes for a transmembrane protein, it is of particular interest as prospective marker to isolate a defined HSC subpopulation, which must be further evaluated by functional analysis. Similar approaches should be taken for *ADGRG6* which encodes for the G-protein coupled receptor 126. Notably, GPR56 (encoded by *ADGRG1*) has been described as prospective marker for leukemia stem cells and was proposed as diagnostic marker for poor clinical outcome in AML (Daga et al., 2019; Pabst et al., 2016). However, GPR56 knockout models did not impair functional consequences and demonstrated a fully functional HSPCs compartments (Rao et al., 2015). Along that line, the functionality of GPR126 in regards of human HSC biology should further be evaluated.

4.3. Targeted sequencing approach allowed better profiling of low-expressed genes

HSCs are characterized by their quiescent nature, persisting in the G0 phase outside the cell cycle and operating gene transcription at low levels (Cheshier et al., 1999). This unique property presents challenges for comprehensive gene expression analysis using WTA sequencing which displays a good sensitivity for high and mid-expressed genes. Recent WTA datasets published by the Haas group and the Grimes group may have inadvertently missed certain low-abundance transcripts due to technical limitations (Triana et al., 2021; X. Zhang et al., 2024). These limitations arise from the need to incorporate ~20,000 protein-coding genes of the human genome, which can result in lower reads per gene. This issue is particularly pronounced for genes expressed at low levels in quiescent cells like HSCs. Furthermore, the presence of unspecific reads for mitochondrial genes can further compromise sequencing depth. This study was performed with a more cost-efficient pre-selected gene panel of 596 genes specifically chosen for low abundant transcripts which are of particular interest for HSC biology (Mair et al., 2020). The analysis revealed a subset of genes highly upregulated in the HSC-1/HSC-2 clusters that were almost undetected in the aforementioned datasets (**Appendix Figure 1**). As example, *MPL* was one of the key genes upregulated in HSC-1 cluster among all age groups, which was neglectable in Zhang *et al*. and Triana *et al*. This discrepancy underscores the importance of considering the quiescent nature of HSCs when designing transcriptomic studies and highlights the need for specialized approaches to capture the full range of gene expression in these cells. Besides the loss of information in reducing the transcriptomic analysis to a subset of genes, the presented study was able to resolve a continuous map of early human HSPCs with similar efficiency as the referred datasets using the WTA approach.

4.4. Age-group comparison displayed balanced lineage output

The expansion of the HSC compartment and a concomitant shift towards myeloid lineage output represent well-characterized hallmarks of aging in murine hematopoietic systems (Beerman et al., 2010; Challen et al., 2010; Chambers et al., 2007; Dykstra et al., 2011; Harrison & Astle, 1982; Morrison et al., 1996; Rossi et al., 2005; Young et al., 2016). Similar findings have been made for the human compartment, with transplantation and computational analysis showing an age-driven enlargement of the HSC pool and decrease abundance of lymphoid precursors (Ainciburu et al., 2023; Pang et al., 2011). Surprisingly, this statement could only be partially confirmed by this study. Indeed, stem cells (HSC-1/HSC-2) demonstrated an increased percentage for mid-aged and old donors being aligned with the reported literature. In contrast, young, mid-aged and old donors displayed an equal frequency of LYP cells (**Figure 20**). Interestingly, young donors had an increased abundance in the GMP, MDP-1 and MDP-2 cluster. On the other hand, pseudotime and tradeSeq analyses mapped the differentiation trajectories across age groups, revealing a balanced and efficient differentiation of HSPCs from young donors, whereas differentiation was delayed across all lineages in mid-aged and older donors. This impairment was most pronounced in lymphoid commitment. Genes involved in differentiation regulation and lineage-choice induction were expressed later in

pseudotime in aged HSPCs, while stemness-associated genes remained active (data not shown). These findings suggest an age-dependent molecular regulation of progenitor production during early HSC differentiation. The observed delay in differentiation may contribute to the increased frequency of HSCs in older healthy adults and could be linked to reduced lymphopoiesis and the lower normal range of hemoglobin observed in aging individuals. Further studies are needed to determine whether these changes are driven intrinsically or influenced by the aged environment.

4.5. Surface proteome analysis of HSC-1 cells revealed exclusive upregulation of CD273/PD-L2

Until today, one of the biggest challenges in studying HSC biology is the isolation of this rare cell type, which is present at a frequency of approximately 1 in 10^6 cells in human BM (Doulatov et al., 2012b; Wang et al., 1997). In contrast to the human system, the stem cell compartment has been extensively characterized in mice. While hematopoiesis is largely conserved across vertebrate evolution, allowing for some experimental findings in mice to be extrapolated to humans, many discoveries cannot be directly translated due to fundamental interspecies differences. A striking example is the marker CD34: in humans, HSCs can be enriched based on CD34 expression, which has been instrumental for isolating HSCs and progenitors and has proven clinical applications in hematopoietic stem cell transplantation (HSCT) studies. Despite CD34 being expressed on less than 5 % of all blood cells, it is present on the majority of human HSCs (Civin et al., 1984; Vogel et al., 2000). In contrast, murine HSCs are typically characterized as CD34 low (Civin et al., 1984; Osawa et al., 1996). Similarly, SLAM markers that define long-term HSCs (LT-HSCs) in mice are largely irrelevant for identifying human HSCs (Larochelle et al., 2011). These differences demand further efforts to characterize the human stem cell compartment to advance clinical applications such as transplantation, gene therapy, stem cell expansion and tumor-cell purging.

Over the past decades, significant progress has been made in refining strategies to isolate human HSCs and obtain pure, homogeneous populations for downstream analysis. A major breakthrough came with single-cell sorting approaches. For example, Notta *et al*. further defined the CD34+ HSPC subpopulation by incorporating CD90 and CD49f expression, identifying HSCs as CD90+CD49f+ and multipotent progenitors (MPPs) as CD90-CD49f- (Notta et al., 2011, 2016). Advances in single-cell RNA sequencing have further revolutionized the field by enabling more precise characterization of human HSCs. This approach was utilized by Anjos-Afonso *et al*., who identified a multipotent subset within CD34+ HSCs expressing EPCR in cord blood samples. Xenograft studies demonstrated that EPCR+ HSCs exhibit high repopulating and self-renewal capacities, achieving a remarkable stem cell frequency of 1 in 3 cells (Anjos-Afonso et al., 2022).

Building on these advancements, technologies have evolved further by integrating transcriptomic analysis with surface proteomics. The described multi-omics approach has enabled the identification of a relatively homogeneous HSC subpopulation characterized by low expression of traditional stem cell marker genes. Subsequent analysis of upregulated surface proteins using AbSeq staining has provided deeper molecular

insights into these cells and identified potential novel stem cell markers. These markers hold promise for facilitating the prospective isolation of these rare cells through FACS-based enrichment for functional validation.

In this analysis, differential protein expression between HSC-1 and HSC-2 populations revealed significant upregulation of CD273 and CD62L in HSC-1 cells (**Figure 24**). CD62L, also known as L-selectin, is well-documented for its critical role in lymphocyte homing to peripheral lymph nodes (Warnock et al., 1998). Functional studies on CD10-CD62L+ HSPCs sorted from Lin-CD34+ BM samples demonstrated full lymphoid and monocytic potential but lacked erythroid differentiation capacity (L. Kohn, 2012). Consistent results were obtained in this study using Lin-CD34+CD38-CD45RA- HSPCs as the parental population to characterize CD62L+ and CD62L- cells. Colony-forming unit (CFU) assays revealed that CD62L+ HSPCs lacked the ability to form BFU-E and CFU-E colonies (data not shown), aligning with findings from the Crooks lab. Interestingly, contrasting results were reported in fetal bone marrow samples, where a refined sorting strategy incorporating Lin-CD34+CD38-CD52+CD62L+CD133+ cells (defined as the CD-REF panel) enriched immunophenotypic HSCs/MPPs capable of full lineage formation, including erythroid differentiation (Ranzoni et al., 2021). This discrepancy highlights the need for further evaluation to resolve conflicting scientific findings.

Besides CD62L, HSC-1 showed a significant upregulation for CD273. CD273, also described as programmed cell death ligand 2 (PD-L2) functions as second ligand to PD-1 and is well described in its function as immunomodulatory role in the context of cancer evasion mechanism (Latchman et al., 2001; Lin et al., 2024). Before focusing on its potential immunomodulatory function in HSPCs, CD273 was evaluated as a potential stem cell marker. Notably, datasets from human HSCs available on BloodSpot and findings from Triana *et al*. also demonstrated distinct upregulation of CD273 in the most immature subpopulations (**Figure 25**).

4.6. Functional analysis confirmed CD273/PD-L2 as marker on HSPCs with enhanced quiescence

Flow cytometry analysis of different HSPC populations showed a higher surface expression of CD273 on a subset of human HSCs (**Figure 26**). Prospectively isolated HSPCs with high CD273 expression were found to display delayed differentiation, low mitochondrial potential, multi-lineage potential and decreased cell expansion in culture. The most striking example for an enhanced quiescence of $CD273^{high}$ HSPCs was the significantly increased expression of CDK6 in $CD273^{low}$ HSPCs, which corrected with a ~13h earlier entry into cell-cycle (**Figure 31**). A study by Laurenti *et al*. established that the level of CDK6 functions as master regulator during quiescence exit and entry into cell cycle, with the absence of this cyclin protein resulting in a 5 - 6 hour delay in G0 exit, preserving the HSC long-term integrity and preventing further damage. While these are good hints for true stem cell phenotypes, a defined HSC must demonstrate durable self-renewal and multilineage differentiation potential conventionally tested by serial transplantations. The previously

described xenograft model, transplanted with 30,000 CD34+CD273^{high} or ^{low} per recipients, only gave limited insights into the self-renewal and multilineage reconstitution potential and present one of the major technical limitations of this study. The results showed no significant differences between all transplanted groups and only demonstrated low overall engraftment potential after 18 weeks post transplantation (**Figure 35**). Since overall chimerism analysis in the PB only decreased over time the BM and spleens were analyzed 18 weeks post transplantation as experimental endpoint. Defined endpoints to functionally validate and separate ST-HSCs from LT-HSCs remain a matter of discussions in the field. For syngeneic mouse transplantations long-term reconstituting HSCs (LTRCs) regenerate all blood lineages and sustainable throughout 6-8 months post transplantation, whereas ST-HSCs are defined by detectable engraftment at 12 weeks post-transplant (Benveniste, 2010). Adapting these endpoints for human cells in xenografts is difficult and performed studies testing human reconstitution potential used different timepoints from 6 to >30 weeks as end-analysis depending on the used marker combination (Goyama et al., 2015). For this study, an earlier timepoint maybe would have been feasible, to detect short-term engraftment between different HSPC populations.

In addition, lineage reconstitution of certain cell types is limited in xenograft model and highly dependent on the used mouse model. The most widely used stain is IL2rg^{null} mice on a non-obese-diabetic (NOD) background, referred to as NSG (Ishikawa et al., 2005; Shultz et al., 2005). These models are highly effective for examining hematopoietic malignancies like acute leukemia, but do not present a suitable homing environment which mediates self-renewal for normal stem cells as illustrated in **Figure 50** (Bonnet & Dick, 1997; Goyama et al., 2015; Nicolini et al., 2003; Rongvaux et al., 2014; Wunderlich et al., 2010).

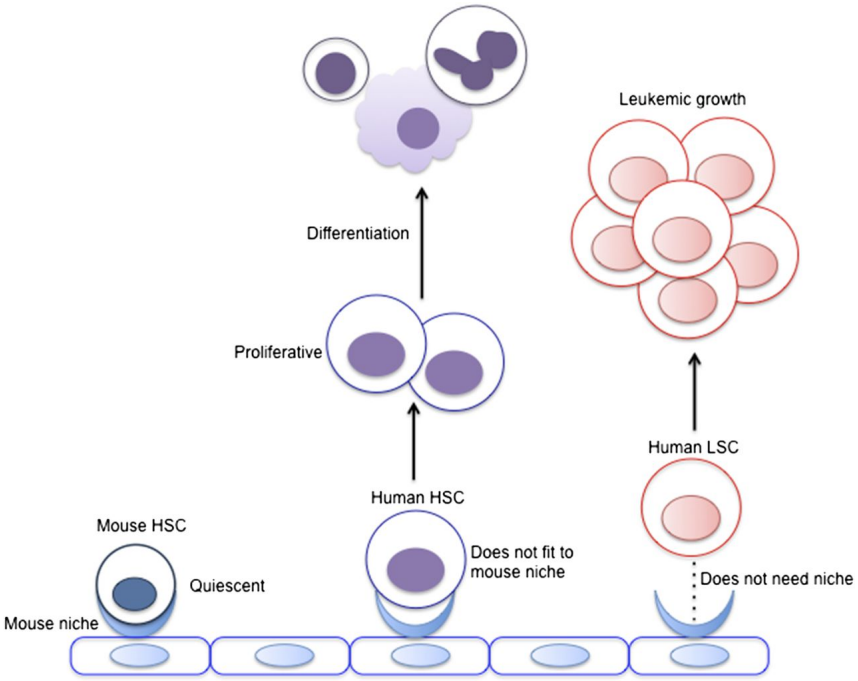

Figure 50. Interaction of mouse niche and human HSCs in Xenograft model.

Hematopoietic stem cells (HSCs) rely on interactions with the bone marrow niche to maintain quiescence. In xenograft models, the murine niche fails to provide the necessary signals to support human HSC self-renewal, leading to a decline in their stemness and

reconstitution potential. In hematopoietic malignancies, leukemia stem cells exhibit intrinsic differences from normal HSCs, retaining their self-renewal capacity without exhaustion (Goyama et al., 2015).

The introduction of the loss-of-function *Kit* allele (NSGW41$^{-/-}$) increased the HSC niche space through impairment of endogenous mouse HSCs and enabled an efficient and stable engraftment of human HSCs with > 60 % human leukocyte frequency in the PB 20 weeks post transplantation (Cosgun et al., 2014).
Besides the used mouse model, overall engraftment and multilineage reconstitution in xenograft models can be influenced by the transplanted subpopulation, source material and cell number, mouse model and gender, injection technique and time point of analysis. For example, erythrocytes are only persistent in the earliest weeks after transplantation. Lymphoid cells occur after 12 weeks in PB - with B-cells declining after 16 weeks and T-cells begin to increase beyond this timepoint- which could be nicely confirmed by this study (**Figure 34**) (Audigé et al., 2017; Harris & Badowski, 2014; Hayakawa et al., 2009; J. Lang et al., 2013; Rongvaux et al., 2013).
The low overall engraftment observed in these experiments may also be attributed to the source material used. Studies have shown that CB samples yield higher engraftment rates in xenografts compared to BM or mPB (Dong Ku et al., 1999; Walcher et al., 2020). Therefore, it is not surprising that most studies prefer CB samples as source material for their xenograft experiments. However, this preference raises questions about how comparable CB-based studies are when investigating adult hematopoiesis.
Despite these technical challenges, *in vivo* xenograft assays remain the gold standard for testing self-renewal and multilineage reconstitution potential of HSCs—a benchmark established since 1988 (GJ Spangrude, 1988). The presented findings indicate that CD273 cannot be classified as a definitive stem cell marker but rather as a marker associated with HSPCs. Improved experimental designs are needed to validate putative HSC markers and overcome limitations inherent to xenotransplantation models.

4.7. CD273 expressing HSPCs are immunomodulating cells suppressing T-cell activation and proliferation

The longstanding paradigm of HSPCs as progenitors solely responsible for blood cell formation has been fundamentally challenged by emerging evidence highlighting their potential immunomodulatory roles. Recent publications have shown that HSPCs can function as antigen presenting cells via major histocompatibility complex II (MHC-II) and regulate T-cell responses; as well as interact with macrophages utilizing Beta-2-microglobulin expression to mediate a "don't eat me" signal and thereby enhancing their survival (Hernández-Malmierca et al., 2022; Rodrigues et al., 2024). Additional studies showed that during inflammation, murine HSPCs upregulate the immune-checkpoint ligands PD-L1 (B7-H1/CD274) and PD-L2 (B7-DC/CD273), which suppress cytotoxic T-cell activity while promoting emergency myelopoiesis (Yamashita & Passegué, 2019). This dual role safeguards HSC functionality by mitigating immune-mediated damage to maintaining the integrity of the HSC pool, ensuring lifelong hematopoiesis, while meeting increased demands for immune cell production. Interestingly, these studies have not thoroughly explored

how the upregulation of PD-L1/PD-L2 protect HSCs from T-cell-mediated cytotoxicity. Given the significant upregulation of PD-L2/CD273 in the immature HSC subset, these findings are particularly striking in the context of their potential immunomodulatory functions within the human stem cell compartment. To advance our understanding in this area, a co-culture system was established to investigate the effect of PD-L2/CD273-expressing HSPCs on allogeneic T-cells using an experimental setting known as mixed lymphoid reaction assay (**Figure 9**).

The subsequent results outlined that blocking PD-L2/CD273 led to increased activation and proliferation of allogeneic T-cells, indicating an immunosuppressive role for CD273-expressing HSPCs (**Figure 39 + Figure 40**). The suppressive function of members of the B7-protein family are well studied in the context of tumor evasion mechanisms. Multiple studies have shown that the increased expression of B7 molecules on the tumor microenvironment inhibits tumor-specific T-cell immunity (W. Zou & Chen, 2008). Thinking of HSC immunosurveillance mechanism in regard of inflammatory responses or autoimmunity, this modulation raises particular interest and could indicate that HSPCs actively modulate the adaptive immune system to evade their potential attacks. Similar mechanisms have been shown by the upregulation of CD274/PD-L1 on cultured murine HSCs which inhibit T-cell proliferation of their host upon allogenic transplantation resulting in improved engraftment rates (J. Zheng et al., 2011).

Additional evidence of an immunomodulating role of $CD273^{high}$ HSPCs could be demonstrated by the decreased abundance of regulatory T-cells (T_{reg}) and increased secretion of pro-inflammatory cytokines like IL-6, TNF- α, IFN-γ and IL-17A upon CD273/PD-L2 inhibition (**Figure 42 + Figure 43**). Tregs function as gatekeeper of our immune tolerance by suppressing effector T-cells, inducing their apoptosis through cytokine releases and limiting chronic inflammation and autoimmunity (Vignali et al., 2008). Notably, studies have shown a higher frequency of T_{regs} in the BM niche, an immune-privileged site which assures HSC self-renewal capacity, and T_{reg} co-localization with HSPCs supporting their stem-cell function (Fujisaki et al., 2011; L. Zou et al., 2004). Therefore, the higher frequency of T_{regs} observed in the MLR assay suggests a potential role in supporting HSC functionality by fostering immune tolerance and mitigating inflammatory stress, which may reflect their protective influence in maintaining stem cell persistence under immune-challenging conditions. Whether the interaction of HSPCs directly modulate T-cell specification, or indirect effects cause the selection for T_{reg} abundance requires further investigation.

Modulating immune responses is particularly critical in the context of allogeneic HSCT, which is widely used as a therapeutic intervention following BM ablation for hematopoietic malignancies (Gyurkocza et al., 2010). GVHD remains a significant complication in allogeneic transplantation, arising from donor immune cells attacking the recipient's tissues and organs (Malard et al., 2023). Since CD274/PD-L1 high HSCs exhibited significantly reduced GVHD in allogeneic mouse models, it would be valuable to explore if these findings apply to CD273-expressing HSPCs (J. Zheng et al., 2011). However, translating these results to human models using CD273/PD-L2-expressing HSPCs and xenografts remains challenging due to technical limitations in reconstructing the lymphoid system and replicating complex cross-species immune

interactions. Humanized mouse models, lack sufficient human epitopes necessary for allogeneic T-cell development, which in turn affects their activity (Kooreman et al., 2017; Lee et al., 2019; Obenaus et al., 2015; Shultz et al., 2005). Recent advancements, such as the incorporation of interleukin-7 (IL-7), have shown promise in enhancing the differentiation of functional human T-cells within NSGW41 mouse models, thereby optimizing lymphoid reconstitution and improving experimental frameworks to study immunosuppressive responses (Coppin et al., 2021). This model could be utilized to study the immunosuppressive effects of CD273^{high} HSPCs *in vivo*.

In addition to their extrinsic adaptation to an inflammatory environment—allowing HSPCs to sustain the necessary cellular output while regulating their activation to preserve the HSC pool and maintain self-renewal—intrinsic mechanisms safeguard HSPCs from excessive immune responses and facilitate the resolution of emergency hematopoiesis. Besides many upregulated myeloid-specific differentiation marker, co-cultured HSPCs displayed an increased expression level of *CXCL10*, *STAT1* and *JunB* (**Figure 48 + Table Appendix 1**). The chemokine CXCL10 has been reported to regulate the self-renewal potential of hematopoietic stem cells (F. Liu et al., 2024). In this context, *STAT1* expression is crucial for normal HSC function and maintaining a subset of HSCs during stress-induced proliferation (J. Li et al., 2022). Additionally, the transcription factor JunB has been shown to regulate HSC proliferation by modulating the expression of key cell cycle regulators and control the rate at which HSCs generate early myeloid progenitors to ensure their proper responsiveness to stress-induced signaling pathways (Passegué, 2008).

All these intrinsic and extrinsic factors act as key regulators of HSPC integrity, playing a crucial role in resolving emergency hematopoiesis and maintaining the delicate balance between HSC activation and quiescence. This balance is essential, as prolonged inflammatory responses can impair HSC function, leading to diminished repopulating capacity and a myeloid bias, which increases the risk of myeloid oncogenesis or bone marrow failure (Caiado et al., 2021).

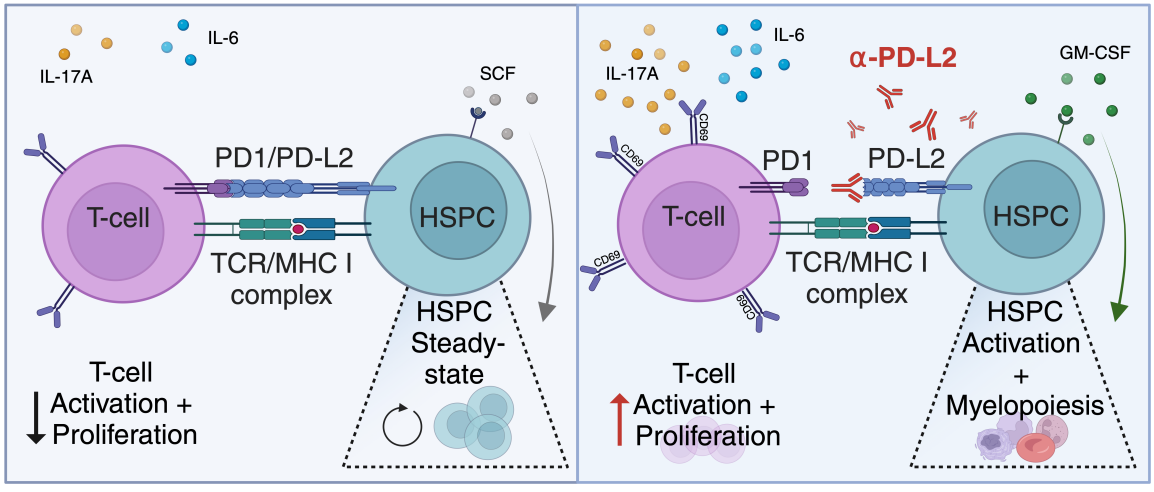

Figure 51. Graphical abstract displaying the immunomodulating function of CD273-expressing HSPCs.

Co-culture of CD273/PD-L2-expressing HSPCs and allogenic mixed T-cells showed balanced inflammatory reactions which was elevated upon blockade of CD273/PD-L2. Neutralization of CD273/PD-L2 increases the release of pro-inflammatory cytokines (IL-17A, IL-6); activation and proliferation of T-cells and showed increased myelopoiesis of co-cultured HSPCs.

Collectively, the newly established co-culture system demonstrated that CD273/PD-L2-expressing HSPCs exhibit a distinct immunomodulatory phenotype by suppressing T-cell activation and proliferation, reducing the secretion of pro-inflammatory cytokines and initiating transcriptional programs that preserve HSPC functionality to safeguard blood formation (**Figure 51**).

5. Conclusions

This study provides significant insights into the early differentiation processes of HSCs and their changes across the human lifespan, as well as CD273 as immunomodulating surface marker on human HSPCs. The key findings are:

- Four major differentiation trajectories were identified through pseudotime analysis, which remain consistent with aging.
- An early branching point into megakaryocyte-erythroid progenitors was observed, but tradeSeq analysis imply a stepwise differentiation process instead of a continuum of low-primed HSPCs.
- Young donors showed more productive differentiation from HSPCs to committed progenitors across all lineages.
- Continuous changes in gene expression of HSPC-related genes (*DLK1*, *ADGRG6*) were observed using tradeSeq analysis.
- CD273/PD-L2 was identified as highly expressed in a subfraction of immature multipotent HSPCs with enhanced quiescence.
- Functional experiments confirmed the immunomodulatory role of CD273/PD-L2 on HSPCs in regulating allogeneic T-cell activation, proliferation and cytokine release.

In summary, this molecular map of early HSPC differentiation across human life provides a valuable resource for understanding hematopoietic development, in addition to the discovery of an immunoregulatory HSPC subset, with potential therapeutic applications in treating hematological malignancies and underscores that our bone marrow is far more than the “waste product” once described by Aristotle.

6. Future perspective

Future studies should refine the functional validation of CD273/PD-L2 as a human HSC marker and checkpoint by combining improved xenotransplantation and immune-competent models. First, limiting-dilution and serial xenotransplantations of prospectively isolated CD273/PD-L2^{high} versus CD273/PD-L2^{low} CD34^{+} HSPCs in optimized humanized systems such as NSGW41- or NSGW41-IL7–based W41$^{-/-}$ models would allow a more stringent assessment of long-term, multilineage repopulating activity and clarify whether CD273/PD-L2 truly enriches for LT-HSCs rather than broadly marking quiescent HSPCs. In parallel, a conditional *Pdcd1lg2* knockout using the Mx1-Cre system in mice could be used to delete CD273/PD-L2 in adult hematopoietic stem and progenitor cells and thereby interrogate its role in maintaining bone marrow homeostasis, lineage output and stress responses in a fully immunocompetent setting. Such an inducible model would enable analysis of how loss of CD273/PD-L2 affects HSC quiescence, self-renewal and recovery after cytotoxic or inflammatory challenge, providing complementary mechanistic insight to the human xenograft data and allowing direct comparison between human and murine stem cell compartments. Building on the MLR data, *in vivo* experiments using CD273/PD-L2^{high} HSPCs in humanized autoimmunity-like or chronic inflammation models, with PD-L2 blockade or genetic perturbation, could determine whether CD273/PD-L2 provides a *bona fide* “immune-privileged” shield that protects HSPCs from T-cell–mediated damage while orchestrating balanced emergency myelopoiesis and preserving stem cell integrity under inflammatory pressure. Finally, integrating barcoding or clonal tracking with single-cell multi-omics in these models would link CD273/PD-L2–dependent immunomodulation to clonal HSC fate decisions over time, thereby connecting stemness, stress responses and immune evasion within the human HSC compartment and paving the way for CD273/PD-L2-targeted strategies to improve transplantation outcomes and prevent immune-mediated stem cell failure in clinical settings.

7. Appendix

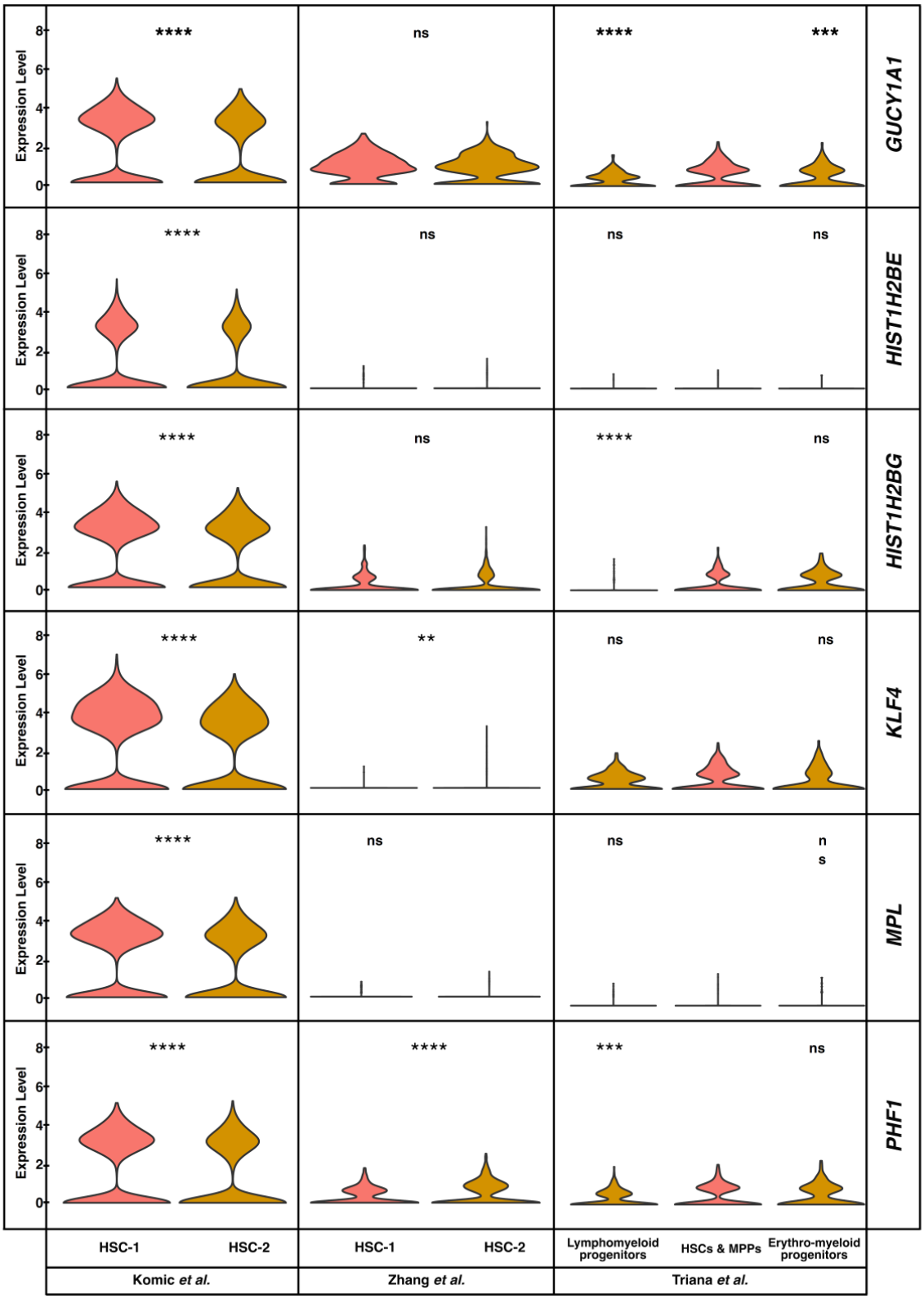

Appendix Figure 1. Comparison of upregulated stem cell genes between different published datasets.

Table Appendix 1. Differentially expressed genes HSPCs vs Co-culture.

	p_val	avg_log2FC	HSPCs	Co-culture	p_val_adj
SPINK2	1,24E-136	4,743470921	0,499	0,067	4,44E-132
CYTL1	1,54E-110	3,152665519	0,561	0,148	5,49E-106
AIF1L	1,09E-43	2,826830731	0,28	0,074	3,90E-39
MYCN	4,02E-44	2,672889453	0,287	0,076	1,44E-39
SMIM24	7,13E-85	2,538944527	0,51	0,157	2,55E-80
GLIPR1	2,52E-53	2,426599968	0,454	0,189	9,03E-49
BAALC	2,24E-35	2,053246114	0,3	0,104	8,02E-31
ZFP36L2	2,67E-99	2,016373413	0,806	0,521	9,55E-95
BAHCC1	1,30E-24	1,931293051	0,251	0,097	4,64E-20
MEST	4,59E-27	1,923494388	0,299	0,127	1,64E-22
STAB1	3,23E-33	1,903657033	0,314	0,118	1,16E-28
CAT	9,08E-69	1,823125435	0,804	0,572	3,25E-64
SLC2A5	4,37E-23	1,818119527	0,255	0,106	1,56E-18
SORL1	5,91E-39	1,814449199	0,461	0,235	2,11E-34
CSF3R	5,82E-36	1,794359269	0,493	0,287	2,08E-31
CABLES1	1,35E-34	1,789524706	0,436	0,221	4,85E-30
XACT	2,68E-25	1,786349027	0,311	0,139	9,59E-21
RAB31	1,28E-17	1,761345452	0,267	0,134	4,58E-13
ZBED3	1,83E-32	1,729962776	0,333	0,134	6,54E-28
NEURL1B	9,25E-24	1,704285888	0,252	0,098	3,31E-19
IL12A-AS1	7,83E-23	1,667739262	0,359	0,193	2,80E-18
MPIG6B	1,82E-18	1,663201022	0,253	0,116	6,51E-14
MMP2	2,15E-56	1,628011876	0,57	0,276	7,68E-52
ABLIM1	3,48E-34	1,625818374	0,371	0,157	1,25E-29
ATP9A	1,01E-20	1,593866417	0,253	0,11	3,63E-16
SNHG19	1,32E-30	1,567522688	0,361	0,163	4,71E-26
CLEC11A	1,65E-33	1,541033296	0,552	0,33	5,91E-29
ADA2	4,96E-13	1,531993331	0,36	0,249	1,78E-08
CDK6-AS1	2,22E-24	1,468062744	0,377	0,203	7,94E-20
TMEM170B	3,10E-19	1,449612561	0,286	0,141	1,11E-14
PLAC8	4,03E-40	1,425365047	0,423	0,177	1,44E-35
CDCA7L	2,30E-33	1,417164969	0,466	0,248	8,22E-29
ACSM3	8,23E-27	1,400691982	0,499	0,323	2,95E-22
CLEC12A	3,84E-14	1,393794831	0,258	0,141	1,38E-09
NREP	1,07E-45	1,390710849	0,723	0,533	3,82E-41
F2R	7,01E-27	1,390306077	0,388	0,195	2,51E-22
ZNF395	1,26E-25	1,383771628	0,353	0,17	4,50E-21
CST7	2,98E-10	1,369756173	0,502	0,422	1,07E-05
TIMP2	1,17E-29	1,364115009	0,495	0,298	4,18E-25
CD9	6,44E-08	1,343701067	0,281	0,193	0,00230309
TENT5A	5,75E-26	1,342709872	0,477	0,29	2,06E-21
CMBL	3,71E-28	1,331140229	0,419	0,219	1,33E-23
IGFBP7	2,19E-48	1,292114177	0,698	0,455	7,84E-44
LTA4H	4,04E-38	1,290833757	0,59	0,355	1,45E-33
APLP2	8,83E-65	1,281952253	0,834	0,607	3,16E-60
BEX1	1,71E-11	1,274454256	0,346	0,231	6,10E-07
PADI4	2,39E-13	1,270123677	0,263	0,148	8,54E-09
DEPTOR	1,22E-26	1,263007259	0,401	0,206	4,37E-22
LIPA	3,97E-07	1,262107424	0,598	0,526	0,014191993
CPNE3	1,24E-23	1,246980984	0,372	0,195	4,45E-19
SOX12	7,59E-26	1,231340047	0,433	0,245	2,71E-21
CD34	9,20E-52	1,225343106	0,77	0,607	3,29E-47
SERPINB1	1,88E-74	1,225272673	0,946	0,891	6,73E-70
MGST1	5,38E-39	1,200160633	0,629	0,393	1,92E-34
SCARB1	1,25E-15	1,197575551	0,272	0,145	4,49E-11
CD302	1,24E-21	1,1875285	0,47	0,309	4,44E-17
PDLIM1	1,36E-25	1,18000664	0,449	0,256	4,87E-21
FAM30A	3,80E-15	1,177553332	0,422	0,287	1,36E-10
CEBPA	3,31E-24	1,171535274	0,44	0,251	1,18E-19
METTL7A	1,49E-25	1,169590927	0,458	0,263	5,34E-21
LMO2	5,72E-38	1,160327655	0,686	0,498	2,05E-33
CD109	1,23E-20	1,159600259	0,473	0,313	4,41E-16
PTPRE	2,88E-14	1,153275372	0,446	0,313	1,03E-09
KCNQ5	4,25E-12	1,146617751	0,293	0,177	1,52E-07
IMPA2	1,45E-35	1,144071555	0,577	0,348	5,20E-31
SCAMP1	5,02E-16	1,143023873	0,353	0,221	1,80E-11
ZNF711	8,31E-13	1,140081423	0,269	0,154	2,97E-08
RASAL2	5,28E-31	1,136155715	0,535	0,325	1,89E-26
ABRAXAS1	1,68E-11	1,135713461	0,255	0,149	6,00E-07
CDCA7	3,97E-11	1,125070864	0,266	0,162	1,42E-06
ERG	1,18E-19	1,117550116	0,419	0,26	4,22E-15
DANCR	1,35E-31	1,104310702	0,563	0,348	4,84E-27
SPARC	1,88E-21	1,098593137	0,507	0,337	6,73E-17
SNHG29	2,11E-147	1,084770485	0,993	0,992	7,56E-143
TESMIN	5,03E-10	1,077755333	0,276	0,179	1,80E-05
LRP5	1,76E-20	1,076580635	0,428	0,253	6,30E-16
DMTN	9,66E-20	1,07104696	0,545	0,393	3,46E-15
SLA	1,35E-10	1,069296318	0,261	0,157	4,81E-06
MTURN	3,09E-19	1,066843784	0,64	0,528	1,11E-14
SLA2	1,51E-23	1,055606216	0,582	0,423	5,40E-19
ALDH3B1	1,92E-11	1,043911796	0,257	0,152	6,86E-07
SNHG25	2,02E-15	1,036481735	0,373	0,24	7,21E-11
ZNF385A	5,12E-12	1,025063985	0,39	0,277	1,83E-07

DNAAF5	1,54E-09	1,018780817	0,269	0,175	5,53E-05
MYC	1,64E-16	1,014657433	0,382	0,232	5,87E-12
CENPV	2,20E-16	1,008238603	0,422	0,279	7,88E-12
KIAA0930	4,55E-20	1,006886482	0,604	0,437	1,63E-15
RNF24	3,08E-40	0,999278905	0,746	0,535	1,10E-35
OSBPL1A	3,07E-15	0,992582367	0,351	0,214	1,10E-10
TNFRSF1A	9,39E-21	0,988625986	0,483	0,316	3,36E-16
UBASH3B	1,78E-09	0,987931635	0,276	0,179	6,39E-05
C11orf1	3,53E-12	0,973110841	0,327	0,209	1,26E-07
PROSER2	1,49E-10	0,972361943	0,255	0,151	5,33E-06
EDEM3	4,38E-14	0,972217505	0,365	0,242	1,57E-09
DNMT3B	5,10E-08	0,972059014	0,267	0,182	0,001826058
ITM2A	1,77E-34	0,971030833	0,775	0,62	6,34E-30
SELL	5,28E-32	0,970793677	0,748	0,614	1,89E-27
RGS18	8,33E-22	0,959868728	0,588	0,431	2,98E-17
BEX3	1,49E-35	0,946322464	0,713	0,542	5,34E-31
MMRN1	2,43E-09	0,941141447	0,272	0,176	8,68E-05
PCDH9	3,90E-09	0,936982555	0,334	0,233	0,000139557
PKP4	1,25E-08	0,927982493	0,289	0,196	0,000445746
TBC1D14	4,19E-13	0,921528485	0,406	0,288	1,50E-08
SNHG14	1,67E-08	0,911661733	0,252	0,161	0,000595785
CITED2	6,55E-21	0,911031606	0,572	0,412	2,34E-16
PGM1	9,38E-13	0,909528639	0,34	0,215	3,35E-08
XYLT1	8,21E-12	0,906839324	0,343	0,222	2,94E-07
MYO18A	4,08E-12	0,906639957	0,395	0,28	1,46E-07
FAM210B	2,82E-18	0,906558686	0,46	0,305	1,01E-13
PLEKHA7	2,31E-09	0,902299829	0,312	0,215	8,26E-05
ALDH6A1	4,07E-12	0,901025817	0,318	0,198	1,46E-07
EVI2B	9,37E-11	0,893299772	0,423	0,316	3,35E-06
CDIP1	2,59E-09	0,892731994	0,302	0,202	9,26E-05
POLE	8,61E-11	0,8887123	0,317	0,21	3,08E-06
PXK	5,96E-18	0,881579456	0,545	0,386	2,13E-13
CASP6	9,33E-16	0,878274136	0,453	0,312	3,34E-11
PROM1	6,70E-10	0,876420056	0,416	0,316	2,40E-05
ITGA4	2,87E-26	0,874614151	0,711	0,582	1,03E-21
SMYD3	1,36E-15	0,867124315	0,636	0,526	4,87E-11
MXI1	7,65E-13	0,865388494	0,282	0,161	2,74E-08
AKR1C3	7,93E-10	0,862581973	0,302	0,198	2,84E-05
SATB1	4,08E-22	0,856638985	0,616	0,452	1,46E-17
GPSM2	3,13E-15	0,855975099	0,399	0,255	1,12E-10
RNASE2	1,96E-10	0,853462901	0,319	0,208	7,02E-06
ICAM3	4,16E-12	0,851338402	0,4	0,277	1,49E-07
HMGN5	4,48E-15	0,850373619	0,449	0,311	1,60E-10
MLC1	2,18E-17	0,839593498	0,5	0,346	7,82E-13
MAML3	2,99E-11	0,834500893	0,346	0,231	1,07E-06
CBX6	8,54E-10	0,833125488	0,306	0,202	3,06E-05
INAFM2	4,84E-16	0,831932113	0,512	0,368	1,73E-11
ERMP1	4,22E-12	0,831085542	0,343	0,22	1,51E-07
GCNT1	3,62E-07	0,830792598	0,304	0,224	0,012937978
TAL1	1,63E-10	0,827415803	0,384	0,271	5,82E-06
TGFBRAP1	1,73E-17	0,825742552	0,546	0,397	6,21E-13
EEF1B2	5,73E-98	0,824806718	0,992	0,986	2,05E-93
NFE2	2,46E-19	0,818615141	0,563	0,393	8,80E-15
ISYNA1	6,50E-11	0,818303931	0,349	0,236	2,33E-06
ALDH3A2	4,28E-07	0,816252755	0,28	0,195	0,015313521
ANGPT1	2,68E-11	0,814252953	0,511	0,402	9,60E-07
STOM	1,60E-15	0,813952502	0,601	0,473	5,71E-11
BTBD2	5,30E-12	0,813062134	0,393	0,271	1,90E-07
IGLL1	1,60E-13	0,812471458	0,347	0,211	5,73E-09
EGFL7	1,53E-17	0,812454888	0,635	0,506	5,48E-13
PCMTD2	1,04E-06	0,804936992	0,273	0,195	0,037285708
ZMYM2	9,66E-16	0,802814622	0,467	0,328	3,46E-11
DPM3	5,92E-10	0,800530779	0,306	0,198	2,12E-05
AIF1	5,61E-41	0,793727844	0,914	0,801	2,01E-36
HOXA9	1,98E-09	0,793162525	0,402	0,3	7,10E-05
KDM5B	2,52E-20	0,792775136	0,648	0,505	9,02E-16
LINC00342	6,41E-11	0,790442795	0,345	0,229	2,29E-06
DOK3	2,48E-20	0,789039813	0,618	0,47	8,89E-16
CORO2A	2,15E-09	0,788856907	0,31	0,202	7,68E-05
ZSCAN16-AS1	1,31E-10	0,787384977	0,317	0,206	4,70E-06
SCARNA9	1,08E-29	0,784852547	0,792	0,654	3,85E-25
ZDHHC9	4,51E-10	0,777489655	0,307	0,198	1,61E-05
LAPTM4B	6,23E-24	0,776473084	0,839	0,815	2,23E-19
NADK2	6,88E-08	0,773838347	0,281	0,193	0,002462072
FAM189B	1,22E-08	0,773425492	0,329	0,235	0,000438033
GAS7	1,21E-07	0,769404371	0,372	0,283	0,004321324
MPST	6,98E-13	0,767437519	0,455	0,331	2,50E-08
LRPAP1	5,59E-11	0,762899119	0,399	0,287	2,00E-06
PDZD8	4,92E-10	0,762684249	0,533	0,453	1,76E-05
GLG1	5,29E-13	0,760672458	0,463	0,327	1,89E-08
QPRT	6,03E-07	0,759135439	0,32	0,24	0,021585899
SESN1	4,47E-08	0,755965308	0,354	0,263	0,001597792
SNHG7	1,42E-22	0,755856207	0,77	0,63	5,07E-18
FLI1	5,61E-11	0,751407586	0,422	0,31	2,01E-06
PECAM1	2,52E-26	0,750343131	0,694	0,53	9,03E-22
GIHCG	7,24E-14	0,749495783	0,457	0,321	2,59E-09

ZBTB44	8,36E-24	0,746806073	0,633	0,439	2,99E-19
JADE1	2,64E-08	0,746606825	0,333	0,238	0,000945763
ENSG00000290832	9,39E-09	0,745459014	0,339	0,239	0,000335953
EPB41L4A-AS1	1,63E-17	0,744040876	0,578	0,421	5,82E-13
KDM1A	1,75E-10	0,743059998	0,464	0,363	6,25E-06
MEN1	1,84E-13	0,739095465	0,429	0,292	6,58E-09
ABCB10	3,32E-08	0,738348278	0,365	0,274	0,001189387
QSER1	3,04E-09	0,735789825	0,324	0,224	0,000108612
ATF7IP2	9,49E-08	0,735431939	0,436	0,359	0,003396529
DSG2	5,17E-11	0,735426494	0,376	0,261	1,85E-06
MRPS2	7,23E-11	0,731800677	0,382	0,267	2,59E-06
SLC26A2	1,05E-06	0,729316677	0,36	0,284	0,037549903
ARID3A	1,10E-09	0,728965116	0,42	0,313	3,93E-05
ADGRL1	4,84E-09	0,726803279	0,317	0,211	0,000173146
CD38	3,11E-08	0,726650116	0,325	0,229	0,001111661
NAP1L1	3,33E-62	0,726264145	0,995	0,99	1,19E-57
IL18	4,76E-08	0,726060403	0,371	0,28	0,001701521
SLC43A1	5,21E-09	0,719646349	0,334	0,232	0,000186281
MRPS26	2,35E-08	0,719241692	0,335	0,24	0,000839209
MSRA	7,04E-09	0,718732006	0,351	0,254	0,000251881
APEX1	1,62E-35	0,718235498	0,92	0,84	5,78E-31
ZKSCAN8	3,05E-10	0,715262185	0,355	0,24	1,09E-05
DIS3L	7,39E-10	0,712261514	0,425	0,322	2,65E-05
PRKAG2	8,11E-08	0,711350686	0,36	0,274	0,002901678
SNTB1	4,73E-07	0,703839437	0,327	0,244	0,016920556
RCSD1	3,58E-11	0,701260742	0,567	0,454	1,28E-06
HGSNAT	1,15E-12	0,701044766	0,431	0,307	4,12E-08
PRSS57	1,75E-08	0,700299343	0,442	0,339	0,00062688
RASGRP2	2,09E-15	0,699536001	0,592	0,479	7,49E-11
RPS24	1,35E-132	0,696535723	1	1	4,82E-128
NLN	5,00E-08	0,690323151	0,381	0,292	0,001788197
PAM	4,22E-09	0,690206609	0,257	0,155	0,000151103
PPT1	6,37E-08	0,688728354	0,523	0,438	0,002280725
MSI2	4,79E-19	0,687947113	0,817	0,761	1,71E-14
TTC3	5,24E-24	0,686896993	0,792	0,66	1,87E-19
RPS26	2,77E-39	0,684613661	0,966	0,957	9,91E-35
RPS3A	1,91E-103	0,683604231	0,999	0,997	6,85E-99
EIF4B	2,40E-53	0,682107244	0,983	0,96	8,58E-49
VAT1	1,93E-10	0,681218898	0,559	0,464	6,90E-06
TFDP2	1,27E-16	0,680734044	0,67	0,55	4,54E-12
HADH	9,59E-07	0,680409812	0,305	0,224	0,034304365
NPM3	4,00E-14	0,679751777	0,531	0,393	1,43E-09
POLR1B	5,27E-07	0,678357693	0,292	0,206	0,018864953
EBPL	1,32E-19	0,678309258	0,69	0,564	4,72E-15
MRI1	7,29E-08	0,677553943	0,335	0,242	0,002610044
ANPEP	1,57E-14	0,676450842	0,543	0,389	5,62E-10
SNHG3	1,11E-27	0,676393121	0,808	0,67	3,98E-23
QSOX1	2,94E-15	0,672913558	0,657	0,552	1,05E-10
MRPS27	1,10E-11	0,672017497	0,467	0,345	3,94E-07
BCL11A	1,35E-12	0,671419092	0,423	0,288	4,81E-08
RHEX	1,54E-12	0,669236005	0,541	0,4	5,51E-08
APPL1	7,30E-19	0,666014311	0,676	0,539	2,61E-14
RPL3	4,17E-94	0,662701116	0,998	0,996	1,49E-89
TTLL12	1,86E-07	0,660163775	0,408	0,323	0,006666491
RSBN1	3,64E-08	0,659956226	0,4	0,305	0,001302853
ZMYM3	4,67E-07	0,659230041	0,273	0,188	0,01669541
NCOA4	1,98E-22	0,658962355	0,86	0,792	7,08E-18
REV3L	1,68E-07	0,656107205	0,366	0,285	0,005998416
RNASET2	3,96E-11	0,655141442	0,496	0,384	1,42E-06
RPS4X	2,69E-84	0,653538404	0,996	0,992	9,62E-80
SOX4	3,50E-11	0,651203679	0,575	0,472	1,25E-06
CPD	4,64E-07	0,651026362	0,329	0,242	0,016586317
KLHL24	6,70E-07	0,647472878	0,335	0,247	0,023973324
MACROH2A1	9,79E-53	0,646118168	0,993	0,974	3,50E-48
RPL5	9,92E-99	0,645442611	0,998	0,997	3,55E-94
HACD4	1,80E-07	0,645438093	0,376	0,288	0,006426705
RPLP0	9,85E-88	0,644665796	0,993	0,985	3,52E-83
ZNF22	4,58E-08	0,644596289	0,508	0,426	0,00163983
SYK	4,93E-24	0,643823337	0,816	0,706	1,76E-19
EI24	2,57E-21	0,642363584	0,772	0,665	9,21E-17
C1orf162	1,34E-06	0,640074791	0,39	0,314	0,047925029
KCNAB2	2,59E-39	0,637241184	0,934	0,823	9,25E-35
ANKRD28	1,18E-08	0,637164052	0,5	0,41	0,000422309
GOLGA8B	8,25E-07	0,634306047	0,36	0,275	0,029508764
LINC01500	1,70E-07	0,633538808	0,371	0,285	0,006098133
RPS18	8,76E-110	0,633385901	1	0,999	3,13E-105
APBB1IP	7,65E-10	0,631803539	0,567	0,474	2,74E-05
CDK6	7,70E-25	0,627357406	0,922	0,914	2,75E-20
RPL7	2,83E-92	0,627315569	0,998	0,997	1,01E-87
TKT	3,16E-21	0,626046301	0,751	0,611	1,13E-16
CCDC34	3,39E-10	0,625954507	0,419	0,304	1,21E-05
ATP2B4	2,14E-13	0,624157066	0,613	0,492	7,67E-09
FBL	1,73E-23	0,622517343	0,786	0,655	6,20E-19
TSPAN3	6,75E-16	0,622385604	0,604	0,464	2,42E-11
STK10	1,28E-09	0,621745576	0,451	0,344	4,57E-05
MFSD1	8,84E-29	0,621543084	0,864	0,758	3,16E-24

TRD-AS1	2,95E-07	0,620884681	0,569	0,501	0,01057198
FAM216A	1,79E-10	0,620879768	0,427	0,305	6,40E-06
RPL7A	2,50E-84	0,619755863	0,994	0,99	8,94E-80
RPS8	2,09E-134	0,617315251	1	1	7,48E-130
BRI3BP	2,07E-18	0,614804323	0,688	0,535	7,42E-14
MYB	1,07E-17	0,613316891	0,82	0,796	3,82E-13
AKR7A2	9,56E-08	0,613169534	0,453	0,37	0,003420649
HSH2D	2,47E-13	0,6104704	0,657	0,54	8,83E-09
COLGALT1	5,44E-12	0,607239086	0,648	0,566	1,95E-07
MDFIC	1,11E-06	0,606764682	0,313	0,229	0,039728807
CREBZF	2,74E-09	0,606713552	0,477	0,377	9,82E-05
ARMH1	6,02E-15	0,604115151	0,648	0,514	2,15E-10
STAT5B	1,05E-13	0,603495077	0,588	0,465	3,77E-09
RPS6	1,07E-120	0,603166619	1	0,999	3,83E-116
ZBTB16	1,36E-07	0,601399642	0,553	0,488	0,004883465
ZNF574	1,01E-07	0,6007212 8	0,375	0,279	0,003618233
PYGL	1,96E-16	0,598604028	0,607	0,443	7,01E-12
FAM78A	3,67E-08	0,597414429	0,407	0,311	0,001313749
ERLIN1	6,51E-07	0,596054246	0,463	0,381	0,023293973
VKORC1	1,55E-09	0,596001306	0,48	0,382	5,55E-05
RPS15A	7,56E-92	0,595621665	0,998	0,996	2,71E-87
ZMYM4	3,35E-09	0,593441411	0,494	0,401	0,000119966
RPL10A	1,12E-82	0,593423703	0,998	0,994	4,00E-78
IL17RA	5,29E-08	0,592271726	0,459	0,365	0,001893607
PPM1F	1,03E-06	0,590708874	0,412	0,332	0,036732541
LSM7	6,10E-10	0,587680958	0,48	0,368	2,18E-05
VPS26B	2,25E-09	0,586475372	0,531	0,429	8,05E-05
DHX40	2,06E-11	0,586168193	0,52	0,394	7,37E-07
EHMT2	1,51E-09	0,580325066	0,493	0,39	5,41E-05
RPL31	1,08E-112	0,579292841	0,999	0,999	3,86E-108
NOA1	6,26E-10	0,578846965	0,487	0,377	2,24E-05
RPL23A	2,07E-85	0,577013766	0,994	0,99	7,40E-81
SUMF2	2,91E-13	0,576149164	0,633	0,524	1,04E-08
IVD	2,75E-12	0,5743930 1	0,541	0,4	9,84E-08
GOT2	1,89E-09	0,572290827	0,459	0,352	6,76E-05
MIR223HG	2,18E-07	0,569707 69	0,44	0,355	0,007798167
RPS5	2,50E-81	0,569534372	0,999	0,995	8,95E-77
MIS18BP1	4,64E-13	0,568379472	0,725	0,617	1,66E-08
RFX7	3,42E-07	0,566391272	0,395	0,305	0,012249841
NPDC1	5,05E-09	0,564318775	0,536	0,456	0,00018068
EEF2	8,88E-51	0,560902683	0,989	0,985	3,18E-46
BLMH	8,92E-15	0,558188076	0,708	0,609	3,19E-10
RALGAPA2	2,66E-08	0,557946216	0,404	0,3	0,000952678
GAPT	8,34E-15	0,557479749	0,694	0,589	2,99E-10
PPA2	7,95E-20	0,556916549	0,793	0,68	2,85E-15
EIF3E	6,84E-36	0,555914103	0,96	0,94	2,45E-31
RRP1B	4,25E-08	0,555823623	0,402	0,307	0,001520489
RPL22	4,42E-74	0,555455508	0,998	0,992	1,58E-69
AHCY	8,76E-12	0,555231488	0,623	0,526	3,13E-07
HNRNPA1	7,34E-53	0,554978275	0,982	0,978	2,63E-48
NME4	4,44E-16	0,554322612	0,731	0,597	1,59E-11
FRAT2	1,39E-06	0,552055881	0,345	0,262	0,049892098
SEL1L3	1,23E-06	0,551719327	0,382	0,299	0,043899547
PLEKHA2	6,28E-07	0,551459789	0,443	0,359	0,022477057
RPL18	1,07E-59	0,550411188	0,986	0,983	3,82E-55
ELK3	1,26E-06	0,548865411	0,455	0,374	0,0452364
RCC1	2,49E-07	0,547487169	0,442	0,35	0,008906633
CUX1	9,17E-14	0,547310305	0,731	0,614	3,28E-09
TMEM97	1,52E-10	0,547131048	0,618	0,523	5,44E-06
APP	4,21E-18	0,545699028	0,599	0,427	1,51E-13
SLC40A1	3,12E-08	0,543306938	0,633	0,549	0,001114706
CCNG1	8,12E-19	0,543295553	0,816	0,723	2,91E-14
GNPTAB	1,63E-07	0,541243336	0,494	0,413	0,005815653
CTSC	3,77E-12	0,540571203	0,734	0,645	1,35E-07
PTDSS1	2,43E-18	0,538591926	0,804	0,693	8,71E-14
OPN3	9,14E-07	0,537133998	0,266	0,186	0,032704113
RPS14	5,47E-77	0,536374906	0,998	0,996	1,96E-72
RPS2	2,74E-85	0,535950 61	0,999	1	9,79E-81
RPLP1	2,93E-91	0,532759318	1	0,998	1,05E-86
PRKAR2A	1,84E-09	0,532244196	0,577	0,49	6,57E-05
RPS21	4,56E-95	0,530774938	1	0,997	1,63E-90
RPS16	7,23E-104	0,530219977	0,999	0,999	2,59E-99
RPL12	4,91E-52	0,529777227	0,999	0,996	1,76E-47
TCF3	2,26E-09	0,529446391	0,498	0,391	8,08E-05
RPS3	5,66E-73	0,529287672	0,996	0,989	2,02E-68
TIMM13	8,15E-13	0,529227406	0,646	0,534	2,91E-08
RPL11	2,53E-82	0,529108122	1	0,997	9,05E-78
RPL29	3,42E-69	0,527679903	0,999	0,997	1,22E-64
NCBP3	3,86E-08	0,527365879	0,53	0,449	0,001381883
CAMLG	2,83E-11	0,524903535	0,702	0,637	1,01E-06
ZNF714	3,39E-07	0,524564815	0,36	0,266	0,012145623
GCSH	3,57E-07	0,522459991	0,461	0,375	0,012786116
GIT1	9,62E-07	0,520241259	0,387	0,301	0,034438272
CXXC5	3,13E-16	0,519320156	0,784	0,679	1,12E-11
RPL14	1,03E-77	0,517437276	1	0,998	3,69E-73
INPP5D	9,80E-21	0,513939822	0,889	0,802	3,51E-16

CBFA2T3	1,73E-09	0,513495683	0,633	0,546	6,21E-05
CTSD	1,13E-08	0,512421514	0,688	0,608	0,000405408
RPL39	1,02E-89	0,508969547	0,999	1	3,64E-85
SLC25A36	3,57E-08	0,507088517	0,553	0,469	0,001276313
RACK1	8,39E-58	0,506702129	0,994	0,988	3,00E-53
RPS4Y1	1,07E-14	0,506277154	0,742	0,635	3,81E-10
NNT	8,84E-10	0,502390982	0,541	0,429	3,16E-05
RPS12	2,10E-62	0,500431525	0,994	0,999	7,53E-58
MTA1	1,50E-07	0,500375413	0,482	0,398	0,005352159
MSRB3	3,85E-11	0,499667324	0,673	0,59	1,38E-06
CSTB	1,93E-25	0,499072637	0,675	0,833	6,91E-21
RPSA	2,76E-52	0,498961885	0,98	0,977	9,89E-48
RPL13	5,66E-58	0,498205131	0,995	0,997	2,03E-53
TAOK3	4,44E-21	0,496246715	0,945	0,904	1,59E-16
DCAF12	3,93E-11	0,496219488	0,593	0,473	1,41E-06
MTF2	1,11E-12	0,494292443	0,654	0,549	3,96E-08
TRIM27	3,60E-08	0,493683948	0,539	0,448	0,001288574
GLUL	6,40E-19	0,493378071	0,764	0,61	2,29E-14
RPS25	1,71E-69	0,493168555	0,999	0,997	6,11E-65
RPL32	1,54E-88	0,492708991	1	0,999	5,52E-84
PEBP1	3,36E-29	0,492470975	0,973	0,956	1,20E-24
PABPC1	9,63E-67	0,489476855	1	1	3,44E-62
IKBIP	3,04E-07	0,489463404	0,422	0,328	0,010864057
PPIP5K2	5,84E-08	0,488501052	0,519	0,414	0,002090798
ADK	3,00E-07	0,487378723	0,536	0,462	0,010718547
RPL27A	6,16E-90	0,487263678	1	1	2,20E-85
CCNB1IP1	1,64E-07	0,484875243	0,476	0,386	0,005885782
RPL18A	1,06E-42	0,484331667	0,989	0,983	3,78E-38
ARMC10	4,45E-08	0,483627641	0,518	0,429	0,001591491
RPL27	7,12E-72	0,482498128	0,995	0,993	2,55E-67
RPL9	2,62E-66	0,481201936	1	1	9,39E-62
RPL26	7,51E-46	0,481153324	0,977	0,978	2,69E-41
SPTAN1	7,26E-07	0,480537653	0,453	0,366	0,025974786
TM7SF3	1,61E-17	0,478226858	0,888	0,831	5,75E-13
RPL13A	2,53E-68	0,478156551	0,998	1	9,04E-64
MFNG	7,00E-09	0,478005001	0,565	0,472	0,000250467
METTL26	2,35E-09	0,477632123	0,622	0,535	8,42E-05
MAPK14	2,85E-12	0,477202749	0,748	0,654	1,02E-07
GAS5	1,98E-20	0,473945072	0,859	0,733	7,10E-16
NUCB2	1,53E-19	0,473366477	0,907	0,801	5,49E-15
CASP2	3,64E-10	0,473250113	0,643	0,548	1,30E-05
TNRC18	5,74E-09	0,470537389	0,604	0,512	0,000205524
RPL34	2,00E-82	0,470348008	1	1	7,17E-78
QARS1	4,21E-11	0,469953334	0,759	0,666	1,51E-06
BTF3	2,27E-35	0,467484999	0,969	0,967	8,13E-31
RPS7	3,48E-72	0,467218554	0,998	0,999	1,25E-67
DRAM1	5,14E-08	0,464962999	0,572	0,48	0,001838695
PTEN	6,49E-12	0,464446526	0,77	0,695	2,32E-07
BPTF	5,23E-10	0,460413874	0,786	0,721	1,87E-05
RPS28	4,27E-81	0,458963627	0,999	0,999	1,53E-76
PIK3R1	2,86E-07	0,458429471	0,546	0,472	0,010225418
ZMIZ1	4,24E-10	0,458119748	0,705	0,619	1,52E-05
CLK1	2,14E-09	0,457474119	0,613	0,517	7,66E-05
DCXR	2,05E-07	0,457456254	0,598	0,536	0,007327136
ATP2B1	1,90E-13	0,456567295	0,607	0,483	6,81E-09
RPL6	1,21E-76	0,455801201	0,999	0,999	4,32E-72
TMEM256	3,76E-10	0,453510284	0,687	0,596	1,34E-05
CPNE1	6,46E-08	0,451628101	0,546	0,459	0,002312456
SMAD5	1,24E-10	0,451520486	0,645	0,541	4,45E-06
RPS29	4,11E-97	0,451162068	1	1	1,47E-92
LRPPRC	2,86E-11	0,448520876	0,73	0,631	1,02E-06
RPS23	5,21E-75	0,446670506	1	0,999	1,87E-70
RPL15	3,80E-55	0,445157998	1	0,999	1,36E-50
NOP53	9,34E-13	0,444113738	0,802	0,744	3,34E-08
SLC12A6	5,37E-09	0,443019856	0,67	0,584	0,000192029
MT-CYB	1,30E-102	0,442125444	1	1	4,65E-98
RPL37A	2,25E-89	0,441266545	1	1	8,04E-85
SCCPDH	9,76E-08	0,440790922	0,611	0,53	0,003491393
PTCD3	9,85E-07	0,439044688	0,53	0,463	0,035228238
RPL4	8,65E-45	0,439002643	0,999	0,993	3,10E-40
BCAP31	7,61E-08	0,433262174	0,708	0,664	0,002722245
NOP56	8,64E-12	0,427204105	0,773	0,702	3,09E-07
UQCRB	4,87E-26	0,426279016	0,935	0,909	1,74E-21
MAT2A	4,84E-07	0,426228499	0,59	0,526	0,017332431
SNHG8	9,19E-15	0,425132812	0,807	0,708	3,29E-10
SLC25A6	8,83E-24	0,424581704	0,972	0,947	3,16E-19
RCOR1	3,02E-07	0,424478867	0,537	0,458	0,010792657
EIF3F	9,29E-20	0,421406746	0,927	0,889	3,32E-15
IPO7	9,15E-14	0,419403326	0,827	0,757	3,27E-09
RPL10	6,67E-22	0,416533775	0,977	0,948	2,39E-17
GALNT2	8,47E-09	0,41653268	0,814	0,772	0,000303186
LAMP2	1,48E-12	0,408863653	0,794	0,668	5,28E-08
NBEAL1	6,23E-08	0,408690125	0,683	0,614	0,002228499
RPL30	3,64E-55	0,405916011	0,999	0,999	1,30E-50
RPLP2	2,21E-63	0,405812682	1	0,999	7,90E-59
MTHFD1L	3,17E-09	0,405332138	0,729	0,654	0,000113437

CCNY	1,07E-08	0,404214547	0,713	0,644	0,000382397
MT-CO3	3,47E-119	0,403159232	1	1	1,24E-114
LDHB	1,82E-16	0,401667816	0,892	0,839	6,51E-12
RPL37	1,08E-79	0,401015047	0,999	1	3,87E-75
RPL24	1,38E-35	0,400223857	0,989	0,983	4,95E-31
TMED3	6,14E-11	0,399575237	0,846	0,774	2,20E-06
RPL23	3,39E-52	0,399188168	0,999	1	1,21E-47
METTL9	6,06E-07	0,397003437	0,729	0,662	0,021697955
CPT1A	6,14E-14	0,389661748	0,89	0,823	2,20E-09
RPL38	1,20E-54	0,389064795	0,999	0,999	4,29E-50
PPA1	3,10E-10	0,388599025	0,736	0,668	1,11E-05
ATXN7L3B	8,08E-08	0,388531744	0,66	0,581	0,002891514
KDELR1	1,68E-13	0,388394408	0,828	0,742	6,02E-09
SEPTIN6	2,55E-08	0,387147861	0,864	0,836	0,000910737
RPL36	2,98E-37	0,385215694	1	0,998	1,07E-32
SRGN	8,15E-11	0,383063803	0,908	0,981	2,92E-06
C1QBP	5,03E-09	0,380915905	0,719	0,628	0,000179905
RPS11	6,65E-52	0,379422216	1	0,998	2,38E-47
PRDX2	7,49E-09	0,378488382	0,718	0,64	0,000268122
LUC7L3	3,42E-14	0,377155897	0,902	0,85	1,22E-09
SMARCC1	3,49E-11	0,376856747	0,806	0,751	1,25E-06
VAMP8	6,89E-20	0,376511604	0,978	0,934	2,47E-15
CRTAP	3,86E-09	0,376503384	0,794	0,707	0,000138291
HTATSF1	2,00E-08	0,375088129	0,683	0,589	0,000713935
RPL21	4,61E-54	0,370418337	0,999	1	1,65E-49
ESYT2	3,05E-07	0,369704445	0,671	0,595	0,010904593
NDUFB9	5,54E-07	0,366229641	0,731	0,686	0,019837087
RPL35A	2,09E-36	0,366121293	0,998	0,99	7,46E-32
NPM1	2,90E-32	0,361897184	0,995	0,992	1,04E-27
SARAF	8,16E-09	0,359771662	0,795	0,74	0,000291822
NCL	1,57E-19	0,356518771	0,989	0,974	5,61E-15
NACA	1,23E-25	0,355944168	0,99	0,993	4,41E-21
PRKDC	4,89E-07	0,355898132	0,759	0,715	0,017479932
POLR1D	1,24E-08	0,355111514	0,851	0,807	0,000445296
RPS13	1,11E-60	0,354470868	0,999	0,999	3,98E-56
TOMM7	3,77E-19	0,353304375	0,975	0,944	1,35E-14
RPL28	4,80E-30	0,347499958	0,999	0,993	1,72E-25
RPS9	6,29E-24	0,346515232	0,983	0,981	2,25E-19
RSL1D1	1,13E-08	0,342733872	0,843	0,789	0,000404746
PABPC4	1,12E-10	0,341039457	0,789	0,684	4,02E-06
YY1	1,11E-14	0,340008251	0,911	0,84	3,97E-10
NONO	2,85E-16	0,337162899	0,966	0,935	1,02E-11
APMAP	1,35E-08	0,337017848	0,814	0,756	0,000482934
HMGA1	9,21E-13	0,333981298	0,901	0,835	3,30E-08
TCERG1	1,09E-06	0,329007274	0,754	0,731	0,03889697
HADHA	1,56E-10	0,327504244	0,882	0,838	5,58E-06
TPT1	2,69E-47	0,326891999	1	1	9,61E-43
GPI	1,31E-08	0,325371665	0,854	0,798	0,000467486
PNRC2	1,10E-07	0,325363901	0,795	0,73	0,0039224
ATP5MC2	9,90E-30	0,325324882	0,999	0,993	3,54E-25
EIF2S3	1,72E-10	0,325190683	0,934	0,882	6,14E-06
FABP5	1,95E-09	0,324826276	0,76	0,647	6,97E-05
RPL41	7,07E-53	0,323994118	1	0,999	2,53E-48
EIF3A	1,56E-18	0,323539595	0,975	0,952	5,58E-14
PRPF38B	5,62E-07	0,321705007	0,795	0,718	0,020117376
ARID1A	6,83E-08	0,314232678	0,819	0,758	0,002443888
CCDC88A	1,75E-08	0,313298974	0,867	0,821	0,000625579
FXYD5	1,73E-07	0,312199808	0,698	0,613	0,006205795
DDX17	4,44E-16	0,309832807	0,975	0,96	1,59E-11
RPS15	3,60E-12	0,306105442	0,96	0,945	1,29E-07
RPS27	4,47E-41	0,3024809	1	1	1,60E-36
GMFG	9,92E-10	0,296588362	0,872	0,805	3,55E-05
USP22	8,33E-07	0,292498	0,804	0,739	0,029813215
MT-ND4	3,99E-76	0,290915907	1	1	1,43E-71
GNL3	1,29E-06	0,289849684	0,764	0,699	0,046025931
MT-ND3	1,76E-60	0,288108816	1	1	6,30E-56
SSRP1	1,11E-06	0,287761449	0,723	0,627	0,039774952
CLNS1A	2,13E-08	0,286329667	0,857	0,804	0,000763382
TUFM	5,67E-13	0,28467787	0,943	0,919	2,03E-08
MT-ATP8	1,44E-35	0,283714752	1	0,999	5,14E-31
RPL8	6,03E-24	0,280130095	0,994	0,99	2,16E-19
UQCRH	2,29E-16	0,279001975	0,976	0,947	8,18E-12
MBP	1,39E-07	0,276111831	0,86	0,805	0,004970038
CERS2	5,79E-11	0,273763158	0,908	0,852	2,07E-06
CD37	1,92E-09	0,271645098	0,866	0,805	6,89E-05
NDUFS5	2,09E-12	0,271045647	0,959	0,928	7,47E-08
RNF130	2,09E-08	0,270765148	0,961	0,887	0,000749452
RPL19	2,94E-20	0,257769463	0,995	0,992	1,05E-15
PNN	2,23E-07	0,257572545	0,842	0,825	0,007986207
SLC25A5	1,71E-14	0,256286833	0,988	0,927	6,10E-10
CKS2	3,48E-08	0,255729957	0,755	0,638	0,001245433
H3-3A	5,53E-17	0,2545417	0,994	0,983	1,98E-12
TOMM20	4,58E-07	0,254165663	0,887	0,843	0,016387695
ENSG00000289901	6,61E-08	0,252219438	0,86	0,815	0,002364084
SERBP1	9,94E-10	0,251794742	0,964	0,947	3,56E-05
PHB2	7,91E-07	0,248152021	0,896	0,836	0,02829112

TOP2B	3,05E-07	0,247702008	0,858	0,814	0,010926245
RPS20	6,06E-42	0,247073124	1	0,999	2,17E-37
MT-ND4L	3,87E-19	0,242623007	0,999	0,996	1,39E-14
EEF1A1	8,36E-27	0,239917727	1	1	2,99E-22
MT-ATP6	6,20E-50	0,236727435	1	1	2,22E-45
HSP90AB1	1,40E-18	0,236579547	0,999	0,997	5,03E-14
PTMA	3,35E-18	0,234796339	1	0,999	1,20E-13
EIF3H	2,44E-08	0,226174558	0,965	0,947	0,000874173
HNRNPR	4,54E-08	0,225249528	0,919	0,916	0,001624506
SLC25A3	1,14E-10	0,223973041	0,977	0,967	4,07E-06
CXCR4	1,25E-07	0,221892382	0,454	0,325	0,004475535
STMN1	7,45E-08	0,220561109	0,92	0,805	0,002667229
RPS19	4,80E-24	0,220224691	0,999	0,999	1,72E-19
COMT	5,74E-07	0,217487239	0,925	0,926	0,020548862
RPL35	2,70E-15	0,216571758	0,996	0,994	9,65E-11
SPN	8,91E-08	0,214912111	0,954	0,9	0,003187321
MT-CO2	1,16E-50	0,207497797	1	1	4,16E-46
MT-CO1	8,89E-48	0,207016583	1	1	3,18E-43
PCBP2	9,48E-08	0,206332687	0,987	0,972	0,003392202
HDGF	3,44E-10	0,204627928	0,98	0,954	1,23E-05
ARHGDIB	4,57E-16	0,201386357	0,995	0,964	1,63E-11
MT-ND1	9,45E-40	0,187867478	1	1	3,38E-35
SNHG6	7,53E-07	0,183650991	0,949	0,937	0,026949463
MT-ND2	1,03E-27	0,177223557	1	1	3,69E-23
ANP32B	2,60E-08	0,157517402	0,996	0,988	0,000929891
YBX1	4,48E-10	0,157259867	0,998	0,997	1,60E-05
GNAS	1,63E-09	0,149094446	0,998	0,993	5,84E-05
CCNI	1,31E-07	0,139789335	0,993	0,991	0,004673875
FTL	8,19E-17	0,102926141	0,994	0,981	2,93E-12
ANXA2	3,35E-32	0,085286827	0,528	0,757	1,20E-27
FGR	1,23E-09	-0,036622837	0,23	0,364	4,39E-05
GSN	1,29E-09	-0,046990708	0,637	0,758	4,62E-05
CIR1	1,76E-11	-0,086753952	0,523	0,657	6,30E-07
GRN	3,62E-14	-0,088867621	0,813	0,893	1,30E-09
PSAP	1,06E-32	-0,093772534	0,966	0,978	3,78E-28
SH3BGRL3	1,60E-09	-0,094083837	1	0,998	5,74E-05
CTSS	6,37E-13	-0,101727578	0,589	0,722	2,28E-08
RAB7A	8,22E-07	-0,127425685	0,958	0,983	0,029414049
HNRNPA2B1	2,75E-08	-0,139119682	0,999	0,998	0,00098317
MAX	1,24E-06	-0,139530736	0,908	0,933	0,044447403
ARPC2	4,51E-08	-0,141563995	0,992	0,999	0,001615208
TPI1	5,90E-07	-0,148458474	0,988	0,967	0,02110275
COX6C	1,06E-08	-0,171835486	0,984	0,987	0,000377821
CLTC	2,21E-07	-0,174183278	0,907	0,943	0,007909509
MORF4L1	1,09E-08	-0,176451994	0,969	0,985	0,0003906
RAN	7,87E-07	-0,182956512	0,987	0,99	0,028167917
TBCA	1,36E-06	-0,186316212	0,889	0,888	0,048758523
COX6A1	6,96E-07	-0,186760938	0,898	0,935	0,024896158
GNAI2	3,99E-09	-0,187056488	0,964	0,976	0,000142904
GRB2	1,16E-06	-0,187098978	0,941	0,952	0,041434235
ATP6V0B	7,96E-07	-0,188548437	0,86	0,902	0,028487744
SAMHD1	5,29E-10	-0,188583862	0,227	0,363	1,89E-05
KPNB1	2,05E-08	-0,188888412	0,973	0,983	0,000734752
CALM1	5,71E-12	-0,203509108	0,946	0,967	2,04E-07
PKM	1,58E-10	-0,209785848	0,971	0,982	5,66E-06
CAPG	5,65E-12	-0,213096414	0,783	0,866	2,02E-07
PCBP1	3,62E-12	-0,213522799	0,98	0,988	1,30E-07
GNB1	8,00E-14	-0,220011845	0,993	0,994	2,86E-09
LDHA	5,28E-07	-0,221415111	0,954	0,937	0,018902058
TLE5	3,62E-07	-0,226581328	0,919	0,943	0,012948597
PLEKHB2	4,85E-07	-0,227970179	0,64	0,738	0,017370226
YWHAB	1,86E-17	-0,229136614	0,987	0,994	6,66E-13
AK2	2,99E-07	-0,229680174	0,907	0,927	0,010692844
MRPL51	8,97E-07	-0,233897528	0,793	0,837	0,032109161
TPM4	1,26E-12	-0,234221787	0,939	0,96	4,50E-08
RTN4	2,13E-09	-0,236601432	0,919	0,942	7,61E-05
EWSR1	1,41E-12	-0,242679533	0,948	0,968	5,06E-08
MTCH2	8,37E-07	-0,243392858	0,782	0,837	0,029943081
CFL1	4,03E-32	-0,245118164	1	1	1,44E-27
TFRC	5,20E-10	-0,248479064	0,699	0,795	1,86E-05
TRA2B	5,94E-07	-0,249019802	0,812	0,85	0,021271679
GGNBP2	4,54E-07	-0,249394766	0,789	0,855	0,016250395
CHCHD2	1,02E-12	-0,250999318	0,955	0,967	3,65E-08
MLF2	8,67E-09	-0,252868197	0,819	0,889	0,000310288

NDUFAB1	6,03E-08	-0,258645787	0,804	0,868	0,002157418
YWHAZ	7,30E-18	-0,260421599	0,983	0,99	2,61E-13
CYRIB	6,45E-07	-0,260826954	0,618	0,731	0,023062775
JUND	3,56E-08	-0,262019133	0,875	0,925	0,001272134
RBX1	4,37E-09	-0,262421627	0,845	0,903	0,000156366
ARL6IP1	4,77E-08	-0,263872413	0,81	0,89	0,001707735
PSMC2	1,77E-08	-0,264517976	0,782	0,834	0,000633901
UBE2I	4,25E-08	-0,265496699	0,812	0,857	0,001520218
ADD1	2,15E-08	-0,26551775	0,836	0,9	0,000768618
COX8A	2,10E-10	-0,265682686	0,882	0,932	7,50E-06
DAZAP2	1,61E-11	-0,265915442	0,883	0,936	5,76E-07
NDUFA4	5,83E-15	-0,266678874	0,93	0,958	2,09E-10
FCER1G	2,42E-16	-0,266797572	0,348	0,539	8,65E-12
BRI3	6,78E-18	-0,268419182	0,787	0,888	2,43E-13
CAPZA1	6,65E-17	-0,270254	0,967	0,979	2,38E-12
RPL36AL	4,60E-11	-0,271985111	0,869	0,92	1,64E-06
PRMT1	9,74E-07	-0,276241555	0,782	0,839	0,034858186
STARD7	4,20E-07	-0,278508058	0,78	0,83	0,015019396
BZW1	8,00E-10	-0,279083755	0,729	0,833	2,86E-05
FTH1	1,70E-88	-0,279374291	0,982	0,991	6,07E-84
RAC1	1,23E-18	-0,279735198	0,957	0,988	4,41E-14
ARPC3	2,93E-14	-0,279831559	0,902	0,954	1,05E-09
TMBIM6	1,51E-25	-0,280856943	0,972	0,994	5,42E-21
CAST	1,18E-06	-0,281589734	0,525	0,64	0,042334715
GPSM3	9,65E-08	-0,282680401	0,704	0,783	0,003453081
EIF4G2	4,55E-17	-0,283391944	0,949	0,979	1,63E-12
SSBP1	1,43E-13	-0,283715659	0,936	0,958	5,12E-09
H2AZ1	5,22E-07	-0,284521852	0,946	0,949	0,018685515
UBXN4	7,14E-10	-0,285284714	0,84	0,885	2,55E-05
COPA	8,66E-09	-0,285502331	0,828	0,886	0,000309997
PSMF1	1,89E-08	-0,289228635	0,761	0,826	0,00067738
WDR1	2,17E-10	-0,290096231	0,796	0,875	7,77E-06
ARF6	3,48E-09	-0,293111189	0,783	0,85	0,000124559
PARK7	8,92E-11	-0,297262832	0,816	0,884	3,19E-06
GTF2A2	1,25E-06	-0,297408546	0,561	0,669	0,044780137
PTGS1	2,26E-08	-0,299030852	0,466	0,606	0,000809548
EIF4E2	8,65E-07	-0,299251738	0,681	0,759	0,030951687
BRK1	2,39E-11	-0,300917043	0,864	0,902	8,55E-07
TPP1	6,22E-11	-0,303323993	0,914	0,94	2,22E-06
PSMD2	1,67E-07	-0,303553025	0,655	0,756	0,005976576
PPP4C	3,32E-10	-0,30449912	0,77	0,853	1,19E-05
SRPRA	9,36E-13	-0,304731191	0,869	0,918	3,35E-08
CDC123	5,12E-07	-0,30576099	0,517	0,637	0,018324515
DOCK2	6,66E-07	-0,305971113	0,761	0,819	0,023817707
SLC7A11	5,88E-22	-0,308013354	0,131	0,321	2,10E-17
UBE2D3	1,40E-13	-0,310969167	0,869	0,929	5,02E-09
ARPC5L	5,47E-07	-0,311597368	0,629	0,713	0,019576365
C11orf58	2,46E-16	-0,312231431	0,898	0,937	8,79E-12
UQCRQ	1,82E-15	-0,313870039	0,918	0,94	6,50E-11
CMPK1	2,81E-08	-0,314208849	0,669	0,769	0,001005339
KIF5B	4,66E-12	-0,314612719	0,819	0,902	1,67E-07
MTPN	2,06E-20	-0,314675472	0,963	0,973	7,37E-16
LASP1	9,84E-10	-0,315399477	0,692	0,803	3,52E-05
NDUFA12	3,81E-11	-0,315862282	0,767	0,841	1,36E-06
GSTO1	1,97E-12	-0,317058773	0,887	0,915	7,05E-08
ACO2	1,35E-08	-0,318047682	0,733	0,792	0,000481628
EMC4	2,13E-08	-0,318553375	0,687	0,775	0,000760371
PSME3	5,96E-11	-0,318728978	0,757	0,828	2,13E-06
CAP1	1,02E-23	-0,321674216	0,945	0,986	3,64E-19
SEM1	3,88E-08	-0,321928207	0,711	0,795	0,001388975
ANAPC11	9,70E-07	-0,322907669	0,528	0,635	0,034693737
MRPL52	9,11E-13	-0,323519198	0,81	0,853	3,26E-08
VASP	2,15E-10	-0,324039366	0,773	0,843	7,69E-06
NOP10	8,21E-16	-0,324988297	0,835	0,924	2,94E-11
HCLS1	2,36E-13	-0,32570229	0,864	0,935	8,45E-09
SMIM12	2,54E-09	-0,326432402	0,583	0,712	9,09E-05
UBE2D2	1,47E-15	-0,326658235	0,913	0,949	5,27E-11
SOD1	9,14E-18	-0,329292333	0,935	0,952	3,27E-13

C6orf62	4,88E-09	-0,330321799	0,771	0,839	0,000174697
LIMD2	3,11E-07	-0,33093208	0,545	0,654	0,011119306
TMEM9B	3,12E-07	-0,331043193	0,46	0,578	0,011153214
COPZ1	1,17E-07	-0,331132904	0,661	0,747	0,004184149
MAP3K20	9,69E-07	-0,331540163	0,561	0,666	0,034684804
NDUFA6	8,89E-08	-0,332286514	0,504	0,629	0,003181942
UBE2A	5,07E-09	-0,335529811	0,701	0,778	0,000181363
ANKRD12	1,57E-08	-0,337098598	0,727	0,81	0,000560579
UBE2Q1	7,65E-11	-0,337245235	0,784	0,86	2,74E-06
ABCF1	6,65E-11	-0,337562521	0,706	0,803	2,38E-06
MAT2B	1,14E-06	-0,339160566	0,582	0,673	0,040757996
ATP2C1	2,91E-07	-0,340789601	0,552	0,643	0,010417763
COX20	1,57E-07	-0,341047036	0,665	0,741	0,005625119
CD55	1,60E-09	-0,342138644	0,549	0,679	5,73E-05
PTBP3	2,04E-10	-0,343181848	0,899	0,915	7,31E-06
PRDX5	2,30E-10	-0,343311172	0,735	0,821	8,22E-06
UBE2B	2,66E-07	-0,343484408	0,535	0,65	0,009512763
SAT1	4,50E-09	-0,343756797	0,689	0,795	0,00016092
UBL5	2,49E-09	-0,344780051	0,663	0,772	8,89E-05
GHITM	5,41E-15	-0,345130808	0,895	0,936	1,94E-10
PDIA3	9,53E-17	-0,345242151	0,883	0,947	3,41E-12
AP2B1	6,63E-09	-0,345841982	0,708	0,785	0,000237377
COTL1	2,98E-12	-0,348129138	0,634	0,774	1,07E-07
TPM3	1,89E-40	-0,349320468	0,993	0,997	6,77E-36
CLIC1	2,16E-17	-0,350627875	0,887	0,918	7,72E-13
FKBP1A	4,27E-16	-0,351073189	0,836	0,913	1,53E-11
DDX5	4,90E-23	-0,352380808	0,988	0,996	1,75E-18
AKR1A1	7,56E-11	-0,356241562	0,676	0,8	2,71E-06
FIBP	4,69E-07	-0,356809096	0,535	0,659	0,016767074
MBD2	2,94E-07	-0,357061377	0,436	0,566	0,010517012
COPB2	7,50E-10	-0,357295749	0,677	0,762	2,69E-05
NFE2L2	2,27E-09	-0,357997552	0,683	0,769	8,12E-05
USP16	9,57E-07	-0,358156872	0,565	0,661	0,034226105
ATP5F1E	1,10E-46	-0,358833919	0,999	1	3,93E-42
PLP2	3,50E-18	-0,359718127	0,966	0,931	1,25E-13
BCL7B	3,71E-07	-0,360718407	0,536	0,634	0,013258382
HSD17B4	3,98E-08	-0,361566105	0,617	0,707	0,001423317
PRR13	1,94E-16	-0,362324362	0,836	0,899	6,93E-12
ATP5PD	3,34E-20	-0,365149949	0,9	0,949	1,20E-15
CD47	2,92E-15	-0,3657487	0,864	0,903	1,04E-10
XPO6	6,27E-08	-0,366239135	0,465	0,586	0,002244594
SCYL2	7,33E-07	-0,366693647	0,546	0,646	0,02624446
TIMM23	5,89E-07	-0,369708568	0,453	0,566	0,021059029
SLC16A3	2,46E-08	-0,371245525	0,4	0,537	0,000878554
IFITM2	9,41E-11	-0,371870892	0,878	0,902	3,37E-06
MYL6	2,15E-18	-0,371964208	0,896	0,945	7,70E-14
KARS1	2,31E-08	-0,371985313	0,572	0,666	0,000825967
PSMD7	5,00E-14	-0,372318096	0,793	0,868	1,79E-09
RAC2	2,78E-23	-0,373299736	0,989	0,946	9,94E-19
VBP1	8,79E-07	-0,374357384	0,514	0,607	0,031446692
LAMTOR3	1,15E-07	-0,374412329	0,542	0,627	0,004103276
GNS	1,16E-06	-0,374540433	0,388	0,51	0,04147041
STXBP5	1,02E-09	-0,377562956	0,658	0,754	3,64E-05
ATF4	1,64E-10	-0,378329468	0,872	0,91	5,87E-06
SRI	4,21E-11	-0,378528857	0,769	0,833	1,51E-06
DAP3	2,67E-07	-0,378725328	0,563	0,661	0,009562238
TAX1BP1	2,11E-17	-0,378958266	0,834	0,931	7,56E-13
SLC2A3	8,71E-10	-0,379279215	0,36	0,504	3,12E-05
ATXN2L	3,96E-15	-0,3793836	0,907	0,934	1,42E-10
TRMT112	1,02E-11	-0,380837883	0,752	0,843	3,64E-07
ZNF511	4,55E-08	-0,381235746	0,425	0,553	0,001629815
TARS1	7,30E-07	-0,382009602	0,551	0,633	0,026104193
VIM	3,66E-26	-0,382178916	0,965	0,991	1,31E-21
MEF2D	5,98E-08	-0,382268263	0,434	0,566	0,002139016
PPP1R18	1,24E-14	-0,384815871	0,869	0,94	4,44E-10
RELA	1,64E-07	-0,385126079	0,664	0,736	0,005858876
POLR2G	2,39E-14	-0,3854737	0,747	0,842	8,54E-10
AAGAB	8,95E-07	-0,385687602	0,361	0,472	0,032033748

VCP	6,51E-11	-0,386375413	0,681	0,789	2,33E-06	USP14	3,64E-16	-0,413096349	0,717	0,841	1,30E-11
OST4	1,61E-20	-0,386855785	0,92	0,964	5,75E-16	C21orf91	1,17E-06	-0,413974773	0,398	0,508	0,041691481
ARPP19	2,79E-08	-0,388452747	0,547	0,658	0,000998621	PSTPIP2	3,42E-14	-0,414819949	0,533	0,69	1,22E-09
UBE2M	6,30E-10	-0,388739711	0,634	0,731	2,26E-05	PSIP1	8,64E-13	-0,415606253	0,881	0,918	3,09E-08
PAFAH1B1	1,60E-12	-0,388829622	0,62	0,759	5,74E-08	BTG2	1,01E-06	-0,416574788	0,452	0,551	0,036066755
ALS2	1,22E-06	-0,388892447	0,501	0,6	0,043618936	DPM1	1,14E-07	-0,417946974	0,44	0,557	0,004064539
ATP2A2	2,53E-14	-0,389726517	0,823	0,882	9,05E-10	SRF	5,14E-08	-0,418314697	0,475	0,596	0,001840813
ARPC4	4,46E-12	-0,389810199	0,673	0,788	1,59E-07	MAPRE1	5,46E-18	-0,418382061	0,793	0,875	1,95E-13
ELOVL5	2,85E-08	-0,390847858	0,567	0,668	0,00101951	ARF4	3,58E-17	-0,418427088	0,76	0,875	1,28E-12
UBB	1,66E-21	-0,391624705	0,895	0,949	5,94E-17	HPGD	3,54E-07	-0,418833511	0,266	0,372	0,012657164
ARL8B	1,15E-16	-0,391664284	0,808	0,911	4,10E-12	EIF2S1	7,26E-08	-0,419166231	0,414	0,531	0,002597531
ATP5IF1	1,47E-12	-0,391839353	0,777	0,834	5,25E-08	TIMMDC1	1,90E-07	-0,420231849	0,404	0,521	0,006792354
CAMTA1	2,21E-12	-0,392273336	0,747	0,839	7,90E-08	ME2	2,52E-09	-0,420817333	0,588	0,679	9,03E-05
PRRC2C	6,80E-15	-0,393124526	0,878	0,931	2,43E-10	POLR1F	5,59E-10	-0,423026535	0,592	0,715	2,00E-05
UBE2N	1,07E-15	-0,396700458	0,755	0,865	3,83E-11	ZNF655	2,21E-09	-0,423371462	0,511	0,624	7,92E-05
PSMB3	3,01E-16	-0,399370975	0,804	0,865	1,08E-11	COPG1	5,14E-13	-0,425621136	0,565	0,708	1,84E-08
RAE1	6,20E-07	-0,399523022	0,476	0,576	0,022179553	PSMA1	1,19E-12	-0,427512677	0,692	0,792	4,25E-08
PSMD12	2,85E-08	-0,400826279	0,552	0,653	0,001018905	KCTD10	3,64E-07	-0,428075322	0,373	0,485	0,013031652
DCAF11	1,63E-09	-0,401462547	0,536	0,663	5,82E-05	SNX9	9,79E-07	-0,428849978	0,29	0,397	0,035046178
PFDN2	3,47E-07	-0,401665138	0,423	0,529	0,01241257	CALM3	2,29E-14	-0,429529015	0,714	0,834	8,20E-10
CHUK	3,32E-07	-0,402321403	0,361	0,476	0,011889313	DUSP23	1,87E-07	-0,429812951	0,517	0,616	0,006683316
ARRB1	1,45E-07	-0,402348818	0,546	0,634	0,005175668	LRRFIP2	8,35E-08	-0,430538475	0,59	0,683	0,002986141
RB1	7,06E-09	-0,404132211	0,549	0,645	0,000252659	SRSF7	3,33E-14	-0,431077422	0,819	0,873	1,19E-09
KCMF1	3,01E-08	-0,405732999	0,501	0,623	0,001076986	SNRNP27	4,48E-08	-0,43129651	0,371	0,495	0,001601932
TXNL4A	2,45E-10	-0,406111281	0,587	0,697	8,76E-06	TESPA1	1,18E-08	-0,432785566	0,578	0,681	0,000423953
PDCD10	5,38E-07	-0,407001759	0,466	0,571	0,019248603	CCDC59	2,62E-11	-0,434090833	0,648	0,735	9,38E-07
STK40	5,90E-07	-0,407417891	0,376	0,488	0,021099414	RHOQ	1,67E-12	-0,434350984	0,443	0,607	5,97E-08
ARHGDIA	1,50E-15	-0,408594897	0,731	0,828	5,36E-11	CHMP2A	2,25E-09	-0,434727422	0,439	0,575	8,06E-05
TSG101	9,64E-10	-0,410088141	0,467	0,607	3,45E-05	SPINT2	1,25E-18	-0,435508942	0,848	0,943	4,47E-14
PLAA	5,17E-07	-0,411168885	0,396	0,518	0,018500781	GABPB1	2,87E-07	-0,436137217	0,454	0,56	0,010271674
RAP1B	1,31E-15	-0,411503357	0,752	0,866	4,69E-11	VSIR	7,02E-07	-0,437383707	0,311	0,424	0,025132275
RAP1A	3,51E-10	-0,411644465	0,624	0,738	1,26E-05	ARHGAP30	2,48E-10	-0,437612807	0,573	0,699	8,87E-06
TMEM167A	4,10E-09	-0,412081882	0,524	0,638	0,000146813	ARPC5	3,10E-37	-0,437639245	0,941	0,985	1,11E-32
RHOG	6,62E-24	-0,412905844	0,919	0,965	2,37E-19	ETS2	1,52E-07	-0,437947337	0,499	0,601	0,005445203

NSFL1C	4,57E-07	-0,439513052	0,383	0,492	0,016362332
ATP5MK	2,60E-28	-0,440052446	0,869	0,938	9,31E-24
LGALS1	2,00E-26	-0,440959418	0,814	0,925	7,16E-22
AP1B1	2,40E-10	-0,443594106	0,516	0,65	8,60E-06
EIF2S2	1,55E-17	-0,444639482	0,908	0,925	5,55E-13
CNOT9	1,22E-13	-0,445103797	0,687	0,781	4,38E-09
CASP8	2,51E-09	-0,446509277	0,525	0,647	8,98E-05
MRPL20	3,44E-15	-0,447371716	0,694	0,809	1,23E-10
DCTD	1,42E-15	-0,447671269	0,773	0,864	5,08E-11
PSMD8	2,47E-17	-0,448245455	0,71	0,832	8,84E-13
CLDND1	1,70E-08	-0,448344581	0,667	0,754	0,000609312
PEX14	1,24E-07	-0,448762316	0,312	0,437	0,004449626
EIF5A	1,37E-25	-0,449266727	0,894	0,956	4,90E-21
ST3GAL2	1,07E-07	-0,451457124	0,431	0,547	0,003819318
PHACTR2	4,95E-08	-0,452550851	0,537	0,645	0,001771083
ADIPOR1	2,01E-08	-0,452693462	0,43	0,547	0,000718201
PSMD4	7,11E-22	-0,454310569	0,807	0,905	2,54E-17
SRP54	4,64E-15	-0,455532865	0,628	0,764	1,66E-10
CHMP1A	6,66E-11	-0,455541976	0,566	0,687	2,38E-06
CAPZB	2,17E-46	-0,455735559	0,972	0,993	7,75E-42
LIF	2,51E-09	-0,456367264	0,206	0,326	9,00E-05
ATP6V1A	2,68E-12	-0,457268806	0,687	0,774	9,60E-08
NAPA	5,59E-18	-0,457744012	0,741	0,86	2,00E-13
RIC8A	1,09E-06	-0,458029331	0,345	0,445	0,038976463
PPP1R12A	2,17E-18	-0,459305577	0,818	0,884	7,77E-14
TRAPPC4	4,50E-07	-0,460714987	0,33	0,442	0,016107225
CD2AP	1,09E-07	-0,461055453	0,477	0,571	0,00389897
CORO1B	1,07E-06	-0,461945279	0,219	0,322	0,038386453
MZT1	1,23E-08	-0,462912666	0,471	0,582	0,000440202
CIAO2B	1,51E-08	-0,463535696	0,407	0,542	0,000540388
RIT1	3,63E-07	-0,464033697	0,255	0,367	0,012992418
FLOT2	1,27E-08	-0,464367219	0,514	0,614	0,000453498
VPS29	9,96E-09	-0,465597973	0,477	0,593	0,000356303
EDF1	1,29E-11	-0,466627181	0,516	0,65	4,63E-07
ELOC	3,51E-19	-0,467043866	0,67	0,82	1,25E-14
CDC42SE2	1,66E-15	-0,469154261	0,654	0,785	5,94E-11
PATL1	2,60E-09	-0,469550419	0,547	0,655	9,29E-05
LITAF	1,11E-09	-0,470322841	0,51	0,65	3,97E-05
ITM2B	1,34E-28	-0,470723368	0,911	0,959	4,79E-24
FERMT3	5,47E-11	-0,471354165	0,518	0,654	1,96E-06
UBE2L3	6,92E-28	-0,471891447	0,847	0,93	2,48E-23
JAK1	6,72E-16	-0,472974223	0,675	0,814	2,41E-11
RAB5A	7,66E-09	-0,473387036	0,418	0,537	0,000274226
RAD23A	6,16E-14	-0,474841296	0,694	0,79	2,21E-09
SLC7A5	2,43E-11	-0,475413929	0,549	0,674	8,69E-07
LCP2	3,16E-10	-0,476679955	0,576	0,689	1,13E-05
CTTNBP2	4,77E-08	-0,477543302	0,189	0,294	0,001708054
SUB1	4,06E-27	-0,479223727	0,864	0,936	1,45E-22
GLRX2	6,91E-09	-0,479584552	0,355	0,485	0,000247218
SNRPA1	2,29E-08	-0,479714572	0,448	0,553	0,000820427
ACOT13	1,49E-07	-0,479969024	0,28	0,395	0,00533039
FLCN	7,35E-07	-0,481919606	0,306	0,412	0,026310213
TTC7B	2,12E-09	-0,482134358	0,311	0,444	7,59E-05
KYAT3	1,70E-07	-0,4826903	0,341	0,454	0,00608463
SUSD1	1,83E-07	-0,483077082	0,312	0,419	0,00655587
MRPL28	1,49E-07	-0,483943094	0,382	0,494	0,005337505
SH2B3	1,76E-11	-0,484765226	0,493	0,65	6,29E-07
KRT10	4,78E-12	-0,485386423	0,524	0,64	1,71E-07
CEP55	1,12E-06	-0,486180865	0,254	0,35	0,0401392
LEO1	2,48E-12	-0,486374097	0,554	0,675	8,86E-08
ERLEC1	6,82E-10	-0,486426085	0,427	0,554	2,44E-05
BUD31	1,04E-08	-0,487995132	0,308	0,435	0,000371578
CDK2AP2	7,25E-12	-0,488044245	0,504	0,652	2,60E-07
COA6	1,31E-10	-0,490150942	0,459	0,594	4,69E-06
PRDX1	4,70E-18	-0,491144605	0,883	0,945	1,68E-13
PDCD5	4,09E-07	-0,491697559	0,49	0,587	0,014635683
CLEC2B	3,11E-07	-0,492904289	0,32	0,425	0,011119848
DEDD	8,59E-12	-0,492992243	0,424	0,582	3,07E-07

NUP62	1,04E-14	-0,493489923	0,6	0,732	3,72E-10
HSPA5	8,49E-12	-0,495127136	0,813	0,87	3,04E-07
PHF11	7,36E-12	-0,495520351	0,489	0,64	2,63E-07
SELENOT	2,47E-20	-0,496251898	0,702	0,839	8,83E-16
PSMC3	3,57E-14	-0,496757997	0,601	0,725	1,28E-09
ADGRE5	2,28E-07	-0,497193533	0,373	0,483	0,008165
ZFAND3	1,76E-08	-0,498852244	0,524	0,623	0,000629406
TMEM214	1,63E-10	-0,499285557	0,53	0,645	5,82E-06
OSTF1	2,53E-07	-0,499449557	0,328	0,431	0,009057347
AIDA	1,73E-08	-0,499553451	0,489	0,593	0,000618149
STAM	4,35E-09	-0,500214629	0,343	0,46	0,000155543
MIEN1	6,00E-07	-0,500518467	0,293	0,4	0,021467618
PSMD13	9,17E-15	-0,501095235	0,599	0,735	3,28E-10
ARID4B	1,15E-13	-0,501759648	0,72	0,822	4,11E-09
PSMC5	5,13E-20	-0,502179334	0,728	0,834	1,84E-15
TMEM14A	1,34E-06	-0,502630695	0,219	0,316	0,04779328
LAPTM5	5,76E-16	-0,504141673	0,923	0,915	2,06E-11
MRPL41	1,99E-14	-0,504230514	0,567	0,709	7,12E-10
ILRUN	6,63E-11	-0,5047541	0,476	0,612	2,37E-06
RAB13	2,03E-07	-0,507198863	0,323	0,438	0,007262368
PML	1,25E-08	-0,507494287	0,325	0,454	0,000448103
SNRPG	3,57E-36	-0,508112853	0,922	0,974	1,28E-31
ATP6V1B2	9,50E-34	-0,508448983	0,747	0,874	3,40E-29
SLC35B1	3,36E-10	-0,508553599	0,442	0,58	1,20E-05
DNAJB12	2,10E-08	-0,508669359	0,296	0,416	0,000752384
EZR	5,38E-12	-0,508674772	0,502	0,648	1,92E-07
CLSTN3	1,35E-06	-0,508858262	0,255	0,359	0,04825435
LCP1	5,99E-40	-0,509161877	0,935	0,983	2,14E-35
STX17	3,30E-08	-0,509742747	0,382	0,497	0,001182037
BLOC1S2	2,32E-12	-0,509819116	0,519	0,654	8,31E-08
TTC32	5,00E-07	-0,510368707	0,248	0,354	0,01788558
COMMD4	4,90E-09	-0,511064741	0,428	0,547	0,00017543
PSMD14	8,29E-17	-0,511091324	0,635	0,76	2,97E-12
S100A11	4,03E-53	-0,511144347	0,637	0,88	1,44E-48
TAF13	2,23E-07	-0,511482455	0,359	0,463	0,007965098
IL4R	1,72E-07	-0,511567352	0,246	0,355	0,006160686
NMT1	4,18E-09	-0,511788141	0,43	0,548	0,000149667
TYK2	7,02E-10	-0,512767682	0,492	0,627	2,51E-05
SEPTIN11	9,11E-14	-0,512792539	0,672	0,784	3,26E-09
PSMD6	5,21E-15	-0,512839742	0,584	0,726	1,86E-10
PRELID1	1,63E-15	-0,513192931	0,554	0,696	5,84E-11
TIMM10	1,32E-13	-0,513433372	0,652	0,757	4,72E-09
STAT3	5,10E-18	-0,514845277	0,654	0,771	1,82E-13
CLU	2,49E-11	-0,514851612	0,445	0,58	8,91E-07
FAM50A	2,89E-07	-0,515236894	0,21	0,319	0,010331164
SLC50A1	7,53E-09	-0,515960731	0,359	0,491	0,000269283
FKBP5	1,61E-08	-0,516085102	0,458	0,564	0,000575724
UBE2S	7,86E-11	-0,516576158	0,552	0,67	2,81E-06
MAP4	1,01E-06	-0,519227766	0,341	0,447	0,036296185
DRAP1	7,13E-13	-0,519603125	0,604	0,723	2,55E-08
APOBEC3C	6,68E-16	-0,521208086	0,717	0,792	2,39E-11
PPP1R9B	6,96E-07	-0,521304506	0,308	0,419	0,024911118
MCL1	1,24E-22	-0,521504196	0,777	0,898	4,44E-18
ESYT1	5,77E-16	-0,521645167	0,693	0,794	2,07E-11
TFG	4,38E-13	-0,522112833	0,601	0,722	1,57E-08
MAP7D1	4,68E-21	-0,523455512	0,689	0,811	1,68E-16
ACOT9	3,00E-08	-0,523933606	0,305	0,427	0,001072822
EMC7	4,07E-13	-0,524232908	0,487	0,631	1,46E-08
VRK2	5,14E-07	-0,524395648	0,324	0,428	0,018380474
YKT6	2,72E-10	-0,525805865	0,399	0,526	9,74E-06
EDEM1	1,52E-09	-0,526019463	0,342	0,472	5,45E-05
SLC39A11	7,82E-07	-0,527146972	0,353	0,452	0,027997691
RAB12	5,32E-07	-0,527373252	0,257	0,361	0,019043446
SRP19	2,72E-20	-0,528288355	0,717	0,827	9,74E-16
TIPRL	2,05E-16	-0,531051157	0,593	0,732	7,33E-12
ELK1	8,53E-10	-0,531181493	0,358	0,497	3,05E-05
SFT2D1	1,02E-17	-0,531313236	0,53	0,719	3,67E-13
GTF2H3	2,29E-08	-0,535544851	0,46	0,556	0,000818689

LST1	6,20E-12	-0,537540847	0,384	0,531	2,22E-07	PSMB1	1,22E-54	-0,556955765	0,937	0,984	4,37E-50
CD53	1,52E-20	-0,537785884	0,527	0,74	5,45E-16	NCF4	2,67E-15	-0,557550778	0,602	0,724	9,57E-11
XRN1	4,39E-08	-0,538260656	0,404	0,51	0,001571504	PTK2	1,07E-06	-0,558341289	0,175	0,269	0,038205875
DLC1	5,97E-09	-0,538798165	0,163	0,274	0,000213633	COX19	1,95E-07	-0,558961286	0,269	0,373	0,006982374
SLC1A4	8,37E-11	-0,538940322	0,516	0,627	3,00E-06	MKNK2	7,59E-07	-0,559302924	0,382	0,492	0,027151982
CAMK1D	6,53E-08	-0,539217902	0,358	0,466	0,002335561	TMEM50A	4,76E-24	-0,559767356	0,717	0,857	1,70E-19
COPS7A	5,41E-08	-0,540150777	0,354	0,473	0,001934167	PPP2R3C	3,90E-13	-0,559963345	0,493	0,632	1,39E-08
VMP1	6,73E-25	-0,540416952	0,692	0,835	2,41E-20	TIMP1	7,56E-20	-0,560149756	0,486	0,678	2,70E-15
PPP1R11	9,77E-10	-0,541508549	0,353	0,486	3,50E-05	DPYSL2	3,87E-08	-0,560173634	0,439	0,543	0,001385041
PCGF5	7,42E-11	-0,542414997	0,477	0,596	2,65E-06	BCL2L1	1,05E-15	-0,560454906	0,554	0,709	3,77E-11
IFNGR2	6,18E-10	-0,542488621	0,458	0,575	2,21E-05	RHOH	1,35E-13	-0,560908132	0,495	0,641	4,81E-09
CMAS	2,75E-22	-0,542688636	0,733	0,84	9,85E-18	CYB5B	1,12E-18	-0,561643374	0,631	0,76	4,00E-14
ACOT7	8,93E-10	-0,544475413	0,381	0,504	3,19E-05	EXOSC8	4,38E-07	-0,562934504	0,364	0,456	0,015660986
PRKCD	4,17E-12	-0,544769577	0,36	0,514	1,49E-07	PTMS	1,50E-23	-0,564138011	0,827	0,92	5,38E-19
TGFBR1	4,24E-07	-0,547103131	0,328	0,434	0,015167856	SH3KBP1	2,10E-22	-0,564321606	0,716	0,858	7,52E-18
PAPSS1	1,81E-14	-0,547245064	0,619	0,751	6,47E-10	SVIP	2,44E-21	-0,565070326	0,68	0,816	8,74E-17
ACTR3	2,72E-58	-0,547385797	0,948	0,987	9,72E-54	SMG1	5,70E-08	-0,566275405	0,382	0,494	0,002038644
ZBTB20	3,57E-07	-0,547973147	0,272	0,376	0,012788133	H3-3B	3,67E-52	-0,568133591	0,965	0,99	1,31E-47
SCAMP3	1,33E-21	-0,550188897	0,654	0,802	4,77E-17	SZRD1	5,57E-11	-0,569120239	0,425	0,562	1,99E-06
SNAP23	7,57E-15	-0,551941591	0,559	0,699	2,71E-10	MYCBP2	8,77E-11	-0,569214494	0,634	0,739	3,14E-06
ITPR1	7,89E-12	-0,552018349	0,425	0,582	2,82E-07	DLD	1,01E-17	-0,570037108	0,471	0,654	3,63E-13
LIMK2	4,16E-09	-0,552671119	0,357	0,489	0,000148803	MAP2K1	3,49E-09	-0,571393542	0,387	0,509	0,000125046
TPSB2	1,42E-09	-0,552802534	0,575	0,636	5,09E-05	TACC1	1,79E-22	-0,571576208	0,68	0,821	6,42E-18
RDX	2,10E-09	-0,553075353	0,617	0,713	7,50E-05	UBE2Z	7,97E-12	-0,572958408	0,593	0,706	2,85E-07
STARD4	9,89E-09	-0,553711046	0,323	0,441	0,0003538	CMC2	1,17E-07	-0,573580139	0,266	0,377	0,004190462
SLC3A2	4,90E-11	-0,554273401	0,566	0,657	1,75E-06	NIT2	7,42E-07	-0,574165086	0,263	0,359	0,026541989
PSMC4	5,83E-12	-0,554410625	0,439	0,58	2,09E-07	ACVR1B	2,93E-07	-0,576355818	0,234	0,339	0,010470295
BCAT1	3,03E-15	-0,554643565	0,704	0,796	1,09E-10	TRIM22	4,81E-13	-0,576360342	0,505	0,636	1,72E-08
PSMD11	7,99E-25	-0,554649647	0,723	0,857	2,86E-20	CCDC167	2,61E-07	-0,578255102	0,234	0,335	0,009336681
POP4	8,51E-08	-0,554757622	0,265	0,38	0,003045943	ANP32E	8,56E-23	-0,579199829	0,673	0,818	3,06E-18
INO80C	4,16E-11	-0,555623351	0,265	0,403	1,49E-06	PDRG1	7,15E-08	-0,579909484	0,261	0,373	0,002557354
ATXN7	1,22E-07	-0,555922123	0,276	0,388	0,004371813	PFN1	4,92E-102	-0,579993265	1	1	1,76E-97
TMSB4X	1,46E-42	-0,556240847	0,999	1	5,21E-38	MED19	4,03E-08	-0,580583454	0,248	0,358	0,001443543
EPS15	2,97E-11	-0,556794037	0,49	0,621	1,06E-06	TMEM199	5,89E-08	-0,58094087	0,199	0,309	0,00210916

GARS1	5,99E-09	-0,582257848	0,484	0,589	0,000214505	PSMA5	2,65E-14	-0,61183491	0,501	0,632	9,48E-10
PLEKHO1	2,00E-07	-0,582837223	0,271	0,378	0,007162351	C17orf58	1,19E-07	-0,612284664	0,172	0,274	0,004265634
SCNM1	6,07E-12	-0,583106499	0,429	0,557	2,17E-07	RTCA	2,41E-08	-0,612675002	0,211	0,325	0,00086335
RECQL	1,96E-13	-0,585839353	0,463	0,605	7,01E-09	MAP1LC3B	2,11E-22	-0,612919843	0,581	0,764	7,56E-18
UFD1	1,54E-13	-0,586921168	0,461	0,605	5,53E-09	SRA1	3,96E-09	-0,613064202	0,231	0,349	0,000141634
RAB2B	1,13E-06	-0,587137104	0,242	0,339	0,040336723	SEL1L	1,95E-11	-0,613389511	0,411	0,548	6,97E-07
CCND2	2,21E-14	-0,587338307	0,572	0,7	7,90E-10	SLC35A4	1,82E-08	-0,613907709	0,267	0,385	0,000650597
GK	3,75E-10	-0,591239303	0,23	0,366	1,34E-05	POLR2K	7,48E-14	-0,614264906	0,442	0,584	2,68E-09
CCDC82	9,93E-10	-0,592145225	0,399	0,517	3,55E-05	MID1IP1	2,75E-07	-0,616093504	0,269	0,371	0,009856001
IQGAP1	6,37E-30	-0,592169142	0,612	0,814	2,28E-25	CDKN3	1,09E-08	-0,617302036	0,272	0,387	0,000388866
ADPRH	5,56E-09	-0,593138356	0,269	0,394	0,000198896	UFM1	2,92E-23	-0,617608374	0,61	0,775	1,05E-18
UBE2D1	1,04E-08	-0,593181773	0,228	0,345	0,000371682	MCTP1	3,70E-09	-0,617841737	0,277	0,402	0,000132481
EHD4	6,94E-08	-0,593462405	0,247	0,354	0,002483159	ACSL4	1,15E-15	-0,617842141	0,522	0,688	4,13E-11
PLEKHF2	5,41E-07	-0,594412022	0,243	0,341	0,019341185	CMTM6	3,48E-57	-0,619370017	0,913	0,99	1,24E-52
GCLM	2,35E-10	-0,594423907	0,364	0,495	8,41E-06	PSMA7	1,72E-44	-0,619459156	0,827	0,934	6,15E-40
FAM117A	1,33E-11	-0,597064548	0,495	0,632	4,76E-07	ATP6V1E1	1,00E-30	-0,619528926	0,72	0,872	3,58E-26
MAFG	8,15E-16	-0,597491633	0,525	0,68	2,92E-11	MITD1	3,21E-10	-0,619702327	0,316	0,453	1,15E-05
OSTM1	3,24E-12	-0,59781593	0,26	0,413	1,16E-07	WBP2	4,49E-23	-0,622462562	0,68	0,822	1,61E-18
EPB41L2	2,47E-10	-0,598378763	0,324	0,458	8,82E-06	CD63	7,83E-51	-0,622504385	0,933	0,969	2,80E-46
PHF1	1,52E-08	-0,598530204	0,245	0,358	0,000544998	PTP4A2	4,62E-59	-0,622555696	0,946	0,982	1,65E-54
FBRS	1,34E-09	-0,599013437	0,31	0,44	4,78E-05	SQLE	2,97E-08	-0,624540735	0,359	0,47	0,001063972
PIK3CD	9,54E-11	-0,599053838	0,396	0,539	3,41E-06	S100A6	1,39E-33	-0,625781793	0,772	0,913	4,96E-29
RAP2C	1,03E-09	-0,602862173	0,311	0,441	3,69E-05	PDLIM5	1,73E-11	-0,626111763	0,299	0,438	6,19E-07
MOB1A	4,76E-35	-0,604122565	0,792	0,927	1,70E-30	CLIC4	3,49E-09	-0,626830004	0,357	0,476	0,000125003
DOCK10	1,40E-07	-0,605710272	0,292	0,401	0,005025459	GRIPAP1	1,13E-07	-0,628447048	0,295	0,409	0,004054824
PTPN1	8,94E-13	-0,605738873	0,558	0,686	3,20E-08	EMP3	8,11E-28	-0,629400668	0,819	0,885	2,90E-23
DENND11	3,76E-09	-0,606688738	0,41	0,528	0,000134366	DNPEP	6,91E-09	-0,630772412	0,323	0,438	0,000247303
ZDHHC12	2,00E-07	-0,606923659	0,176	0,277	0,007150154	C19orf12	8,60E-07	-0,630957155	0,222	0,319	0,030775615
ERP44	8,98E-20	-0,607483735	0,601	0,751	3,21E-15	FAM241A	1,07E-06	-0,631299548	0,184	0,277	0,038244465
DDA1	7,71E-12	-0,607566689	0,359	0,5	2,76E-07	TSEN15	2,60E-07	-0,631883002	0,272	0,375	0,009304961
VAMP2	3,71E-24	-0,608128119	0,596	0,777	1,33E-19	CPPED1	4,70E-12	-0,632713704	0,446	0,582	1,68E-07
NCOA3	1,82E-09	-0,609036952	0,486	0,614	6,50E-05	PIP4K2C	2,04E-08	-0,632746538	0,251	0,362	0,000729088
USP12	7,35E-10	-0,610188407	0,454	0,574	2,63E-05	CBR1	1,70E-11	-0,633421121	0,246	0,391	6,10E-07
SAP30	3,87E-08	-0,611690336	0,288	0,4	0,001386071	SNCA	1,29E-13	-0,634109706	0,427	0,575	4,61E-09

TEX30	2,21E-18	-0,636158507	0,473	0,642	7,90E-14	RNF14	4,94E-07	-0,66500268	0,184	0,277	0,017660234
ADAR	2,93E-32	-0,638097655	0,741	0,875	1,05E-27	ORMDL2	1,16E-27	-0,666115826	0,581	0,778	4,15E-23
NAMPT	3,59E-08	-0,638676888	0,36	0,481	0,00128335	ALOX5AP	1,41E-46	-0,668393744	0,301	0,661	5,05E-42
ANXA7	4,56E-32	-0,640232144	0,708	0,855	1,63E-27	GUK1	3,40E-08	-0,671950774	0,207	0,318	0,001216589
IFI27L2	1,94E-12	-0,640738389	0,295	0,447	6,94E-08	SAMD9	8,93E-12	-0,672293722	0,284	0,43	3,20E-07
MYL12A	1,54E-30	-0,641185708	0,753	0,876	5,50E-26	WSB2	6,33E-20	-0,674173267	0,411	0,605	2,26E-15
HIGD1A	1,57E-08	-0,642016527	0,263	0,375	0,000561562	SCO2	1,67E-08	-0,677685214	0,26	0,376	0,000598561
HDGFL3	1,83E-18	-0,642353586	0,507	0,652	6,55E-14	RNF11	3,37E-09	-0,678998408	0,257	0,381	0,000120417
PTPRC	2,56E-28	-0,642986721	0,807	0,895	9,16E-24	RASSF5	2,88E-15	-0,679862597	0,376	0,551	1,03E-10
FLNA	1,40E-30	-0,643500901	0,69	0,837	4,99E-26	ACTB	1,68E-65	-0,682162478	1	1	6,01E-61
PSMC1	2,17E-25	-0,643729332	0,625	0,785	7,77E-21	SLC1A5	2,30E-16	-0,682732938	0,701	0,772	8,23E-12
RAB8B	1,95E-13	-0,643843015	0,395	0,549	6,99E-09	BLOC1S1	2,65E-08	-0,683052115	0,148	0,252	0,000947906
RBCK1	4,51E-20	-0,646283631	0,545	0,702	1,61E-15	MTMR14	9,71E-12	-0,68436867	0,258	0,401	3,47E-07
YRDC	2,10E-08	-0,646596222	0,218	0,332	0,000752334	TRIM44	6,38E-11	-0,685968745	0,366	0,494	2,28E-06
PNPLA8	2,56E-10	-0,647438152	0,245	0,377	9,15E-06	HMGCS1	2,30E-09	-0,686049024	0,32	0,447	8,24E-05
C5orf15	8,11E-12	-0,647520374	0,302	0,456	2,90E-07	DPH3	4,27E-11	-0,687323634	0,261	0,398	1,53E-06
ISCU	6,75E-16	-0,648165778	0,646	0,763	2,42E-11	ERAP2	3,12E-18	-0,690125159	0,453	0,634	1,12E-13
NPLOC4	1,04E-10	-0,649142843	0,376	0,505	3,71E-06	PSMD1	3,89E-40	-0,690344073	0,713	0,868	1,39E-35
HERC1	2,25E-12	-0,649143335	0,387	0,539	8,03E-08	LONRF1	4,84E-07	-0,690473726	0,195	0,289	0,017332389
ENSG00000223393	1,74E-14	-0,649880279	0,584	0,726	6,22E-10	DYNLT1	9,46E-12	-0,691455169	0,346	0,487	3,39E-07
WBP4	2,62E-14	-0,654521864	0,398	0,549	9,37E-10	DERL1	7,47E-18	-0,692033567	0,418	0,603	2,67E-13
CASP4	7,16E-22	-0,655684602	0,601	0,753	2,56E-17	EIF1	1,72E-65	-0,694840 39	0,98	0,995	6,17E-61
GNPDA2	2,39E-07	-0,655689776	0,176	0,271	0,008553029	CDC42SE1	4,81E-37	-0,696213392	0,714	0,895	1,72E-32
FOXN3	1,01E-21	-0,659680027	0,701	0,819	3,62E-17	LGALS9	5,18E-29	-0,698179943	0,813	0,909	1,85E-24
CNDP2	3,15E-17	-0,660997245	0,455	0,617	1,13E-12	UBLCP1	5,62E-22	-0,700115164	0,499	0,686	2,01E-17
HJURP	2,40E-07	-0,661055155	0,258	0,354	0,008601737	MAGEF1	1,31E-09	-0,701117081	0,254	0,38	4,69E-05
FAM177A1	5,96E-11	-0,661251238	0,31	0,452	2,13E-06	TNIP1	1,55E-14	-0,701500066	0,365	0,521	5,56E-10
BCL10	4,61E-10	-0,661666392	0,289	0,418	1,65E-05	SEC61G	9,65E-57	-0,701958765	0,857	0,962	3,45E-52
ATP6V0E1	1,06E-62	-0,662203 99	0,89	0,978	3,80E-58	SERTAD2	5,12E-15	-0,702793395	0,434	0,585	1,83E-10
SELENOK	6,76E-16	-0,662540527	0,435	0,587	2,42E-11	RPL39L	3,34E-07	-0,703063088	0,176	0,265	0,011953192
NOTCH2	1,58E-08	-0,662680618	0,205	0,315	0,000566699	BMP2K	5,07E-23	-0,708264459	0,507	0,707	1,82E-18
UBE2H	5,37E-12	-0,662927665	0,42	0,555	1,92E-07	PIK3R5	2,67E-09	-0,708834804	0,241	0,359	9,55E-05
HMGN4	1,88E-21	-0,664111454	0,543	0,723	6,74E-17	IMPA1	8,39E-14	-0,711803994	0,351	0,501	3,00E-09
TM6SF1	1,11E-07	-0,664541338	0,16	0,256	0,003976548	PPP3CC	6,42E-09	-0,711862031	0,219	0,334	0,000229806

CMPK2	1,21E-10	-0,716531803	0,28	0,41	4,33E-06	RASSF2	1,01E-22	-0,751927325	0,514	0,691	3,62E-18
UBC	3,73E-26	-0,717734548	0,601	0,779	1,33E-21	NBN	2,16E-29	-0,753002116	0,673	0,83	7,72E-25
PSMB4	6,36E-66	-0,718523148	0,876	0,971	2,28E-61	LFNG	4,97E-09	-0,754751852	0,16	0,273	0,000177679
ERAP1	7,70E-16	-0,720057855	0,311	0,497	2,76E-11	GTPBP2	1,29E-13	-0,755186319	0,367	0,512	4,63E-09
DNAJA1	4,76E-45	-0,720201294	0,769	0,92	1,70E-40	DBI	2,91E-65	-0,755497015	0,83	0,961	1,04E-60
SEC61B	6,78E-43	-0,720500734	0,796	0,924	2,43E-38	SYT11	9,39E-09	-0,756929429	0,217	0,327	0,000335807
PIM1	3,33E-43	-0,720603802	0,706	0,901	1,19E-38	KIFAP3	1,40E-10	-0,757470989	0,261	0,391	5,00E-06
PLAUR	3,71E-10	-0,721463341	0,271	0,407	1,33E-05	CCDC6	8,30E-11	-0,75771624	0,347	0,471	2,97E-06
IL18R1	1,64E-11	-0,721973362	0,178	0,31	5,88E-07	PSMA4	1,53E-50	-0,759532686	0,796	0,895	5,49E-46
RIPK2	1,35E-11	-0,722406857	0,286	0,427	4,85E-07	GATA2	9,89E-31	-0,762222638	0,658	0,811	3,54E-26
FAM102A	7,18E-08	-0,723855727	0,184	0,284	0,00256966	RALA	2,45E-24	-0,764754793	0,63	0,782	8,75E-20
BIRC2	1,10E-09	-0,723973442	0,323	0,444	3,93E-05	PLGRKT	9,66E-10	-0,765814756	0,167	0,278	3,46E-05
RBMXL1	1,90E-09	-0,727505495	0,239	0,36	6,80E-05	ZNFX1	4,13E-11	-0,766631188	0,253	0,383	1,48E-06
HAX1	4,43E-14	-0,731509684	0,355	0,506	1,59E-09	TASL	8,42E-10	-0,767194707	0,146	0,26	3,01E-05
CD58	4,31E-13	-0,731573576	0,352	0,499	1,54E-08	C4orf46	3,35E-12	-0,768767061	0,333	0,477	1,20E-07
DDX60L	1,63E-10	-0,732388129	0,134	0,251	5,83E-06	PALM2AKAP2	2,70E-25	-0,770166413	0,465	0,682	9,66E-21
PLEK	2,06E-15	-0,733153516	0,876	0,895	7,36E-11	GABARAPL2	8,73E-20	-0,774390516	0,423	0,616	3,12E-15
SBNO2	5,15E-09	-0,733339581	0,194	0,309	0,000184333	MTMR4	3,06E-07	-0,775118854	0,284	0,382	0,010932627
YPEL5	1,92E-09	-0,734750771	0,527	0,629	6,89E-05	IL1B	8,58E-13	-0,775414468	0,602	0,697	3,07E-08
MSMO1	5,76E-09	-0,737249432	0,213	0,325	0,000206192	PSMB6	3,27E-29	-0,776593992	0,547	0,738	1,17E-24
EFHD2	1,18E-23	-0,738028941	0,483	0,693	4,23E-19	TNFAIP8	1,85E-24	-0,777050096	0,611	0,777	6,64E-20
TUBA1A	5,97E-07	-0,738718402	0,414	0,491	0,021376748	ATP6V0A2	8,28E-28	-0,777627532	0,593	0,777	2,96E-23
ADRM1	8,79E-14	-0,741149189	0,288	0,443	3,14E-09	MIIP	1,54E-09	-0,778521275	0,17	0,279	5,51E-05
SQOR	8,39E-13	-0,741163405	0,241	0,397	3,00E-08	EIF2AK2	2,79E-25	-0,781915636	0,586	0,74	9,99E-21
GIPC1	4,85E-08	-0,743991516	0,199	0,302	0,001733788	SLC38A1	6,87E-15	-0,783971106	0,428	0,569	2,46E-10
MARS1	8,08E-19	-0,744166737	0,43	0,601	2,89E-14	SRBD1	1,25E-13	-0,784001312	0,259	0,415	4,47E-09
RNF213	3,25E-21	-0,744515084	0,433	0,625	1,16E-16	RUBCN	1,65E-07	-0,785330301	0,2	0,301	0,005894781
ALG2	4,49E-11	-0,746180912	0,325	0,461	1,61E-06	COX17	4,07E-35	-0,792703393	0,567	0,79	1,46E-30
PCK2	2,47E-11	-0,747364401	0,353	0,481	8,82E-07	RCN1	2,48E-19	-0,795978725	0,518	0,688	8,86E-15
HTRA2	4,07E-12	-0,748036874	0,328	0,47	1,46E-07	TRPV2	6,13E-10	-0,801964082	0,183	0,301	2,19E-05
IL6ST	1,98E-08	-0,749867417	0,206	0,318	0,000709983	PPP1R15A	1,76E-25	-0,802079535	0,548	0,73	6,29E-21
NRAS	2,28E-23	-0,7500203	0,447	0,648	8,14E-19	DESI1	1,08E-10	-0,80508451	0,159	0,28	3,86E-06
ST6GAL1	5,80E-10	-0,750662931	0,39	0,506	2,08E-05	TANK	1,89E-20	-0,805107862	0,429	0,618	6,78E-16
UBA7	9,04E-11	-0,751715807	0,2	0,328	3,23E-06	C9orf64	3,24E-10	-0,805690466	0,189	0,303	1,16E-05

HMGA2	2,04E-07	-0,806555187	0,26	0,354	0,007304478
LY75	6,85E-09	-0,80713717	0,17	0,28	0,000245061
SYNGR2	1,94E-20	-0,807711818	0,494	0,668	6,94E-16
FAR2	1,94E-16	-0,809746965	0,367	0,53	6,93E-12
ATOX1	1,18E-14	-0,812524589	0,313	0,47	4,22E-10
PSMB2	8,75E-88	-0,817010444	0,888	0,966	3,13E-83
PYROXD1	4,72E-10	-0,819453194	0,198	0,319	1,69E-05
LMNA	1,48E-12	-0,821514114	0,286	0,429	5,30E-08
COQ10B	1,25E-19	-0,821775785	0,311	0,498	4,49E-15
TPSAB1	9,76E-12	-0,822557628	0,248	0,381	3,49E-07
CFLAR	1,01E-21	-0,827488491	0,571	0,741	3,62E-17
NET1	9,03E-18	-0,830187778	0,528	0,671	3,23E-13
ARL6IP5	3,41E-46	-0,832081855	0,854	0,946	1,22E-41
PRDM8	2,95E-08	-0,839986865	0,16	0,262	0,001055594
COMMD1	7,65E-08	-0,845118081	0,199	0,301	0,002735971
LY6E	3,91E-17	-0,846046897	0,316	0,492	1,40E-12
ENSG00000290032	1,69E-09	-0,8463557	0,253	0,375	6,06E-05
CLPTM1	2,95E-09	-0,846749095	0,424	0,542	0,000105408
CD82	8,09E-82	-0,848461157	0,923	0,978	2,89E-77
PPFIBP1	2,17E-10	-0,849846698	0,312	0,434	7,76E-06
CHMP5	1,54E-30	-0,851041802	0,478	0,686	5,51E-26
AARS1	1,04E-15	-0,855280463	0,295	0,46	3,71E-11
POMP	8,28E-97	-0,856305162	0,886	0,978	2,96E-92
AHR	2,61E-14	-0,859260177	0,249	0,408	9,33E-10
SMAP2	1,31E-41	-0,865142523	0,669	0,848	4,67E-37
PPID	6,10E-15	-0,865737158	0,267	0,429	2,18E-10
FLOT1	2,70E-17	-0,866922011	0,271	0,446	9,65E-13
RAB9A	5,66E-07	-0,872552631	0,212	0,306	0,020251465
LPXN	1,23E-51	-0,873660634	0,682	0,891	4,41E-47
BLVRA	1,53E-11	-0,875637642	0,208	0,343	5,48E-07
RAB29	1,34E-08	-0,875924919	0,276	0,39	0,000480705
SHMT2	2,62E-20	-0,876357237	0,676	0,738	9,38E-16
JAK2	1,83E-08	-0,877459825	0,206	0,312	0,000654467
SHFL	5,34E-22	-0,882198879	0,445	0,628	1,91E-17
TNFSF12	1,44E-13	-0,883841688	0,159	0,301	5,16E-09
RNF145	6,08E-24	-0,885284934	0,455	0,654	2,17E-19
NFKBIB	2,04E-19	-0,885407364	0,331	0,512	7,30E-15
NFE2L1	8,82E-14	-0,888641037	0,38	0,512	3,15E-09
HYOU1	9,26E-20	-0,889193473	0,343	0,533	3,31E-15
PHGDH	3,29E-10	-0,889352576	0,32	0,437	1,18E-05
MLLT11	3,79E-24	-0,891234347	0,364	0,575	1,35E-19
MOV10	2,63E-10	-0,891273779	0,146	0,259	9,40E-06
GPX4	4,28E-99	-0,898761526	0,907	0,985	1,53E-94
TLNRD1	2,55E-18	-0,899597702	0,286	0,463	9,13E-14
RAB27B	1,25E-19	-0,904923619	0,319	0,501	4,49E-15
RAB33A	3,70E-13	-0,909775834	0,184	0,325	1,32E-08
TMEM131L	3,55E-11	-0,912686651	0,277	0,4	1,27E-06
DDHD1	1,56E-09	-0,915094438	0,241	0,357	5,58E-05
FYB1	1,43E-23	-0,919852091	0,516	0,7	5,12E-19
TBCB	2,12E-22	-0,923136852	0,369	0,562	7,57E-18
SP110	2,00E-33	-0,923723056	0,541	0,752	7,14E-29
CGAS	7,14E-21	-0,924486104	0,32	0,515	2,56E-16
NAGK	2,03E-17	-0,925471869	0,24	0,411	7,28E-13
PSMA3	4,04E-76	-0,925526488	0,755	0,914	1,45E-71
NMI	1,27E-50	-0,926985 7	0,605	0,829	4,55E-46
CRELD2	4,12E-16	-0,929121172	0,306	0,462	1,47E-11
GDI1	2,60E-22	-0,932008436	0,336	0,546	9,31E-18
IL2RG	4,64E-73	-0,936156716	0,795	0,958	1,66E-68
PEA15	1,25E-25	-0,936249 32	0,423	0,623	4,48E-21
PAG1	6,43E-21	-0,937219984	0,283	0,485	2,30E-16
TRIM8	9,63E-18	-0,943020724	0,327	0,492	3,45E-13
MMD	1,72E-07	-0,944292882	0,211	0,305	0,006142474
HTATIP2	4,50E-29	-0,949484775	0,36	0,593	1,61E-24
GLIPR2	1,80E-11	-0,951960853	0,146	0,268	6,44E-07
DUSP10	2,35E-16	-0,960708389	0,251	0,425	8,40E-12
SOCS2	8,52E-25	-0,964291337	0,561	0,729	3,05E-20
IRF2	1,89E-16	-0,965844777	0,254	0,423	6,75E-12
SMIM29	6,94E-19	-0,965932095	0,253	0,438	2,48E-14

SESN2	2,68E-07	-0,970108632	0,195	0,287	0,009575607
LYSMD2	9,29E-13	-0,974315276	0,213	0,354	3,33E-08
PSMB8-AS1	1,43E-24	-0,974729479	0,31	0,526	5,11E-20
CYTH1	1,32E-07	-0,976489824	0,233	0,325	0,004706695
TAPBPL	3,64E-12	-0,989348466	0,151	0,278	1,30E-07
SPPL2A	4,42E-27	-0,992154529	0,387	0,601	1,58E-22
ARL4A	2,43E-18	-0,992903791	0,242	0,418	8,68E-14
SH3BP2	1,02E-14	-0,997635566	0,192	0,341	3,66E-10
HERPUD1	8,40E-15	-0,998160944	0,314	0,467	3,00E-10
NECAP2	2,06E-22	-0,999800008	0,328	0,519	7,36E-18
SNX10	6,20E-39	-1,002041999	0,501	0,746	2,22E-34
CARS1	4,95E-19	-1,0062588	0,252	0,431	1,77E-14
TMSB10	8,37E-66	-1,008435396	0,914	0,963	3,00E-61
AGPAT3	3,38E-16	-1,011768035	0,282	0,443	1,21E-11
BTG3	5,99E-15	-1,016113726	0,183	0,336	2,14E-10
SQSTM1	5,05E-62	-1,024154491	0,663	0,89	1,81E-57
SAMSN1	9,75E-58	-1,025924116	0,566	0,851	3,49E-53
ERICH1	5,33E-07	-1,033433636	0,381	0,478	0,019078826
ZMIZ2	1,22E-16	-1,034646046	0,247	0,415	4,36E-12
SREBF1	9,42E-15	-1,044293652	0,122	0,26	3,37E-10
LACTB	3,42E-37	-1,046234016	0,351	0,62	1,23E-32
SNX20	5,82E-39	-1,046468002	0,4	0,668	2,08E-34
IL18BP	1,75E-19	-1,053549447	0,116	0,284	6,25E-15
CEP135	4,63E-10	-1,053695803	0,287	0,402	1,66E-05
EHD1	1,11E-09	-1,063019622	0,166	0,279	3,97E-05
ITGA2B	1,02E-49	-1,063767808	0,489	0,785	3,64E-45
SMIM14	5,46E-11	-1,073534538	0,16	0,282	1,95E-06
TRIM26	3,02E-20	-1,078507634	0,229	0,42	1,08E-15
CYTIP	2,85E-13	-1,082615081	0,231	0,37	1,02E-08
SELENOS	2,07E-50	-1,100694359	0,522	0,762	7,40E-46
CDK17	2,29E-14	-1,103487137	0,166	0,311	8,20E-10
WT1	1,23E-13	-1,103870432	0,133	0,264	4,41E-09
TXN	7,18E-61	-1,103917227	0,953	0,987	2,57E-56
C2orf76	9,70E-11	-1,105716152	0,152	0,265	3,47E-06
STK17B	5,02E-30	-1,105962416	0,323	0,554	1,80E-25
CSF2RB	1,85E-66	-1,106205864	0,449	0,801	6,63E-62
NABP1	2,13E-15	-1,106764218	0,189	0,34	7,63E-11
NIBAN1	2,60E-32	-1,107295989	0,596	0,763	9,30E-28
PARP14	1,85E-35	-1,108141011	0,447	0,685	6,61E-31
ENSG00000282885	1,02E-16	-1,108465107	0,189	0,35	3,65E-12
NFKB1	1,61E-24	-1,109035519	0,425	0,618	5,76E-20
VOPP1	1,77E-24	-1,112865842	0,53	0,695	6,34E-20
GRINA	7,22E-25	-1,113190201	0,389	0,583	2,58E-20
BTN3A1	4,16E-13	-1,120526281	0,125	0,255	1,49E-08
PLSCR1	2,75E-54	-1,125797405	0,524	0,772	9,85E-50
STAT2	5,32E-24	-1,144433228	0,241	0,449	1,90E-19
SRC	2,51E-18	-1,144596608	0,239	0,413	8,98E-14
TMEM154	1,42E-17	-1,144688639	0,196	0,364	5,07E-13
MAFF	1,43E-21	-1,146331116	0,188	0,381	5,11E-17
MED10	5,29E-20	-1,148634751	0,163	0,343	1,89E-15
ENSG00000265975	6,52E-13	-1,149726424	0,134	0,26	2,33E-08
RFX5	1,64E-25	-1,151383345	0,255	0,467	5,86E-21
ADAP1	4,03E-18	-1,153555586	0,164	0,332	1,44E-13
STAT4	7,60E-18	-1,156410379	0,167	0,334	2,72E-13
ACSL1	4,88E-14	-1,158869802	0,127	0,259	1,75E-09
IFI44	7,94E-25	-1,161586001	0,164	0,38	2,84E-20
ARNTL2	4,52E-22	-1,165001343	0,218	0,413	1,62E-17
ARHGEF7	2,28E-18	-1,165590503	0,316	0,481	8,14E-14
ZC3H12A	1,10E-15	-1,171039897	0,158	0,307	3,94E-11
ZNF267	2,16E-28	-1,175905584	0,318	0,539	7,74E-24
DENND5A	5,58E-22	-1,178602601	0,243	0,445	2,00E-17
CARD16	1,69E-16	-1,187424825	0,111	0,26	6,06E-12
MAST4	2,81E-27	-1,190359001	0,442	0,634	1,00E-22
APOBEC3G	6,59E-24	-1,195408217	0,219	0,424	2,36E-19
FMNL3	1,68E-24	-1,197364687	0,245	0,447	5,99E-20
BTG1	7,08E-15	-1,199229035	0,472	0,612	2,53E-10
HLA-DMA	1,42E-93	-1,199981998	0,64	0,891	5,09E-89
TRAF3	4,79E-35	-1,200499623	0,292	0,554	1,71E-30

BST2	4,13E-54	-1,204426966	0,458	0,739	1,48E-49
TRIM21	3,79E-19	-1,204968689	0,177	0,348	1,36E-14
ZFP36L1	3,49E-60	-1,206151336	0,436	0,777	1,25E-55
PSME1	7,27E-102	-1,218998032	0,635	0,904	2,60E-97
FAS	7,64E-18	-1,225610929	0,218	0,389	2,73E-13
CYLD	6,35E-56	-1,225935281	0,394	0,714	2,27E-51
CYB5A	9,65E-25	-1,231760741	0,245	0,452	3,45E-20
SOD2	3,52E-16	-1,234075535	0,557	0,701	1,26E-11
MALT1	4,84E-11	-1,241678161	0,167	0,288	1,73E-06
TNIP2	2,14E-20	-1,251541429	0,208	0,39	7,64E-16
SLC27A2	1,80E-35	-1,252393445	0,382	0,609	6,46E-31
WWC2	2,70E-22	-1,255501907	0,193	0,388	9,65E-18
ZFAND2A	4,37E-16	-1,255650226	0,125	0,269	1,56E-11
IFIT5	6,53E-16	-1,258244479	0,112	0,254	2,34E-11
GCH1	2,45E-16	-1,299283822	0,155	0,304	8,76E-12
NFKBIE	5,84E-36	-1,301052466	0,318	0,574	2,09E-31
NCOA7	2,69E-37	-1,318007705	0,401	0,635	9,61E-33
NLRC5	3,82E-23	-1,319651647	0,169	0,364	1,37E-18
STX11	1,91E-25	-1,323404619	0,188	0,394	6,84E-21
IER5	1,20E-19	-1,330299571	0,199	0,374	4,29E-15
CTSH	5,76E-36	-1,335615336	0,081	0,32	2,06E-31
FAM219A	3,72E-19	-1,336244803	0,13	0,292	1,33E-14
TIFA	2,12E-24	-1,336438372	0,219	0,418	7,58E-20
ENPP3	1,89E-15	-1,351016951	0,148	0,29	6,75E-11
RFTN1	2,41E-19	-1,387574173	0,355	0,518	8,63E-15
ENPP4	2,42E-09	-1,392721613	0,167	0,271	8,67E-05
SLC66A2	2,16E-31	-1,395367828	0,281	0,519	7,73E-27
TAPBP	1,46E-99	-1,400991157	0,6	0,897	5,21E-95
MTHFD2	7,69E-67	-1,402425779	0,52	0,812	2,75E-62
CASP1	2,07E-35	-1,405556141	0,202	0,463	7,41E-31
ENO2	8,20E-20	-1,413693853	0,137	0,301	2,93E-15
UBE2L6	5,25E-64	-1,418942914	0,383	0,695	1,88E-59
HLA-E	1,02E-194	-1,426016763	0,947	0,996	3,65E-190
JUNB	6,60E-44	-1,431049096	0,471	0,724	2,36E-39
SNX11	3,46E-20	-1,433492682	0,253	0,431	1,24E-15
VAMP5	2,02E-46	-1,440733475	0,258	0,56	7,24E-42
FAM110A	3,37E-37	-1,444721567	0,335	0,579	1,21E-32
HLA-DMB	2,51E-96	-1,453912	0,267	0,725	8,97E-92
ATF5	3,11E-14	-1,454130823	0,149	0,283	1,11E-09
PMAIP1	1,11E-23	-1,454589808	0,213	0,402	3,98E-19
IL3RA	1,14E-20	-1,470816923	0,188	0,362	4,06E-16
NUB1	4,80E-45	-1,473098839	0,564	0,778	1,72E-40
NFKBIZ	2,05E-14	-1,473109375	0,123	0,254	7,34E-10
VEGFA	4,39E-20	-1,477918188	0,169	0,339	1,57E-15
ZC4H2	4,03E-18	-1,480192088	0,118	0,269	1,44E-13
BTN3A2	6,28E-39	-1,482902257	0,184	0,453	2,25E-34
HLA-DPB1	1,41E-187	-1,488744174	0,873	0,992	5,03E-183
CDKN1A	7,60E-40	-1,491249238	0,322	0,598	2,72E-35
DTX3L	1,35E-40	-1,495825528	0,224	0,499	4,85E-36
CLIC2	2,51E-23	-1,498337234	0,151	0,343	8,98E-19
GPR68	6,30E-34	-1,507930318	0,105	0,341	2,26E-29
JAK3	2,10E-56	-1,527158781	0,31	0,64	7,51E-52
PSMB8	5,07E-105	-1,535718648	0,505	0,833	1,81E-100
GBP2	5,21E-31	-1,557172438	0,181	0,418	1,86E-26
HLA-DRA	6,22E-224	-1,559913079	0,958	0,999	2,23E-219
TRIP10	4,18E-11	-1,586130722	0,142	0,252	1,49E-06
ELL2	2,65E-54	-1,598283923	0,271	0,591	9,47E-50
MTSS1	1,74E-27	-1,621561071	0,164	0,37	6,22E-23
HLA-A	0	-1,636965339	1	1	0
LTB	1,21E-27	-1,640681331	0,182	0,39	4,33E-23
ENSG00000290574	1,35E-23	-1,648581421	0,67	0,694	4,83E-19
HIVEP1	8,13E-20	-1,651222618	0,093	0,25	2,91E-15
SEMA7A	9,21E-51	-1,654287504	0,249	0,56	3,29E-46
SEMA4A	3,18E-45	-1,659102433	0,249	0,535	1,14E-40
TRAFD1	3,43E-59	-1,676263673	0,305	0,639	1,23E-54
DDX60	1,04E-33	-1,679782556	0,096	0,327	3,72E-29
RSAD2	4,69E-44	-1,681203121	0,314	0,596	1,68E-39
ARHGAP31	1,97E-33	-1,690105819	0,12	0,351	7,03E-29

CAVIN2	3,96E-20	-1,698876675	0,169	0,335	1,42E-15
B2M	0	-1,707498065	1	1	0
NINJ1	2,00E-32	-1,709511667	0,141	0,373	7,16E-28
HLA-DPA1	8,86E-228	-1,712965634	0,936	0,991	3,17E-223
RUNX3	2,30E-53	-1,716389184	0,564	0,78	8,24E-49
PIM3	1,04E-50	-1,742466892	0,26	0,561	3,73E-46
OPTN	6,44E-55	-1,766502101	0,241	0,557	2,30E-50
ADAM8	7,58E-60	-1,778919582	0,227	0,577	2,71E-55
SOCS1	2,97E-73	-1,786857763	0,233	0,627	1,06E-68
BTN2A2	1,12E-42	-1,791250876	0,163	0,442	4,00E-38
HLA-DRB1	3,65E-229	-1,795971426	0,888	0,997	1,31E-224
DAPP1	1,61E-26	-1,799954227	0,137	0,338	5,76E-22
GBP3	9,09E-31	-1,812985935	0,086	0,297	3,25E-26
SDC4	1,86E-23	-1,822472093	0,089	0,262	6,67E-19
BHLHE40	5,98E-95	-1,8320469	0,399	0,796	2,14E-90
DDIT4	3,92E-36	-1,834041869	0,178	0,422	1,40E-31
HLA-C	3,08E-290	-1,853356555	0,992	1	1,10E-285
HLA-DRB6	1,05E-90	-1,880914221	0,265	0,697	3,77E-86
CD83	5,24E-22	-1,892928993	0,14	0,319	1,88E-17
PSME2	5,84E-160	-1,920455168	0,508	0,893	2,09E-155
TAP2	3,03E-147	-1,923424295	0,506	0,899	1,08E-142
CD74	9,52E-280	-1,945809887	0,995	0,999	3,41E-275
IER3	9,12E-24	-1,948045862	0,145	0,333	3,26E-19
LGALS3BP	1,68E-95	-1,973014048	0,288	0,714	6,00E-91
PARP9	2,02E-98	-1,977595119	0,324	0,729	7,22E-94
MAP3K8	2,03E-66	-1,978187212	0,3	0,643	7,25E-62
BCL3	7,98E-48	-1,985995123	0,157	0,454	2,86E-43
IFI6	2,75E-56	-1,995386542	0,212	0,535	9,85E-52
DMD	1,93E-27	-2,000846086	0,086	0,274	6,92E-23
IFIH1	1,22E-86	-2,035750884	0,248	0,666	4,38E-82
BCL2A1	2,19E-30	-2,064645889	0,073	0,272	7,83E-26
MVP	1,02E-27	-2,080866004	0,071	0,256	3,63E-23
GDF11	1,33E-106	-2,094975997	0,434	0,789	4,76E-102
HLA-B	0	-2,101106989	1	1	0
OAS3	2,54E-65	-2,129719229	0,172	0,527	9,09E-61
APOL3	6,70E-33	-2,153116306	0,073	0,286	2,40E-28
KLF6	3,87E-97	-2,165002272	0,429	0,797	1,39E-92
IL21R	8,33E-33	-2,169492033	0,083	0,296	2,98E-28
RNF19B	3,01E-63	-2,203439711	0,307	0,623	1,08E-58
APOL2	2,30E-46	-2,223842018	0,129	0,411	8,23E-42
CIITA	7,62E-56	-2,231525677	0,152	0,471	2,73E-51
AFDN	5,23E-35	-2,233151341	0,077	0,294	1,87E-30
HLA-DQB1	9,23E-191	-2,264040405	0,49	0,943	3,30E-186
IFI35	3,23E-42	-2,265287024	0,092	0,35	1,16E-37
LAP3	5,18E-98	-2,281497505	0,263	0,675	1,85E-93
SNN	5,82E-27	-2,284784949	0,104	0,295	2,08E-22
HCP5	1,43E-108	-2,308495555	0,205	0,682	5,13E-104
ISG15	1,86E-60	-2,308608962	0,204	0,537	6,65E-56
HLA-DOA	1,10E-88	-2,322425302	0,146	0,583	3,94E-84
SERPINB9	3,88E-32	-2,322685333	0,305	0,539	1,39E-27
TNFRSF4	5,99E-48	-2,326673266	0,116	0,4	2,14E-43
NFE2L3	3,42E-106	-2,375031689	0,248	0,702	1,22E-101
IFITM3	1,52E-143	-2,388772068	0,411	0,83	5,45E-139
MX1	8,67E-36	-2,397947176	0,11	0,346	3,10E-31
RELB	7,23E-48	-2,407773834	0,096	0,375	2,59E-43
MIR155HG	1,38E-28	-2,443138004	0,157	0,363	4,92E-24
TRIM69	1,69E-59	-2,502388753	0,096	0,419	6,06E-55
APOL6	6,24E-141	-2,515143464	0,253	0,771	2,23E-136
IRF7	6,13E-43	-2,564902781	0,064	0,31	2,19E-38
GBP5	1,42E-90	-2,587552256	0,24	0,65	5,08E-86
PTGIR	6,20E-37	-2,599583989	0,067	0,292	2,22E-32
APOL1	1,39E-72	-2,643191105	0,107	0,481	4,97E-68
GBP4	1,73E-157	-2,687255599	0,363	0,856	6,18E-153
PTAFR	6,26E-102	-2,713986871	0,12	0,588	2,24E-97
SLC2A6	2,13E-84	-2,720646599	0,148	0,552	7,61E-80
PSMB9	7,03E-215	-2,742442972	0,336	0,89	2,52E-210
IL10RA	1,19E-38	-2,766914591	0,052	0,273	4,24E-34
IRF1	1,25E-183	-2,784092486	0,443	0,892	4,46E-179

SAMD9L	8,57E-102	-2,813865754	0,147	0,602	3,07E-97
EPSTI1	9,13E-157	-2,830787887	0,236	0,789	3,27E-152
IFI44L	1,69E-42	-2,894462714	0,075	0,323	6,05E-38
NFKBIA	3,33E-105	-2,894621699	0,451	0,807	1,19E-100
HLA-F	2,54E-162	-2,952070583	0,189	0,779	9,09E-158
NFKB2	3,36E-67	-2,954247157	0,075	0,415	1,20E-62
STAT1	6,61E-285	-2,965438826	0,761	0,987	2,36E-280
MT2A	5,17E-30	-3,028148422	0,11	0,316	1,85E-25
ICAM1	2,61E-82	-3,049886996	0,102	0,498	9,35E-78
MAOA	3,62E-44	-3,122749121	0,054	0,298	1,30E-39
TNFAIP2	1,02E-42	-3,175411782	0,145	0,413	3,64E-38
TVP23A	9,72E-57	-3,184439107	0,042	0,333	3,48E-52
WARS1	9,16E-122	-3,221606392	0,16	0,653	3,28E-117
CD40	2,62E-44	-3,306787748	0,082	0,339	9,39E-40
FSCN1	1,40E-56	-3,356184153	0,445	0,685	5,02E-52
MARCKS	1,30E-21	-3,364132211	0,111	0,267	4,65E-17
IL32	9,28E-122	-3,410543895	0,224	0,69	3,32E-117
BIRC3	9,86E-137	-3,440817457	0,152	0,683	3,53E-132
TNFAIP3	3,24E-131	-3,441491737	0,13	0,65	1,16E-126
HLA-DQA2	2,38E-46	-3,507590906	0,025	0,265	8,51E-42
PLAAT4	6,67E-48	-3,524044483	0,029	0,276	2,39E-43
GP1BA	2,62E-77	-3,579077117	0,066	0,436	9,38E-73
IFIT3	1,31E-106	-3,593581255	0,098	0,563	4,69E-102
TAP1	0	-3,615661264	0,637	0,999	0
XAF1	6,14E-119	-3,637557373	0,096	0,595	2,20E-114
TRAF1	1,18E-55	-3,664187064	0,052	0,339	4,24E-51
TNFSF10	1,11E-169	-3,694194366	0,223	0,783	3,98E-165
HLA-DQA1	1,33E-259	-3,999216504	0,235	0,923	4,77E-255
GBP1	4,32E-179	-4,519820439	0,128	0,742	1,55E-174
TNFRSF9	6,30E-59	-4,711938535	0,024	0,307	2,25E-54
CCL5	6,55E-65	-5,042647117	0,022	0,327	2,34E-60
RGS1	1,76E-52	-5,212506535	0,017	0,271	6,31E-48
KLHDC7B	7,80E-109	-5,734967101	0,025	0,477	2,79E-104
EBI3	7,83E-93	-6,333151049	0,034	0,436	2,80E-88
CXCL9	3,81E-44	-6,451645139	0,029	0,254	1,36E-39
CXCL11	9,14E-60	-6,744370735	0,008	0,284	3,27E-55
CXCL10	6,44E-52	-7,073186493	0,01	0,255	2,31E-47

8. References

Abkowitz, J. L., Catlin, S. N., McCallie, M. T., & Guttorp, P. (2002). Evidence that the number of hematopoietic stem cells per animal is conserved in mammals. *Blood*, *100*(7), 2665–2667. https://doi.org/10.1182/blood-2002-03-0822

Acar, M., Kocherlakota, K. S., Murphy, M. M., Peyer, J. G., Oguro, H., Inra, C. N., Jaiyeola, C., Zhao, Z., Luby-Phelps, K., & Morrison, S. J. (2015). Deep imaging of bone marrow shows non-dividing stem cells are mainly perisinusoidal. *Nature*, *526*(7571), 126–130. https://doi.org/10.1038/NATURE15250

Adolfsson, J. (2005). Identification of Flt3+ lympho-myeloid stem cells lacking erythro-megakaryocytic potential a revised road map for adult blood lineage commitment. *Cell*, *121*, 295–306.

Ainciburu, M., Ezponda, T., Berastegui, N., Alfonso-Pierola, A., Vilas-Zornoza, A., Martin-Uriz, P. S., Alignani, D., Lamo-Espinosa, J., San-Julian, M., Jiménez-Solas, T., Lopez, F., Muntion, S., Sanchez-Guijo, F., Molero, A., Montoro, J., Serrano, G., Diaz-Mazkiaran, A., Lasaga, M., Gomez-Cabrero, D., … Prosper, F. (2023). Uncovering perturbations in human hematopoiesis associated with healthy aging and myeloid malignancies at single-cell resolution. *ELife*, *12*. https://doi.org/10.7554/ELIFE.79363

AJ Becker, E. M. J. T. (1963). Cytological demonstration of the clonal nature of spleen colonies derived from transplanted mouse marrow cells. *Nature*, *197*, 452–454.

Akashi, K., Traver, D., Miyamoto, T., & Weissman, I. L. (2000). A clonogenic common myeloid progenitor that gives rise to all myeloid lineages. *Nature*, *404*, 193–197.

Alejo E. Rodriguez-Fraticelli, S. L. W. C. S. W. R. P. S. H. P. M. J. J. S. R. A. C. A. M. K. F. D. C. (2018). Clonal analysis of lineage fate in native haematopoiesis. *Nature*, *553*(7687), 212–216.

Anjos-Afonso, F., & Bonnet, D. (2023). Human CD34+ hematopoietic stem cell hierarchy: how far are we with its delineation at the most primitive level? *Blood*, *142*(6), 509–518. https://doi.org/10.1182/BLOOD.2022018071

Anjos-Afonso, F., Buettner, F., Mian, S. A., Rhys, H., Perez-Lloret, J., Garcia-Albornoz, M., Rastogi, N., Ariza-McNaughton, L., & Bonnet, D. (2022). Single cell analyses identify a highly regenerative and homogenous human CD34+ hematopoietic stem cell population. *Nature Communications*, *13*(1). https://doi.org/10.1038/S41467-022-29675-W

Anthony, B. A., & Link, D. C. (2014). Regulation of hematopoietic stem cells by bone marrow stromal cells. *Trends in Immunology*, *35*(1), 32–37. https://doi.org/10.1016/j.it.2013.10.002

Asada, N., Kunisaki, Y., Pierce, H., Wang, Z., Fernandez, N. F., Birbrair, A., Ma'ayan, A., & Frenette, P. S. (2017). Differential cytokine contributions of perivascular haematopoietic stem cell niches. *Nature Cell Biology*, *19*(3), 214–223. https://doi.org/10.1038/NCB3475

Audigé, A., Rochat, M. A., Li, D., Ivic, S., Fahrny, A., Muller, C. K. S., Gers-Huber, G., Myburgh, R., Bredl, S., Schlaepfer, E., Scherrer, A. U., Kuster, S. P., & Speck, R. F. (2017). Long-term leukocyte reconstitution in NSG mice transplanted with human cord blood hematopoietic stem and progenitor cells. *BMC Immunology*, *18*(1), 1–15. https://doi.org/10.1186/S12865-017-0209-9/FIGURES/12

Bagger, F. O., Sasivarevic, D., Sohi, S. H., Laursen, L. G., Pundhir, S., Sønderby, C. K., Winther, O., Rapin, N., & Porse, B. T. (2016). BloodSpot: a database of gene expression profiles and transcriptional programs for healthy and malignant haematopoiesis. *Nucleic Acids Research*, *44*(D1), D917–D924. https://doi.org/10.1093/NAR/GKV1101

Baldridge, M. T., King, K. Y., Boles, N. C., Weksberg, D. C., & Goodell, M. A. (2010a). Quiescent haematopoietic stem cells are activated by IFN-γ in response to chronic infection. *Nature*, *465*(7299), 793–797. https://doi.org/10.1038/NATURE09135

Baldridge, M. T., King, K. Y., Boles, N. C., Weksberg, D. C., & Goodell, M. A. (2010b). Quiescent haematopoietic stem cells are activated by IFN-γ in response to chronic infection. *Nature 2010 465:7299*, *465*(7299), 793–797. https://doi.org/10.1038/nature09135

Baldus, C. D., Tanner, S. M., Kusewitt, D. F., Liyanarachchi, S., Choi, C., Caligiuri, M. A., Bloomfield, C. D., & De La Chapelle, A. (2003). BAALC, a novel marker of human hematopoietic progenitor cells. *Experimental Hematology*, *31*(11), 1051–1056. https://doi.org/10.1016/j.exphem.2003.08.004

Balogh, P., Adelman, E. R., Pluvinage, J. V., Capaldo, B. J., Freeman, K. C., Singh, S., Elagib, E., Nakamura, Y., Kurita, R., Sashida, G., Zunder, E. R., Li, H., Gru, A. A., Price, E. A., Schrier, S. L., Weissman, I. L., Figueroa, M. E., Pang, W. W., & Goldfarb, A. N. (2020). RUNX3 levels in human hematopoietic progenitors are regulated by aging and dictate erythroid-myeloid balance. *Haematologica*, *105*(4), 905–913. https://doi.org/10.3324/HAEMATOL.2018.208918

Baum, C. M., Weissman, I. L., Tsukamoto, A. S., Buckle, A. M., & Peault, B. (1992). Isolation of a candidate human hematopoietic stem-cell population. *Proceedings of the National Academy of Sciences of the United States of America*, *89*(7), 2804–2808. https://doi.org/10.1073/PNAS.89.7.2804

Beckmann, J., Scheitza, S., Wernet, P., Fischer, J. C., & Giebel, B. (2007). Asymmetric cell division within the human hematopoietic stem and progenitor cell compartment: Identification of asymmetrically segregating proteins. *Blood*, *109*(12), 5494–5501. https://doi.org/10.1182/blood-2006-11-055921

Beerman, I., Bhattacharya, D., Zandi, S., Sigvardsson, M., Weissman, I. L., Brydere, D., & Rossia, D. J. (2010). Functionally distinct hematopoietic stem cells modulate hematopoietic lineage potential during aging by a mechanism of clonal expansion. *Proceedings of the National Academy of Sciences of the United States of America*, *107*(12), 5465–5470. https://doi.org/10.1073/PNAS.1000834107

Beerman, I., Bock, C., Garrison, B. S., Smith, Z. D., Gu, H., Meissner, A., & Rossi, D. J. (2013). Proliferation-dependent alterations of the DNA methylation landscape underlie hematopoietic stem cell aging. *Cell Stem Cell*, *12*(4), 413–425. https://doi.org/10.1016/j.stem.2013.01.017

Benveniste, P. (2010). Intermediate-term hematopoietic stem cells with extended but time-limited reconstitution potential. *Cell Stem Cell*, *6*, 48–58.

Bertrand, J. Y., & Traver, D. (2009). Hematopoietic cell development in the zebrafish embryo. *Current Opinion in Hematology*, *16*(4), 243–248. https://doi.org/10.1097/MOH.0B013E32832C05E4

Bexte, T., Albinger, N., Al Ajami, A., Wendel, P., Buchinger, L., Gessner, A., Alzubi, J., Särchen, V., Vogler, M., Rasheed, H. M., Jung, B. A., Wolf, S., Bhayadia, R., Oellerich, T., Klusmann, J.-H., Penack, O., Möker, N., Cathomen, T., Rieger, M. A., … Ullrich, E. (2024). CRISPR/Cas9 editing of NKG2A improves the efficacy of primary CD33-directed chimeric antigen receptor natural killer cells. *Nature Communications*, *15*(1), 8439. https://doi.org/10.1038/S41467-024-52388-1

Bhatia, M., Wang, J. C. Y., Kapp, U., Bonnet, D., & Dick, J. E. (1997). Purification of primitive human hematopoietic cells capable of repopulating immune-deficient mice. *Proceedings of the National Academy of Sciences of the United States of America*, *94*(10), 5320–5325. https://doi.org/10.1073/PNAS.94.10.5320

Bian, Z., Gong, Y., Huang, T., Lee, C. Z. W., Bian, L., Bai, Z., Shi, H., Zeng, Y., Liu, C., He, J., Zhou, J., Li, X., Li, Z., Ni, Y., Ma, C., Cui, L., Zhang, R., Chan, J. K. Y., Ng, L. G., … Liu, B. (2020). Deciphering human macrophage development at single-cell resolution. *Nature 2020 582:7813*, *582*(7813), 571–576. https://doi.org/10.1038/s41586-020-2316-7

Biasco, L., Pellin, D., Scala, S., Dionisio, F., Basso-Ricci, L., Leonardelli, L., Scaramuzza, S., Baricordi, C., Ferrua, F., Cicalese, M. P., Giannelli, S., Neduva, V., Dow, D. J., Schmidt, M., Von Kalle, C., Roncarolo, M. G., Ciceri, F., Vicard, P., Wit, E., … Aiuti, A. (2016). In Vivo Tracking of Human Hematopoiesis Reveals Patterns of Clonal Dynamics during Early and Steady-State Reconstitution Phases. *Cell Stem Cell*, *19*(1), 107–119. https://doi.org/10.1016/j.stem.2016.04.016

Bigas, A., & Waskow, C. (2016). Blood stem cells: from beginning to end. *Development (Cambridge, England)*, *143*(19), 3429–3433. https://doi.org/10.1242/DEV.142828

Blümich, S., Zdimerova, H., Münz, C., Kipar, A., & Pellegrini, G. (2021). Human CD34+ Hematopoietic Stem Cell–Engrafted NSG Mice: Morphological and Immunophenotypic Features. *Veterinary Pathology*, *58*(1), 161–180. https://doi.org/10.1177/0300985820948822/SUPPL_FILE/COMBINED_SUPPLEMENTAL_MATERIALS-BLUMICH_ET_AL.PDF

Bock, C., Beerman, I., Lien, W. H., Smith, Z. D., Gu, H., Boyle, P., Gnirke, A., Fuchs, E., Rossi, D. J., & Meissner, A. (2012). DNA Methylation Dynamics during In Vivo Differentiation of Blood and Skin Stem Cells. *Molecular Cell*, *47*(4), 633–647. https://doi.org/10.1016/j.molcel.2012.06.019

Boettcher, S., & Manz, M. G. (2017). Regulation of Inflammation- and Infection-Driven Hematopoiesis. *Trends in Immunology*, *38*(5), 345–357. https://doi.org/10.1016/J.IT.2017.01.004/ASSET/86564558-9ADE-4B8B-9197-944081F71264/MAIN.ASSETS/GR1.JPG

Boles, N. C., Lin, K. K., Lukov, G. L., Bowman, T. V., Baldridge, M. T., & Goodell, M. A. (2011). CD48 on hematopoietic progenitors regulates stem cells and suppresses tumor formation. *Blood*, *118*(1), 80. https://doi.org/10.1182/BLOOD-2010-12-322339

Bonnet, D., & Dick, J. E. (1997). Human acute myeloid leukemia is organized as a hierarchy that originates from a primitive hematopoietic cell. *Nature Medicine*, *3*(7), 730–737. https://doi.org/10.1038/nm0797-730

Bradley, T. R., & Metcalf, D. (1966). The growth of mouse bone marrow cells in vitro. *The Australian Journal of Experimental Biology and Medical Science*, *44*(3), 287–299. https://doi.org/10.1038/ICB.1966.28

Bruns, I., Lucas, D., Pinho, S., Ahmed, J., Lambert, M. P., Kunisaki, Y., Scheiermann, C., Schiff, L., Poncz, M., Bergman, A., & Frenette, P. S. (2014). Megakaryocytes regulate hematopoietic stem cell quiescence through CXCL4 secretion. *Nature Medicine*, *20*(11), 1315–1320. https://doi.org/10.1038/NM.3707

Busch, K., Klapproth, K., Barile, M., Flossdorf, M., Holland-Letz, T., Schlenner, S. M., Reth, M., Höfer, T., & Rodewald, H. R. (2015). Fundamental properties of unperturbed haematopoiesis from stem cells in vivo. *Nature*, *518*(7540), 542–546. https://doi.org/10.1038/NATURE14242

Busque, L., Patel, J. P., Figueroa, M. E., Vasanthakumar, A., Provost, S., Hamilou, Z., Mollica, L., Li, J., Viale, A., Heguy, A., Hassimi, M., Socci, N., Bhatt, P. K., Gonen, M., Mason, C. E., Melnick, A., Godley, L. A., Brennan, C. W., Abdel-Wahab, O., & Levine, R. L. (2012). Recurrent somatic TET2 mutations in normal elderly individuals with clonal hematopoiesis. *Nature Genetics 2012 44:11*, *44*(11), 1179–1181. https://doi.org/10.1038/ng.2413

C, P., AR, M., G, M., M, P., M, C., G, R., G, M., M, P., AM, G., & P, C. (1984). Embryonic----Fetal Hb switch in humans: studies on erythroid bursts generated by embryonic progenitors from yolk sac and liver. *Proceedings of the National Academy of Sciences of the United States of America*, *81*(8), 2416–2420. https://doi.org/10.1073/PNAS.81.8.2416

Cabezas-Wallscheid, N. (2014). Identification of regulatory networks in HSCs and their immediate progeny via integrated proteome, transcriptome, and DNA methylome analysis. *Cell Stem Cell*, *15*, 507–522.

Caiado, F., Pietras, E. M., & Manz, M. G. (2021). Inflammation as a regulator of hematopoietic stem cell function in disease, aging, and clonal selection. *The Journal of Experimental Medicine*, *218*(7), e20201541. https://doi.org/10.1084/JEM.20201541

Calvanese, V., Capellera-Garcia, S., Ma, F., Fares, I., Liebscher, S., Ng, E. S., Ekstrand, S., Aguadé-Gorgorió, J., Vavilina, A., Lefaudeux, D., Nadel, B., Li, J. Y., Wang, Y., Lee, L. K., Ardehali, R., Iruela-Arispe, M. L., Pellegrini, M., Stanley, E. G., Elefanty, A. G., … Mikkola, H. K. A. (2022). Mapping human haematopoietic stem cells from haemogenic endothelium to birth. *Nature*, *604*(7906), 534–540. https://doi.org/10.1038/s41586-022-04571-x

Calvanese, V., & Mikkola, H. K. A. (2023). The genesis of human hematopoietic stem cells. *Blood*, *142*(6), 519–532. https://doi.org/10.1182/BLOOD.2022017934

Canu, G., & Ruhrberg, C. (2021). First blood: the endothelial origins of hematopoietic progenitors. *Angiogenesis*, *24*(2), 199–211. https://doi.org/10.1007/s10456-021-09783-9

Carrelha, J., Mazzi, S., Winroth, A., Hagemann-Jensen, M., Ziegenhain, C., Högstrand, K., Seki, M., Brennan, M. S., Lehander, M., Wu, B., Meng, Y., Markljung, E., Norfo, R., Ishida, H., Belander Strålin, K., Grasso, F., Simoglou Karali, C., Aliouat, A., Hillen, A., … Jacobsen, S. E. W. (2024). Alternative platelet differentiation pathways initiated by nonhierarchically related hematopoietic stem cells. *Nature Immunology*, *25*(6), 1007. https://doi.org/10.1038/S41590-024-01845-6

Carrelha, J., Meng, Y., Kettyle, L. M., Luis, T. C., Norfo, R., Alcolea, V., Boukarabila, H., Grasso, F., Gambardella, A., Grover, A., Högstrand, K., Lord, A. M., Sanjuan-Pla, A., Woll, P. S., Nerlov, C., & Jacobsen, S. E. W. (2018). Hierarchically related lineage-restricted fates of multipotent haematopoietic stem cells. *Nature*, *554*(7690), 106–111. https://doi.org/10.1038/nature25455

CE Müller-Sieburg, R. C. M. T. B. A. H. S. (2002). Deterministic regulation of hematopoietic stem cell self-renewal and differentiation. *Blood*, *100*, 1302–1309.

Çelebi, B., Mantovani, D., & Pineault, N. (2011). Effects of extracellular matrix proteins on the growth of haematopoietic progenitor cells. *Biomedical Materials*, *6*(5). https://doi.org/10.1088/1748-6041/6/5/055011

Challen, G. A., Boles, N. C., Chambers, S. M., & Goodell, M. A. (2010). Distinct Hematopoietic Stem Cell Subtypes Are Differentially Regulated by TGF-β1. *Cell Stem Cell*, *6*(3), 265–278. https://doi.org/10.1016/j.stem.2010.02.002

Chambers, S. M., Shaw, C. A., Gatza, C., Fisk, C. J., Donehower, L. A., & Goodell, M. A. (2007). Aging Hematopoietic Stem Cells Decline in Function and Exhibit Epigenetic Dysregulation. *PLOS Biology*, *5*(8), e201. https://doi.org/10.1371/JOURNAL.PBIO.0050201

Chang, Y. T., Prompsy, P., Kimeswenger, S., Tsai, Y. C., Ignatova, D., Pavlova, O., Iselin, C., French, L. E., Levesque, M. P., Kuonen, F., Bobrowicz, M., Brunner, P. M., Pascolo, S., Hoetzenecker, W., & Guenova, E. (2024). MHC-I upregulation safeguards neoplastic T cells in the skin against NK cell-mediated eradication in mycosis fungoides. *Nature Communications 2024 15:1*, *15*(1), 1–18. https://doi.org/10.1038/s41467-024-45083-8

Charbord, P., Tavian, M., Humeau, L., & Peault, B. (1996). Early ontogeny of the human marrow from long bones: an immunohistochemical study of hematopoiesis and its microenvironment [see comments]. *Blood*, *87*(10), 4109–4119. https://doi.org/10.1182/blood.V87.10.4109.bloodjournal87104109

Cheshier, S. H., Morrison, S. J., Liao, X., & Weissman, I. L. (1999). In vivo proliferation and cell cycle kinetics of long-term self-renewing hematopoietic stem cells. *Proceedings of the National Academy of Sciences*, *96*(6), 3120–3125. https://doi.org/10.1073/PNAS.96.6.3120

Chin, C. J., Li, S., Corselli, M., Casero, D., Zhu, Y., He, C. Bin, Hardy, R., Péault, B., & Crooks, G. M. (2018). Transcriptionally and Functionally Distinct Mesenchymal Subpopulations Are Generated from Human Pluripotent Stem Cells. *Stem Cell Reports*, *10*(2), 436. https://doi.org/10.1016/J.STEMCR.2017.12.005

Choi, J. S., Mahadik, B. P., & Harley, B. A. C. (2015). Engineering the hematopoietic stem cell niche: Frontiers in biomaterial science. *Biotechnology Journal*, *10*(10), 1529–1545. https://doi.org/10.1002/BIOT.201400758

Civin, C. I., Strauss, L. C., Brovall, C., Fackler, M. J., Schwartz, J. F., & Shaper, J. H. (1984). Antigenic analysis of hematopoiesis. III. A hematopoietic progenitor cell surface antigen defined by a monoclonal antibody raised against KG-1a cells. *The Journal of Immunology*, *133*(1), 157–165. https://doi.org/10.4049/JIMMUNOL.133.1.157

Collado, M., Blasco, M. A., & Serrano, M. (2007). Cellular Senescence in Cancer and Aging. *Cell*, *130*(2), 223–233. https://doi.org/10.1016/J.CELL.2007.07.003/ASSET/2C8FF50D-F0F0-4E0D-8BB6-DA58F4436302/MAIN.ASSETS/GR3.JPG

Conneally, E., Cashman, J., Petzer, A., & Eaves, C. (1997). Expansion in vitro of transplantable human cord blood stem cells demonstrated using a quantitative assay of their lympho-myeloid repopulating activity in

nonobese diabetic-scid/scid mice. *Proceedings of the National Academy of Sciences of the United States of America*, *94*(18), 9836–9841. https://doi.org/10.1073/PNAS.94.18.9836

Cooper, B. (2011). The origins of bone marrow as the seedbed of our blood: from antiquity to the time of Osler. *Proceedings (Baylor University. Medical Center)*, *24*(2), 115. https://doi.org/10.1080/08998280.2011.11928697

Coppin, E., Sundarasetty, B. S., Rahmig, S., Blume, J., Verheyden, N. A., Bahlmann, F., Ravens, S., Schubert, U., Schmid, J., Ludwig, S., Geissler, K., Guntinas-Lichius, O., von Kaisenberg, C., Groten, T., Platz, A., Naumann, R., Ludwig, B., Prinz, I., Waskow, C., & Krueger, A. (2021). Enhanced differentiation of functional human T cells in NSGW41 mice with tissue-specific expression of human interleukin-7. *Leukemia 2021 35:12*, *35*(12), 3561–3567. https://doi.org/10.1038/s41375-021-01259-5

Cosgun, K. N., Rahmig, S., Mende, N., Reinke, S., Hauber, I., Schäfer, C., Petzold, A., Weisbach, H., Heidkamp, G., Purbojo, A., Cesnjevar, R., Platz, A., Bornhäuser, M., Schmitz, M., Dudziak, D., Hauber, J., Kirberg, J., & Waskow, C. (2014). Kit regulates HSC engraftment across the human-mouse species barrier. *Cell Stem Cell*, *15*(2), 227–238. https://doi.org/10.1016/J.STEM.2014.06.001

Cronkite, D. A., & Strutt, T. M. (2018). The Regulation of Inflammation by Innate and Adaptive Lymphocytes. *Journal of Immunology Research*, *2018*(1), 1467538. https://doi.org/10.1155/2018/1467538

Cui, K., Zang, C., Roh, T. Y., Schones, D. E., Childs, R. W., Peng, W., & Zhao, K. (2009). Chromatin Signatures in Multipotent Human Hematopoietic Stem Cells Indicate the Fate of Bivalent Genes during Differentiation. *Cell Stem Cell*, *4*(1), 80–93. https://doi.org/10.1016/j.stem.2008.11.011

Daga, S., Rosenberger, A., Quehenberger, F., Krisper, N., Prietl, B., Reinisch, A., Zebisch, A., Sill, H., & Wölfler, A. (2019). High GPR56 surface expression correlates with a leukemic stem cell gene signature in CD34-positive AML. *Cancer Medicine*, *8*(4), 1771. https://doi.org/10.1002/CAM4.2053

De Bruin, A. M., Demirel, Ö., Hooibrink, B., Brandts, C. H., & Nolte, M. A. (2013). Interferon-γ impairs proliferation of hematopoietic stem cells in mice. *Blood*, *121*(18), 3578–3585. https://doi.org/10.1182/BLOOD-2012-05-432906

Dechambre A, L. L. H. L. (1877). *Dictionnaire encyclopédique des sciences médicales.*

Dey, S., Ashwin, H., Milross, L., Hunter, B., Majo, J., Filby, A. J., Fisher, A. J., Kaye, P. M., & Lagos, D. (2023). Downregulation of MALAT1 is a hallmark of tissue and peripheral proliferative T cells in COVID-19. *Clinical and Experimental Immunology*, *212*(3), 262–275. https://doi.org/10.1093/CEI/UXAD034

Dick, J. E. (1996). Normal and leukemic human stem cells assayed in SCID mice. *Seminars in Immunology*, *8*(4), 197–206. https://doi.org/10.1006/SMIM.1996.0025

Dick, J. E. (2008). Stem cell concepts renew cancer research. *Blood*, *112*(13), 4793–4807. https://doi.org/10.1182/BLOOD-2008-08-077941

Ding, L., & Morrison, S. J. (2013). Haematopoietic stem cells and early lymphoid progenitors occupy distinct bone marrow niches. *Nature*, *495*(7440), 231–235. https://doi.org/10.1038/NATURE11885

Dobin, A., Davis, C. A., Schlesinger, F., Drenkow, J., Zaleski, C., Jha, S., Batut, P., Chaisson, M., & Gingeras, T. R. (2013). STAR: ultrafast universal RNA-seq aligner. *Bioinformatics (Oxford, England)*, *29*(1), 15–21. https://doi.org/10.1093/BIOINFORMATICS/BTS635

Dong Ku, K., Fujiki, Y., Fukushima, T., Hideo, E., Shibuya, A., & Nakauchi, H. (1999). Comparison of Hematopoietic Activities of Human Bone Marrow and Umbilical Cord Blood CD34 Positive and Negative Cells. *STEM CELLS*, *17*(5), 286–294. https://doi.org/10.1002/STEM.170286

Dorsheimer, L., Assmus, B., Rasper, T., Ortmann, C. A., Ecke, A., Abou-El-Ardat, K., Schmid, T., Brüne, B., Wagner, S., Serve, H., Hoffmann, J., Seeger, F., Dimmeler, S., Zeiher, A. M., & Rieger, M. A. (2019). Association of Mutations Contributing to Clonal Hematopoiesis With Prognosis in Chronic Ischemic Heart Failure. *JAMA Cardiology*, *4*(1), 25–33. https://doi.org/10.1001/JAMACARDIO.2018.3965

Dorshkind, K., Montecino-Rodriguez, E., & Signer, R. A. J. (2009). The ageing immune system: is it ever too old to become young again? *Nature Reviews Immunology 2009 9:1*, *9*(1), 57–62. https://doi.org/10.1038/nri2471

Doulatov, S. (2010). Revised map of the human progenitor hierarchy shows the origin of macrophages and dendritic cells in early lymphoid development. *Nat. Immunol.*, *11*, 585–593.

Doulatov, S., Notta, F., Laurenti, E., & Dick, J. E. (2012a). Hematopoiesis: A Human Perspective. *Cell Stem Cell*, *10*(2), 120–136. https://doi.org/10.1016/j.stem.2012.01.006

Doulatov, S., Notta, F., Laurenti, E., & Dick, J. E. (2012b). Hematopoiesis: A human perspective. *Cell Stem Cell*, *10*(2), 120–136. https://doi.org/10.1016/j.stem.2012.01.006

Drize, N., Keller, J., & Chertkov, J. (1996). Local clonal analysis of the hematopoietic system shows that multiple small short-living clones maintain life-long hematopoiesis in reconstituted mice. *Blood*, *88*(8), 2927–2938. https://doi.org/10.1182/blood.V88.8.2927.bloodjournal8882927

Dykstra, B., Kent, D., Bowie, M., McCaffrey, L., Hamilton, M., Lyons, K., Lee, S. J., Brinkman, R., & Eaves, C. (2007). Long-Term Propagation of Distinct Hematopoietic Differentiation Programs In Vivo. *Cell Stem Cell*, *1*(2), 218–229. https://doi.org/10.1016/J.STEM.2007.05.015/ATTACHMENT/28296E2B-E926-4990-8D08-D3593E5F82CB/MMC1.PDF

Dykstra, B., Olthof, S., Schreuder, J., Ritsema, M., & Haan, G. De. (2011). Clonal analysis reveals multiple functional defects of aged murine hematopoietic stem cells. *Journal of Experimental Medicine*, *208*(13), 2691–2703. https://doi.org/10.1084/JEM.20111490

Dzierzak, E., & Bigas, A. (2018). Blood Development: Hematopoietic Stem Cell Dependence and Independence. *Cell Stem Cell*, *22*(5), 639–651. https://doi.org/10.1016/j.stem.2018.04.015

Edvardsson, L., Dykes, J., & Olofsson, T. (2006). Isolation and characterization of human myeloid progenitor populations—TpoR as discriminator between common myeloid and megakaryocyte/erythroid progenitors. *Experimental Hematology*, *34*(5), 599–609. https://doi.org/10.1016/J.EXPHEM.2006.01.017

Ehninger, A., & Trumpp, A. (2011). The bone marrow stem cell niche grows up: Mesenchymal stem cells and macrophages move in. *Journal of Experimental Medicine*, *208*(3), 421–428. https://doi.org/10.1084/JEM.20110132

Eilken, H. M., Nishikawa, S. I., & Schroeder, T. (2009). Continuous single-cell imaging of blood generation from haemogenic endothelium. *Nature 2009 457:7231*, *457*(7231), 896–900. https://doi.org/10.1038/nature07760

El Bannoudi, H., Cornwell, M., Luttrell-Williams, E., Engel, A., Rolling, C., Barrett, T. J., Izmirly, P., Belmont, H. M., Ruggles, K., Clancy, R., Buyon, J., & Berger, J. S. (2023). Platelet LGALS3BP as a Mediator of Myeloid Inflammation in Systemic Lupus Erythematosus. *Arthritis & Rheumatology (Hoboken, N.J.)*, *75*(5), 711–722. https://doi.org/10.1002/ART.42382

Elowitz, M. B., Levine, A. J., Siggia, E. D., & Swain, P. S. (2002). Stochastic gene expression in a single cell. *Science*, *297*(5584), 1183–1186. https://doi.org/10.1126/SCIENCE.1070919/SUPPL_FILE/ELOWITZSOM.PDF

Essers, M. A., Offner, S., Blanco-Bose, W. E., Waibler, Z., Kalinke, U., Duchosal, M. A., & Trumpp, A. (2009). IFNalpha activates dormant haematopoietic stem cells in vivo. *Nature*, *458*, 904–908.

Falix, F. A., Aronson, D. C., Lamers, W. H., & Gaemers, I. C. (2012). Possible roles of DLK1 in the Notch pathway during development and disease. *Biochimica et Biophysica Acta (BBA) - Molecular Basis of Disease*, *1822*(6), 988–995. https://doi.org/10.1016/J.BBADIS.2012.02.003

Farlik, M., Halbritter, F., Müller, F., Choudry, F. A., Ebert, P., Klughammer, J., Farrow, S., Santoro, A., Ciaurro, V., Mathur, A., Uppal, R., Stunnenberg, H. G., Ouwehand, W. H., Laurenti, E., Lengauer, T., Frontini, M., & Bock, C. (2016). DNA Methylation Dynamics of Human Hematopoietic Stem Cell Differentiation. *Cell Stem Cell*, *19*(6), 808–822. https://doi.org/10.1016/j.stem.2016.10.019

Ferreira, R., Wai, A., Shimizu, R., Gillemans, N., Rottier, R., Von Lindern, M., Ohneda, K., Grosveld, F., Yamamoto, M., & Philipsen, S. (2007). Dynamic regulation of Gata factor levels is more important than their identity. *Blood*, *109*(12), 5481–5490. https://doi.org/10.1182/BLOOD-2006-11-060491

Finch, C. E. (2009). Evolution of the human lifespan and diseases of aging: Roles of infection, inflammation, and nutrition. *Proceedings of the National Academy of Sciences*, *107*(suppl_1), 1718–1724. https://doi.org/10.1073/PNAS.0909606106

Florez, M. A., Matatall, K. A., Jeong, Y., Ortinau, L., Shafer, P. W., Lynch, A. M., Jaksik, R., Kimmel, M., Park, D., & King, K. Y. (2020). Interferon Gamma Mediates Hematopoietic Stem Cell Activation and Niche Relocalization through BST2. *Cell Reports*, *33*(12), 108530. https://doi.org/10.1016/J.CELREP.2020.108530/ATTACHMENT/FAC95336-308C-4487-8BB6-246A60B1CBDF/MMC3.MP4

Florian, M. C., Dö Rr, K., Niebel, A., Daria, D., Schrezenmeier, H., Rojewski, M., Filippi, M.-D., Hasenberg, A., Gunzer, M., Scharffetter-Kochanek, K., Zheng, Y., & Geiger, H. (2012). *Cell Stem Cell Article Cdc42 Activity Regulates Hematopoietic Stem Cell Aging and Rejuvenation*. https://doi.org/10.1016/j.stem.2012.04.007

Forsberg, E. C., Serwold, T., Kogan, S., Weissman, I. L., & Passegué, E. (2006). New evidence supporting megakaryocyte-erythrocyte potential of flk2/flt3+ multipotent hematopoietic progenitors. *Cell*, *126*, 415–426.

Fraser, S. T., Isern, J., & Baron, M. H. (2007). Maturation and enucleation of primitive erythroblasts during mouse embryogenesis is accompanied by changes in cell-surface antigen expression. *Blood*, *109*(1), 343. https://doi.org/10.1182/BLOOD-2006-03-006569

Fröbel, J., Landspersky, T., Percin, G., Schreck, C., Rahmig, S., Ori, A., Nowak, D., Essers, M., Waskow, C., & Oostendorp, R. A. J. (2021). The Hematopoietic Bone Marrow Niche Ecosystem. *Frontiers in Cell and Developmental Biology*, *9*, 705410. https://doi.org/10.3389/fcell.2021.705410

Fujisaki, J., Wu, J., Carlson, A. L., Silberstein, L., Putheti, P., Larocca, R., Gao, W., Saito, T. I., Celso, C. Lo, Tsuyuzaki, H., Sato, T., Côté, D., Sykes, M., Strom, T. B., Scadden, D. T., & Lin, C. P. (2011). In vivo imaging of Treg cells providing immune privilege to the haematopoietic stem-cell niche. *Nature*, *474*(7350), 216–220. https://doi.org/10.1038/NATURE10160

Ganuza, M., Hall, T., Myers, J., Nevitt, C., Sánchez-Lanzas, R., Chabot, A., Ding, J., Kooienga, E., Caprio, C., Finkelstein, D., Kang, G., Obeng, E., & McKinney-Freeman, S. (2022). Murine foetal liver supports limited detectable expansion of life-long haematopoietic progenitors. *Nature Cell Biology*, *24*(10), 1475–1486. https://doi.org/10.1038/s41556-022-00999-5

Gao, X., Xu, C., Asada, N., & Frenette, P. S. (2018). The hematopoietic stem cell niche: from embryo to adult. *Development*, *145*(2). https://doi.org/10.1242/dev.139691

Gazit, R., Mandal, P. K., Ebina, W., Ben-Zvi, A., Nombela-Arrieta, C., Silberstein, L. E., & Rossi, D. J. (2014). Fgd5 identifies hematopoietic stem cells in the murine bone marrow. *Journal of Experimental Medicine*, *211*(7), 1315–1331. https://doi.org/10.1084/JEM.20130428/VIDEO-1

Genovese, G., Kähler, A. K., Handsaker, R. E., Lindberg, J., Rose, S. A., Bakhoum, S. F., Chambert, K., Mick, E., Neale, B. M., Fromer, M., Purcell, S. M., Svantesson, O., Landén, M., Höglund, M., Lehmann, S., Gabriel, S. B., Moran, J. L., Lander, E. S., Sullivan, P. F., … McCarroll, S. A. (2014). Clonal Hematopoiesis and Blood-Cancer Risk Inferred from Blood DNA Sequence. *New England Journal of Medicine*, *371*(26), 2477–2487. https://doi.org/10.1056/NEJMOA1409405/SUPPL_FILE/NEJMOA1409405_DISCLOSURES.PDF

Gerdes, J., Schwab, U., Lemke, H., & Stein, H. (1983). Production of a mouse monoclonal antibody reactive with a human nuclear antigen associated with cell proliferation. *International Journal of Cancer*, *31*(1), 13–20. https://doi.org/10.1002/IJC.2910310104

Gerrits, A., Dykstra, B., Kalmykowa, O. J., Klauke, K., Verovskaya, E., Broekhuis, M. J. C., de Haan, G., & Bystrykh, L. V. (2010). Cellular barcoding tool for clonal analysis in the hematopoietic system. *Blood*, *115*(13), 2610–2618. https://doi.org/10.1182/blood-2009-06-229757

GJ Spangrude, S. H. I. W. (1988). Purification and characterization of mouse hematopoietic stem cells. *Science*, *241*, 58–62.

Glimm, H., Ball, C. R., & von Kalle, C. (2011). You Can Count on This: Barcoded Hematopoietic Stem Cells. *Cell Stem Cell*, *9*(5), 390–392. https://doi.org/10.1016/j.stem.2011.10.013

Gobran, M., Politi, A. Z., Welp, L., Jakobi, J., Urlaub, H., & Lenart, P. (2025). PLK1 inhibition delays mitotic entry revealing changes to the phosphoproteome of mammalian cells early in division. *EMBO Journal*. https://doi.org/10.1038/S44318-025-00400-9/SUPPL_FILE/44318_2025_400_MOESM12_ESM.PDF

Goodman, W. A., Omenetti, S., Date, D., Di Martino, L., De Salvo, C., Kim, G. D., Chowdhry, S., Bamias, G., Cominelli, F., Pizarro, T. T., & Mahabeleshwar, G. H. (2016). KLF6 contributes to myeloid cell plasticity in the pathogenesis of intestinal inflammation. *Mucosal Immunology*, *9*(5), 1250–1262. https://doi.org/10.1038/MI.2016.1

Goyal, S., & Zandstra, P. W. (2015). Chasing blood. *Nature*, *518*(7540), 488–490. https://doi.org/10.1038/nature14203

Goyama, S., Wunderlich, M., & Mulloy, J. C. (2015). Xenograft models for normal and malignant stem cells. *Blood*, *125*(17), 2630 LP – 2640. https://doi.org/10.1182/blood-2014-11-570218

Granja, J. M., Klemm, S., McGinnis, L. M., Kathiria, A. S., Mezger, A., Corces, M. R., Parks, B., Gars, E., Liedtke, M., Zheng, G. X. Y., Chang, H. Y., Majeti, R., & Greenleaf, W. J. (2019). Single-cell multiomic analysis identifies regulatory programs in mixed-phenotype acute leukemia. *Nature Biotechnology 2019 37:12*, *37*(12), 1458–1465. https://doi.org/10.1038/s41587-019-0332-7

Greenbaum, A., Hsu, Y. M. S., Day, R. B., Schuettpelz, L. G., Christopher, M. J., Borgerding, J. N., Nagasawa, T., & Link, D. C. (2013). CXCL12 in early mesenchymal progenitors is required for haematopoietic stem-cell maintenance. *Nature*, *495*(7440), 227–230. https://doi.org/10.1038/NATURE11926

Grover, A., Sanjuan-Pla, A., Thongjuea, S., Carrelha, J., Giustacchini, A., Gambardella, A., Macaulay, I., Mancini, E., Luis, T. C., Mead, A., Jacobsen, S. E. W., & Nerlov, C. (2016). Single-cell RNA sequencing reveals molecular and functional platelet bias of aged haematopoietic stem cells. *Nature Communications*, *7*. https://doi.org/10.1038/NCOMMS11075

Gyurkocza, B., Rezvani, A., & Storb, R. F. (2010). Allogeneic hematopoietic cell transplantation: the state of the art. *Expert Review of Hematology*, *3*(3), 285. https://doi.org/10.1586/EHM.10.21

Haar, J. L., & Ackerman, G. A. (1971). A phase and electron microscopic study of vasculogenesis and erythropoiesis in the yolk sac of the mouse. *The Anatomical Record*, *170*(2), 199–223. https://doi.org/10.1002/AR.1091700206

Haas, S. (2015). Inflammation-induced emergency megakaryopoiesis driven by hematopoietic stem cell-like megakaryocyte progenitors. *Cell Stem Cell*, *17*, 422–434.

Haas, S., Trumpp, A., & Milsom, M. D. (2018). Causes and consequences of hematopoietic stem cell heterogeneity. *Cell Stem Cell*, *22*(5), 627–638. https://doi.org/10.1016/j.stem.2018.04.003

Hao, Y., Hao, S., Andersen-Nissen, E., Mauck, W. M., Zheng, S., Butler, A., Lee, M. J., Wilk, A. J., Darby, C., Zager, M., Hoffman, P., Stoeckius, M., Papalexi, E., Mimitou, E. P., Jain, J., Srivastava, A., Stuart, T., Fleming, L. M., Yeung, B., … Satija, R. (2021). Integrated analysis of multimodal single-cell data. *Cell*, *184*(13), 3573-3587.e29. https://doi.org/10.1016/J.CELL.2021.04.048/ASSET/13B1132E-1BA1-48C0-89F4-2EE6D8AB8FBA/MAIN.ASSETS/FIGS7.JPG

Hao, Y., Stuart, T., Kowalski, M. H., Choudhary, S., Hoffman, P., Hartman, A., Srivastava, A., Molla, G., Madad, S., Fernandez-Granda, C., & Satija, R. (2023). Dictionary learning for integrative, multimodal and scalable single-cell analysis. *Nature Biotechnology 2023 42:2*, *42*(2), 293–304. https://doi.org/10.1038/s41587-023-01767-y

Harris, D. T., & Badowski, M. (2014). Long term human reconstitution and immune aging in NOD-Rag (-)-γ chain (-) mice. *Immunobiology*, *219*(2), 131–137. https://doi.org/10.1016/J.IMBIO.2013.08.013

Harrison, D. E., & Astle, C. M. (1982). Loss of stem cell repopulating ability upon transplantation. Effects of donor age, cell number, and transplantation procedure. *Journal of Experimental Medicine*, *156*(6), 1767–1779. https://doi.org/10.1084/JEM.156.6.1767

Hayakawa, J., Hsieh, M. M., Uchida, N., Phang, O., & Tisdale, J. F. (2009). Busulfan produces efficient human cell engraftment in NOD/LtSz-scid IL2Rγ null mice. *Stem Cells (Dayton, Ohio)*, *27*(1), 175. https://doi.org/10.1634/STEMCELLS.2008-0583

He, X., & Xu, C. (2020). Immune checkpoint signaling and cancer immunotherapy. *Cell Research 2020 30:8*, *30*(8), 660–669. https://doi.org/10.1038/s41422-020-0343-4

Hernández-Malmierca, P., Vonficht, D., Schnell, A., Uckelmann, H. J., Bollhagen, A., Mahmoud, M. A. A., Landua, S. L., van der Salm, E., Trautmann, C. L., Raffel, S., Grünschläger, F., Lutz, R., Ghosh, M., Renders, S., Correia, N., Donato, E., Dixon, K. O., Hirche, C., Andresen, C., … Haas, S. (2022). Antigen presentation safeguards the integrity of the hematopoietic stem cell pool. *Cell Stem Cell*, *29*(5), 760-775.e10. https://doi.org/10.1016/J.STEM.2022.04.007

Hikspoors, J. P. J. M., Kruepunga, N., Mommen, G. M. C., Köhler, S. E., Anderson, R. H., & Lamers, W. H. (2022). A pictorial account of the human embryonic heart between 3.5 and 8 weeks of development. *Communications Biology 2022 5:1*, *5*(1), 1–22. https://doi.org/10.1038/s42003-022-03153-x

Hirche, C., Frenz, T., Haas, S. F., Döring, M., Borst, K., Tegtmeyer, P. K., Brizic, I., Jordan, S., Keyser, K., Chhatbar, C., Pronk, E., Lin, S., Messerle, M., Jonjic, S., Falk, C. S., Trumpp, A., Essers, M. A. G., & Kalinke, U. (2017). Systemic Virus Infections Differentially Modulate Cell Cycle State and Functionality of Long-Term Hematopoietic Stem Cells In Vivo. *Cell Reports*, *19*(11), 2345–2356. https://doi.org/10.1016/J.CELREP.2017.05.063

Hirsch, E., Iglesias, A., Potocnik, A. J., Hartmann, U., & Fässler, R. (1996). Impaired migration but not differentiation of haematopoietic stem cells in the absence of β1 integrins. *Nature*, *380*(6570), 171–175. https://doi.org/10.1038/380171A0

Houssaint, E. (1981). Differentiation of the mouse hepatic primordium. II. Extrinsic origin of the haemopoietic cell line. *Cell Differentiation*, *10*(5), 243–252. https://doi.org/10.1016/0045-6039(81)90007-5

Huang, D., Han, Y., Tang, T., Yang, L., Jiang, P., Qian, W., Zhang, Z., Qian, X., Zeng, X., & Qian, P. (2023). Dlk1 maintains adult mice long-term HSCs by activating Notch signaling to restrict mitochondrial metabolism. *Experimental Hematology and Oncology*, *12*(1). https://doi.org/10.1186/S40164-022-00369-9

Hung, C. H., Wang, K. Y., Liou, Y. H., Wang, J. P., Huang, A. Y. S., Lee, T. L., Jiang, S. T., Liao, N. S., Shyu, Y. C., & Shen, C. K. J. (2020). Negative Regulation of the Differentiation of Flk2− CD34− LSK Hematopoietic Stem Cells by EKLF/KLF1. *International Journal of Molecular Sciences*, *21*(22), 8448. https://doi.org/10.3390/IJMS21228448

Ishikawa, F., Livingston, A. G., Wingard, J. R., Nishikawa, S. ichi, & Ogawa, M. (2002). An assay for long-term engrafting human hematopoietic cells based on newborn NOD/SCID/β2-microglobulinnull mice. *Experimental Hematology*, *30*(5), 488–494. https://doi.org/10.1016/S0301-472X(02)00784-1

Ishikawa, F., Yasukawa, M., Lyons, B., Yoshida, S., Miyamoto, T., Yoshimoto, G., Watanabe, T., Akashi, K., Shultz, L. D., & Harada, M. (2005). Development of functional human blood and immune systems in NOD/SCID/IL2 receptor γ chainnull mice. *Blood*, *106*(5), 1565. https://doi.org/10.1182/BLOOD-2005-02-0516

Ito, K., Carracedo, A., Weiss, D., Arai, F., Ala, U., Avigan, D. E., Schafer, Z. T., Evans, R. M., Suda, T., Lee, C. H., & Pandolfi, P. P. (2012). A PML-PPAR-δ pathway for fatty acid oxidation regulates hematopoietic stem cell maintenance. *Nature Medicine*, *18*(9), 1350–1358. https://doi.org/10.1038/NM.2882

Ito, K., & Suda, T. (2014). Metabolic requirements for the maintenance of self-renewing stem cells. *Nature Reviews Molecular Cell Biology*, *15*(4), 243–256. https://doi.org/10.1038/NRM3772

Ito, M., Hiramatsu, H., Kobayashi, K., Suzue, K., Kawahata, M., Hioki, K., Ueyama, Y., Koyanagi, Y., Sugamura, K., Tsuji, K., Heike, T., & Nakahata, T. (2002). NOD/SCID/γcnull mouse: An excellent recipient mouse model for engraftment of human cells. *Blood*, *100*(9), 3175–3182. https://doi.org/10.1182/blood-2001-12-0207

Jaiswal, S., & Ebert, B. L. (2019). Clonal hematopoiesis in human aging and disease. *Science*, *366*(6465). https://doi.org/10.1126/SCIENCE.AAN4673/ASSET/93051C95-6898-41BD-B5F2-A1135C364DCF/ASSETS/GRAPHIC/366_AAN4673_FA.JPEG

Jaiswal, S., Fontanillas, P., Flannick, J., Manning, A., Grauman, P. V., Mar, B. G., Lindsley, R. C., Mermel, C. H., Burtt, N., Chavez, A., Higgins, J. M., Moltchanov, V., Kuo, F. C., Kluk, M. J., Henderson, B., Kinnunen, L., Koistinen, H. A., Ladenvall, C., Getz, G., … Ebert, B. L. (2014). Age-Related Clonal Hematopoiesis Associated with Adverse Outcomes. *New England Journal of Medicine*, *371*(26), 2488–2498. https://doi.org/10.1056/NEJMOA1408617/SUPPL_FILE/NEJMOA1408617_DISCLOSURES.PDF

JE Till, E. M. (1961). A direct measurement of the radiation sensitivity of normal mouse bone marrow cells. *Radiat. Res.*, *14*, 213–222.

Jia, L., Zhang, Q., & Zhang, R. (2018). PD-1/PD-L1 pathway blockade works as an effective and practical therapy for cancer immunotherapy. *Cancer Biology & Medicine*, *15*(2), 116–123. https://doi.org/10.20892/J.ISSN.2095-3941.2017.0086

JM, M., R, N., H, K., LD, S., M, L., & IL, W. (1988). The SCID-hu mouse: murine model for the analysis of human hematolymphoid differentiation and function. *Science (New York, N.Y.)*, *241*(4873), 1632–1639. https://doi.org/10.1126/SCIENCE.241.4873.1632

Karamitros, D., Stoilova, B., Aboukhalil, Z., Hamey, F., Reinisch, A., Samitsch, M., Quek, L., Otto, G., Repapi, E., Doondeea, J., Usukhbayar, B., Calvo, J., Taylor, S., Goardon, N., Six, E., Pflumio, F., Porcher, C., Majeti, R., Göttgens, B., & Vyas, P. (2018). Single-cell analysis reveals the continuum of human lympho-myeloid progenitor cells article. *Nature Immunology*, *19*(1), 85–97. https://doi.org/10.1038/S41590-017-0001-2

Kaufmann, K. B., Zeng, A. G. X., Coyaud, E., Garcia-Prat, L., Papalexi, E., Murison, A., Laurent, E. M. N., Chan-Seng-Yue, M., Gan, O. I., Pan, K., McLeod, J., Boutzen, H., Zandi, S., Takayanagi, S. ichiro, Satija, R., Raught, B., Xie, S. Z., & Dick, J. E. (2021). A latent subset of human hematopoietic stem cells resists regenerative stress to preserve stemness. *Nature Immunology 2021 22:6*, *22*(6), 723–734. https://doi.org/10.1038/s41590-021-00925-1

Kim, I., Saunders, T. L., & Morrison, S. J. (2007). Sox17 Dependence Distinguishes the Transcriptional Regulation of Fetal from Adult Hematopoietic Stem Cells. *Cell*, *130*(3), 470–483. https://doi.org/10.1016/j.cell.2007.06.011

Kim, J. M., Kim, N. I., Oh, Y. K., Kim, Y. J., Youn, J., & Ahn, M. J. (2005). CpG oligodeoxynucleotides induce IL-8 expression in CD34+ cells via mitogen-activated protein kinase-dependent and NF-kappaB-independent pathways. *International Immunology*, *17*(12), 1525–1531. https://doi.org/10.1093/INTIMM/DXH345

Kim, S., Kim, N., Presson, A. P., Metzger, M. E., Bonifacino, A. C., Sehl, M., Chow, S. A., Crooks, G. M., Dunbar, C. E., An, D. S., Donahue, R. E., & Chen, I. S. Y. (2014). Dynamics of HSPC Repopulation in Nonhuman Primates Revealed by a Decade-Long Clonal-Tracking Study. *Cell Stem Cell*, *14*(4), 473–485. https://doi.org/10.1016/j.stem.2013.12.012

King, K. Y., & Goodell, M. A. (2011). Inflammatory modulation of HSCs: Viewing the HSC as a foundation for the immune response. *Nature Reviews Immunology*, *11*(10), 685–692. https://doi.org/10.1038/NRI3062

Kingsley, P. D., Malik, J., Fantauzzo, K. A., & Palis, J. (2004). Yolk sac-derived primitive erythroblasts enucleate during mammalian embryogenesis. *Blood*, *104*, 19–25.

Kode, A., Manavalan, J. S., Mosialou, I., Bhagat, G., Rathinam, C. V., Luo, N., Khiabanian, H., Lee, A., Murty, V. V., Friedman, R., Brum, A., Park, D., Galili, N., Mukherjee, S., Teruya-Feldstein, J., Raza, A., Rabadan, R., Berman, E., & Kousteni, S. (2014). Leukaemogenesis induced by an activating β-catenin mutation in osteoblasts. *Nature*, *506*(7487), 240–244. https://doi.org/10.1038/NATURE12883

Kohn, L. A., Hao, Q. L., Sasidharan, R., Parekh, C., Ge, S., Zhu, Y., Mikkola, H. K. A., & Crooks, G. M. (2012). Lymphoid priming in human bone marrow begins before expression of CD10 with upregulation of L-selectin. *Nature Immunology 2012 13:10*, *13*(10), 963–971. https://doi.org/10.1038/ni.2405

Komic, H., Schmachtel, T., Simoes, C., Külp, M., Yu, W., Jolly, A., Nilsson, M. S., Gonzalez, C., Prosper, F., Bonig, H., Paiva, B., Thorén, F. B., & Rieger, M. A. (2025). Continuous map of early hematopoietic stem cell differentiation across human lifetime. *Nature Communications 2025 16:1*, *16*(1), 1–17. https://doi.org/10.1038/s41467-025-57096-y

Komorowska, K., Doyle, A., Wahlestedt, M., Subramaniam, A., Debnath, S., Chen, J., Soneji, S., Van Handel, B., Mikkola, H. K. A., Miharada, K., Bryder, D., Larsson, J., & Magnusson, M. (2017). Hepatic Leukemia Factor Maintains Quiescence of Hematopoietic Stem Cells and Protects the Stem Cell Pool during Regeneration. *Cell Reports*, *21*(12), 3514–3523. https://doi.org/10.1016/J.CELREP.2017.11.084

Kondo, M., Weissman, I. L., & Akashi, K. (1997). Identification of clonogenic common lymphoid progenitors in mouse bone marrow. *Cell*, *91*(5), 661–672. https://doi.org/10.1016/S0092-8674(00)80453-5

Kooreman, N. G., de Almeida, P. E., Stack, J. P., Nelakanti, R. V., Diecke, S., Shao, N. Y., Swijnenburg, R. J., Sanchez-Freire, V., Matsa, E., Liu, C., Connolly, A. J., Hamming, J. F., Quax, P. H. A., Brehm, M. A., Greiner, D. L., Shultz, L. D., & Wu, J. C. (2017). Alloimmune Responses of Humanized Mice to Human Pluripotent Stem Cell Therapeutics. *Cell Reports*, *20*(8), 1978–1990. https://doi.org/10.1016/j.celrep.2017.08.003

Kovtonyuk, L. V., Fritsch, K., Feng, X., Manz, M. G., & Takizawa, H. (2016). Inflamm-Aging of Hematopoiesis, Hematopoietic Stem Cells, and the Bone Marrow Microenvironment. *Frontiers in Immunology*, *7*(NOV). https://doi.org/10.3389/FIMMU.2016.00502

Krause, D., Fackler, M., Civin, C., & May, W. (1996). CD34: Structure, Biology, and Clinical Utility. *Blood*, *87*(1), 1–13. https://doi.org/10.1182/BLOOD.V87.1.1.1

Kumaravelu, P., Hook, L., Morrison, A. M., Ure, J., Zhao, S., Zuyev, S., Ansell, J., & Medvinsky, A. (2002). Quantitative developmental anatomy of definitive haematopoietic stem cells/long-term repopulating units (HSC/RUs): role of the aorta-gonad-mesonephros (AGM) region and the yolk sac in colonisation of the mouse embryonic liver. *Development*, *129*, 4891–4899.

Lang, J., Kelly, M., Freed, B. M., McCarter, M. D., Kedl, R. M., Torres, R. M., & Pelanda, R. (2013). Studies of lymphocyte reconstitution in a humanized mouse model reveal a requirement of T cells for human B cell maturation. *Journal of Immunology (Baltimore, Md. : 1950)*, *190*(5), 2090–2101. https://doi.org/10.4049/JIMMUNOL.1202810

Lang, R. A., Metcalf, D., Cuthbertson, R. A., Lyons, I., Stanley, E., Kelso, A., Kannourakis, G., Williamson, D. J., Klintworth, G. K., Gonda, T. J., & Dunn, A. R. (1987). Transgenic mice expressing a hemopoietic growth factor gene (GM-CSF) develop accumulations of macrophages, blindness, and a fatal syndrome of tissue damage. *Cell*, *51*(4), 675–686. https://doi.org/10.1016/0092-8674(87)90136-X

Lansdorp, P. M., Sutherland, H. J., & Eaves, C. J. (1990). Selective expression of CD45 isoforms on functional subpopulations of CD34+ hemopoietic cells from human bone marrow. *The Journal of Experimental Medicine*, *172*(1), 363–366. https://doi.org/10.1084/JEM.172.1.363

Lara-Astiaso, D., Weiner, A., Lorenzo-Vivas, E., Zaretsky, I., Jaitin, D. A., David, E., Keren-Shaul, H., Mildner, A., Winter, D., Jung, S., Friedman, N., & Amit, I. (2014). Chromatin state dynamics during blood formation. *Science*, *345*(6199), 943–949. https://doi.org/10.1126/SCIENCE.1256271/SUPPL_FILE/LARAASTIASO.SM.PDF

Larochelle, A., Savona, M., Wiggins, M., Anderson, S., Ichwan, B., Keyvanfar, K., Morrison, S. J., & Dunbar, C. E. (2011). Human and rhesus macaque hematopoietic stem cells cannot be purified based only on SLAM family markers. *Blood*, *117*(5), 1550–1554. https://doi.org/10.1182/BLOOD-2009-03-212803

Latchman, Y., Wood, C. R., Chernova, T., Chaudhary, D., Borde, M., Chernova, I., Iwai, Y., Long, A. J., Brown, J. A., Nunes, R., Greenfield, E. A., Bourque, K., Boussiotis, V. A., Carter, L. L., Carreno, B. M., Malenkovich,

N., Nishimura, H., Okazaki, T., Honjo, T., … Freeman, G. J. (2001). PD-L2 is a second ligand for PD-1 and inhibits T cell activation. *Nature Immunology*, *2*(3), 261–268. https://doi.org/10.1038/85330

Laurenti, E., Frelin, C., Xie, S., Ferrari, R., Dunant, C. F., Zandi, S., Neumann, A., Plumb, I., Doulatov, S., Chen, J., April, C., Fan, J. B., Iscove, N., & Dick, J. E. (2015). CDK6 levels regulate quiescence exit in human hematopoietic stem cells. *Cell Stem Cell*, *16*(3), 302–313. https://doi.org/10.1016/j.stem.2015.01.017

Laurenti, E., & Göttgens, B. (2018). From haematopoietic stem cells to complex differentiation landscapes. *Nature 2018 553:7689*, *553*(7689), 418–426. https://doi.org/10.1038/nature25022

Lee, J. Y., Han, A.-R., & Lee, D. R. (2019). T Lymphocyte Development and Activation in Humanized Mouse Model. *Development & Reproduction*, *23*(2), 79. https://doi.org/10.12717/DR.2019.23.2.079

Lee-Thedieck, C., Rauch, N., Fiammengo, R., Klein, G., & Spatz, J. P. (2012). Impact of substrate elasticity on human hematopoietic stem and progenitor cell adhesion and motility. *Journal of Cell Science*, *125*(16), 3765–3775. https://doi.org/10.1242/JCS.095596/258417/AM/IMPACT-OF-SUBSTRATE-ELASTICITY-ON-HUMAN

Lehnertz, B., Chagraoui, J., MacRae, T., Tomellini, E., Corneau, S., Mayotte, N., Boivin, I., Durand, A., Gracias, D., & Sauvageau, G. (2021). HLF expression defines the human hematopoietic stem cell state. *Blood*, *138*(25), 2642–2654. https://doi.org/10.1182/BLOOD.2021010745

Li, J. M., Kim, S., Zhang, Y., Bian, F., Hu, J., Lu, R., Pflugfelder, S. C., Chen, R., & Li, D. Q. (2021). Single-Cell Transcriptomics Identifies a Unique Entity and Signature Markers of Transit-Amplifying Cells in Human Corneal Limbus. *Investigative Ophthalmology & Visual Science*, *62*(9), 36. https://doi.org/10.1167/IOVS.62.9.36

Li, J., Williams, M. J., Park, H. J., Bastos, H. P., Wang, X., Prins, D., Wilson, N. K., Johnson, C., Sham, K., Wantoch, M., Watcham, S., Kinston, S. J., Pask, D. C., Hamilton, T. L., Sneade, R., Waller, A. K., Ghevaert, C., Vassiliou, G. S., Laurenti, E., … Green, A. R. (2022). STAT1 is essential for HSC function and maintains MHCIIhi stem cells that resist myeloablation and neoplastic expansion. *Blood*, *140*(14), 1592–1606. https://doi.org/10.1182/BLOOD.2021014009

Li, Q., Huo, A., Li, M., Wang, J., Yin, Q., Chen, L., Chu, X., Qin, Y., Qi, Y., Li, Y., Cui, H., & Cong, Q. (2024). Structure, ligands, and roles of GPR126/ADGRG6 in the development and diseases. *Genes & Diseases*, *11*(1), 294–305. https://doi.org/10.1016/J.GENDIS.2023.02.016

Lin, X., Kang, K., Chen, P., Zeng, Z., Li, G., Xiong, W., Yi, M., & Xiang, B. (2024). Regulatory mechanisms of PD-1/PD-L1 in cancers. *Molecular Cancer 2024 23:1*, *23*(1), 1–50. https://doi.org/10.1186/S12943-024-02023-W

Link, H., Arseniev, L., Bähre, O., Kadar, J. G., Diedrich, H., & Poliwoda, H. (1996). Transplantation of allogeneic CD34+ blood cells. *Blood*, *87*(11), 4903–4909. https://doi.org/10.1182/BLOOD.V87.11.4903.BLOODJOURNAL87114903

Linton, P. J., & Dorshkind, K. (2004). Age-related changes in lymphocyte development and function. *Nature Immunology 2004 5:2*, *5*(2), 133–139. https://doi.org/10.1038/ni1033

Lipka, D. B., Wang, Q., Cabezas-Wallscheid, N., Klimmeck, D., Weichenhan, D., Herrmann, C., Lier, A., Brocks, D., Von Paleske, L., Renders, S., Wünsche, P., Zeisberger, P., Gu, L., Haas, S., Essers, M. A., Brors, B., Eils, R., Trumpp, A., Milsom, M. D., & Plass, C. (2014). Identification of dna methylation changes at cis-regulatory elements during early steps of hsc differentiation using tagmentation-based whole genome bisulfite sequencing. *Cell Cycle*, *13*(22), 3476–3487. https://doi.org/10.4161/15384101.2014.973334

Liu, F., Sun, X., Deng, S., Wu, Y., Liu, X., Wu, C., Huang, K., Li, Y., Dong, Z., Xiao, W., Li, M., Chen, Z., Ju, Z., Xiao, J., Du, J., & Zeng, H. (2024). Cxcl10 and Cxcr3 regulate self-renewal and differentiation of hematopoietic stem cells. *Stem Cell Research & Therapy*, *15*(1). https://doi.org/10.1186/S13287-024-03861-7

Liu, Y., Gao, Y., Hao, H., & Hou, T. (2020). CD279 mediates the homeostasis and survival of regulatory T cells by enhancing T cell and macrophage interactions. *FEBS Open Bio*, *10*(6), 1162. https://doi.org/10.1002/2211-5463.12865

LO Jacobson, E. S. E. M. J. E. (1951). Recovery from radiation injury. *Science*, *113*, 510–511.

Love, M. I., Huber, W., & Anders, S. (2014). Moderated estimation of fold change and dispersion for RNA-seq data with DESeq2. *Genome Biology*, *15*(12), 1–21. https://doi.org/10.1186/S13059-014-0550-8/FIGURES/9

Lu, B., Fernandino, A. F., & Flavell, R. A. (2004). Gadd45beta is important for perpetuating cognate and inflammatory signals in T cells. *Nature Immunology*, *5*(1), 38–44. https://doi.org/10.1038/NI1020

Lu, R. (2014). Sleeping Beauty Wakes Up the Clonal Succession Model for Homeostatic Hematopoiesis. *Cell Stem Cell*, *15*(6), 677–678. https://doi.org/10.1016/j.stem.2014.11.015

Luckett, W. P. (1978). Origin and differentiation of the yolk sac and extraembryonic mesoderm in presomite human and rhesus monkey embryos. *American Journal of Anatomy*, *152*(1), 59–97. https://doi.org/10.1002/AJA.1001520106

Ma, O., Hong, S. H., Guo, H., Ghiaur, G., & Friedman, A. D. (2014). Granulopoiesis requires increased C/EBPα compared to monopoiesis, correlated with elevated Cebpa in immature G-CSF receptor versus M-CSF receptor expressing cells. *PloS One*, *9*(4). https://doi.org/10.1371/JOURNAL.PONE.0095784

Maiga, A., Lemieux, S., Pabst, C., Lavallée, V. P., Bouvier, M., Sauvageau, G., & Hébert, J. (2016). Transcriptome analysis of G protein-coupled receptors in distinct genetic subgroups of acute myeloid leukemia: identification of potential disease-specific targets. *Blood Cancer Journal 2016 6:6*, *6*(6), e431–e431. https://doi.org/10.1038/bcj.2016.36

Mair, F., Erickson, J. R., Voillet, V., Simoni, Y., Bi, T., Tyznik, A. J., Martin, J., Gottardo, R., Newell, E. W., & Prlic, M. (2020). A Targeted Multi-omic Analysis Approach Measures Protein Expression and Low-Abundance Transcripts on the Single-Cell Level. *Cell Reports*, *31*(1), 107499. https://doi.org/10.1016/J.CELREP.2020.03.063

Malard, F., Holler, E., Sandmaier, B. M., Huang, H., & Mohty, M. (2023). Acute graft-versus-host disease. *Nature Reviews Disease Primers*, *9*(1), 27. https://doi.org/10.1038/s41572-023-00438-1

Mangelinck, A., Dubuisson, A., Becht, E., Dromaint-Catesson, S., Fasquel, M., Provost, N., Walas, D., Darville, H., Galizzi, J. P., Lefebvre, C., Blanc, V., & Lombardi, V. (2023). Characterization of CD4+ and CD8+ T cells responses in the mixed lymphocyte reaction by flow cytometry and single cell RNA sequencing. *Frontiers in Immunology*, *14*, 1320481. https://doi.org/10.3389/FIMMU.2023.1320481/BIBTEX

Manning, J. M., Manning, L. R., Dumoulin, A., Padovan, J. C., & Chait, B. (2020). Embryonic and Fetal Human Hemoglobins: Structures, Oxygen Binding, and Physiological Roles. *Sub-Cellular Biochemistry*, *94*, 275–296. https://doi.org/10.1007/978-3-030-41769-7_11

Mansell, E., Lin, D. S., Loughran, S. J., Milsom, M. D., & Trowbridge, J. J. (2023). New insight into the causes, consequences, and correction of hematopoietic stem cell aging. *Experimental Hematology*, *125–126*, 1–5. https://doi.org/10.1016/J.EXPHEM.2023.07.002

Manz, M. G., Miyamoto, T., Akashi, K., & Weissman, I. L. (2002). Prospective isolation of human clonogenic common myeloid progenitors. *Proceedings of the National Academy of Sciences of the United States of America*, *99*(18), 11872–11877. https://doi.org/10.1073/PNAS.172384399

Matsuoka, Y., Sumide, K., Kawamura, H., Nakatsuka, R., Fujioka, T., Sasaki, Y., & Sonoda, Y. (2015). Human cord blood-derived primitive CD34-negative hematopoietic stem cells (HSCs) are myeloid-biased long-term repopulating HSCs. *Blood Cancer Journal 2015 5:3*, *5*(3), e290–e290. https://doi.org/10.1038/bcj.2015.22

Maximow, A. (1909). Der Lymphozyt als gemeinsame Stammzelle der ver- schiedenen Blutelemente in der embryonalen Entwicklung und im postfetalen Leben der Säugetiere. *Folia Haematol. (Frankf.)*, *8*, 125–134.

McGrath, K. E., Frame, J. M., Fegan, K. H., Bowen, J. R., Conway, S. J., Catherman, S. C., Kingsley, P. D., Koniski, A. D., & Palis, J. (2015). Distinct Sources of Hematopoietic Progenitors Emerge before HSCs and Provide Functional Blood Cells in the Mammalian Embryo. *Cell Reports*, *11*(12), 1892–1904. https://doi.org/10.1016/J.CELREP.2015.05.036

Medvinsky, A., & Dzierzak, E. (1996). Definitive hematopoiesis is autonomously initiated by the AGM region. *Cell*, *86*(6), 897–906. https://doi.org/10.1016/S0092-8674(00)80165-8

Medvinsky, A., Rybtsov, S., & Taoudi, S. (2011). Embryonic origin of the adult hematopoietic system: advances and questions. *Development*, *138*(6), 1017–1031. https://doi.org/10.1242/DEV.040998

Metcalf, D., Begley, C. G., & Johnson, G. R. (1986). Hemopoietic effects of purified bacterially synthesized multi-CSF in normal and marrow-transplanted mice. *Immunobiology*, *172*(3–5), 158–167. https://doi.org/10.1016/S0171-2985(86)80095-X

Miller, J. P., & Allman, D. (2003). The Decline in B Lymphopoiesis in Aged Mice Reflects Loss of Very Early B-Lineage Precursors. *The Journal of Immunology*, *171*(5), 2326–2330. https://doi.org/10.4049/JIMMUNOL.171.5.2326

Mitchell, E., Spencer Chapman, M., Williams, N., Dawson, K. J., Mende, N., Calderbank, E. F., Jung, H., Mitchell, T., Coorens, T. H. H., Spencer, D. H., Machado, H., Lee-Six, H., Davies, M., Hayler, D., Fabre, M. A., Mahbubani, K., Abascal, F., Cagan, A., Vassiliou, G. S., … Campbell, P. J. (2022). Clonal dynamics of haematopoiesis across the human lifespan. *Nature 2022 606:7913*, *606*(7913), 343–350. https://doi.org/10.1038/s41586-022-04786-y

Moore, M. A. S., & Metcalf, D. (1970). Ontogeny of the Haemopoietic System: Yolk Sac Origin of In Vivo and In Vitro Colony Forming Cells in the Developing Mouse Embryo. *British Journal of Haematology*, *18*(3), 279–296. https://doi.org/10.1111/J.1365-2141.1970.TB01443.X

Moriguchi, T., & Yamamoto, M. (2014). A regulatory network governing Gata1 and Gata2 gene transcription orchestrates erythroid lineage differentiation. *International Journal of Hematology*, *100*(5), 417–424. https://doi.org/10.1007/S12185-014-1568-0

Morrison, S. J., Wandycz, A. M., Akashi, K., Globerson, A., & Weissman, I. L. (1996). The aging of hematopoietic stem cells. *Nature Medicine 1996 2:9*, *2*(9), 1011–1016. https://doi.org/10.1038/nm0996-1011

Morrison, S. J., Wandycz, A. M., Hemmati, H. D., Wright, D. E., & Weissman, I. L. (1997). Identification of a lineage of multipotent hematopoietic progenitors. *Development*, *124*.

Mossadegh-Keller, N., Sarrazin, S., Kandalla, P. K., Espinosa, L., Richard Stanley, E., Nutt, S. L., Moore, J., & Sieweke, M. H. (2013). M-CSF instructs myeloid lineage fate in single haematopoietic stem cells. *Nature*, *497*(7448), 239–243. https://doi.org/10.1038/NATURE12026

Müller, A. M., Medvinsky, A., Strouboulis, J., Grosveld, F., & Dzierzak, E. (1994). Development of hematopoietic stem cell activity in the mouse embryo. *Immunity*, *1*, 291–301.

Murray, L., Chen, B., Galy, A., Chen, S., Tushinski, R., Uchida, N., Negrin, R., Tricot, G., Jagannath, S., & Vesole, D. (1995). Enrichment of Human Hematopoietic Stem Cell Activity in the CD34+Thy-1+Lin- Subpopulation From Mobilized Peripheral Blood. *Blood*, *85*(2), 368–378. https://doi.org/10.1182/BLOOD.V85.2.368.368

Musa, G., Cazorla-Vázquez, S., van Amerongen, M. J., Stemmler, M. P., Eckstein, M., Hartmann, A., Braun, T., Brabletz, T., & Engel, F. B. (2019). Gpr126 (Adgrg6) is expressed in cell types known to be exposed to mechanical stimuli. *Annals of the New York Academy of Sciences*, *1456*(1), 96–108. https://doi.org/10.1111/NYAS.14135

Nagai, Y., Garrett, K. P., Ohta, S., Bahrun, U., Kouro, T., Akira, S., Takatsu, K., & Kincade, P. W. (2006). Toll-like receptors on hematopoietic progenitor cells stimulate innate immune system replenishment. *Immunity*, *24*(6), 801–812. https://doi.org/10.1016/J.IMMUNI.2006.04.008

Nakajima-Takagi, Y., Osawa, M., & Iwama, A. (2014). Manipulation of hematopoietic stem cells for regenerative medicine. *Anatomical Record*, *297*(1), 111–120. https://doi.org/10.1002/ar.22804

Nestorowa, S., Hamey, F. K., Pijuan Sala, B., Diamanti, E., Shepherd, M., Laurenti, E., Wilson, N. K., Kent, D. G., & Göttgens, B. (2016). A single-cell resolution map of mouse hematopoietic stem and progenitor cell differentiation. *Blood*, *128*(8), e20–e31. https://doi.org/10.1182/BLOOD-2016-05-716480

Neumann, E. (1868). Über die Bedeutung des Knochenmarks für die Blutbildung. *Zentralblatt Für Die Medizinischen Wissenschaften*, *44*, 122.

Nguyen, U., Squaglia, N., Boge, A., & Fung, P. A. (2011). The Simple Western™: a gel-free, blot-free, hands-free Western blotting reinvention. *Nature Methods 2011 8:11*, *8*(11), v–vi. https://doi.org/10.1038/nmeth.f.353

Nicolini, F. E., Cashman, J. D., Hogge, D. E., Humphries, R. K., & Eaves, C. J. (2003). NOD/SCID mice engineered to express human IL-3, GM-CSF and Steel factor constitutively mobilize engrafted human progenitors and compromise human stem cell regeneration. *Leukemia 2004 18:2*, *18*(2), 341–347. https://doi.org/10.1038/sj.leu.2403222

Notta, F. (2016). Distinct routes of lineage development reshape the human blood hierarchy across ontogeny. *Science*, *351*, aab2116.

Notta, F., Doulatov, S., Laurenti, E., Poeppl, A., Jurisica, I., & Dick, J. E. (2011). Isolation of single human hematopoietic stem cells capable of long-term multilineage engraftment. *Science*, *333*(6039), 218–221. https://doi.org/10.1126/SCIENCE.1201219

Notta, F., Zandi, S., Takayama, N., Dobson, S., Gan, O. I., Wilson, G., Kaufmann, K. B., McLeod, J., Laurenti, E., Dunant, C. F., McPherson, J. D., Stein, L. D., Dror, Y., & Dick, J. E. (2016). Distinct routes of lineage development reshape the human blood hierarchy across ontogeny. *Science*, *351*(6269). https://doi.org/10.1126/SCIENCE.AAB2116

Obenaus, M., Leitão, C., Leisegang, M., Chen, X., Gavvovidis, I., Van Der Bruggen, P., Uckert, W., Schendel, D. J., & Blankenstein, T. (2015). Identification of human T-cell receptors with optimal affinity to cancer antigens using antigen-negative humanized mice. *Nature Biotechnology*, *33*(4), 402–407. https://doi.org/10.1038/NBT.3147

O'Connell, R. M., Rao, D. S., Chaudhuri, A. A., Boldin, M. P., Taganov, K. D., Nicoll, J., Paquette, R. L., & Baltimore, D. (2008). Sustained expression of microRNA-155 in hematopoietic stem cells causes a myeloproliferative disorder. *The Journal of Experimental Medicine*, *205*(3), 585. https://doi.org/10.1084/JEM.20072108

Oetjen, K. A., Lindblad, K. E., Goswami, M., Gui, G., Dagur, P. K., Lai, C., Dillon, L. W., McCoy, J. P., & Hourigan, C. S. (2018). Human bone marrow assessment by single-cell RNA sequencing, mass cytometry, and flow cytometry. *JCI Insight*, *3*(23). https://doi.org/10.1172/JCI.INSIGHT.124928

O'Flaherty, E., Wong, W. K., Pettit, S. J., Seymour, K., Ali, S., & Kirby, J. A. (2000). Regulation of T-cell apoptosis: a mixed lymphocyte reaction model. *Immunology*, *100*(3), 289. https://doi.org/10.1046/J.1365-2567.2000.00048.X

Olson, O. C., Kang, Y. A., & Passegué, E. (2020a). Normal Hematopoiesis Is a Balancing Act of Self-Renewal and Regeneration. *Cold Spring Harbor Perspectives in Medicine*, *10*(12), 1–23. https://doi.org/10.1101/CSHPERSPECT.A035519

Orteu, C. H., Poulter, L. W., Rustin, M. H. A., Sabin, C. A., Salmon, M., & Akbar, A. N. (1998). The Role of Apoptosis in the Resolution of T Cell-Mediated Cutaneous Inflammation. *The Journal of Immunology*, *161*(4), 1619–1629. https://doi.org/10.4049/JIMMUNOL.161.4.1619

Osawa, M., Hanada, K., Hamada, H., & Nakauchi, H. (1996). Long-term lymphohematopoietic reconstitution by a single CD34-low/negative hematopoietic stem cell. *Science*, *273*, 242–245.

Pabst, C., Bergeron, A., Lavallée, V. P., Yeh, J., Gendron, P., Norddahl, G. L., Krosl, J., Boivin, I., Deneault, E., Simard, J., Imren, S., Boucher, G., Eppert, K., Herold, T., Bohlander, S. K., Humphries, K., Lemieux, S., Hébert, J., Sauvageau, G., & Barabé, F. (2016). GPR56 identifies primary human acute myeloid leukemia cells with high repopulating potential in vivo. *Blood*, *127*(16), 2018–2027. https://doi.org/10.1182/BLOOD-2015-11-683649

Palis, J. (2014). Primitive and definitive erythropoiesis in mammals. *Front Physiol*, *5*, 3.

Pang, W. W., Price, E. A., Sahoo, D., Beerman, I., Maloney, W. J., Rossi, D. J., Schrier, S. L., & Weissman, I. L. (2011). Human bone marrow hematopoietic stem cells are increased in frequency and myeloid-biased with age. *Proceedings of the National Academy of Sciences of the United States of America*, *108*(50), 20012–20017. https://doi.org/10.1073/PNAS.1116110108/-/DCSUPPLEMENTAL

Pardali, E., Dimmeler, S., Zeiher, A. M., & Rieger, M. A. (2020). Clonal hematopoiesis, aging, and cardiovascular diseases. *Experimental Hematology*, *83*, 95–104. https://doi.org/10.1016/J.EXPHEM.2019.12.006

Passegué, E. (2008). The JunB Transcriptional Network: from Hematopoietic Stem Cells to Myeloid Function. *Blood*, *112*(11), sci-32. https://doi.org/10.1182/BLOOD.V112.11.SCI-32.SCI-32

Pastore, F., & Levine, R. L. (2016). Epigenetic regulators and their impact on therapy in acute myeloid leukemia. *Haematologica*, *101*(3), 269–278. https://doi.org/10.3324/HAEMATOL.2015.140822

Paul, F. (2015). Transcriptional heterogeneity and lineage commitment in myeloid progenitors. *Cell*, *163*, 1663–1677.

Perié, L., Duffy, K. R., Kok, L., de Boer, R. J., & Schumacher, T. N. (2015). The branching point in erythro-myeloid differentiation. *Cell*, *163*. https://doi.org/10.1016/j.cell.2015.11.059

Pietras, E. (2015). Functionally distinct subsets of lineage-biased multipotent progenitors control blood production in normal and regenerative conditions. *Cell Stem Cell*, *17*, 35–46.

Pietras, E. M. (2017). Inflammation: a key regulator of hematopoietic stem cell fate in health and disease. *Blood*, *130*(15), 1693–1698. https://doi.org/10.1182/BLOOD-2017-06-780882

Pietras, E. M., Lakshminarasimhan, R., Techner, J. M., Fong, S., Flach, J., Binnewies, M., & Passegué, E. (2014). Re-entry into quiescence protects hematopoietic stem cells from the killing effect of chronic exposure to type I interferons. *The Journal of Experimental Medicine*, *211*(2), 245–262. https://doi.org/10.1084/JEM.20131043

Pina, C., Fugazza, C., Tipping, A. J., Brown, J., Soneji, S., Teles, J., Peterson, C., & Enver, T. (2012). Inferring rules of lineage commitment in haematopoiesis. *Nature Cell Biology*, *14*(3), 287–294. https://doi.org/10.1038/NCB2442

Pines, J., & Hunter, T. (1991). Human cyclins A and B1 are differentially located in the cell and undergo cell cycle-dependent nuclear transport. *Journal of Cell Biology*, *115*(1), 1–17. https://doi.org/10.1083/JCB.115.1.1

Pinho, S., & Frenette, P. S. (2019). Haematopoietic stem cell activity and interactions with the niche. *Nature Reviews. Molecular Cell Biology*, *20*(5), 303–320. https://doi.org/10.1038/S41580-019-0103-9

Potocnik, A. J., Brakebusch, C., & Fässler, R. (2000). Fetal and adult hematopoietic stem cells require β1 integrin function for colonizing fetal liver, spleen, and bone marrow. *Immunity*, *12*(6), 653–663. https://doi.org/10.1016/S1074-7613(00)80216-2

Qian, P., He, X. C., Paulson, A., Kono, T., Ferguson-Smith, A. C., & Li, L. (2016). The Dlk1-Gtl2 Locus Preserves LT-HSC Function by Inhibiting the PI3K-mTOR Pathway to Restrict Mitochondrial Metabolism. *Stem Cell*, *18*, 214–228. https://doi.org/10.1016/j.stem.2015.11.001

R Majeti, C. P. I. W. (2007). Identification of a hierarchy of multipotent hematopoietic progenitors in human cord blood. *Cell Stem Cell*, *1*, 635–645.

Radtke, S., Haworth, K. G., Kiem, H.-P., Kevin Haworth, fredhutchorg G., & Hans-Peter Kiem, fredhutchorg. (2016). The frequency of multipotent CD133+CD45RA−CD34+ hematopoietic stem cells is not increased in fetal liver compared to adult stem cell sources. *Experimental Hematology*, *44*(6), 502. https://doi.org/10.1016/J.EXPHEM.2016.02.011

Raj, A., & van Oudenaarden, A. (2008). Nature, nurture, or chance: stochastic gene expression and its consequences. *Cell*, *135*(2), 216–226. https://doi.org/10.1016/J.CELL.2008.09.050

Ranzoni, A. M., Tangherloni, A., Berest, I., Riva, S. G., Myers, B., Strzelecka, P. M., Xu, J., Panada, E., Mohorianu, I., Zaugg, J. B., & Cvejic, A. (2021). Integrative single-cell RNA-seq and ATAC-seq analysis of human developmental hematopoiesis. *Cell Stem Cell*, *28*(3), 472–487. https://doi.org/10.1016/j.stem.2020.11.015

Rao, T. N., Marks-Bluth, J., Sullivan, J., Gupta, M. K., Chandrakanthan, V., Fitch, S. R., Ottersbach, K., Jang, Y. C., Piao, X., Kulkarni, R. N., Serwold, T., Pimanda, J. E., & Wagers, A. J. (2015). High-level Gpr56 expression is dispensable for the maintenance and function of hematopoietic stem and progenitor cells in mice. *Stem Cell Research*, *14*(3), 307. https://doi.org/10.1016/J.SCR.2015.02.001

Regan-Komito, D., Swann, J. W., Demetriou, P., Cohen, E. S., Horwood, N. J., Sansom, S. N., & Griseri, T. (2020). GM-CSF drives dysregulated hematopoietic stem cell activity and pathogenic extramedullary myelopoiesis in experimental spondyloarthritis. *Nature Communications 2020 11:1*, *11*(1), 1–15. https://doi.org/10.1038/s41467-019-13853-4

Rieger, M. A., Hoppe, P. S., Smejkal, B. M., Eitelhuber, A. C., & Schroeder, T. (2009). Hematopoietic cytokines can instruct lineage choice. *Science*, *325*(5937), 217–218. https://doi.org/10.1126/SCIENCE.1171461

Rieger, M. A., & Schroeder, T. (2012a). Hematopoiesis. *Cold Spring Harbor Perspectives in Biology*, *4*(12). https://doi.org/10.1101/cshperspect.a008250

Ringnér, M. (2008). What is principal component analysis? *Nature Biotechnology*, *26*(3), 303–304. https://doi.org/10.1038/NBT0308-303

Robin C. (1875). Dictionnaire encyclopédique des sciences médicales. Title. *In DeChambre A (Ed.)*, *Vol. 2*, 1–33.

Rodrigues, C. P., Collins, J. M., Yang, S., Martinez, C., Kim, J. W., Lama, C., Nam, A. S., Alt, C., Lin, C., & Zon, L. I. (2024). Transcripts of repetitive DNA elements signal to block phagocytosis of hematopoietic stem cells. *Science*, *385*(6714). https://doi.org/10.1126/SCIENCE.ADN1629

Rongvaux, A., Takizawa, H., Strowig, T., Willinger, T., Eynon, E. E., Flavell, R. A., & Manz, M. G. (2013). Human hemato-lymphoid system mice: current use and future potential for medicine. *Annual Review of Immunology*, *31*, 635–674. https://doi.org/10.1146/ANNUREV-IMMUNOL-032712-095921

Rongvaux, A., Willinger, T., Martinek, J., Strowig, T., Gearty, S. V., Teichmann, L. L., Saito, Y., Marches, F., Halene, S., Palucka, A. K., Manz, M. G., & Flavell, R. A. (2014). Development and function of human innate immune cells in a humanized mouse model. *Nature Biotechnology 2014 32:4*, *32*(4), 364–372. https://doi.org/10.1038/nbt.2858

Rossi, D. J., Bryder, D., Zahn, J. M., Ahlenius, H., Sonu, R., Wagers, A. J., & Weissman, I. L. (2005). Cell intrinsic alterations underlie hematopoietic stem cell aging. *Proceedings of the National Academy of Sciences of the United States of America*, *102*(26), 9194–9199. https://doi.org/10.1073/PNAS.0503280102/SUPPL_FILE/03280TABLE5.XLS

Rossi, D. J., Seita, J., Czechowicz, A., Bhattacharya, D., Bryder, D., & Weissman, I. L. (2007). Hematopoietic Stem Cell Quiescence Attenuates DNA Damage Response and Permits DNA Damage Accumulation During Aging. *Cell Cycle*, *6*(19), 2371–2376. https://doi.org/10.4161/cc.6.19.4759

Rumfelt, L. L., Zhou, Y., Rowley, B. M., Shinton, S. A., & Hardy, R. R. (2006). Lineage specification and plasticity in CD19- early B cell precursors. *The Journal of Experimental Medicine*, *203*(3), 675–687. https://doi.org/10.1084/JEM.20052444

Salvador, J. M., Mittelstadt, P. R., Belova, G. I., Fornace, A. J., & Ashwell, J. D. (2005). The autoimmune suppressor Gadd45alpha inhibits the T cell alternative p38 activation pathway. *Nature Immunology*, *6*(4), 396–402. https://doi.org/10.1038/NI1176

Sanjuan-Pla, A., Macaulay, I. C., Jensen, C. T., Woll, P. S., Luis, T. C., Mead, A., Moore, S., Carella, C., Matsuoka, S., Jones, T. B., Chowdhury, O., Stenson, L., Lutteropp, M., Green, J. C. A., Facchini, R., Boukarabila, H., Grover, A., Gambardella, A., Thongjuea, S., … Jacobsen, S. E. W. (2013). Platelet-biased stem cells reside at the apex of the haematopoietic stem-cell hierarchy. *Nature*, *502*(7470), 232–236. https://doi.org/10.1038/NATURE12495

Santagostino, S. F., Arbona, R. J. R., Nashat, M. A., White, J. R., & Monette, S. (2017). Pathology of Aging in NOD scid gamma Female Mice. *Veterinary Pathology*, *54*(5), 855–869. https://doi.org/10.1177/0300985817698210

Scheuermann, R. H., & Racila, E. (1995). CD19 antigen in leukemia and lymphoma diagnosis and immunotherapy. *Leukemia & Lymphoma*, *18*(5–6), 385–397. https://doi.org/10.3109/10428199509059636

Schmachtel, T., Bonig, H., & Rieger, M. A. (2025). FACS-Based Assessment of Human Hematopoietic Stem and Progenitor Cells. *International Journal of Molecular Sciences*, *26*(17), 8381. https://doi.org/10.3390/IJMS26178381

Schuettpelz, L. G., & Link, D. C. (2013). Regulation of hematopoietic stem cell activity by inflammation. *Frontiers in Immunology*, *4*(JUL), 55771. https://doi.org/10.3389/FIMMU.2013.00204/BIBTEX

Seita, J., & Weissman, I. L. (2010b). Hematopoietic stem cell: Self-renewal versus differentiation. *Wiley Interdisciplinary Reviews: Systems Biology and Medicine*, *2*(6), 640–653. https://doi.org/10.1002/WSBM.86

Sezaki, M., Hayashi, Y., Wang, Y., Johansson, A., Umemoto, T., & Takizawa, H. (2020). Immuno-Modulation of Hematopoietic Stem and Progenitor Cells in Inflammation. *Frontiers in Immunology*, *11*, 585367. https://doi.org/10.3389/FIMMU.2020.585367/PDF

Shultz, L. D., Lyons, B. L., Burzenski, L. M., Gott, B., Chen, X., Chaleff, S., Kotb, M., Gillies, S. D., King, M., Mangada, J., Greiner, D. L., & Handgretinger, R. (2005). Human Lymphoid and Myeloid Cell Development in NOD/LtSz-scid IL2Rγnull Mice Engrafted with Mobilized Human Hemopoietic Stem Cells. *The Journal of Immunology*, *174*(10), 6477–6489. https://doi.org/10.4049/JIMMUNOL.174.10.6477

Sioud, M., Fløisand, Y., Forfang, L., & Lund-Johansen, F. (2006). Signaling through toll-like receptor 7/8 induces the differentiation of human bone marrow CD34+ progenitor cells along the myeloid lineage. *Journal of Molecular Biology*, *364*(5), 945–954. https://doi.org/10.1016/J.JMB.2006.09.054

Six, E., Guilloux, A., Denis, A., Lecoules, A., Magnani, A., Vilette, R., Male, F., Cagnard, N., Delville, M., Magrin, E., Caccavelli, L., Roudaut, C., Plantier, C., Sobrino, S., Gregg, J., Nobles, C. L., Everett, J. K., Hacein-Bey-Abina, S., Galy, A., … Bushman, F. D. (2020). Clonal tracking in gene therapy patients reveals a diversity of human hematopoietic differentiation programs. *Blood*, *135*(15), 1219–1231. https://doi.org/10.1182/blood.2019002350

Song, Y., Rongvaux, A., Taylor, A., Jiang, T., Tebaldi, T., Balasubramanian, K., Bagale, A., Terzi, Y. K., Gbyli, R., Wang, X., Fu, X., Gao, Y., Zhao, J., Podoltsev, N., Xu, M., Neparidze, N., Wong, E., Torres, R., Bruscia, E. M., … Halene, S. (2019). A highly efficient and faithful MDS patient-derived xenotransplantation model for pre-clinical studies. *Nature Communications 2019 10:1*, *10*(1), 1–14. https://doi.org/10.1038/s41467-018-08166-x

Steensma, D. P., Bejar, R., Jaiswal, S., Lindsley, R. C., Sekeres, M. A., Hasserjian, R. P., & Ebert, B. L. (2015). Clonal hematopoiesis of indeterminate potential and its distinction from myelodysplastic syndromes. *Blood*, *126*(1), 9–16. https://doi.org/10.1182/BLOOD-2015-03-631747

Steiner, R., & Vogel, H. (1973). On the kinetics of erythroid cell differentiation in fetal mice. I. Microspectrophotometric determination of the hemoglobin content in erythroid cells during gestation. *Journal of Cellular Physiology*, *81*(3), 323–337. https://doi.org/10.1002/JCP.1040810305

Stuart, T., Butler, A., Hoffman, P., Hafemeister, C., Papalexi, E., Mauck, W. M., Hao, Y., Stoeckius, M., Smibert, P., & Satija, R. (2019). Comprehensive Integration of Single-Cell Data. *Cell*, *177*(7), 1888-1902.e21. https://doi.org/10.1016/J.CELL.2019.05.031/ATTACHMENT/2F8B9EBE-54E6-43EB-9EF2-949B6BDA8BA2/MMC3.PDF

Su, T. Y., Hauenstein, J., Somuncular, E., Dumral, Ö., Leonard, E., Gustafsson, C., Tzortzis, E., Forlani, A., Johansson, A. S., Qian, H., Månsson, R., & Luc, S. (2024). Aging is associated with functional and molecular changes in distinct hematopoietic stem cell subsets. *Nature Communications 2024 15:1*, *15*(1), 1–16. https://doi.org/10.1038/s41467-024-52318-1

Sudo, K., Ema, H., Morita, Y., & Nakauchi, H. (2000). Age-Associated Characteristics of Murine Hematopoietic Stem Cells. *Journal of Experimental Medicine*, *192*(9), 1273–1280. https://doi.org/10.1084/JEM.192.9.1273

Sugimura, R., He, X. C., Venkatraman, A., Arai, F., Box, A., Semerad, C., Haug, J. S., Peng, L., Zhong, X. B., Suda, T., & Li, L. (2012). Noncanonical Wnt signaling maintains hematopoietic stem cells in the niche. *Cell*, *150*, 351–365.

Sun, J., Ramos, A., Chapman, B., Johnnidis, J. B., Le, L., Ho, Y. J., Klein, A., Hofmann, O., & Camargo, F. D. (2014). Clonal dynamics of native haematopoiesis. *Nature*, *514*(7522), 322–327. https://doi.org/10.1038/NATURE13824

Takizawa, H., Boettcher, S., & Manz, M. G. (2012). Demand-adapted regulation of early hematopoiesis in infection and inflammation. *Blood*, *119*(13), 2991–3002. https://doi.org/10.1182/BLOOD-2011-12-380113

Tang, W., He, J., Huang, T., Bai, Z., Wang, C., Wang, H., Yang, R., Ni, Y., Hou, J., Wang, J., Zhou, J., Yao, Y., Gong, Y., Hou, S., Liu, B., & Lan, Y. (2021). Hlf Expression Marks Early Emergence of Hematopoietic Stem Cell Precursors With Adult Repopulating Potential and Fate. *Frontiers in Cell and Developmental Biology*, *9*, 728057. https://doi.org/10.3389/FCELL.2021.728057/FULL

Tavian, M., Hallais, M. F., & Péault, B. (1999). Emergence of intraembryonic hematopoietic precursors in the pre-liver human embryo. *Development*, *126*(4), 793–803. https://doi.org/10.1242/DEV.126.4.793

Tober, J., Koniski, A., McGrath, K. E., Vemishetti, R., Emerson, R., Mesy-Bentley, K. K. de, Waugh, R., & Palis, J. (2007). The megakaryocyte lineage originates from hemangioblast precursors and is an integral component both of primitive and of definitive hematopoiesis. *Blood*, *109*, 1433–1441.

Topalian, S. L., Drake, C. G., & Pardoll, D. M. (2015). Immune checkpoint blockade: a common denominator approach to cancer therapy. *Cancer Cell*, *27*(4), 450. https://doi.org/10.1016/J.CCELL.2015.03.001

Triana, S., Vonficht, D., Jopp-Saile, L., Raffel, S., Lutz, R., Leonce, D., Antes, M., Hernández-Malmierca, P., Ordoñez-Rueda, D., Ramasz, B., Boch, T., Jann, J. C., Nowak, D., Hofmann, W. K., Müller-Tidow, C., Hübschmann, D., Alexandrov, T., Benes, V., Trumpp, A., … Haas, S. (2021). Single-cell proteo-genomic reference maps of the hematopoietic system enable the purification and massive profiling of precisely defined cell states. *Nat. Immunol.*, *22*(12), 1577–1589. https://doi.org/10.1038/s41590-021-01059-0

Tusi, B. K., Wolock, S. L., Weinreb, C., Hwang, Y., Hidalgo, D., Zilionis, R., Waisman, A., Huh, J. R., Klein, A. M., & Socolovsky, M. (2018). Population snapshots predict early haematopoietic and erythroid hierarchies. *Nature*, *555*(7694), 54–60. https://doi.org/10.1038/NATURE25741

Uckelmann, H., Blaszkiewicz, S., Nicolae, C., Haas, S., Schnell, A., Wurzer, S., Wagener, R., Aszodi, A., & Essers, M. A. G. (2016). Extracellular matrix protein Matrilin-4 regulates stressinduced HSC proliferation via CXCR4. *Journal of Experimental Medicine*, *213*(10), 1961–1971. https://doi.org/10.1084/JEM.20151713

Umemoto, T., Hashimoto, M., Matsumura, T., Nakamura-Ishizu, A., & Suda, T. (2018). Ca2+-mitochondria axis drives cell division in hematopoietic stem cells. *The Journal of Experimental Medicine*, *215*(8), 2097–2113. https://doi.org/10.1084/JEM.20180421

van der Loo, J. C. M., Hanenberg, H., Cooper, R. J., Luo, F.-Y., Lazaridis, E. N., & Williams, D. A. (1998). Nonobese Diabetic/Severe Combined Immunodeficiency (NOD/SCID) Mouse as a Model System to Study the Engraftment and Mobilization of Human Peripheral Blood Stem Cells. *Blood*, *92*(7), 2556–2570. https://doi.org/10.1182/BLOOD.V92.7.2556

Van Overmeire, E., Stijlemans, B., Heymann, F., Keirsse, J., Morias, Y., Elkrim, Y., Brys, L., Abels, C., Lahmar, Q., Ergen, C., Vereecke, L., Tacke, F., De Baetselier, P., Van Ginderachter, J. A., & Laoui, D. (2016). M-CSF and GM-CSF receptor signaling differentially regulate monocyte maturation and macrophage polarization in the tumor microenvironment. *Cancer Research*, *76*(1), 35–42. https://doi.org/10.1158/0008-5472.CAN-15-0869/652040/AM/M-CSF-AND-GM-CSF-RECEPTOR-SIGNALING-DIFFERENTIALLY

Vasto, S., Candore, G., Balistreri, C. R., Caruso, M., Colonna-Romano, G., Grimaldi, M. P., Listi, F., Nuzzo, D., Lio, D., & Caruso, C. (2007). Inflammatory networks in ageing, age-related diseases and longevity. *Mechanisms of Ageing and Development*, *128*(1), 83–91. https://doi.org/10.1016/J.MAD.2006.11.015

Velten, L., Haas, S. F., Raffel, S., Blaszkiewicz, S., Islam, S., Hennig, B. P., Hirche, C., Lutz, C., Buss, E. C., Nowak, D., Boch, T., Hofmann, W. K., Ho, A. D., Huber, W., Trumpp, A., Essers, M. A. G., & Steinmetz, L. M. (2017). Human haematopoietic stem cell lineage commitment is a continuous process. *Nat. Cell Biol.*, *19*(4), 271–281. https://doi.org/10.1038/ncb3493

Verovskaya, E., Broekhuis, M. J. C., Zwart, E., Ritsema, M., van Os, R., de Haan, G., & Bystrykh, L. V. (2013). Heterogeneity of young and aged murine hematopoietic stem cells revealed by quantitative clonal analysis using cellular barcoding. *Blood*, *122*(4), 523–532. https://doi.org/10.1182/blood-2013-01-481135

Vignali, D. A. A., Collison, L. W., & Workman, C. J. (2008). How regulatory T cells work. *Nature Reviews Immunology 2008 8:7*, *8*(7), 523–532. https://doi.org/10.1038/nri2343

Villani, A. C., Satija, R., Reynolds, G., Sarkizova, S., Shekhar, K., Fletcher, J., Griesbeck, M., Butler, A., Zheng, S., Lazo, S., Jardine, L., Dixon, D., Stephenson, E., Nilsson, E., Grundberg, I., McDonald, D., Filby, A., Li, W., De Jager, P. L., … Hacohen, N. (2017). Single-cell RNA-seq reveals new types of human blood dendritic cells, monocytes and progenitors. *Science (New York, N.Y.)*, *356*(6335), eaah4573. https://doi.org/10.1126/SCIENCE.AAH4573

Vink, C. S., Mariani, S. A., & Dzierzak, E. (2022). Embryonic Origins of the Hematopoietic System: Hierarchies and Heterogeneity. *HemaSphere*, *6*(6), e737. https://doi.org/10.1097/HS9.0000000000000737

Vogel, W., Scheding, S., Kanz, L., & Brugger, W. (2000). Clinical applications of CD34(+) peripheral blood progenitor cells (PBPC). *Stem Cells (Dayton, Ohio)*, *18*(2), 87–92. https://doi.org/10.1634/STEMCELLS.18-2-87

von Mering, C., Jensen, L. J., Snel, B., Hooper, S. D., Krupp, M., Foglierini, M., Jouffre, N., Huynen, M. A., & Bork, P. (2005). STRING: known and predicted protein-protein associations, integrated and transferred across organisms. *Nucleic Acids Research*, *33*(Database issue). https://doi.org/10.1093/NAR/GKI005

Walcher, L., Hilger, N., Wege, A. K., Lange, F., Tretbar, U. S., Blaudszun, A. R., & Fricke, S. (2020). Humanized mouse model: Hematopoietic stemcell transplantation and tracking using short tandem repeat technology. *Immunity, Inflammation and Disease*, *8*(3), 363–370. https://doi.org/10.1002/IID3.317

Walkley, C. R., Olsen, G. H., Dworkin, S., Fabb, S. A., Swann, J., McArthur, G. A. A., Westmoreland, S. V., Chambon, P., Scadden, D. T., & Purton, L. E. (2007). A Microenvironment-Induced Myeloproliferative Syndrome Caused by Retinoic Acid Receptor γ Deficiency. *Cell*, *129*(6), 1097–1110. https://doi.org/10.1016/J.CELL.2007.05.014

Walsh, K., Raghavachari, N., Kerr, C., Bick, A. G., Cummings, S. R., Druley, T., Dunbar, C. E., Genovese, G., Goodell, M. A., Jaiswal, S., Maciejewski, J., Natarajan, P., Shindyapina, A. V., Shuldiner, A. R., Van Den Akker, E. B., & Vijg, J. (2022). Clonal Hematopoiesis Analyses in Clinical, Epidemiologic, and Genetic Aging Studies to Unravel Underlying Mechanisms of Age-Related Dysfunction in Humans. *Frontiers in Aging*, *3*, 841796. https://doi.org/10.3389/FRAGI.2022.841796/BIBTEX

Wang, J. C. Y., Doedens, M., & Dick, J. E. (1997). Primitive Human Hematopoietic Cells Are Enriched in Cord Blood Compared With Adult Bone Marrow or Mobilized Peripheral Blood as Measured by the Quantitative In Vivo SCID-Repopulating Cell Assay. *Blood*, *89*(11), 3919–3924. https://doi.org/10.1182/BLOOD.V89.11.3919

Warnock, R. A., Askari, S., Butcher, E. C., & Von Andrian, U. H. (1998). Molecular Mechanisms of Lymphocyte Homing to Peripheral Lymph Nodes. *Journal of Experimental Medicine*, *187*(2), 205–216. https://doi.org/10.1084/JEM.187.2.205

Watson, C. J., Papula, A. L., Poon, G. Y. P., Wong, W. H., Young, A. L., Druley, T. E., Fisher, D. S., & Blundell, J. R. (2020). The evolutionary dynamics and fitness landscape of clonal hematopoiesis. *Science*, *367*(6485), 1449–1454. https://doi.org/10.1126/science.aay9333

Weissman, I. L., & Shizuru, J. A. (2008). The origins of the identification and isolation of hematopoietic stem cells, and their capability to induce donor-specific transplantation tolerance and treat autoimmune diseases. *Blood*, *112*(9), 3543–3553. https://doi.org/10.1182/BLOOD-2008-08-078220

Weng, C., Yu, F., Yang, D., Poeschla, M., Liggett, L. A., Jones, M. G., Qiu, X., Wahlster, L., Caulier, A., Hussmann, J. A., Schnell, A., Yost, K. E., Koblan, L. W., Martin-Rufino, J. D., Min, J., Hammond, A., Ssozi, D., Bueno, R., Mallidi, H., … Sankaran, V. G. (2024). Deciphering cell states and genealogies of human haematopoiesis. *Nature 2024 627:8003*, *627*(8003), 389–398. https://doi.org/10.1038/s41586-024-07066-z

Wilkinson, D. G., Bailes, J. A., Champion, J. E., & McMahon, A. P. (1987). A molecular analysis of mouse development from 8 to 10 days post coitum detects changes only in embryonic globin expression. *Development (Cambridge, England)*, *99*(4), 493–500. https://doi.org/10.1242/DEV.99.4.493

Wilson, A. (2008). Hematopoietic stem cells reversibly switch from dormancy to self-renewal during homeostasis and repair. *Cell*, *135*, 1118–1129.

Wunderlich, M., Chou, F. S., Link, K. A., Mizukawa, B., Perry, R. L., Carroll, M., & Mulloy, J. C. (2010). AML xenograft efficiency is significantly improved in NOD/SCID-IL2RG mice constitutively expressing human SCF, GM-CSF and IL-3. *Leukemia 2010 24:10*, *24*(10), 1785–1788. https://doi.org/10.1038/leu.2010.158

Wunderlich, M., Chou, F. S., Sexton, C., Presicce, P., Chougnet, C. A., Aliberti, J., & Mulloy, J. C. (2018). Improved multilineage human hematopoietic reconstitution and function in NSGS mice. *PLoS ONE*, *13*(12), e0209034. https://doi.org/10.1371/JOURNAL.PONE.0209034

Xie, M., Lu, C., Wang, J., McLellan, M. D., Johnson, K. J., Wendl, M. C., McMichael, J. F., Schmidt, H. K., Yellapantula, V., Miller, C. A., Ozenberger, B. A., Welch, J. S., Link, D. C., Walter, M. J., Mardis, E. R., Dipersio, J. F., Chen, F., Wilson, R. K., Ley, T. J., & Ding, L. (2014). Age-related mutations associated with clonal hematopoietic expansion and malignancies. *Nature Medicine 2014 20:12*, *20*(12), 1472–1478. https://doi.org/10.1038/nm.3733

Yamashita, M., & Passegué, E. (2019). TNFα coordinates hematopoietic stem cell survival and myeloid regeneration. *Cell Stem Cell*, *25*(3), 357. https://doi.org/10.1016/J.STEM.2019.05.019

Yang, L., Bryder, D., Adolfsson, J., Nygren, J., Månsson, R., Sigvardsson, M., & Jacobsen, S. E. W. (2005). Identification of Lin–Sca1+kit+CD34+Flt3– short-term hematopoietic stem cells capable of rapidly reconstituting and rescuing myeloablated transplant recipients. *Blood*, *105*(7), 2717–2723. https://doi.org/10.1182/BLOOD-2004-06-2159

Young, K., Borikar, S., Bell, R., Kuffler, L., Philip, V., & Trowbridge, J. J. (2016). Progressive alterations in multipotent hematopoietic progenitors underlie lymphoid cell loss in aging. *The Journal of Experimental Medicine*, *213*(11), 2259–2267. https://doi.org/10.1084/JEM.20160168

Yu, V. (2016). Epigenetic memory underlies cell-autonomous heterogeneous behavior of hematopoietic stem cells. *Cell*, *167*, 1310–1322.

Zafar, A., Ng, H. P., Kim, G. D., Chan, E. R., & Mahabeleshwar, G. H. (2021). BHLHE40 promotes macrophage pro-inflammatory gene expression and functions. *FASEB Journal : Official Publication of the Federation of American Societies for Experimental Biology*, *35*(10). https://doi.org/10.1096/FJ.202100944R

Zanetti, C., & Krause, D. S. (2020). "Caught in the net": the extracellular matrix of the bone marrow in normal hematopoiesis and leukemia. *Experimental Hematology*, *89*, 13–25. https://doi.org/10.1016/J.EXPHEM.2020.07.010

Zappia, L., & Oshlack, A. (2018). Clustering trees: a visualization for evaluating clusterings at multiple resolutions. *GigaScience*, *7*(7), 1–9. https://doi.org/10.1093/GIGASCIENCE/GIY083

Zeng, A. G. X., Nagree, M. S., Jakobsen, N. A., Shah, S., Murison, A., Cheong, J.-G., Turkalj, S., Lim, I. N. X., Jin, L., Araújo, J., Aguilar-Navarro, A. G., Parris, D., McLeod, J., Kim, H., Lee, H. S., Zhang, L., Boulanger, M., Wagenblast, E., Flores-Figueroa, E., … Xie, S. Z. (2023). A hematopoietic stem cell subset that retains memory of prior inflammatory stress accumulates in aging and clonal hematopoiesis. *BioRxiv*, 2023.09.11.557271. https://doi.org/10.1101/2023.09.11.557271

Zhang, C. C., Kaba, M., Ge, G., Xie, K., Tong, W., Hug, C., & Lodish, H. F. (2006). Angiopoietin-like proteins stimulate ex vivo expansion of hematopoietic stem cells. *Nature Medicine 2006 12:2*, *12*(2), 240–245. https://doi.org/10.1038/nm1342

Zhang, X., Song, B., Carlino, M. J., Li, G., Ferchen, K., Chen, M., Thompson, E. N., Kain, B. N., Schnell, D., Thakkar, K., Kouril, M., Jin, K., Hay, S. B., Sen, S., Bernardicius, D., Ma, S., Bennett, S. N., Croteau, J., Salvatori, O., … Grimes, H. L. (2024). An immunophenotype-coupled transcriptomic atlas of human hematopoietic progenitors. *Nature Immunology 2024*, 1–13. https://doi.org/10.1038/s41590-024-01782-4

Zhao, J. L., Ma, C., O'Connell, R. M., Mehta, A., Diloreto, R., Heath, J. R., & Baltimore, D. (2014). Conversion of danger signals into cytokine signals by hematopoietic stem and progenitor cells for regulation of stress-induced hematopoiesis. *Cell Stem Cell*, *14*(4), 445–459. https://doi.org/10.1016/j.stem.2014.01.007

Zhao, M., Perry, J. M., Marshall, H., Venkatraman, A., Qian, P., He, X. C., Ahamed, J., & Li, L. (2014). Megakaryocytes maintain homeostatic quiescence and promote post-injury regeneration of hematopoietic stem cells. *Nature Medicine*, *20*(11), 1321–1326. https://doi.org/10.1038/NM.3706

Zheng, J., Umikawa, M., Zhang, S., Huynh, H., Silvany, R., Chen, B. P. C., Chen, L., & Zhang, C. C. (2011). Ex vivo expanded hematopoietic stem cells overcome the MHC barrier in allogeneic transplantation. *Cell Stem Cell*, *9*(2), 119. https://doi.org/10.1016/J.STEM.2011.06.003

Zheng, Z., He, H., Tang, X. T., Zhang, H., Gou, F., Yang, H., Cao, J., Shi, S., Yang, Z., Sun, G., Xie, X., Zeng, Y., Wen, A., Lan, Y., Zhou, J., Liu, B., Zhou, B. O., Cheng, T., & Cheng, H. (2022). Uncovering the emergence of HSCs in the human fetal bone marrow by single-cell RNA-seq analysis. *Cell Stem Cell*, *29*(11), 1562-1579.e7. https://doi.org/10.1016/j.stem.2022.10.005

Zhu, H., Traver, D., Davidson, A. J., Dibiase, A., Thisse, C., Thisse, B., Nimer, S., & Zon, L. I. (2005). Regulation of the lmo2 promoter during hematopoietic and vascular development in zebrafish. *Developmental Biology*, *281*(2), 256–269. https://doi.org/10.1016/J.YDBIO.2005.01.034

Zou, L., Barnett, B., Safah, H., LaRussa, V. F., Evdemon-Hogan, M., Mottram, P., Wei, S., David, O., Curiel, T. J., & Zou, W. (2004). Bone marrow is a reservoir for CD4+CD25+ regulatory T cells that traffic through CXCL12/CXCR4 signals. *Cancer Research*, *64*(22), 8451–8455. https://doi.org/10.1158/0008-5472.CAN-04-1987

Zou, W., & Chen, L. (2008). Inhibitory B7-family molecules in the tumour microenvironment. *Nature Reviews Immunology 2008 8:6*, *8*(6), 467–477. https://doi.org/10.1038/nri2326

Acknowledgments

I would like to express my deepest gratitude to **Prof. Dr. Michael A. Rieger** for giving me the opportunity to pursue my PhD thesis in his laboratory. His supervision, guidance and the many opportunities he provided over the years have been instrumental in enabling me to complete my research and grow professionally throughout this journey.

I am also sincerely grateful to **PD Dr. Oliver Rossbach**, who has accompanied me since my Bachelor's studies, through my Master's and now as a reviewer of my PhD thesis. His valuable ideas, constructive suggestions and support have been greatly appreciated.

A heartfelt thank you goes to all the amazing people both within and beyond our research group. Without the support of my colleagues and friends at work, this project would not have been possible. I would particularly like to thank all current and former members of the AG Rieger as well as my collaborators: **Adrien, Tjeerd, Ramona, Malak, Lena, Ika, Jassi, Domi** and **Hana**.

A special thanks goes to **Alec, Marius** and **Daniel**, whose scientific input and immense help with experiments were invaluable. More importantly, their presence made the past years a joyful and memorable experience, full of laughter and friendship.

I would also like to thank **Ariana**. We went through this PhD journey side by side, and I cannot imagine doing it any other way.

To my friends outside the lab: thank you for being part of this ride and providing your support beyond the world of research.

Finally, and most importantly, I would like to thank my wonderful family — especially my parents — who stood by me through every challenge. Your unwavering support, encouragement and belief in me made it possible to complete this journey. This accomplishment is as much yours as it is mine and I could not have done it without you. Thank you!